THE THERMAL DECOMPOSITION OF UNIRRADIATED AND IRRADIATED LITHIUM AZIDE

by

V C LIDDIARD B.Sc. (Hons), (Rhodes)

A thesis submitted to the University of Cape Town in fulfilment of the requirements for the Degree of Doctor of Philosophy.

Department of Chemistry,
University of Cape Town,
Rondebosch, Cape,
South Africa.

JANUARY 1969.

The copyright of this thesis vests in the author. No quotation from it or information derived from it is to be published without full acknowledgement of the source. The thesis is to be used for private study or non-commercial research purposes only.

Published by the University of Cape Town (UCT) in terms of the non-exclusive license granted to UCT by the author.

University of Cape Town

ACKNOWLEDGEMENTS

The author wishes to express his grateful appreciation to Professor E G Prout, Professor of Physical Chemistry, University of Cape Town, for his invaluable advice, direction and interest throughout the period of the research and during the writing of this thesis.

The author also wishes to express his appreciation and thanks to Mr. S G Harris for assistance in the technical aspects of the work, to Miss A Stylianou, the typist, to the Radio Isotope Section of the Food and Fruit Institute, Stellenbosch, for use of the ^{60}Co source, and to his wife for assistance in the proof-reading and preparation of the manuscript.

Finally, the author is indebted to African Explosives and Chemical Industries Limited for financial assistance and for appointment as a Research Officer at University during the course of this research.

CONTENTS

Page

Page

7. THE THERMAL DECOMPOSITION OF LITHIUM AZIDE PRE-IRRADIATED WITH X-RAYS 150

SUMMARY

The thermal decomposition in vacuo of lithium azide, in powder and pellet form, has been investigated. The temperature range was 160° - 220°C. The results obtained were highly reproducible, and a study of the reaction kinetics was made for both the pelleted and powdered forms of the azide.

Mathematical analysis of the results obtained indicated that discrete nuclei are formed over the induction period which then grow two-dimensionally over the acceleratory period. The nuclei increase in number linearly with time and overlap and ingestion of the nuclei occurs during the acceleratory period. This was shown by the applicability of the Avrami-Erofeyev equation with the exponent n assuming the value 3, for the analysis of the acceleratory period p/t plot. The nuclei are formed mainly over the external surfaces of the decomposing particles.

The effects produced by pre-irradiation with γ-, X- and U.V.- radiation on the subsequent thermal decomposition have been studied. These studies were largely on the powdered lithium azide, but some attention was also given to pre-irradiating the pelleted material. Pre-irradiation of the powdered material resulted in a marked shortening of the length of the induction period followed by an increased acceleratory rate, for the types of radiation employed. X- and U.V.-radiation did not have any significant effect on the decay period reaction rate. The p/t plots were sigmoid, as found for the unirradiated azide.

Applicability of the Avrami-Enofeyev equation in the analysis of the acceleratory period for the irradiated azide indicated that two-dimensional nuclei formed and grew on the surfaces of the particles, except in the case of γ-irradiated lithium azide when the reaction was largely confined to internal grain boundaries.

Similar mechanisms operate over the induction periods for the unirradiated and irradiated azide. A change in the value of the activation energy for the acceleratory periods, indicated that the rate determining step for this stage of the reaction is altered after pre-irradiation. The same mechanism was applicable for the decay stages of the unirradiated and irradiated azide.

The effects of pre-irradiation with all three types of radiation, resulted in a double-sigmoid p/t plot in the case of pelleted lithium azide. The initial reaction was confined to the surface of the pellet pre-irradiated with U.V., and occured throughout the bulk of the pellets pre-irradiated with γ- and X-rays.

1. INTRODUCTION

The work presented in this thesis involves a study of the thermal decomposition of lithium azide and then the effects of various radiations, namely γ, X and U.V., on the subsequent thermal decomposition of lithium azide. Consequently it is deemed necessary to review thermal decomposition studies alone, and then the work associated with the interaction of the above radiations with solids.

1.1 THE THERMAL DECOMPOSITION OF SOLIDS

Chemical reactions involving one solid phase and producing another invariably proceed preferentially at the interface between the two phases. The thermal decomposition of solids is generally a reaction that proceeds via this process. Reaction is usually initiated at some specific locality and is termed the nucleation process. This results in the formation of sub-microscopic particles of the solid product phase called nuclei. These may be distributed over the surface of, or embedded in, the bulk of the reactant matrix. Further decomposition is localised at the interface between the nuclei and the reactant matrix, so that the nuclei grow in size as the reaction proceeds. As the nuclei grow, the area of this interface increases.

The chemical reactivity is influenced to a marked extent by the numerous types of imperfections or defects in the solid. Although it is not immediately obvious why, on electronic grounds, solid state reactions such as the thermal decomposition of carbonates(1) and azides(2,3) should be favoured at dislocations, growth defects and mosaic block boundaries, it is nevertheless reasonable to expect that chemical transformation may be facilitated at these points on the internal and external surfaces of a crystal because both the chemical potential and steriochemical environment of ionic species in the immediate vicinity of these imperfections differ from those of similar species at "ideal"lattice sites. It has been shown that many thermal decomposition reactions of solid substances begin at the point of emergence of dislocations at the crystal surface and at the boundaries of their groupings(4-7). Besides being influenced by the line defects mentioned above, the thermal decomposition process may be influenced by point defects in the lattice, such as anionic and cationic vacancies, interstitial ions, impurity atoms or ions and electronic defects (free electrons, excitons, colour-centres and positive holes). The mechanisms of all thermal decompositions in the solid state have tentatively been divided into two groups by Boldyrev(8-10). One group involves reaction proceeding through cleavage of bonds within an anionic or cationic lattice component (for example the decomposition of potassium permanganate(11,12)) and the other group comprises reactions in which the decomposition process occurs as a result of transfer of an electron from anion to cation. Decompositions of the latter group are exemplified by the inorganic azides(13).

As mentioned above nucleation may occur over the surface of the crystal or be embedded in the bulk of the reactant matrix. Chemical reaction is generally accepted as proceeding via this (i) nucleus formation, followed by (ii) nucleus growth. The nature of the nuclei formed is not always clearly defined but it is generally accepted that they are composed of solid reaction product. This general type of mechanism involving the two stages of formation and growth is rarely in dispute and, at least in many solid decompositions, no alternative analysis having sufficient flexibility to account for the variable kinetics and for rates ranging from times of half-change of a few seconds to many days, has been advanced. It is now customary to associate the unique sites at which nucleation takes place with imperfections at both the internal and external surfaces, as has been mentioned above (these in turn reflect the imperfect structure of the solid).

The nuclei may be classified into two main groups, namely compact nuclei and diffuse nuclei. The latter nuclei are spread uniformly throughout the solid. In support of this classification visual examinations of decomposing barium azide(14,15) sodium azide(16,17) and lead, cadmium and silver azides(18) have been made, and the nuclei observed directly.

Generally the activation energy for nucleus formation is greater than that for nucleus growth, with the consequence that compact nuclei are formed. Similar activation energies for nuclear formation and growth generally favours the formation of diffuse nuclei. Compact nuclei are observed to have characteristic shapes and in sodium azide platelets(17), these were observed to be two-dimensional and approximately circular, initially, and were formed on preferred crystallographic faces. The reaction then moved along a two-dimensional path towards the centre of the crystal. Hexagonal nuclei were observed in the thermal decomposition of potassium hydrogen oxalate(19).

The number of nuclei formed during thermal decomposition may be greatly influenced by the pre-reaction treatment of the sample, thereby increasing greatly the number of potential nucleus forming sites. Grinding(20,21), scratching of the crystal surface(22) and the method of sample preparation(23) have been shown to play an important role in this respect. Pre-irradiation of the solid prior to decomposition with ionizing radiations (γ- and X-rays(24-27)), ultra-violet light(28,29), electrons(30) or reactor radiation(31,32) has generally been found to enhance the subsequent thermal decomposition of the solid as a result of the formation of crystal defects and deposition of radiolysis products in the crystal lattice.

The majority of thermal decompositions investigated are of the type:

$$A_{solid} \longrightarrow B_{solid} + C_{gas}$$

The reaction is performed isothermally and the course of the decomposition is followed by pressure measurements of the evolved gas. A decomposition curve representing the course of the decomposition is obtained by plotting pressure against time (p/t plot) or the fractional decomposition, α, against time. In the general case the decomposition curve has the features illustrated in FIGURE 1.1,

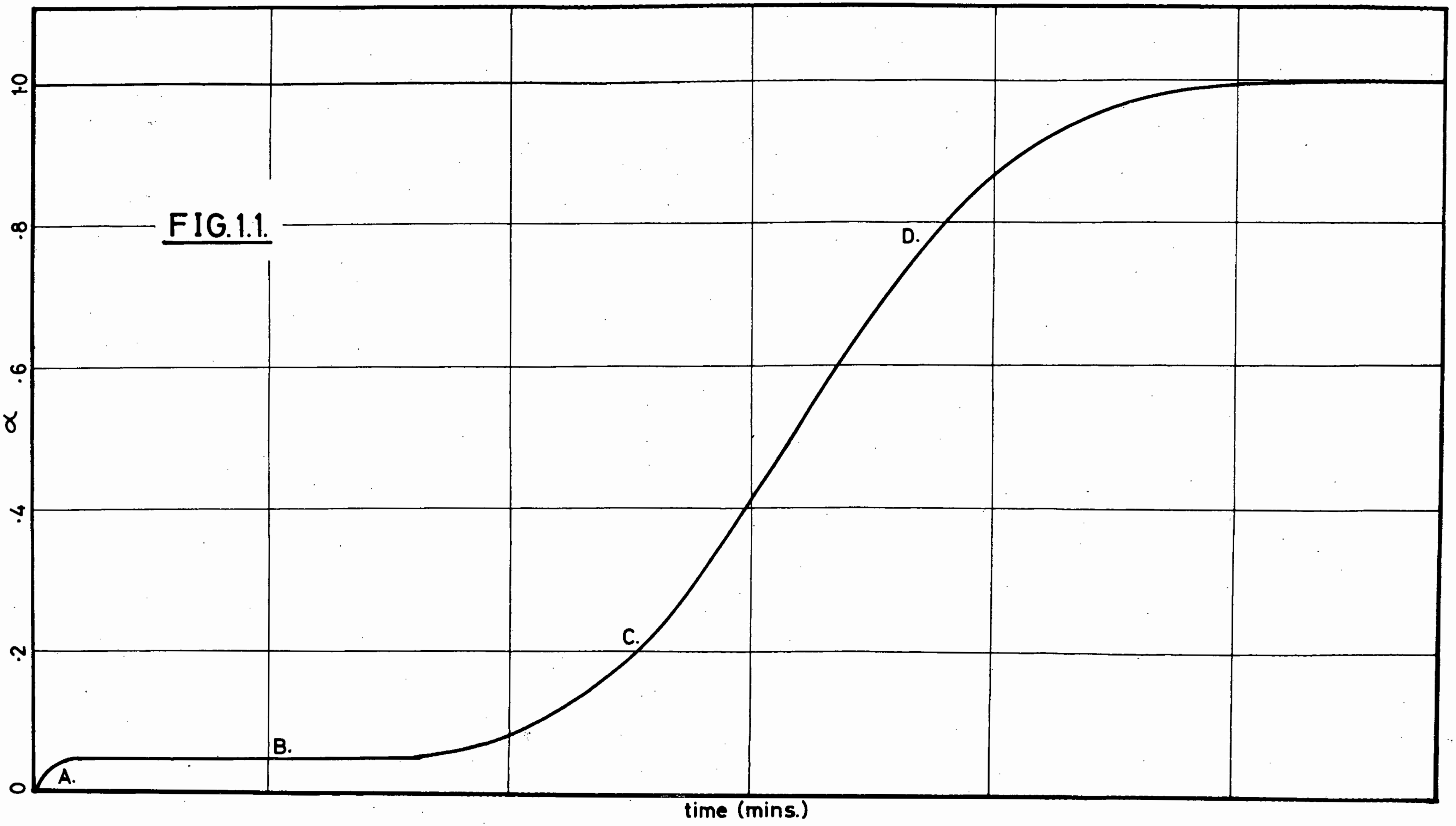

FIG. 1.1.

although any of these features may be absent in specific cases. Features of the decomposition include (i) an initial rapid evolution of gas A, followed by (ii) a section B, termed the <u>induction period</u>, characterised by a slow evolution of gas, which in some cases is scarcely measurable. At the conclusion of the induction period, an (iii) <u>acceleratory period</u>, C, results, which normally extends up to fractional decompositions(α) of 0.1 to 0.5. After the inflexion point the (iv) <u>decay period</u>, D, or period of deceleration operates during the final stages of the decomposition.

These divisions are usually associated with the production of nuclei, their growth, and beyond the inflexion point the overlap and merging of the nuclei and contraction of the product/reactant interface. In the decomposition of inorganic azides (3,20,33) the p/t plot is generally sigmoid and no initial burst of gas is observed, prior to the induction period. The shape of the p/t curve in the thermal decomposition of solid materials offers information regarding the physical nature of the reacting solid and the nature of the chemical process.

The acceleratory period is that part of the decomposition plot that has been studied most intensively, because, when it can be analysed uniquely, it yields the most information. The recognition of numerous types of imperfections in crystals and of the way in which their number and mutual influence may vary suggests that the kinetics of decomposition of a crystal, depending on nucleation and preferential reaction at crystal imperfections, should be a complex process. Nevertheless the good overall fit obtained with relatively simple kinetic equations indicates that complexity of crystal structure is not obviously reflected in chemical decomposition and that it can be made evident only by rather detailed observation and kinetic analysis.

A decomposition model constructed on the basis of the analytical form of the decomposition (p/t) functions should ideally be supported with further data obtained for instance by ionic conductivity (34,35) measurements, observations of the decomposition under light microscope or electron microscope$^{(5,14)}$, structural studies$^{(36)}$, spectroscopic studies$^{(37)}$ and analytical investigations of the reaction products$^{(38)}$.

Nucleation in the reactant matrix may involve a single step and it is assumed that a single molecule will lead to the formation of a nucleus. The formation of nuclei then follows the **EXPONENTIAL LAW:**

$$dN/dt \;=\; k_1 N_o \exp\,(-k_1 t) \quad \ldots\ldots\ldots\ldots\ldots\ldots\ldots\ldots \quad (1.1)$$

where N is the number of nuclei at time t, N_o is the number of nucleus-forming sites and k_1 is the rate constant. In the early stages of the reaction, and especially if the activation energy for nucleus formation is large (i.e. k_1 is small) then:

$$dN/dt \;=\; k_1\, N_o$$

Under these circumstances the number of nuclei increase linearly with time. This was observed in the dehydration of copper sulphate pentahydrate$^{(39)}$.

When multiple steps are required for nucleus formation, the **POWER LAW** describes the decomposition:

$$dN/dt \;=\; D\beta\; t^{\beta-1} \quad \ldots\ldots\ldots\ldots\ldots\ldots\ldots\ldots \quad (1.2)$$

D is a constant related to the rate constant k_2 as

$$D \;=\; \frac{N_o k_2^{\beta}}{\beta!}$$

and where β is an integer, representing the number of successive molecular decompositions at a single site required to form a stable growth nucleus. Nuclei containing less than β product atoms are not growth nuclei but germ nuclei, which may become growth nuclei by acquiring the requisite number of product atoms. This in essence was the theory considered by Bagdassarian$^{(40)}$, but was concerned only with the special case where:

$$k_o = k_1 = k_2 = \;\ldots\ldots\ldots\ldots\ldots = k_{\beta-1}$$

$k_\beta = k_{\beta+1} = k_{\beta+2} = \ldots\ldots\ldots\ldots = k$, and where k is the rate constant for the addition of a product atom to a nucleus containing i atoms. Allnatt and Jacobs(41) recently considered the general solution, where firstly, they consider the situation in which the rate constants are all different and then they consider the modifications to the theory, which are necessary when the k's are all different up to i = r, where r refers to the number of product atoms in a nucleus.

The concept that the reaction interface advances at a constant rate has been confirmed in the majority of cases for which the velocity has been measured directly, but there do exist deviations from this ideal behaviour. The deviations have been attributed to the dipolar nature of the water molecule, in the case of the dehydration of salt hydrates(39) and it has been suggested that the reason is trivial(42,43) for the non-ideal case of the chrome alum decomposition(44). However, Young(45) suggests that this difference arises from detailed changes in the interfacial conditions.

Nuclear formation and growth may be explained using several models which for convenience may be divided into four groups. The mathematical relationships describing these are:

(i) The Power Law
(ii) The Exponential Law
(iii) The Prout-Tompkins equation
(iv) The Avrami-Erofeyev equation.

(i) The power law. This class of thermal decomposition comprises those in which nucleation proceeds according to equation 1.2. Normal growth is assumed and overlap of the growing nuclei is neglected. With these conditions it can be shown(46) that:

$$p = k_3 \, t^n \quad \ldots\ldots\ldots\ldots\ldots\ldots\ldots\ldots\ldots\ldots \quad (1.3)$$

where p is the gas pressure at time t during an isothermal decomposition, k_3 is the rate constant and $n = \beta + \lambda$. β has the same meaning as before and $\lambda = 1$, 2 or 3 depending on whether the nuclei grow 1, 2 or 3-dimensionally, i.e. are rod-like, plate-like or spherical.

The POWER LAW, equation 1.3, has been applied in the above form, and in a slightly modified form, with good results, to a number of compounds. Several workers(20,47,48) have found the power law with n = 3 to hold for the decomposition of calcium azide. Leiga(49) found that n took on values between 3.02 and 5.30 when the power law was used in the decomposition of silver oxalate. As the nuclei were observed to be 3-dimensional (i.e. $\lambda = 3$), β then took on values 0 to 2. A theory of instantaneous nucleation and further nucleation according to the exponential law, was suggested as the mechanism for this reaction.

(ii) The exponential law. Garner and Hailes(50) were led to the concept of linear branching reaction chains, to apply to the decomposition of mercury fulminate. Assuming a constant rate of nucleation and a constant branching coefficient, k_4,

$$p = C \exp (k_4 \; t) \quad \ldots\ldots\ldots\ldots\ldots\ldots\ldots\ldots \quad (1.4)$$

This is termed the EXPONENTIAL LAW. C is a constant and is a function of temperature and contains the rate constants for nucleation, growth and branching. Although the equation was applied with success to the decomposition of mercury fulminate and large crystals of lead styphnate(51), it is now generally accepted that the concept of linear chains required some modification. The rapid propagation of linear chains through the crystal would tend to separate it into mosaic blocks, which would then decompose slowly. Modifying the original assertions so that branching plate-like nuclei propagated through the crystal, was an improvement on the theory. This idea was applied in the decomposition of silver oxalate(52) and it was suggested that decomposition proceeded along grain boundaries and dislocation lines, and branching occurred at intersections of these defects in the crystal lattice.

(iii) The Prout-Tompkins equation. Prout and Tompkins(53) noted that Garner's linear branching chain theory in the form it was originally presented took no account of the overlap of branching chains at higher degrees of decomposition. Modifying the original equation by introducing a term for the probability of chain termination, an equation of the form:

$$\log \frac{p}{p_f - p} = k_5 t + c_1 \quad \ldots\ldots\ldots\ldots\ldots\ldots\ldots\ldots \quad (1.5)$$

was derived on integrating the equation derived to represent the rate of decomposition, $d\alpha/dt$. This equation is termed the **PROUT-TOMPKINS EQUATION.** These workers found that this equation was applicable to the particular preparation of potassium permanganate studied by them. This equation has been found to be applicable to many permanganate decompositions(54).

Prout and Tompkins found that analysis of the decomposition of silver permanganate was improved if a modified form of equation 1.5 was used. The equation:

$$\log \frac{p}{p_f - p} = k_5' \log t + c_2 \quad \ldots\ldots\ldots\ldots\ldots\ldots\ldots \quad (1.6)$$

was derived and is termed the modified Prout-Tompkins equation. This equation takes into account the fact that the branching coefficient k_5 was not constant but varied inversely with time.

Hill(23,56) has postulated a diffusion chain mechanism for the decomposition of potassium permanganate and has found that the appearance in low temperature runs of a low activation energy, 15 k.cals/mole, can be associated with a diffusion process in the dislocation network, resulting in the formation of product nuclei at points throughout the crystal lattice.

(iv) The Avrami-Erofeyev equation. In an attempt to obtain a more general kinetic equation, Avrami(57) dealt with the nucleation process in a study of the kinetics of phase change. He made the assumption that the new phase, as a result of the thermal decomposition of the solid, is nucleated by tiny "germ nuclei" which already exist in the old phase. These germ nuclei are capable of developing into observable "growth nuclei" after commencement of the transformation. The number of germ nuclei decreases in two ways as the reaction proceeds. The first effect is the normal activation and growth of the nuclei and the second effect is the ingestion of germ nuclei by actively growing growth nuclei, which thus renders the germ nuclei inoperative. These nuclei incorporated before activation are termed "phantom nuclei". For convenience, the germ nuclei are now termed "nuclei" and the growth nuclei are termed "grains". The grains (phantom nuclei included) taken to full growth and neglecting the impingement upon one another are referred to as "extended grains".

The rate of disappearance of nuclei during any time interval dt from a system originally containing N_o nuclei per unit volume at t = 0 is given by:

$$- dN' = dN + dN'' \quad \ldots\ldots\ldots\ldots\ldots\ldots\ldots (1.7)$$

where

$$dN = k_1' N' dt \quad \ldots\ldots\ldots\ldots\ldots\ldots\ldots (1.8)$$

and

$$dN'' = \frac{N'}{1 - V} dV \quad \ldots\ldots\ldots\ldots\ldots\ldots (1.9)$$

The number of nuclei at t = 0, N_o, decreases with time and at time = t their number will be N'(t) since N(t) become grains and N"(t) are ingested (phantom nuclei) by the growth of the N(t) grains. Thus, from 1.7, the decrease in the number of potential sites in any time interval dt is equal to the number of grains plus the number of phantom nuclei formed. This is the general case for random nucleation. Equation 1.9 is obtained by considering the number of nuclei per unit volume which the advancing front of the product phase encounters during the time interval dt. This density is given by the number N' of nuclei at time t, divided by the untransformed volume (1 - V), per unit volume. dV is the volume swept out by the grains of the product phase during a time interval dt. Equation 1.9 can be used in the form

$$dN'' = \frac{N'}{1 - \alpha} d\alpha \quad \ldots\ldots\ldots\ldots\ldots (1.10)$$

where $\alpha = {}^{p}/{p_f}$, the fractional decomposition of the solid.

Equations 1.7, 1.8 and 1.10 now give

$$k_1' N' + \frac{N'}{1-\alpha}\frac{d\alpha}{dt} + \frac{dN'}{dt} = 0 \quad \ldots\ldots\ldots\ldots(1.11)$$

Rearranging and integrating this then gives

$$N' = (1-\alpha) N_o \exp(-k_1' t) \quad \ldots\ldots\ldots\ldots\ldots \quad (1.12)$$

Using 1.8 and 1.12 then

$$\frac{dN}{dt} = (1-\alpha) k_1' N_o \exp(-k_1' t) \quad \ldots\ldots\ldots\ldots\ldots \quad (1.13)$$

Integrating 1.13 the equation obtained is

$$N(t) = k_1' N_o \int_o^t e^{-k_1' y}\left[1-\alpha(y)\right] dy \quad \ldots\ldots\ldots\ldots(1.14)$$

which is the expression for the density of grains (growth nuclei) as a function of time. Rewriting 1.14 for the growth of 3-dimensional (spherical) nuclei the expression obtained for the fractional decomposition is

$$\alpha(t) = \frac{Sk' N_o k_2^3}{V_o} \int_o^t e^{-k_1' y} (t-y)^3 \left[1-\alpha(y)\right] dy \quad \ldots\ldots\ldots \quad (1.15)$$

where S is a shape factor and V_o is the final volume of product obtained from complete decomposition of W_o gms of the reactant. Equation 1.15 is not amenable to direct solution but can only be solved approximately. For the particular case of random nucleation, however, Avrami has shown how a solution may be obtained using the concept of "extended volume". The extended volume, (V_{ex}), or fractional decomposition, $(\alpha_{ex}(t))$, was defined as the total volume of all nuclei including overlapping regions and those growth nuclei (grains) which would have been formed from ingested germ nuclei were this a physically realistic process. The assumption was made that cessation of growth due to impingement of grains does not occur in the reactant matrix. The rate of formation of all nuclei is $\frac{dN}{dt}$, whence the extended fractional decomposition is given as

$$\alpha_{ex}(t) = \frac{V_{ex}(t)}{V_o} = \frac{1}{V_o}\int_o^t v(t, y)\left[\frac{dN'}{dt}\right]_{t=y} dy \quad \ldots\ldots\ldots(1.16)$$

where V_o is as defined above. The term $v(t, y)$ is the volume of a nucleus formed at time t, formed at t = y.

$$v\ (t, y) = S\left[k_2'\ (t - y)\right]^3 \quad .... \quad (1.17)$$

where k_2' is the linear rate of isotopic growth and S is a shape factor for 3-dimensional growth. Thus equation 1.16 reduces to

$$\alpha_{ex}\ (t) = \frac{\alpha k_2'^3\ k_1'\ N_o}{V_o} \int_0^t e^{-k_1' y}\ (t - y)^3\ dy \quad ....(1.18)$$

This equation can be evaluated precisely and to obtain $\alpha(t)$ a relationship between the actual volume of the product V, $(\alpha(t))$, and the extended volume $V_{ex}(t)$, $(\alpha_{ex}\ (t))$, must be found. The general method presented by Avrami to this problem produced rather cumbersome formula and as a method of simplification it was stated that on the average the ratio of "non-overlapped volume", v', to extended volume V_{1ex}, is equal to the density of unreacted matter at that time, $(1 - V)$, to give the expression

$$\frac{v'}{V_{1\ ex}} = \frac{1 - V}{V} \quad .... \quad (1.19)$$

where

$$V_{1\ ex} = \int_0^t v\ (t, y)\ \ N'\ (y)\ dy \quad ....(1.20)$$

integrated over the whole crystal. The non-overlapped volume v' is considered to be that part of the volume which contains no product phase whatsoever.

Taking into account the increment of the product grains over the time interval dt,

$$\frac{dv'}{dV_{1\ ex}} = \frac{1 - V}{V} \quad ....(1.21)$$

and whence

$$\frac{d\alpha}{d\alpha_{ex}} = 1 - \alpha \quad .... \quad (1.22)$$

Using equations 1.18 and 1.22,

$$\alpha_{ex} = \int_0^{\infty} \frac{d\alpha}{1 - \alpha} = \frac{S\, k_2'^3 k_1'\, N_o}{V_o} \int_0^t e^{-k_1' y}\, (t - y)^3\, dy \quad \ldots\ldots\ldots(1.23)$$

or

$$- \log\,(1 - \alpha) = \frac{6\, S\, N_o\, k_2'^3}{V_o\, k_1'^3} \left[e^{-k_1' t} - 1 + k_1' t - \frac{(k_1'\, t)^2}{2!} + \frac{(k_1'\, t)^3}{3!} \right] \ldots.(1.24)$$

For simplification, let

$$k = \frac{S\, k_2'^3}{V_o k_1'^3} \quad \ldots\ldots\ldots\ldots\ldots\ldots\ldots\ldots\ldots\ldots\ (1.25)$$

and hence 1.24 becomes

$$- \log\,(1 - \alpha) = 6\, k\, N_o \left[e^{-k_1' t} - 1 + k_1' t - \frac{(k_1' t)^2}{2!} + \frac{(k_1' t)^3}{3!} \right] \quad \ldots..(1.26)$$

This is the most general solution to the case of random nucleation of three-dimensional product nuclei.

Several limiting cases may be obtained from equation 1.24.

(i) <u>α small</u>. When $\alpha \ll 1$, the contribution of overlapping and phantom nuclei will be negligible and α_{ex} may be replaced by α.

Equation 1.24 then becomes:

$$\alpha = 6\, k\, N_o \left[e^{-k_1' t} - 1 + k_1' t - \frac{(k_1' t)^2}{2!} + \frac{(k_1' t)^3}{3!} \right] \quad \ldots\ldots.(1.27)$$

Thus for $k_1' t$ small,

$$\alpha = c_3 t^4 \quad \ldots\ldots\ldots\ldots\ldots\ldots\ldots\ldots\ldots\ldots\ (1.28)$$

or for plate-like nuclei, or instantaneous nucleation followed by three-dimensional growth

$$\alpha = c_4 t^3 \quad \ldots\ldots\ldots\ldots\ldots\ldots\ldots\ldots\ldots\ldots\ (1.29)$$

or for linear growth

$$\alpha = c_5 t^2 \quad \ldots\ldots\ldots\ldots\ldots\ldots\ldots\ldots\ldots\ldots \quad (1.30)$$

Equations 1.28,1.29 and 1.30 are seen to be the power law, $\alpha = c\,t^n$, where $n = \beta + \lambda$, as described by equation 1.3.

(ii) <u>t large</u>. In the decay period, when t is large, equation 1.24 reduces to

$$-\log(1 - \alpha) = k N_o t^3 \quad \ldots\ldots\ldots\ldots\ldots\ldots\ldots\ldots \quad (1.31)$$

or

$$\alpha = 1 - \exp(-k N_o t^3) \quad \ldots\ldots\ldots\ldots\ldots\ldots\ldots\ldots \quad (1.32)$$

The equation 1.32 is applicable for analysis of the decay period.

Mampel (58), using a different approach investigated the problems of overlap and ingestion and considered the various ways in which a surface corresponding to that of a spherical particle could be covered by discs. Discs falling within other discs are phantom nuclei, while discs which partially cover one another represent nuclei which overlap during growth. He derived equations which have the same general form as 1.15 derived by Avrami.

Using a different approach Erofeyev (59) first derived a general kinetic equation

$$\alpha = 1 - \exp\left(-\int_0^t p\,dt\right) \quad \ldots\ldots\ldots\ldots\ldots\ldots\ldots\ldots \quad (1.33)$$

where α = fractional decomposition as before and p is the probability of the reaction of an individual molecule in an interval dt.

Equation 1.33 may also be written

$$-\ln(1 - \alpha) = \int_0^t p\,dt \quad \ldots\ldots\ldots\ldots\ldots\ldots\ldots \quad (1.34)$$

The equation was then applied to the formation and growth of nuclei in the solid state.

If the rate of formation of nuclei is given by dv/dt, then for constant rate of nucleation,

$$dv/dt = \text{const.} \qquad \ldots\ldots \qquad (1.35)$$

and in the second limiting case when the rate is a power of time

$$dv/dt = \text{const.}\ t^{z} \qquad \ldots\ldots \qquad (1.36)$$

In either case the probability p.dt is proportional to the total volume of the spherical layers traced at the instant t around the nuclear centres that have arisen at the instant t*. The radii of the spheres limiting the layers are:

$$r = u\,(t - t^{*}) \quad \text{and} \quad r + dr = u\,(t + dt - t^{*}) \qquad \ldots\ldots (1.37)$$

Accordingly,

$$pdt = dt\int_{0}^{t} 4\ u^{3}\,(t - t^{*})^{2}\ \frac{dv}{dt}\ dt^{*} \qquad \ldots\ldots \qquad (1.38)$$

If the rate of formation of nuclei is dependant upon time, then from equations 1.36 and 1.38

$$p\ dt = \text{const.}\ t^{z+3}\ dt \qquad \ldots\ldots \qquad (1.39)$$

and from this equation and equation 1.33

$$\alpha = 1 - \exp\left(-\ kt^{z\ +\ 4}\right) \qquad \ldots\ldots \qquad (1.40)$$

For the first limiting case, (for constant rate of nucleation),

$$\alpha = 1 - \exp\left(-kt^{4}\right) \qquad \ldots\ldots \qquad (1.41)$$

Considering equation 1.40, if the rate of nucleation is as the square of time, then

$$\alpha = 1 - \exp\left(-kt^{6}\right) \qquad \ldots\ldots (1.42)$$

which for small values of t reduces to

$$p = ct^{6} \qquad \ldots\ldots \qquad (1.43)$$

This is the power law equation postulated by Wischin (14) for the thermal decomposition of barium azide.

Considering equation 1.41, the power 4 corresponds to three-dimensional growth, increasing in number at a constant rate.

For cylindrical nuclei (the centres of formation of the nuclei are edges or surface cracks) the expression analagous to 1.41 is

$$\alpha = 1 - \exp(-kt^3) \quad \ldots\ldots\ldots\ldots\ldots\ldots\ldots\ldots \quad (1.44)$$

and correspondingly, for flat nuclei:

$$\alpha = 1 - \exp(-kt^2) \quad \ldots\ldots\ldots\ldots\ldots\ldots\ldots\ldots \quad (1.45)$$

In general, according to the shape of the nucleus and the number of electrons necessary for the formation of a stable nucleus, Erofeyev states the general equation:

$$\alpha = 1 - \exp(-k_6 t^n) \quad \ldots\ldots\ldots\ldots\ldots\ldots\ldots\ldots \quad (1.46)$$

or

$$-\log(1 - \alpha) = k_6 t^n \quad \ldots\ldots\ldots\ldots\ldots\ldots\ldots\ldots \quad (1.47)$$

where $n \gtrless 4$, and $n = \beta + \lambda$, where β = number of intermediate stages in the formation of the initial centres of a reaction and λ = a value with three possible alternatives depending on whether the reaction nuclei are 1,2 or 3-dimensional.

Equation 1.46 is seen to be of the same form as the equation derived by Avrami, equation 1.26, but is the general equation for the kinetics of reactions which proceed by way of formation and growth of reaction nuclei in a solid. Equations 1.46 and 1.47 are known as the <u>AVRAMI-EROFEYEV EQUATION</u>.

The use of the Avrami-Erofeyev equation is almost universal amongst Russian workers(60 - 63) and has also been widely used by other workers(3, 64 - 68). Ishkin and Dubil(63) examined the kinetics of the thermal decomposition of sodium and potassium bicarbonates, and Acheson and Galwey(65) studied the kinetics of the thermal decomposition of nickel terephthalate, using the Avrami-Erofeyev equation. These latter workers showed that the carbon dioxide formation reaction obeyed the Avrami-Erofeyev equation though the reaction rate and the exponent value, n , varied for different salt preparations. They reported that the value of $n = 1.5$ for pure nickel teraphthalate indicated cosiderable restriction of growth of nuclei so that this process did not exert a major controlling influence on the reaction kinetics. They concluded that after nucleation of a particular crystallite the subsequent growth of that nucleus was largely confined to that particle although there was a small but significant probability that growth may extend to neighbouring salt particles. This model is closely comparable to that proposed(64) by Galwey and Jacobs for the thermal decomposition of powdered (cubic form) ammonium perchlorate, where growth was considered to occur essentially in one dimension, $n = 2$. Later work on ammonium perchlorate(66) was also analysed using the Avrami-Erofeyev equation with $n = 2$ or 3.

Herley and Levy(67) investigated the effects of pre-irradiation (γ-rays) on the thermal decomposition of ammonium perchlorate. For the material used, n had the value 4 for the unirradiated salt, and on irradiating and decomposing the salt, although $n = 4$ held over the range $0.07 < \alpha < 0.25$, in the decay stage with $n = 3$, the fit was over the range $0.40 < \alpha < 0.98$. These workers assumed the mechanism of Galwey and Jacobs(64) to hold for the irradiated salt as well.

Prout and Moore(3) applied the Avrami-Erofeyev equation in the kinetic analysis of the thermal decomposition of unirradiated and irradiated barium azide. The exponent n, was found to be 4 in both cases. It was considered that the reaction proceeded through the formation and growth of 3-dimensional nuclei, which increased in number linearly with time. The effect of pre-irradiation (γ-rays) was to increase the number of nuclei, and so increase the reaction rate on pre-irradiation.

Criticism of the Avrami-Erofeyev equation has recently been offered by some Russian schools(69,70). Razumov(69) and others maintain that the Avrami-Erofeyev has the shortcoming of describing reaction only in a continuous medium during the formation of the nuclei in the volume, during thermal decomposition. They hold that the nuclei are formed only on the surface, and on this assumption have derived a theoretical equation involving two dimensionless variables, to determine the process of thermal decomposition. Sakovich(70) has derived a topokinetic equation and has fitted this to the process of decomposition of solids.

Sakovich offers the equation

$$d\alpha/dt = K/m\alpha^{1-m}(1-\alpha^m) \text{ ....(1.48)}$$

where K is the rate constant, α the fractional decomposition, m a parameter constant and t the time. By integrating for time t one obtains the expression for the part of the substance which underwent reaction,

$$\alpha^m = 1 - e^{-Kt} \text{ ....(1.49)}$$

In virtually all the thermal decompositions that have been studied the acceleratory period can be accounted for topographically in terms of a reaction mechanism described by one of the above rate equations, for the formation and growth of nuclei in solids.

During the decay period, overlap of the compact nuclei has occurred and the reaction then proceeds from a shrinking of the reactant/product interface. Analysis of the decay may be achieved using a <u>FIRST ORDER EQUATION</u> but for this equation to be applicable, two conditions are necessary. First, one can obtain a first order expression if by chance the particle size distribution of completely nucleated particles is exponential, or secondly as a result of separation of the reactant matrix during the acceleratory period one can obtain a large number of precisely equivalent particles which do not contain active growth nuclei. The first-order equation is rarely used and is seldom of real value.

The decay period may be analysed by the AVRAMI-EROFEYEV EQUATION in the form

$$\alpha = 1 - \exp(-k_6 t^3) \quad \ldots\ldots\ldots\ldots\ldots\ldots \quad (1.50)$$

provided the contracting interface remains intact. Because of the difference in molecular volume between product and reactant phases, the interface may collapse leaving isolated blocks of material in which no nuclei are present. The same condition may arise from extensive growth of plate-like nuclei. In these isolated blocks if each molecule has an equal probability for decomposition, then the rate of reaction is simply proportional to the amount of substance undecomposed. Consequently

$$d\alpha/dt = k_7 (1 - \alpha) \quad \ldots\ldots\ldots\ldots\ldots\ldots \quad (1.51)$$

and therefore

$$\log \frac{1}{1 - \alpha} = k_7 t \quad \ldots\ldots\ldots\ldots\ldots\ldots \quad (1.52)$$

Equation 1.52 is referred to as the UNIMOLECULAR DECAY LAW.

If the rate-controlling factor in the decay reaction becomes the number of remaining unreacted molecules, not all of the molecules will be favourably situated next to a product molecule and

$$dp/dt = k' (p_f - p) P \quad \ldots\ldots\ldots\ldots\ldots\ldots \quad (1.53)$$

where P is the probability of the favoured situation, and is determied by p/p_f.

On substitution and integration

$$\log (p/p_f - p) = k_8 t + c_6 \quad \ldots\ldots\ldots\ldots\ldots\ldots \quad (1.54)$$

which is the PROUT-TOMPKINS EQUATION only with a different rate constant than for the acceleratory period.

Frequently, in cases where there is rapid and efficient surface nucleation of particles, the surfaces of the particles become coated with a layer of product in the early stages of the reaction. The rate determining step could then be the rate of penetration of this interface into the particles. For spherical particles of initial radius a, then the fraction decomposed at time t is given by

$$\alpha = 4/3\pi a^3 - 4/3\pi (a - k't)^3 \Big/ 4/3\pi a^3 \qquad (1.55)$$

$$= 1 - (1 - k_9 t)^3 \qquad (1.56)$$

or

$$1 - (1 - \alpha)^{1/3} = k_9 t \qquad (1.57)$$

Equation 1.57 is known as the <u>CONTRACTING SPHERE EQUATION</u>.

For contracting interfaces in geometrical shapes other than spherical i.e. parallelopiped and rectangle, a similar treatment to the contracting sphere method above, may be applied.

Mathematical analysis of the acceleratory and decay periods of the p/t plots for isothermal decomposition of solids can thus yield much information on the reaction mechanisms. Using this analysis, information can be obtained regarding the process of nucleation, the approximate shape of the nuclei and the mechanism by which they grow in size as the reaction progresses through the solid. Growth may be from a constant number of nuclei or from nuclei increasing as a power of time, or via branching chain mechanisms. The exact nature of the nuclei formed, however, is speculative. Further evidence should ideally be sought, as mentioned earlier, and a method suited to this end is the study of the effects of exposure to various types of radiation prior to thermal decomposition. Pre-irradiation of the solid with ultra-violet radiation, X-rays, γ-rays, electrons, heavy particles and reactor radiation has been extensively studied and the effects of these pre-irradiations have often been invaluable in elucidating the nature of the irradiation damage.

1.2 THE EFFECTS OF ULTRA-VIOLET RADIATION ON SOLIDS

Considerable information on the effect of ultra-violet radiation on solids has been obtained by a study of the actual decomposition of solids by light, namely the phenomenon of photolysis. Consequently, it is profitable to review the salient features of this branch of solid state chemistry, in particular the photolysis of the inorganic azides. The concepts developed in these researches have been transferred to other classes of substances and consequently it is furthermore useful to give detailed consideration to such work.

When crystals of certain inorganic solids are irradiated with ultra-violet light of wavelength corresponding to a characteristic absorption band of the solid, photochemical decomposition (photolysis) takes place. The course of the reaction is generally followed by pressure measurements of the evolved gas at fixed time intervals during the photolysis.

In the decomposition of solids under the influence of ultra-violet light, the energy of the quantum is comparable in magnitude with that of a chemical bond and this type of decomposition by radiation represents the simplest type of decomposition of the solid(71). Since on exposure the light flux is incident on the surface of the crystal, any chemical interaction between light and matter which does occur is localised mainly at the surface. Photolysis usually ceases when the crystal surface has become covered with a layer of product, which protects deeper layers of the crystal from the action of light (provided that further development of the reaction by a thermal process, by conversion of the energy of the light quanta into heat energy(72), is excluded).

The rate of photolysis is generally thought to depend both on the probability of transfer of an electron to the conduction band and on the possibility of its recombining with a positive hole. Boldyrev and Medvinskii(73) point out, however, that together with the width of the forbidden zone or other energy characteristics of electronic excitation, no less important characteristics are thought to be the lifetimes of the excitations, their concentrations and their mobilities.

The first real attempt at a theoretical explanation of the mechanism of the photolysis of any inorganic azide was due to Mott(74) when he proposed the mechanism of the reaction occurring in the photolysis of barium azide. The mechanism was based on the results of work done by Garner and Maggs(29) and Wischin(14). The theory was the same as that applied to the photochemical reaction of the silver halides(71, 75). Mott considered the solid to be an ionic conductor with mobile metal ions in interstitial positions and on irradiation electrons and positive holes were formed which diffused through the lattice. The electrons were trapped at some unspecified "sensitivity specks" where the mobile metal ion was subsequently neutralised. Accumulation of the metal atoms at these centres resulted in product nuclei which grew. Further electrons were trapped by the metal to form, in the case of silver bromide, an Ag^- ion, a process favoured by a high concentration of conduction electrons. A mobile Ag^+ ion would then neutralise the negative ion and contribute to a secondary growth mechanism. The mobile positive holes formed were thought to diffuse to the surface and neutralise anions with the evolution of the halogen or nitrogen, for the halides or azides, respectively.

Hence, the overall result was a growing nucleus accompanied by the evolution of gas, accounting for the observed formation of nuclei on the surface of the crystals during photochemical decomposition. This mechanism, one of the first attempts to elucidiate the photolysis mechanism, has since been criticised and modified and other mechanisms postulated. These will be dealt with below.

Thomas and Tompkins(76) made a detailed investigation of the photolysis of barium azide and concluded that Mott's theory required modification. A theory was proposed involving the production and trapping of excitons and it was thought that this would account more satisfactory for the results, and for earlier results (14,29). The original results of this investigation showed that using light of wavelength predominantly 2537Å, there was a constant rate of evolution of gas at constant temperature and constant intensity, and the rate varied as the square of the intensity at constant temperature. At constant intensity, but varying the temperature however, the rate was found to increase in a complex manner.

After a suggestion by Baidins (77) that the metallic reaction product of the photolysis of barium azide was inert, the interpretation of the photolysis of barium azide was re-assessed by Jacobs and Tompkins and others (78,79). New (78) kinetic measurements of the photolysis reaction showed the reaction to be more complex than first realised and a theory involving the production of both excitons and positive holes was postulated. The nature of the light source, the extent of the decomposition and the intensity of the radiation were examined in relation to the rate of the photochemical reaction. One of the most significant results of the whole work was the variation in the rate of photolysis with time. It was observed that the rate first decreased and then increased. This acceleratory region was followed by a period of constant rate of evolution. This behaviour was observed using lamps with (i) 2537Å as the principal line and (ii) a more or less continuous spectrum with principal lines superimposed.

It was found that when barium azide was irradiated with light from a high pressure arc having a 3650Å line, or with a low pressure lamp having essentially the 2537Å line, the initial rate was proportional to the square of the intensity and had an activation energy of approximately 5 k.cals./mole. This was interpreted in terms of bimolecular recombination of excitons at an unidentified trap, T:

$$N_3^- \, T \overset{h\nu}{\rightleftharpoons} N_3^{-*} \, T \rightleftharpoons \left[N_3 \, T\right]^{-*}$$

$$N_3^- \left[N_3 \, T\right]^{-*} \overset{h\nu}{\rightleftharpoons} N_3^{-*} \left[N_3 T\right]^{-*} \rightleftharpoons \left[N_3 T \, N_3\right]^{=**}$$

$$\Big\downarrow \text{5 k.cals./mole}$$

$$3N_2 + Ba + \square + \square$$

where $\square$ represents a vacancy, and * the excited state of the anion or complex. After a while the square law was found to be unapplicable and the rate of N_2 evolution increased. It was assumed that the traps T were consumed prior to this increase in rate. The final rate was constant and was found to have an activation energy of approximately 20 k.cals./mole for the 2537Å and 37.4 k.cals./mole for the 3650Å line.

It was suggested that once the Ba atoms were formed as above, a second process became operative:

$$Ba \overset{h\nu}{\rightleftharpoons} Ba^+ + e$$

$$Ba^+ + N_3^- \xrightarrow{E} Ba + N_3 \quad \text{where } E \sim 1\text{eV}$$

$$N_3^- \overset{h\nu}{\rightleftharpoons} N_3^{-*}$$

$$N_3^{-*} + N_3 \rightarrow 3N_2 + e$$

$$2N_3 \rightarrow 3N_2$$

$$Ba + Ba^{2+} + 2e \rightarrow Ba_2$$

Photoemission from the barium atoms results in acceleration of the reaction with the formation of N_2 by combination of excitons and radicals. The Ba atoms then aggregate to give Ba metal. If the irradiation was terminated when constant rate had been attained, a maximum dark rate was measured. This was considered to be a thermal decomposition due to:

$$Ba + Ba^{2+} \rightarrow (Ba_2)^{2+}$$

followed by electrons transferring from azide ions to the positively charged barium and the positive holes then react together to liberate the "dark rate" N_2.

It was later shown(80) that the acceleratory period could be removed by filtering the 2537Å line radiation with a water filter. It had previously been shown(79) that this could be achieved if the high pressure (3650Å) lamp was filtered with an OY 10 (Choice) filter.

Verneker(81) recently reported an investigation into the photolytic decomposition of barium azide and used ultra-violet light in particular wavelength ranges. It was found that (i) irradiation with U.V. light of wavelength 1849 + 2537Å and (ii) 2000 - 3000Å gave rise to the rate/time plot previously reported(79). However, irradiation with monochromatic U.V. light of wavelength 2537Å produced no acceleratory region. Barium nitride was also detected after each reaction in the product, irrespective of the reaction temperature. Photolysis of barium nitride was found to yield an accelerating rate. It was proposed that the decrease in rate initially, was due to a gradual consumption of defects as previously proposed and that the reaction ought to have proceeded to zero, as these defects are consumed. However, metallic specks are produced and the second process based on the photoemission of electrons from the metal keeps the reaction going. After the minimum value, the acceleratory period was proposed to be due to the photolysis of the nitride formed.

The photochemical decomposition of the azides of sodium, potassium, rubidium, caesium, strontium, mercury(-ous), thallium(-ous), silver and lead(4,29,81-87) have been investigated in addition to barium azide. Similar results have been obtained and related mechanisms have been proposed for the reactions.

Rubidium, potassium and strontium azides have been shown to exhibit similar rate/time characteristics as barium azide, in that an initial deceleratory region was followed by an acceleratory region. This in turn was found to be followed by a constant rate reaction. For potassium azide(82) it was found that if a low pressure lamp was used with a water filter, only a deceleratory process followed by a constant rate process was observed.

In the case of the photolysis of rubidium and caesium azides(84) it was suggested that three mechanisms were responsible for the rate/time plots. Caesium azide displayed an initial deceleratory process on photolysis, which becomes constant briefly, and then decreases before becoming constant again. The first two mechanisms as proposed for barium azide initially were thought to be valid and a third mechanism was proposed in addition to involve the reaction of excitons and excited azide ions at metallic nuclei, with the formation of N_4^-. The subsequent thermal decomposition of these N_4^- ions was thought to be responsible for the dark rate, when the ultra-violet lamp was switched off. The following mechanism was proposed for the acceleratory reaction (the third mechanism in the process of photolysis):

$$N_3^- \overset{h\nu}{\rightleftharpoons} N_3^{-*} \quad \text{(exciton)}$$

$$M_n \xrightarrow{h\nu} M_n^+ + e \quad (M_n = \text{metal nucleus})$$

$$N_3^- \xrightarrow{h\nu} [N_3^-]^* \quad \text{(excited azide ion)}$$

$$[N_3^-]^* + M_n^+ \rightarrow N_3\,M_n$$

$$N_3^{-*} + N_3\,M_n \rightarrow M_n + N_4^- + N_2 + \boxed{-} \qquad \text{(anion vacancy)}$$

$$M_n + M^+ + e \rightarrow M_n + 1$$

Thus the overall kinetics are described by (i) an initial decelerative region, (ii) a region of linear growth (second mechanism for barium azide) and (iii) an accelerative process involving the production of N_4^-.

These previous investigations of the azides contained much speculative work, and measurement of absorption spectra(80), photoelectric(80,88) properties, colour centre absorption bands(4,89,90,91) and electron spin resonance(92-97) results offered considerable support to mechanisms considered by Jacobs(83) and others. They reported that the rate of photolysis of sodium azide does not increase at any stage of the reaction, while that for potassium and strontium did, and proposed that two mechanisms applied in these latter cases. Absorption bands and e.s.r. results show that on ultra-violet radiation of potassium and sodium azides, the products positively identified were F-centres and F_2^+ centres for sodium azide (F_2^+ centre is a single electron associated with a divacancy) and N_2^- and N_4^- ions for potassium azide, as well as nitrogen gas in both cases. Almost nothing is, however, known about the colour centres or e.s.r. results for strontium azide. The information suggested that while excited azide ions formed in the perfect crystal revert to the ground state, those which formed adjacent to imperfections (impurity ions, dislocations, vacancies) decomposed in the following way:

$$N_3^{-*} + N_3^{-*} \rightarrow N_4^- + \boxed{-}\,e + N_2$$

$$N_3^{-*} + N_3^{-*} \rightarrow N_2^- + \boxed{-}\,e + 2N_2$$

$$N_3^{-*} + N_3^{-*} \rightarrow \boxed{-}\,e\,\boxed{-} + e + 3N_2$$

This mechanism can account for the decelerative process, and it was suggested that this may also apply to barium azide, but the N_4^- ion has not yet been identified in the U.V. irradiated salt. Jacobs et alia suggested the second process had the mechanism of photoemission from the metallic specks. The dark rate on switiching off the lamp was proposed to be due to the reaction:

$$N_4^- \rightarrow N_3^- + N$$

$$N + N \rightarrow N_2$$

In a more thorough examination of the kinetics and results of photolysis of sodium azide(86) the constant rate reaction observed after the deceleratory period was proposed to be due to a photoemission process from the metallic nucleus

$$Na_n \xrightleftharpoons{h\nu} Na_n^+ \quad e$$

$$N_3^{-*} + Na_n^+ \rightleftharpoons Na_n + N_3$$

Either by repetition of these steps, or by the reaction of an exciton, (N_3^{-*}), and a positive hole: $N_3^{-*} + N_3 \rightarrow 3N_2 + 2\boxed{-} + e$, there are formed three molecules of nitrogen, two electrons and two anion vacancies. The electrons produced are trapped by anion vacancy pairs forming transient F_2^+ centres, which then react with Na^+ to form Na atoms, the net result being nucleus growth. These workers did not observe any acceleration in the photodecomposition of sodium azide, and they ascribed it to topochemical features.

In a review of the photochemical decomposition of sodium, potassium, barium (reported above), silver and lead azides, it has been reported(81) after using various wavelengths of ultra-violet radiation that except for lead and silver azide, a deceleratory process followed by an acceleratory process was observed during the photochemical decomposition of the azides. It was considered that the work functions of all the metals of the salts studied, were such that irradiation with light of wavelength 1849 + 2537Å could cause photoemission, and yet no acceleratory process was observed in the cases of Pb and Ag azides. As described above for barium azide, the metal is considered to be in the atomic form, and hence the ionization potential of the atom is used. This would account for the loss of electron release from Pb or Ag. Also, for those metals which form the nitride, i.e. Na, K and Ba, it was proposed that the acceleration is caused by the photodecomposition of the nitride. It was also stated that all azides can show an acceleration in their photolytic rate if light capable of photoionizing the metal atoms, formed during photolysis, is used as a photolyzing source.

Apart from the inorganic azides, considerable work has been done on other classes of substances. The photodecomposition of the silver halides has been extensively examined(98,99) and more recently lead iodide and chloride have been investigated(100,101). It was proposed that(100) the primary act on irradiating lead iodide, in agreement with earlier results(102), was the creation of mobile excitons. Two excitons were considered to combine at specific traps (suggested as anion vacancies) yielding a molecule of iodine and an atom of lead. The lead atoms then diffused to form metallic lead nuclei.

The formation of lead in irradiated lead chloride(101) is thought to proceed also by way of trapping at anion vacancies, but it is suggested that excited electrons are trapped. The colour-centres thus formed can induce immediate charge transfer with the subsequent precipitation of the neighbouring lead ions.

Photodecomposition studies have been carried out on several perchlorates, a class of substances the thermal decomposition of which has been widely studied. The photodecomposition of nitronium perchlorate(103) yielded results that suggested that two processes took place during photolysis. Study of the photolysis of silver perchlorate(104) indicated that three mechanisms were possible during U.V. irradiation. The mechanisms proposed were considered to account for the observed rates and involved creation of defect centres leading to an acceleratory rate, consumption of defect centres resulting in deceleration and a steady-state rate originating from the initiation of the reaction from the photoemission from silver specks. This latter mechanism was put forward in the photodecomposition of the inorganic azides.

A multiple atom anion solid that has received attention recently is sodium bromate(105-107). In addition, the effect of pre-irradiation with γ-rays (^{60}Co) on the photoreaction, was investigated. Rate/time plots characterised by an initial deceleratory process followed by a constant rate of gas evolution, as found for sodium(86) and silver and lead(83), azides, were reported. γ-rays had the effect of decreasing the initial rate and decreasing the time required to attain the final constant rate.

A phenomenonological theory was proposed(106,107) to account for the photochemical decomposition of sodium bromate. A rate equation was derived with the assumptions that (i) photolysis is essentially a solid state electronic process and that (ii) decomposition occurs, at least part of the time, at decomposition sites, when these become doubly excited. The sites were suggested to be either fixed or mobile excitons, which yield oxygen on decomposition as:

$$BrO_3^{-**} \rightarrow Br\,O^- + O_2$$

1.3 THE EFFECTS OF PRE-IRRADIATION WITH ULTRA-VIOLET LIGHT ON THE THERMAL DECOMPOSITION OF SOLIDS

The effect of pre-irradiation on the thermal decomposition of many crystalline solids, in particular the azides(20,21,29,74,108,109), has been studied in considerable detail. These studies have led to increased knowledge of the mechanism of the thermal decomposition of the unirradiated solid and also to the nature of the radiation damage. The general effects of pre-irradiation of the solid, on the subsequent thermal decomposition are:

(i) shortening of the induction period,
(ii) acceleration of the reaction,
(iii) changes in the activation energies associated with the decomposition process(es),
(iv) changes in the mathematical analyses governing the p/t plots, and their extent of fit.

The effects of the pre-irradiation are generally long lasting(92) but may undergo ageing. Some substances are insensitive to pre-irradiation by ultra-

evolution, as [illegible]

violet light e.g. silver oxalate(110) and silver permanganate(111), while others show extreme sensitivity e.g. strontium azide(68).

The thermal decomposition of many inorganic solids is thought to proceed by way of an electron-transfer mechanism, and in view of this and the discussion of the effects of ultra-violet radiation on matter and the mechanisms of photochemical decomposition, it is feasible to state that a positive effect may be expected on the thermal decomposition, when solids of this nature are pre-irradiated with ultra-violet light. The inorganic azides are an example in point. Garner and Maggs(29) were the first workers to study the effects of pre-irradiation with ultra-violet light, when they studied its effect on the subsequent thermal decomposition of barium and strontium azides. They found that the induction periods for these two azides were shortened, and in the case of barium azide, noted an increase of the rate constant k, in the equation $\alpha = k\,(t - t_0)^6$, with increasing pre-irradiation with ultra-violet light. No attempts were made to measure the activation energies when the pre-irradiated specimens were thermally decomposed, and it was assumed that the nature of the reaction mechanisms was not markedly affected by pre-illumination with ultra-violet light.

They proposed that ultra-violet irradiation produced "holes" and diffusion of barium atoms, (in the case of barium azide), to these "holes" resulted in the formation of nuclei, from which the reaction initiated. Mott(74), as mentioned previously, proposed that barium azide was an ionic conductor by virtue of the presence of an equilibrium concentration of interstitial barium ions and that under U.V.-irradiation electrons are ejected from azide ions to the conduction band of the crystal. These electrons wander around until they are trapped by a speck of metallic barium, when the resulting electric field attracts interstitial metal ions. The speck therefore grew by a process of internal electrolysis. This reaction occurs on the surface of the crystals and on internal surfaces e.g. cracks.

Later investigation by Thomas and Tompkins(108) confirmed the experimental findings that pre-irradiation of barium azide shortened the induction period and increased the rate of the thermal decomposition. These effects were accounted for in terms of the large number of anion vacancies (Garner and Magg's "holes"). It was found also that the exponent 6 only remained constant at low doses, and large doses reduced the value to 3. They explained their results by stating that at low doses, more potential nucleus forming sites of the type required to sustain the nucleation law $dN/dt = kt^2$, are created. The site involved was assumed to be an anion vacancy. At higher doses it was proposed that these sites became activated, presumably by trapping electrons and so relaxing the requirement for thermal activation. In the limit this means that all the potential nucleus forming sites become both activated and equivalent, and accordingly a cubic acceleratory period is obtained.

Prout and Moore(68) found that the exponent in the Avrami-Erofeyev equation changed from 4 to 6, when barium azide was pre-irradiated with ultra-violet radiation. They proposed the formation of large numbers of F-centres on irradiation, which aggregate and collapse on heating, with the formation of barium atoms. These then migrate and crystallise at favourable sites to yield metallic nuclei, from which the reaction then proceeds. They proposed the same growth mechanism for these nuclei as they proposed for the unirradiated azide(3). The change of n from 4 to 6 was accounted for by assuming that after irradiation the number of nuclei no longer increase linearly with time, but rather with the cube of time (cf. Wischin(14)). Although it was shown that exposure to ultra-violet light effects photochemical decomposition in potassium azide(82), it was subsequently shown(21) that pre-irradiation with ultra-violet radiation, even though the salt was coloured blue, had no effect on the thermal decomposition. However, it was observed that on heating the blue colour rapidly faded. It was proposed that in this case, mobile excitons are formed and the electron from the exciton tunnels to a vacant site forming a single entity, the colouration complex, which comprises an F-centre and a positive hole. A second exciton can then form a complex adjacent to the first and reaction to give three molecules of nitrogen can then result. Nitrogen was observed in the post-irradiation period. On heating it was proposed that the reverse process in fact occurred, when both the bimolecular combination of positive holes and the unimolecular recombination of electrons from F-centres with positive holes by tunnel effect took place. This would account for the failure to detect photoconductance.

Studies of the thermal decomposition of potassium and sodium azides, as may be seen from the above, have been complicated by the volatility of the metal product at the decomposition temperature. This is unfortunate because it is relatively easy to obtain physical data on these salts(4,37,80). For example Miller(92) has shown by using the dual techniques of electron spin resonance and cryoabsorption spectroscopy that under treatment with ultra-violet radiation and heat, sodium azide develops centres of colloidal sodium. The mechanism of formation of the colloidal particles is attributed to photochemical reduction by irradiation, leaving an excess of sodium in the lattice which forms clusters during thermal diffusion. Aggregation of the metal was proposed via vacancy or electron diffusion. No other work on the effect of ultra-violet radiation on the subsequent thermal decomposition of these two azides has been done.

Calcium(20,48,68) and strontium(29,68,109) azides have been examined and similar results have been found for both these azides. Garner and Reeves(109) found that the power law with the exponent n = 3 held for the decomposition of both calcium and strontium azides and for these salts pre-irradiated with a dose of ultra-violet radiation. Shortening of the induction period and a 3 to 4 times increase in the rate constant for the acceleratory period were observed when the salts were irradiated prior to decomposition. It was stated that for the unirradiated azides, the nuclei were three-dimensional and all of approximately the same size at the end of the induction period. On irradiating with ultra-violet light, nuclei are formed and are thought to be more even in size at the end of the induction period as the fit of the power law improved. It was assumed that ultra-violet radiation caused sites (points of emergence of dislocation) to develop into nuclei, which would not normally so develop on thermal treatment. Tompkins and Young(20) confirmed the fit of the power law with n = 3 for calcium azide pre-irradiated with ultra-violet light. They examined the effects of pre-irradiation on aged and annealed calcium azide and on the fresh material. With fresh material it was reported that the rate constant increased continuously with the irradiation dose, unlike the aged material for which the rate constant was a constant for all doses up to 10^{14} photons/cm^2. The difference was attributed to the activation of excess bulk vacancies in the fresh calcium azide. For the aged material it was supposed that an excess of electrons due to irradiation were captured by surface clusters and these transformed into growth nuclei. In the unirradiated material the rate was controlled by the slow rate of production of electrons which were always in short supply. In fresh material containing excess grown-in vacancies, pre-irradiation was reported to activate germ nuclei throughout the system. However, Prout and Brown(48) report no ageing effect for unirradiated calcium azide, over a four month period. They report internal nucleation on pre-irradiating the salt.

In later work, Prout and Moore(68) further studied the effects of pre-irradiation on calcium azide and strontium azide and found the results to be very similar for both salts. They found for both azides that for heavy doses of ultra-violet radiation, the power law with n = 3 was not valid, but rather n = 2 gave a better fit of the decomposition p/t data. Both azides did not darken on pre-irradiation and as previously reported, shortening of the induction period followed by an increase in the rate constant for the acceleratory region was observed and the inflexion point of the p/t plots was seen to fall steadily on increasing the pre-irradiation dose. It was stated that primarily surface damage occurred and two dimensional nuclei growing linearly with time for the highly irradiated azides were supposed. On heavily irradiating the azides prior to decomposition, any further increase in the number of surface nuclei is virtually "swamped" there being such a large number formed as a result of the irradiation and n accordingly changes from 3 to 2.

A study of the effects of pre-irradiation with ultra-violet light on the thermal decomposition of silver azide(2) showed that neither the form of the p/t decomposition curve nor the maximum rate were affected within experimental reproducibility, but it could not be determined if this treatment affected the length of the induction period. Low reproducibility was found for this salt.

In the first study of the effects of pre-irradiation with ultra-violet radiation on the thermal decomposition of mercuric oxalate(112), it was stated that the irradiated salt decomposed with a higher rate than the unirradiated salt. The unirradiated salt decomposed with an initial surface reaction which was acceleratory and was represented as the expansion of discs from a number of point nuclei. After pre-irradiation the acceleratory period, which normally extended to $\alpha = 0.15$, was replaced by an initial burst of gas followed by a short constant rate period. Later investigation by Prout and Moore(113) showed the unirradiated and irradiated decomposition could be represented by the power law with $n = 2$. They proposed that the effect of exposure to sunlight (ultra-violet) was to create an unidentified irradiation product by an electron transfer process which formed and grew under the action of light on the surface of the mercuric oxalate. The product was tentatively suggested to have been mercurous oxalate.

Silver oxalate is another oxalate that has been examined with respect to the influence of ultra-violet radiation on the subsequent thermal decomposition. Benton and Cunningham(114) and Tompkins(115) were the early contributors to the so-called power law school of thought on the decomposition of silver oxalate. They found that the acceleratory period of the decomposition could be represented by an expression of the form: $\alpha = k\ (t - t_o)^n$ where $3.5 < n < 4$. Benton and Cunningham note that after exposure to ultra-violet radiation, the rate constant k increased and as was later confirmed by Tompkins, the value of n fell off towards 3. The effects were attributed to the first-order formation at certain sites of compact nuclei which grow in three-dimensions the number of unfertilized sites decreasing as the ultra-violet dose is increased. Other workers(52,116) on the other hand postulated a branching chain mechanism for the decomposition and found no change in the rate constant for light doses of ultra-violet light, but did observe a change in the pre-exponential factor. Decomposition(117) of single crystals of the unirradiated salt were later observed to follow a cubic law, however. More recently Haynes and Young(118) have indicated that the exponential law appears to offer the best analysis and explanation for the decomposition behaviour. In irradiated silver oxalate they propose that the number of starting points on the surface are increased by pre-irradiation and these then develop into growth nuclei, with simultaneous decomposition along a line joining two of these nuclei, hence explaining the use of the exponential equation.

The mechanism of photolysis has been found to be of great value in achieving a better understanding of the nature of the thermal decomposition of solids, since the photo- and thermal decomposition processes can frequently be equated. This is especially the case for the processes of nuclear formation and growth in solid state decompositions.

1.4 THE EFFECTS OF HIGH ENERGY RADIATION ON THE THERMAL DECOMPOSITION OF SOLIDS

(i) Pre-irradiation of the inorganic azides

Prior to 1954, very little work had been done in this field. The earliest attempt to study the effects of radiation on the thermal decomposition of solids was by Garner and Moon(119) and Muraour(120). Muraour bombarded α - lead azide and silver acetylide with high energy electrons and decomposition at room temperature, analagous to that on heating the compounds, was observed. Garner and Moon, however, after pre-irradiating barium azide at room temperature with a radium needle and finding no effect on the thermal decomposition, irradiated the barium azide during thermal decomposition. In this case a four-fold increase in the reaction rate was observed and the nuclei on the faces of crystals nearest the needle were larger than for other faces. The main effect of the emission was on the nucleus growth and not the formation.

In 1939 the effect of emission from a radium needle on the thermal decomposition of strontium azide was studied(121) in similar fashion. It was found that the induction period was reduced and a large increase in k, in the equation: $\log p = kt + c$, was observed. It was reported that the effect of the radiation was either to increase the rate of growth of the nuclei or to increase their rate of formation.

Interest in the effect of pre-irradiation on the azides was revived in an indirect way in 1954, when Bowden and Singh(122) irradiated among other compounds lithium, cadmium, silver and lead azides, in an attempt to detonate them. They were subjected to irradiation by electrons, neutrons, fission products and X-rays, but other than explosion on irradiating with an electron stream, no success was forthcoming from the investigation. It was explained that detonation in the case of bombardment with electrons was a consequence of a thermal effect due to bulk heating of the crystals. However, it was observed that the effect of irradiation on these azides, did effect their subsequent thermal decomposition. The effect of neutron pre-irradiation on lithium azide and α-lead azide was compared and found to be more marked in the case of lithium azide. Shortening of the induction periods, followed by increased reaction rates, was observed for both the azides. Other than this cursory investigation, no other results concerning the effects of pre-irradiation on the thermal decomposition were reported.

The effect of reactor radiation and high energy X-rays on the subsequent thermal decomposition of α-lead azide has been studied(124,125). Some of the difficulties resulting from the study of lead azide were indicated by Todd(126) who showed that irradiation in air by X-rays led to the formation of a basic carbonate. Groocock irradiated α-lead azide in air with X-rays from a 1 MeV generator and with pile radiation and reported no change in the characteristics of the p/t plot for the thermal decomposition of the irradiated material, for doses less than 10^4r, using both forms of radiation. However, for larger doses of X-rays and pile radiation, a reduction in the activation energies and increase in the reaction rate was observed. No definite conclusions as to the nature of the radiation damage were reached. Jach(124,125) however, reports an explanation for the effects of heavily reactor-irradiated colloidal α-lead azide. As found by Groocock, the effects of pre-irradiation enhanced the subsequent decomposition, and eliminated the induction period. The maximum rate was changed from $\alpha = 0.4$ to $\alpha = 0$, and the activation energies were reduced in agreement with Groocock's findings. The dose was given as 35 hrs. at a flux of $7 - 8 \times 10^{12}$ neutrons/ cm^2. sec.

It was stated that the initial reaction in the unirradiated salt was thought to be complex and occurred along surfaces, cracks and dislocations, and in the acceleratory period there was some indication that a surface and 3-dimensional reaction occurred simultaneously, and it was thought that some cracking of the small single crystals occurred at the beginning of the reaction. The effects of the pre-irradiation were thought to create a large number of nuclei and potential nuclei and on attaining the furnace temperature a rapid surface reaction resulted, followed by a contracting sphere penetration of the surface. The radiation damage in the crystals was considered analagous to that found in nitrate study (127-130), and it was thought that N_2 was produced at internal and external surfaces. Further radiation caused decomposition at normal lattice sites, with build up of gaseous N_2 internally, which would cause cracking of the crystals and so expose further new surface to the radiation. The vacancies and/or clusters of vacancies left behind formed sites where lead atoms accumulated, resulting in nuclei. The decrease in the activation energies was associated with a change in the excitation energy of the electrons resulting from the excessive local strain induced by a radiolysis of 20% prior to thermal decomposition.

The azide that has probably received the most amount of attention has been barium azide. Apart from the effects of ultra-violet light on the subsequent thermal decomposition and studies of the photolysis of this azide, the effects of X-rays and γ-rays on the thermal decomposition have been studied in some detail. Among the earliest work was that of Garner and Moon, mentioned previously. The same acceleration of the decomposition reaction was observed in later work with preliminary exposure to X-rays(131,132), γ-rays(3,133), and electron bombardment(30,134).

Groocock and Tompkins(30), using electron bombardment with accelerating potentials of 100 to 200 V, studied the decomposition of barium azide at room temperature and the effect of pre-irradiation on the subsequent thermal decomposition. They observed similar characteristics of the reaction, as previously found when studying the effect of ultra-violet light on the thermal decomposition(21,76,108). One significant difference was the fact that the exponent n in the equation $p = c\ (t - y)^n$, remained constant at 6, even for prolonged exposure to the electron beam. It was assumed that this was an indication that no nuclei were created during pre-irradiation and it was proposed that the primary act was the ejection of electrons from azide ions, and surface vacancies were rapidly converted to F-centres in the high excess of electrons. These were immobile as their mobility depended upon the presence of anion vacancies, and thus nucleus formation during bombardment, was not considered feasible. During the warm-up period it was considered that regeneration of azide ions and vacancies from positive holes and F-centres took place and these vacancies, (greater in number after pre-irradiation), assist in nucleus formation in the thermal process, which is thus accelerated. Osinovik(134) also reported a large increase in the maximum rate after pre-irradiation of barium azide with electrons. He also stated that there was a marked shortening of the induction period after several days exposure of the salt to γ-rays.

Erofeyev and Sviridov(131) studied the effect of pre-irradiation with X-rays on the subsequent thermal decomposition of barium azide. These authors found that there existed a considerable degree of analogy between the effects produced by different types of radiation, with X-rays producing more discernible changes in the kinetics. The Avrami-Erofeyev equation was used to analyse the p/t plots and the value of n for the irradiated salt was found to vary in a complex fashion, whereas this value was found to be between 8 and 12 for the unirradiated salt. It was found that pre-irradiation steadily decreased the duration of induction period, and radiolysis was detected after long exposures to the beam. A decrease in the total activation energy for thermal decomposition was also detected.

The effect of X-irradiation at the instant of thermal decomposition of barium azide has been studied in some detail(132,135,136). Boldyrev and Skorik(132) found that pre-irradiation at this moment produced a greater irradiation effect than pre-irradiation at ambient temperatures. It was suggested that nuclei, which were only stable above a critical size, were formed and grew by trapping of electrons followed by neutralisation of the charge by migrating vacancies. The nuclei were originally aggregates of atoms or F-centres. At room temperature it was explained that the mobility of vacancies was low and hence only a few stable nuclei were formed, while at the threshold temperature, their mobility had increased. Thus a large number of stable nuclei could form and hence a higher rate of decomposition took place. These authors later(135,136) extended their study to include silver, calcium and strontium azides. Using pellets of silver and barium azides and irradiating with X-rays of up to 400 rads/min at the threshold of decomposition, no effect on the thermal decomposition of silver azide was observed, while a pronounced enhancement of the decomposition of the pelleted barium azide was observed at 125°C. It was stated that the electron transfer from the valence band into the conduction band during the thermal decomposition of ionic salts, can be the limiting stage only when a certain restriction concerning the ratio of free electrons and effective electron traps is satisfied.

The effect of pre-irradiation with high-energy (1 MeV) γ-rays on the thermal decomposition of barium azide was investigated by Prout and Moore recently(3,133). They noted that exposure to 20 M rad. γ-irradiation coloured the salt a buff colour. It was noticed that as the γ-ray dose was increased the induction period was progressively shortened, the rate constant for the acceleratory period increased steadily and the decay reaction commenced at lower α values. A study of the same preparation as used in the pre-irradiation studies showed that the Avrami-Erofeyev equation with $n = 4$ fitted the unirradiated p/t plots, irrespective of the temperature, and this was also found to be the case with the γ-irradiated salt. Although a change in the ionic conductivity was observed on irradiating the material, the activation energy for the ionic (anionic) conductivity was unchanged. A lowering of the activation energy for the induction period on pre-irradiation was observed. It was stated that the γ-ray pre-irradiation was equivalent to an internal bombardment by electrons with varying velocities, and after irradiation the salt could contain N_2, cation and anion vacancies and F-centres, according to a suggested mechanism. It was proposed, with supporting evidence obtained by exposing the partially decomposed irradiated barium azide to water vapour and then continuing the reaction, that the irradiation effect was associated with the production of F-centres, which aggregated and collapsed during the induction period within the particle to form barium atoms. These then migrated to the surface to crystallise and form barium metal nuclei.

Prout and colleagues studied the effects of ionizing radiations on the subsequent thermal decomposition of calcium(48,137) and strontium azides(138,139). They found(48) that similar mechanisms could be applied to calcium azide pre-irradiated with X-rays and 1 MeV γ-rays. It was suggested that vacancies are formed in excess on irradiation, which aggregated at the surface, and accordingly the time taken to reach a critical concentration of calcium atoms to form a metal nucleus should be reduced, shortening the induction period. This was in fact observed. Consequently, the explanation for the increase in the rate constant for the reaction was the result of the creation of many more centres over the un-irradiated azide. The centres or nuclei were proposed to form at internal surfaces along grain boundaries and at external surfaces.

Further investigation on the effects of pre-irradiation on the thermal decomposition of strontium azide, after Maggs(121) and Sviridov(140) had made cursory investigations of the effect of pre-irradiation with a radium source and X-rays respectively, was done by Prout and Moore(138,139). They investigated the effects of pre-irradiation with X-rays and γ-rays (1 MeV) and found that similar argument could be applied to the effects of both these irradiations on the subsequent thermal decomposition. The thermal stability of the strontium azide pre-irradiated with γ-rays from ^{60}Co was found to be considerably reduced. A parallel investigation of the thermal decomposition of the unirradiated and γ-irradiated strontium azide showed that the power law with the exponent as 3 fitted the unirradiated and irradiated salt p/t analysis for doses up to 100,000 rad. For γ-ray doses greater than this, an exponential law was found to apply.

A study of the effects of water vapour at various stages of the decomposition of the irradiated salt established the role of strontium metal product on the reaction rate. For the unirradiated salt, it was proposed that the formation and 2-dimensional growth of nuclei, increasing in number linearly with time, took place at favoured sites of the crystal surfaces. It was suggested that the cores of emergent dislocations would be sites favourable to decomposition. Decomposition of adjacent azide ions resulted in the formation of nitrogen and a strontium atom, which crystallise to form a metallic speck and reaction then spreads from these nuclei. The pre-irradiated material was found not to have different values of the activation energies involved in the decomposition process. It was assumed that a high concentration of F-centres resulted from the γ-pre-irradiation and that nuclei could be expected to grow on the surfaces or in the bulk of the material. Water vapour experiments however indicate that as for barium azide(3,133) and for the unirradiated salt, nucleation and growth takes place only on the surface. This is thought to be as a result of aggregation and collapse of F-centres with the formation of strontium metal within the particles. The strontium atoms then migrate along grain boundaries to the surface where they aggregate and the reaction proceeds as before, for the unirradiated salt. The change in mathematical analysis for heavier doses was attributed to a branching chain mechanism from the nuclei along dislocations, with a mechanism similar to that described for silver oxalate(52).

The effects of radiation on sodium azide have been studied in some detail, but studies of the effect of pre-irradiation on the thermal decomposition, similar to those reported above have not been rigorously attempted. This is also the case for potassium azide. The metallic nuclei formed in both these salts are volatile at the decomposition temperature and this presents a certain amount of difficulty in investigating the decomposition mechanisms, and accordingly, the effects of pre-irradiation.

A study of the effects of γ-rays and fast and slow neutrons on sodium azide(141) by reflection measurements, showed that γ-irradiation produced three absorption bands, two of which decayed completely at room temperature, while the third was stable at temperatures up to 90°C. The stable band was attributed to colour-centres, such as those found in the alkali halides. Nitrogen should be expected to be trapped in the crystal. No identification of these colour-centres, or those attributed to the unstable bands was attempted. An absorption band resulting from fast neutron bombardment at room temperature, which was also identified in material pre-irradiated with slow neutrons, followed by heating at 90°C was attributed to the aggregation of sodium atoms, to form colloidal particles.

Heal(142) investigated the radiation damage due to X-irradiation in sodium azide, by chemical methods, to determine whether the irradiation damage was trapped electrons, or sodium metal dispersed atomically or colloidally as a principal decomposition product. His findings were that azide ions decomposed mainly to molecular nitrogen and electrons, and little if at all to nitride ions. The effect of temperature on the decomposition rate of sodium azide by X-rays between -186°C and 202°C was also studied. The rate of decomposition was reported to be proportional to the rate of energy absorption at all the temperatures studied and the effect was tentatively intepreted in terms of the formation of azide radicals, both directly by the radiation and also by thermal activation of trapped excitons and their subsequent decomposition.

Other investigations on the nature of the irradiation damage when sodium and potassium azides are subjected to X-irradiation, have been done using electron spin resonance(143) and the effects on the photoelectric properties(88), as well as on the absorption spectra(89). Using E.S.R. methods, a N_2 defect stable at room temperature was detected in X-irradiated sodium azide and by use of photoemission spectra it was shown that sodium azide, X-irradiated at 77°K gave rise to a complex spectra, whereas potassium azide yield no such spectra. No explanation was attempted to account for the photocurrent spectra recorded. Earlier investigation by Cunningham and Tompkins(89) on the effects of X-irradiation at low temperatures on sodium and potassium azides yielded some information as to the nature of the damage. By studying the optical absorption spectra of these two azides at liquid nitrogen temperatures, they identified R_1 and R_2 bands, along with the large band attributed to F-centres in potassium azide. Irradiation at -78°C resulted in bleacing of the R_2 bands and it was proposed that the resulting F-centres diffused and formed potassium atoms by donating their electrons at grain boundaries to potassium ions.

The formation of V-centres (trapped positive holes) at -170°C was reported in both azides, along with the F-centre band, and on warming to -100°C, the V-centre band disappeared completely.

Keating and Krasner(144) studied the effects of ^{60}Co γ-rays and pile irradiation on sodium azide and found that decomposition, faulting and strain resulted in the specimen. The faulting was attributed to the motion of dislocations under internal stress resulting from decomposition. Although the two irradiations produced qualitatively similar results, the inhomogeneity of the reactor irradiation was attributed as the cause of the quantitative differences. Annealing did not reduce the faulting and part of the strain. The damage was studied using X-ray diffraction techniques.

(ii) Pre-irradiation of inorganic salts other than the azides

These compounds are generally non-explosive substances although some oxalates and perchlorates and the styphinates are explosive. The azides on the other hand are generally classed as primary or secondary explosives.

The permanganates have probably received more attention than other salts of the above classification and the effects of various types of irradiation on the subsequent thermal decomposition have been studied in some detail. A similarity in the behaviour of potassium and silver permanganate on pre-irradiating the salts with various irradiations, was reported by Prout and others(145,146). They reported that pre-irradiation with reactor irradiation, protons (145 MeV), thermal neutrons and ^{60}Co γ-rays drastically altered the subsequent thermal decomposition, by shortening the length of the induction period and increasing the rate of the reaction. The shattering of the crystals at the end of the induction period was observed to have become more marked after irradiation.

The nature of the damage was considered to be the displacement of potassium ions into interstitial positions by Compton electrons which had energies in excess of the threshold energy for displacement and as a result it was considered that Frenkel-type defects were formed throughout the bulk of the crystals. On heating it was proposed that that recombination occurred with the release of Wigner energy of sufficient magnitude to rupture bonds. A centre of decomposition, a "decomposition spike", which increased in number and size through the induction period, was formed as a result. Severe internal strains caused violet shattering at the end of the induction period. Reaction proceed then by the Prout-Tompkins mechanism, which involved propagation by branching planes through the material.

A systematic study of the effects of pre-irradiation with 1.1 MeV γ-rays on the thermal decomposition of a series of permanganates was then done by Prout and colleagues. The effect of γ-irradiation on lithium, sodium, caesium(54), barium(147) and rubidium(148) permanganates was studied. Lithium and barium permanganates only showed small effects, while larger effects were observed with the other permanganates. On account of a lack of systematic behaviour, as the atomic weight of the cation increased, a mechanism was proposed(54) taking Varley's displacement mechanism(149 -151) into account and involving multiple ionization of permanganate ions. Coulombic repulsion could then occur between the positively charged permanganate ions and cations, with the formation of Frenkel defects. Since crystallographic investigation indicated that the cations have spatially greater degree of freedom, it was proposed that cationic interstitials were formed.

This theory was criticised by Boldyrev and others(152-155) when it was stated that the increased rate on irradiating the permanganates could not be reduced to displacement effects alone, but it was associated to a considerable extent with the catalytic action of radiolysis products formed by ionization effects in the lattice, in analogy with photolysis and thermal decomposition of solids. They showed(111) that exposure of silver permanganate to gamma quanta of lesser energy than is necessary to displace a cation to an interstitial position still accelerated the subsequent thermal decomposition. In a study of the effects of X-radiation on the thermal decomposition of lithium, potassium, rubidium, caesium and silver permanganates(153), the Prout-Tompkins equation, as used by Prout and colleagues for the kinetic analysis of the p/t plots, was found to hold satisfactorily. It was reported that the effect of the pre-irradiation increased with the radii of the cation. No attempt was made to identify the radiolysis products mentioned.

Huang(156) reported that distortion centres in a lattice may be observed by a reduction in the intensity of the Bragg reflections by an artificial temperature factor, by slowly varying background scatter and a diffuse scattering in the neighbourhood of Bragg directions. Senio and Tucker(157) used this analysis as well as electron density profiles drawn through the carbon atoms, when they investigated the effect of reactor radiation on boron carbide. They found displaced carbon atoms.

In a similar fashion, Prout and others attempted to detect displaced atoms in γ-irradiated silver(158) and potassium permanganates(48,159). In the study of silver permanganate no displaced atoms could be detected by the X-ray diffraction technique but Laue photographs taken at the end of the induction period showed marked asterism indicating high internal stresses. It was reported that the difficulty of resolving the oxygen atoms was due to the heavy silver atoms. X-ray diffraction studies of pre-irradiated potassium permanganate indicated that pairs of defects appeared to have been created, basing this assumption on work by Konazaki(160). However, Fourier projection and difference methods were not successful in identifying interstitial oxygen atoms after irradiation, for counter techniques must be applied, as indicated by Azaroff(161), if changes in the electron density distribution due to the lighter oxygen atoms are to be detected. The presence of oxygen in crystals of potassium permanganate after massive γ-preirradiation has subsequently been detected by mass spectrometry.

In light of these investigations(162), it is now considered that irradiation causes rupture of the Mn - O bond, with formation of interstitial oxygen. These atoms, along possibly with additional atoms due to heating and further decomposition, then diffuse through the crystals and form pockets of gas. The stresses set up by these pockets of gas then cause shattering of the crystals, exposing fresh surfaces, which are rapidly nucleated, causing acceleration of the reaction.

Protashchik and Erofeyev(62) recently investigated the effects of varying doses of γ-irradiation on 23 preparations of potassium permanganate having five degrees of surface area. The p/t plots were analysed using the Avrami-Erofeyev equation. They report the effect of irradiation on the decomposition consisted essentially of increasing the number of potential centres on which appear the initial growth centres of solid product.

The oxalates of lead, nickel, mercury(ic) and silver have been studied and the effects of pre-irradiation on the reaction kinetics examined using thermal neutrons, γ-rays and X-rays. Young(163) investigated the decomposition of uranyl oxalate trihydrate. It was found that on irradiation with thermal neutrons, the reactant became traversed with rods of decomposition product at the sites of the fission recoil tracks. It was found when analysing the p/t plots of the irradiated material, that an extra parabolic term had to be added to the function describing the acceleratory period of the unirradiated material. This was taken as proof of the topochemical nature of the reaction.

Mercuric oxalate was first examined by Prout and Tompkins(112) and the effects of ultra-violet light, cathode rays and a high density electron beam on the subsequent thermal decomposition was studied. Radiolysis was observed on irradiating with electron beam, but no effect on the rate of the reaction was detected. However, cathode rays increased the rate of the initial reaction but did not effect the decay stage. It was proposed that surface damage, with the possible production of mercurous oxalate by electron transfer, caused the higher initial rate.

In a recent examination(113) of the effects of X-rays and (1 MeV) γ-rays on the thermal decomposition, Prout and Moore found that considerable radiolysis resulted with γ-pre-irradiation, but not with X-irradiation. The effects of X-irradiation were to increase drastically the rate of the initial reaction and to reduce the duration of the reaction. It was considered that X-irradiation increased the number of potential nuclei in the oxalate particles. This was followed by formation and two-dimensional growth of reaction centres, which touch and overlap earlier, accounting for the decrease in the inflexion point.

On irradiating mercuric oxalate with γ-rays, the salt darkened and the effect on the thermal decomposition was to accelerate it, the acceleration occurring after an initial burst of gas accounting for 22% of the final gas pressure. This was not observed with the unirradiated salt. With increasing γ-ray dose, there was progressive loss of weight of the sample. It was proposed that in addition to a radiolysis product, an "irradiation product" was formed, which decomposed on heating. The decomposition mechanism was proposed to occur through a branching chain mechanism and the initial reaction occurred internally in the particles. This was thought to be the result of the formation of irradiation product along dislocations. The observed difference between the activation energies for the decay reaction of the unirradiated and irradiated salts was explained to be a consequence of the presence of radiolysis/thermal decomposition products and in addition, undecomposed reactant.

Herley and Prout(26) found that pre-irradiation of lead oxalate with γ-rays had the effect of shortening the induction period and slightly increasing the reaction rate. Their p/t plots for the unirradiated material were different from those obtained by Bircumshaw and Harris(164) and this was possibly due(45) to the latter workers using larger particles. It is suggested(45) that the p/t plots of the highly irradiated material be analysed according to a power law of the form: $\alpha = k(t + t_o)^3$.

Although silver oxalate has been studied from 1935, and many conflicting and contrasting theories proposed for the decomposition mechanism of the unirradiated and ultra-violet light irradiated material, a relatively small amount of work has been done on the salt pre-irradiated with γ-rays(60,61,118). Although the Russian workers(60,61) carried out most of their experiments at high temperatures where self-heating occurred, the general conclusion of the effects of γ-irradiation on silver oxalate were that the radiation produced nuclei throughout the crystal and affected the whole decomposition. Haynes and Young(118), studied the thermal decomposition of the salt at much lower temperatures, after pre-irradiation with reactor radiation and γ-rays.

Although different schools had proposed either an exponential law or cube law to account for the acceleratory period of the unirradiated salt, Haynes and Young found that for the fresh material they used, the exponential law gave satisfactory analysis. After irradiation with thermal neutrons, a certain degree of irreproducibility was experienced, but the power law with the exponent at 3 was found to give consistently the best fit to the acceleratory period. It was found that shattering of the particles occurred on initial heating of the irradiated material, but only after 20 mins with the unirradiated salt. The irreproducibility was attributed to the distribution of the reaction product formed during radiolysis. The effect of a light irradiation dose was to poison the branching process and the germ nuclei of the branching process were probably converted to growth nuclei which grew according to a cube law on the surfaces of the crystals. The decay mechanism was found to be the same for the decay period in both the unirradiated and irradiated salts. It was found that thermally annealing the material prior to irradiation, gave a better fit to the cube law, and no cracking of the particles was observed at all. The cracking was attributed to the occlusion of solvent.

γ-irradiation was proposed to create nuclei of low density in the bulk of the material, possibly at residual solvent occlusions not removed by annealing. As the reactor irradiation proceeded electron traps were created by γ-radiolysis on the bulk and germ nuclei were created by fast neutron damage.

The effects of pre-irradiation on the subsequent thermal decomposition of nickel oxalate, a salt which decomposes similarly to the silver salt, were done simultaneously by two independent schools(31,165). These have been the only investigations into the effects of irradiation on this oxalate. Jach and Griffel(31) studied the effects of reactor irradiation in the temperature range 253°- 360°C, while Prout and Brown(165) studied the effects of γ-irradiation on the main decomposition over the range 240° - 260°C. They also investigated the initial reaction over the range 105°- 125°C.

A study of the main acceleratory reaction by Jach and Griffel showed that this could best be described, in the cases of unirradiated and irradiated salt, by a relationship of the form: $(\alpha - \alpha_o) = a(t - t_o)^m$ where m was always found to have the value 2. The rate constant was a and α_o and t_o were constants which separated the complicated initial reaction from the main acceleratory period. This may be seen to be a modified form of the power law. On the other hand, Prout and Brown proposed a branching mechanism for the main acceleratory periods for both the unirradiated and γ-irradiated nickel oxalate. It was proposed that the Prout-Tompkins equation fitted the unirradiated p/t plot, while the modified Prout-Tompkins equation gave more satisfactory results for the analysis of the irradiated salt. These workers also found that the contracting sphere equation was applicable in analysing the decay reaction for both irradiated and unirradiated nickel oxalate, whereas Jach and Griffel proposed an exponential type of relationship for these decay reactions. The equation

$\alpha = D\left\{1 - \exp\left[k_d\ (t - t'_o)\right]\right\}$ was used.

The general effects of pre-irradiation on the subsequent thermal decomposition were found to be the same in both investigations. The induction period was shortened and the rate of the acceleratory reaction was enhanced.

Jach and Griffel propose that the activation energy for nucleation was lower than that for growth, and the effects of irradiation was to greatly enhance the number of potential nuclei but not affect the rate of growth. It was thought that reaction began at the surface of the crystallites from these potential nuclei, and growth then proceeded two dimensionally into the crystal, preferentially along preferred planes, thus explaining the exponent value of 2. On irradiation, as there were so many more potential nuclei and hence more growing nuclei after a certain time, the power law tended to reflect growth and the better fit of the analysis with m = 2 on irradiation was then understandable. The decay reaction was considered to proceed by a contracting sphere mechanism, even though an exponential analysis was applied. The exponential law fit was possibly due to an exponential particle size distribution resulting from break-up due to strains.

Prout and Brown(165), however, made a careful study of the initial reaction, prior to the acceleratory period and expressed the belief that the effects of the irradiation were to be found in the initial deceleratory region. Their analysis of the subsequent acceleratory period was in agreement with that of Daneš and Ponec(166). It was found that the activation energy of the initial reaction for the irradiated salt was ~16 k.cals./mole, whereas that for the acceleratory region was ~33 k.cals./mole, indicating the reaction in the former to be different from the main reaction. The primary act of the radiation was proposed as stripping electrons off oxalate ions with the production of nickel atoms at subgrain boundaries, dislocations and crystal imperfections and the initial reaction was the decomposition of this intermediate product. Further changes in the decomposition after γ-irradiation were assumed to be the result of the formation of anion vacancies. Reaction was proposed to spread through the subgrain boundary network and over free surfaces, and the strain at the resulting interface was responsible for the usual accelerating reaction by the Prout-Tompkins mechanism. It was stated that this acceleration differed from that of the unirradiated salt, in that the probability of branching decreased with time. The decay mechanism in both the unirradiated and irradiated salts was due to the reactant/product interface shrinking in a 3-dimensional contraction.

Of the inorganic perchlorates, ammonium perchlorate has received most attention in view, probably, of its use in rocket propellants. Although the salt has been subjected to extensive research and various mechanisms have been published concerning the kinetics of the thermal decomposition, relatively little has been done concerning the effects of pre-irradiation on the kinetics and mechanism of the subsequent thermal decomposition.

An initial study(167) using differential thermal analysis (DTA), showed that the reaction rate was enhanced, when ammonium perchlorate was pre-irradiated with X-rays. The effects of X-rays and γ-rays on the salt were then observed by Freeman, Anderson and Campisi(24), using DTA and thermogravimetric analysis (TGA) under atmospheric and reduced pressures. The investigation showed that the decomposition was a multistage one and the low temperature stages of the reaction were appreciably enhanced as a result of the irradiation dose. A similar decomposition pattern was found for ammonium perchlorate pre-irradiated with X-rays and γ-rays.

These workers favoured the "electron transfer" mechanism (as opposed to a school of thought on a "proton transfer" mechanism) as the mechanism for the thermal decomposition. It was thought that positive holes were created during irradiation and doping experiments appeared to confirm these findings. Electrical conductivity measurements(167) lent support to the electron transfer mechanism.

It was later reported(168) that E.S.R. spectra on the irradiated salt were interpreted as being the result of NH_3^+, the ammonia radical, trapped in the crystal lattice. Other workers(169,170) have also reported identification of NH_3^+ and the ClO_3 radical in irradiated ammonium perchlorate, using E.P.R. (electron paramagnetic resonance) methods.

The reaction nuclei were considered to be chains that grew by branching and to account for the higher acceleratory and maximum rates observed on irradiating the salt it was proposed that the initial network of nuclei was very extensive and so chain termination became important sooner.

Herley and Levy(67) later investigated the effects of γ-irradiation on the thermal decomposition of carefully selected crystals of ammonium perchlorate. It was observed that on irradiation the clear crystals turned milky white and the sigmoid p/t plot characteristics were retained for the irradiated salt, but the reaction rate was greatly enhanced and the induction period shortened. No cracking or shattering of the crystals during decomposition was observed. These workers found that the Avrami-Erofeyev equation with $n = 4$ described the acceleratory period for both the irradiated and unirradiated material, although a larger fit was found with the unirradiated analysis. The decay period in both cases was analysed by the Avrami-Erofeyev equation with $n = 3$. This acceleratory period analysis was in agreement with that of Galwey and Jacobs(64) for crystals of ammonium perchlorate.

These latter workers proposed the decomposition to occur principally on mosaic boundaries after initiation by defects. Assuming this mechanism to be correct, Herley and Levy stated that the effects of γ-irradiation appeared to be a shortening of the induction period and an increase in the rate of the three-dimensional growth during the acceleratory period until a coherent interface was built up on the material between the mosaic blocks. The increase in the acceleratory rate could be attributed to an increase in the number of decomposition nuclei present.

All the solids discussed above have exhibited a common tendency on pre-irradiation with high energy radiation prior to thermal decomposition. This tendency is the enhancement of the reaction rate, and this is generally explained topochemically in terms of centres of damage, formation of vacancies and clusters and aggregations of associated point defects and electron trapping. A notable exception to this trend, however, is the effect of γ-irradiation on the thermal decomposition of silver nitrite. Schneller and Flanagan(171) recently reported that the effect of an increasing pre-irradiation dose of 1.3 MeV γ-rays on the thermal decomposition was to progressively decelerate the rate of the reaction and the duration of the induction period increased. No significant loss of weight was reported during irradiation. It was further observed that irradiation in poor vacuum or at atmospheric pressure had no effect on the subsequent thermal decomposition. Furthermore, even if the NO_2 formed during decomposition was continually removed, the rate constants determined from the linear slope of the p/t plot, fell below the extrapolated Arrhenius plot, for temperatures above 60°C, thus making it imperative to study the decomposition below this temperature, while previous investigations(172) were above 72°C.

Similar behaviour has also been reported by Boldyrev and Eroshkin(173) in 1966, when they studied the effects of pre-irradiation with X-rays.

Schneller and Flanagan advanced no mechanism for the radiation effect. They suggested that the reason for the fall-off of the rate constants from the extrapolated Arrhenius plot was due to NO_2 which could not be removed quickly enough and had a poisoning effect on the reaction.

2. PREVIOUS WORK ON THE THERMAL DECOMPOSITION OF LITHIUM AZIDE

As a consequence of attempting to initiate explosion in a number of sensitive azides by irradiation with slow neutrons, Bowden and Singh(122) observed that pre-irradiation considerably accelerated the subsequent thermal decomposition of lithium azide.

No exhaustive study, however, was made on the thermal decomposition of the unirradiated or irradiated material.

3. OBJECTS OF THE RESEARCH

The effects of the subsequent thermal decomposition on irradiating the azides of barium, calcium and strontium with ultra-violet light, X-rays and γ-rays have been extensively investigated(3,20,29,48,68,109,131-133,137-140). While it was shown(21) that pre-irradiation of potassium azide with ultra-violet light had no effect on the kinetics of thermal decomposition, no other investigations concerning the effects of pre-irradiation on the kinetics of the thermal decomposition of the alkali metal azides have been reported.

The present work was undertaken in an attempt to determine whether lithium azide could be sensitised in a manner similar to that found for the azides just mentioned. As a precursor it was necessary to study the thermal decomposition of the unirradiated salt.

The objects of the research were thus twofold, namely a study of the decomposition of the unirradiated salt and the decomposition of the sensitised salt.

4. APPARATUS AND EXPERIMENTAL PROCEDURES

4.1 APPARATUS

4.1.1 The high vacuum line

The course of all the thermal decompositions was followed using a constant-volume high vacuum line. This is shown diagrammatically in FIGURE 4.1. It consists essentially of a pump section, a pressure measuring gauge and the decomposition section. The latter two were in duplicate, so that two separate decompositions could be carried out simultaneously.

The pumps comprised a two-stage Edwards "Speedivac" rotary high vacuum pump, model 2SC 20A (A), backing an Edwards "Speedivac" oil diffusion pump model 203B, (B). Pressures of better than 10^{-6} torr, as measured on a Pirani gauge, could be obtained with this system.

Two calibrated McLeod gauges, (C), were employed, one for each decomposition section. The volumes of the McLeod bulbs were 123.1 ml and 111.3 ml at 25°C.

Decompositions were carried out in the decomposition section, (D). This has been described in detail by Herley and Prout$^{(173)}$. The temperature control was ± 0.03°C in the temperature range used. Silicone oil (Midland Silicones Ltd., MS 704) was used in the outer jacket and nitrobenzene in the inner jacket. A temperature range of 130° - 210°C was obtained with these liquids. Replacing the nitrobenzene with ethyl salicylate gave a temperature range of 160° - 230°C.

In order to transfer the weighed sample for a particular decomposition from the drybox to the line, the glass section (E) was used. The sample was loaded into this in the drybox and the two 10 mm taps then closed, sealing the sample off from the atmosphere. Tap (F) was used as a point at which to evacuate the decomposition chamber by using a portable rotary high vacuum pump. This was done prior to opening the bottom 10 mm. tap to the vacuum line and pumps.

Traps (G) and (H) were surrounded with liquid nitrogen to condense out water vapour or any other condensable gases. These were positioned (i) between the rotary pump and the back line/main line and (ii) between the decomposition chambers and the McLeod gauges, to protect the former from mercury and water vapour.

The volumes of the two reaction sections of the line, i.e. with pump section isolated, were found to be (i) 1334 ml and (ii) 1557 ml at 22°C, using dry nitrogen.

4.1.2 The hot-stage microscope

A Leitz Microscope Heating Stage (Vacuum type) 1750°, with a copper-constantan thermocouple capable of measuring temperatures up to 300°C was employed. Temperatures were read directly, using an internally compensated Scalamp Thermocouple Galvanometer connected to the thermocouple.

The hot-stage is illustrated in **FIGURE** 4.2. The essential features of this are:

1. radiation screen
2. gasket
3. vacuum connection
4. heating current connection
5. base plate
6. electrode column with clamp
7. thermocouple flange
8. screw cup
9. cover with quartz window
10. clamping wedges
11. viewing hole, 1.5 mm diameter
12. tantalum sample container
13. capillary tube with thermocouple
14. double-walled vacuum tank
15. bleed valve
16. cooling water connections
17. thermocouple bush
18. base with spherical bearings and magnets

The lower diagram in FIGURE 4.2.1 illustrates the positioning of the tantalum box heating element, with lid and viewing hole. Screws 'a' are used to loosen the wedges which clamp the heating element in position.

The hot stage was mounted on a Leitz Ortholux Microscope fitted with the Ultropak incident light illuminator. Two objectives were used viz. U.0 6.5 and U.0 11, with 10X and 25X eyepieces. Coupled with a magnification factor of 1.25X, this enabled visual observations under magnifications of 81, 138, 203 and 344.

Photomicrographs were taken using a Leitz film-holder and transport mechanism, coupled to the microscope with a Leitz micro-attachment with central shutter. Magnifications of 65X and 110X were possible.

The hot stage was connected via glass tubing and a ball and socket glass junction to the pumps at point (J), (FIGURE 4.1). The volume of the hot stage and line containing the McLeod gauge was found to be 1346 ml. at 22°C, using dry nitrogen, after isolating the pump section.

4.1.3 Pelleting Apparatus

A ten-ton apex Type 341/4 hydraulic press was used to pellet ground lithium azide in an evacuated 5 mm. die (Research and Industrial Instruments Co, Model KB-0)

4.1.4 Pre-irradiation equipment

(a) γ-rays. All pre-irradiations with γ-rays were done at the Radio Isotope Section of the Food and Fruit Institute, Stellenbosch, Cape. A ^{60}Co irradiation unit was used, employing a source of 290 curies(174). For comparative purposes all irradiations for a particular series were carried out simultaneously. The dose given each batch of samples was calculated in roëntgens, from calibration curves derived by using a ferrous dosimeter.

(b) X-rays. A Phillips PW 1009 X-ray generator, using a sealed Cu tube, was employed for the X-irradiations. The tube was mounted horizontally so that the beam was directed vertically onto the sample. Unless otherwise stated, the tube was operated at an applied voltage of 10kV and a filament current of 5mA. White radiation was used throughout.

(c) Ultra-violet light. Irradiations were done using a low intensity Hanovia portable ultra-violet lamp, incorporating a medium pressure mercury straight arc tube in quartz with an effective length of 44 cm. The principal radiation output was at 3650, 3021, 2972, 2650 and 2537 Å. Irradiation with a medium pressure Hanovia U.V.S. 500 lamp of higher intensity was done on a few samples. These will be referred to as being irradiated with the high intensity source.

4.2 EXPERIMENTAL PROCEDURES

Because of the deliquescent and light sensitive nature of lithium azide, all handling was done in a dry-box under dry nitrogen and under darkroom conditions. A weak red light was used as a source of illumination.

4.2.1 Pelleting

Powdered lithium azide, ground for 5 mins. in a vibration mill (Research and Industrial Instruments Co., agate container) was weighed into the die which was then evacuated and sealed. These operations were performed in the drybox. After transfer to the press the die was evacuated for 10 mins. and a steady pressure of 1000 lbs/sq. in. applied for 15 mins. The resulting pellets were 5mm in diameter and 0.1 - 0.2mm in thickness.

Such material is referred to as pelleted lithium azide.

4.2.2 Grinding

The crushed pellets (agate mortar in drybox) were loaded into airtight agate containers with two agate balls per container. These were agitated for 30 secs. in a Grindex (Research and Industrial Instruments Co.) and the material then stored in a vacuum desiccator over P_2O_5, in the drybox in the dark. Such material is referred to as powdered lithium azide.

4.2.3 Pre-irradiations

(a) Pre-irradiations with γ-rays were carried out in blackened, evacuated and sealed Pyrex ampoules. The ampoules were baked before use, and stored in a vacuum dessicator.

The ampoules were L-shaped so that ultra-violet light from the blow-torch flame did not reach the sample when the ampoules were sealed.

(b) On account of the deliquescent nature of lithium azide, all pre-irradiations with X-rays were carried out with the sample in an air-tight glass container using a 0.016mm thick aluminium window, through which the X-ray beam passed. The sample was spread thinly over a brass plate to facilitate sample handling in the drybox where an extremely large electrostatic charge was present. All irradiations were performed under dry nitrogen. The container was placed approximately 27 cm directly below the window of the X-ray tube.

(c) Pre-irradiations with ultra-violet light were performed in the drybox in an atmosphere of dry nitrogen and with the azide in an open glass container. The external surface of the container was covered with aluminium foil to reduce electrostatic effects. The container was placed at a distance of either 6.5 or 28 cm beneath the U.V. lamp. The lamp was allowed to warm up for 15 mins. before the sample was irradiated.

For comparative purposes the pre-irradiations with γ-, X-rays and ultra-violet light (in any one series) were done simultaneously.

4.2.4 Decomposition procedure

Platinum buckets were generally employed to contain the lithium azide in the apparatus. Substitution by Pyrex buckets had no effect on the thermal decomposition, other than to cause a longer heating lag.

The buckets were cleaned in hot concentrated nitric acid and then in distilled water. They were finally heated in a bunsen burner to a red heat and allowed to cool before use. The required weight of sample was placed in the bucket, which was winched into position between the two 10mm taps in the sample-containing section (E). This was done in the drybox. The complete section was then transferred to the high vacuum line and opened to the high vacuum system. The line was pumped hard for 10 - 12 hours prior to commencing a decomposition. (Preliminary tests showed that a satisfactory vacuum with the furnace on and the sample in (E), could be maintained for at least 24 hours).

The pumps were then isolated and the bucket lowered with the winch into the decomposition chamber. A stopclock was simultaneously started and pressure readings were taken at various times throughout the course of the reaction. The liquid nitrogen traps were topped every 10 mins. during a run. The final pressure, p_a, was read after raising the reaction temperature to 220°C and maintaining it at this value for one and a half hours.

4.2.5 Water interruptions

Runs were performed where after the decomposition had proceeded to a certain stage, the decomposition was interrupted, the sample exposed to water vapour for a fixed length of time and then the run was continued. The water vapour was introduced by removing the cold trap (H) prior to evacuation and placing 2 - 3 ml degassed conductivity water in it. The water was then solidified by the liquid nitrogen.

The line was then evacuated, the pump section isolated and the run done in the normal manner to the selected point of interruption. The bucket containing the sample was then raised, allowed to cool for 5 mins. and after noting the pressure the line was evacuated to a hard vacuum (20 - 25 mins.).

The sample and the pumps were then isolated from the trap and the liquid nitrogen Dewar removed from the trap, which was then warmed to room temperature (20°C). The resulting water vapour was allowed to come into contact with the sample for the requisite time. The liquid nitrogen Dewar was replaced and the whole line evacuated for 12 hours. The decomposition was then continued after isolating the pumps.

4.2.6 Interruption followed by irradiation

Decompositions were interrupted at certain points, the sample irradiated and the run continued.

As the product of the thermal decomposition of lithium azide is extremely reactive in air, special precautions were observed when removing the sample and during irradiation.

For γ-irradiations, special Pyrex ampoules were used, these being slightly larger than the normal Pyrex bucket. The sample was loaded into the ampoule, placed in the decomposition line in the normal manner and the decomposition followed to the desired point of interruption. The sample was then raised into the glass section (E) and transferred to the drybox. The ampoule was removed under dry argon, evacuated, painted black and then sealed with a blow-torch flame. After irradiation the paint was removed, the ampoule opened under dry argon and loaded into the section (E). The procedure from this point was as described above (4.2.4).

For X-irradiations, a large amount of azide was decomposed to the desired point of interruption when the bucket was raised into the section (E), which was then transferred to the drybox. The azide and its decomposition products were loaded (under dry argon) into the glass container described above (4.2.3 (b)). After X-irradiation, the procedure of weighing out a specimen, loading it into the decomposition line, pumping and performing a run, was the usual one.

A similar procedure to that followed above for X-irradiations was adopted for ultra-violet irradiations. The large amount of azide was irradiated in the drybox in the aluminium coated glass dish used for all ultra-violet irradiations. The sample was weighed out and the run continued as before.

4.2.7 Photomicrography

Photomicrographic studies were carried out on pelleted lithium azide. The pellets were prepared as described above. The pellet was loaded into the hot-stage, onto a tantalum element shaped like a box. This was carried out in the drybox. The stage was transferred to the microscope, connected to the vacuum line via the ball and socket joint (J) and the whole apparatus evacuated for 12 hours. Pressures of better than 10^{-6} torr were obtained. During a run, for reasons given later, the pumps were not isolated. The "differential method" of plotting the course of the reaction was used.

This method involves isolating the pump section for 30 secs and allowing the pressure to buildup in the decomposition section over this time interval. The pressure was noted on the McLeod gauge and the pump section then re-connected to the line. Readings were taken in this manner during the course of the decomposition.

The light from the 60 watt Ultropak illuminator was shown to affect the thermal decomposition of the specimen and accordingly the light was only used at a low intensity and was exposed to the sample for brief periods, namely for observations and for the purpose of taking a photograph.

The film used for the photomicrographs was Agfa Isopan I.S.S. (100 A.S.A.). Two-second exposures were used. It was not possible when printing the negatives to maintain constant conditions for a series of negatives, as darkening of the background of the photomicrographs increased as the reaction progressed. To obtain good contrast, a hard printing paper and suitable developing times were employed.

FIG. 4.1

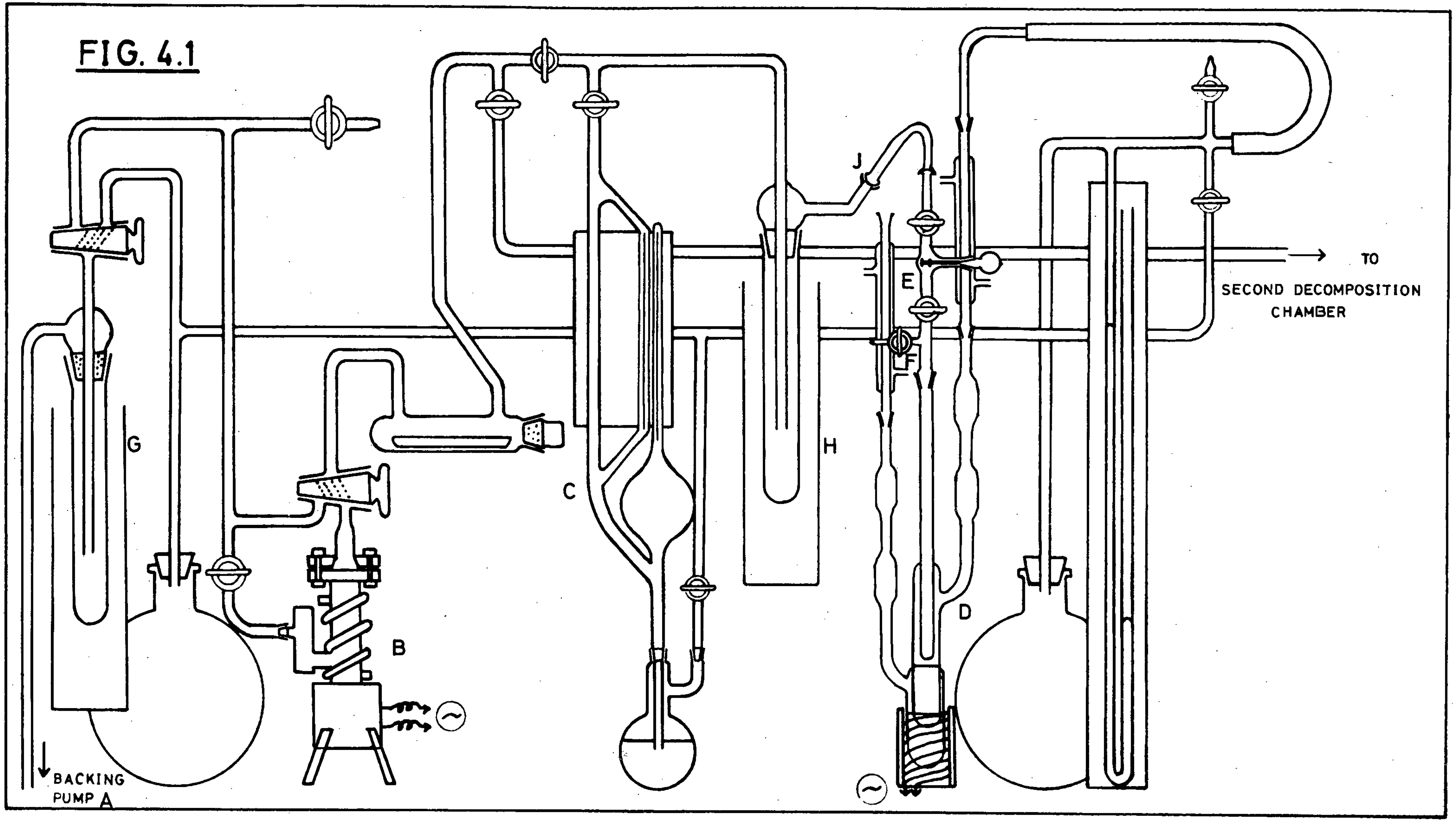

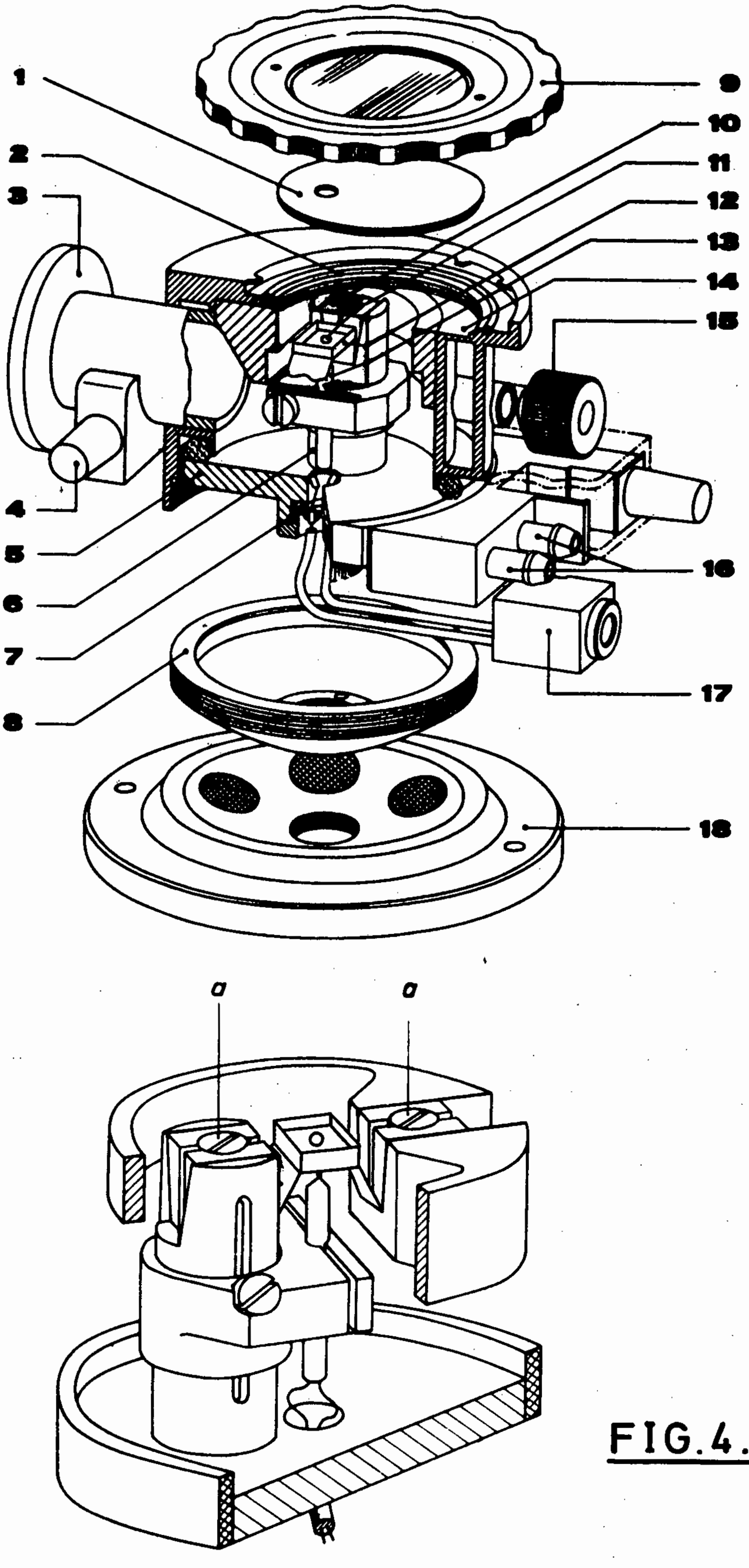

FIG.4.2.

5. THE THERMAL DECOMPOSITION OF LITHIUM AZIDE

THROUGHOUT THIS AND THE FOLLOWING SECTIONS, (6,7,8 and 9), THE RATE CONSTANTS, k , ARE NUMBERED SO THAT THOSE FOR THE ACCELERATORY PERIODS CARRY A LOWER NUMBER THAN THOSE FOR THE DECAY PERIODS. THESE CONSTANTS ARE NOT EQUIVALENT TO ANY CORRESPONDINGLY NUMBERED ONES IN THE INTRODUCTION. THE NUMBERING OF THE MATHEMATICAL EQUATIONS DOES NOT CORRESPOND TO THAT IN THE INTRODUCTION, BUT IS CONSISTENT THROUGHOUT SECTIONS REPORTING THE EXPERIMENTAL RESULTS.

Unless otherwise stated, (i) all pressures are recorded in units of 10^{-2} torr, (ii) in any one series (for comparative purposes) the results are all normalised to a common final pressure, p_f , = 160×10^{-2} torr. The final pressure actually measured before normalisation is p_a . Time is recorded in minutes. The p/t results for the decomposition runs done in this and the following sections (6,7,8 and 9) appear in the Appendix.

5.1 PREPARATION AND ANALYSIS OF ANHYDROUS LITHIUM AZIDE, LiN_3

5.1.1 Preparation

Anhydrous lithium azide $Li N_3$, was prepared by a method similar to that used by Gray and Waddington(175). The relevant chemical reaction is:

$$Li\ OH \cdot H_2O + HN_3 \rightleftharpoons Li\ N_3 + 2H_2O \quad ....(5.1)$$

Conductivity water was used in the preparation of hydrazoic acid, HN_3, and lithium azide. It was found to have a specific conductance of 2.0×10^{-6} ohms^{-1} cms^{-1}, at 20°C.

Hydrazoic acid was obtained by an ion-exchange method, using an "Analar" grade cationic resin in the H^+ form. A 10% solution of sodium azide (British Drug

Houses), NaN_3 , was passed through the bed of the resin. The resulting 3% solution of hydrazoic acid was found to contain no iron or sodium ions as impurities, by the use of "Ferron" reagant and flame photometry.

Lithium azide was obtained by neutralising a concentrated solution of lithium hydroxide with the prepared solution of hydrazoic acid and then adding a slight excess of acid. The water was removed by pumping at 40°C. Throughout this procedure the solution was maintained in an acid state, by external testing using phenolphthalein.

Lithium azide was prepared as a white powder and was dehydrated over P_2O_5 with continuous pumping for 36 hours. These operations were performed in a dark room, using a weak red light. After dehydration all further sample handling was carried out in a glass-fibre dry-box, under dry nitrogen, as the salt is extremely hygroscopic.

5.1.2 Analysis

Differential scanning calorimetry, thermogravimetry and infra-red spectra of the lithium azide dehydrated as described above, showed no traces of water of crystallisation. **FIGURE** 5.1 (a) illustrates the effect of water on the infra-red spectra of lithium azide. Freshly prepared azide and material that had been allowed to become visibly damp by standing in the atmosphere, show absorption peaks at 3360 cms^{-1}. Lithium azide, dehydrated as described above, showed no traces of water.

FIGURE 5.1 (b) shows the thermogravimetric trace of 34.4 mg of lithium azide dehydrated as described above. Decomposition was performed under a nitrogen flow of 1 litre/min. The heating rate was 2.6°C/min. After no detectable loss in weight, that could be expected during a dehydration process, the salt decomposed at 218°C. A steady final weight was obtained after the rapid reaction. A temperature-time plot illustrates the heating rate. The salt was thus considered to be free of any traces of water, within the limits of experimental conditions.

Chemical analysis of the dehydrated lithium azide by Dr. F. Pascher, Bonn, Germany, showed the salt to be better than 99.6% LiN_3, by determination of Li as sulphate and N_2 by combustion.

5.2 REPRODUCIBILITY

Approximately 4.5 - 5.5 mg of lithium azide were used in each run. Initially the unground azide was used and it was found that the decomposition was extremely erratic and irreproducible. Some runs showed no apparent decomposition. Typical p/t curves obtained using the same material at 210°C may be seen in **FIGURE** 5.2, with the results given in **TABLE** 5.1. These results are not normalised.

The material was then ground in a vibration mill for 10 mins. using an air-tight agate container and agate balls. This gave variable results as before. The ground material was annealed "in situ" at 130°C for one hour and then pumped for a further two hours before decomposition. The two runs done showed large discrepancy, as illustrated in **FIGURE** 5.3, with the results in **TABLE** 5.2. Pressures are not normalised.

Unground lithium azide was then pressed into pellets (5 mm diameter, ± 5.0 mg) using an evacuable die. The die was evacuated for 10 mins and then a steady pressure of 1000 lbs/sq.in. applied for 15 mins. Reproducibility improved but was still not satisfactory. Results of two runs at 195°C and two runs at 210°C are given in **TABLE** 5.3 and are seen graphically in **FIGURE** 5.4. The induction period was 29 and 31 mins. at 195°C and 24 and 17 mins. at 210°C. Rate constants k_1 and k_3 (equations 5.2 and 5.3 [see 5.3.2]) for the acceleratory and decay periods respectively, were as follows:

(i) Acceleratory period: (a) 195°C : 1.99×10^{-2}, 1.91×10^{-2} min^{-1}

(b) 210°C : 2.21×10^{-2}, 2.17×10^{-2} min^{-1} respectively

(ii) Decay period : (a) 195°C : 1.26×10^{-2}, 1.23×10^{-2} min^{-1},

(b) 210°C : 1.68×10^{-2}, 1.77×10^{-2} min^{-1} respectively

Ground lithium azide (10 mins vibration mill) was pelleted in a similar manner to the above, when the reproducibility of the thermal decomposition was found to be of a high order. This procedure was adopted throughout the course of this research. The azide used was always less than four weeks old, during which time no change in the reproducibility was detectable. Results of four consecutive runs at 210°C are presented in **TABLE** 5.4 and **FIGURE** 5.5. The induction period was found to be 25, 24, 25 and 25 mins respectively. Rate constants k_1 and k_3 (equation 5.2 and 5.3) for the acceleratory and decay periods respectively, were as follows:

(i) Acceleratory period: 3.36×10^{-2}; 3.20×10^{-2}, 3.14×10^{-2}, 3.09×10^{-2} min^{-1} respectively

(ii) Decay period: 2.82×10^{-2}; 2.72×10^{-2}; 2.79×10^{-2}; 2.72×10^{-2} min^{-1} respectively.

Since pelleting of the material gave the only reproducible results, it was decided to investigate the effect of varying the pelleting pressure to determine whether a critical pressure existed. Duplicate pellets were made using pressures of 1000, 750, 500 and 250 lbs/sq.in. The maximum pressure that could be applied to the 5mm die used was 1000 lbs/sq.in. In the subsequent thermal decomposition of the pellets the reproducibility became poorer with decreasing pelleting pressure. The results appear in **TABLE** 5.5 and are graphically illustrated in **FIGURE** 5.6. The reaction temperature was 195°C.

Having achieved reproducible thermal decomposition with pellets, it was considered advantageous to obtain similar reproducibility with lithium azide powder, so that this study could be compared with previous research on the decomposition of the azides(3,133,138,139,176).

Lithium azide pelleted as above was ground in a Grindex, with agate containers and balls, for 30 secs. The results of three consecutive runs at 195°C are given in **TABLE** 5.6 and depicted graphically in **FIGURE** 5.7. The reproducibility was of a high order. The curves are sigmoid with a well defined induction period. The latter was found to be 33, 33 and 35 mins. respectively. Rate constants k_1 and k_3 (equations 5.2 and 5.3) for the acceleratory and decay periods respectively, were as follows:

(i) Acceleratory period: 1.05×10^{-2}; 0.96×10^{-2}; 1.06×10^{-2} min^{-1} respectively

(ii) Decay period: 0.94×10^{-2}; 0.91×10^{-2}; 0.97×10^{-2} min^{-1} respectively

Measurement of the particle size of the lithium azide powder as determined microscopically was found on the average to be 5.0 microns.

The effect of several pelleting and grinding operations on lithium azide was examined, to determine if a limiting effect had been achieved when the material was pelleted and ground as described above. The results for ground material taken through three consecutive pelleting and grinding stages are given in **TABLE** 5.7 and **FIGURE** 5.8 for a reaction temperature of 190°C. The pellets were ground for 10 secs in the Grindex after each pelleting stage. It appears from the results that the limiting stage has been reached with the single pelleting and grinding operation. The slight discrepancy in the curves can be attributed to variation due to grinding (see below).

An examination of the effect of varying the grinding time in the Grindex, after the initial grinding (10 mins vibration mill) and pelleting, was made.

Reproducibility of material ground for 3 mins. was of a high order and the p/t results for two runs are presented in **TABLE** 5.8 for a reaction temperature of 190°C. Runs were done at 185°C using material that had been ground in the Grindex for 10 secs, 30 secs, 3 mins and 10 mins respectively. These results appear in **TABLE** 5.9 and **FIGURE** 5.9. It is seen that the induction period increases, being found to be 55, 56, 75 and 94 mins respectively and the inflexion point decreases as $\alpha = 0.58$, 0.54, 0.44 and 0.37 (estim.) as the particle size decreases with increasing grinding time. It is observed that the p/t curve is drastically changed for lithium azide ground for 10 mins. Analysis of the acceleratory period shows that the maximum rate (obtained from the slope of the p/t plot) decreased with grinding time (and hence decreasing particle size) as follows:

Maximum rate: 2.20×10^{-2}; 1.84×10^{-2}; 2.20×10^{-2}; 7.04×10^{-2} mm/min. for the 10 secs, 30 secs, 3 mins and 10 mins grinding times respectively.

Mathematical analysis of the 3 mins run however is seen to give a poor fit to the Avrami-Erofeyev equation (see 5.3.2) with $n = 3$. With $n = 2$ a good fit is obtained, for $0.5 < \alpha < 0.58$. Thus it appears that excessive grinding with the Grindex, viz. 3 mins, damages and/or reduces the particles to such a size that a change of the equation fitting the p/t plot occurs. This was shown to be the case with two different preparations, ground separately.

Insufficient grinding of the pelleted lithium azide resulted in non-sigmoid p/t curves. This is illustrated in **FIGURE** 5.10 and the results appear in **TABLE** 5.10. The reaction temperature was 185°C. The samples were of the same preparation but were ground in two portions which were then used. The vibration mill (10 mins) was used for one portion. The action of this mill is very mild compared to that of the Grindex's. The other portion was ground using the

Grindex (3 mins). Optical examination of both samples showed that large lumps of unground pellet were present in the sample ground in the vibration mill. The flat section of the p/t curve is thus attributed to this inefficient grinding. (This in turn appears to stem from the quantity of material placed in the agate container. Larger amounts require longer grinding times for the same effect as when grinding a small amount. In light of this, the figures quoted for the duration the lithium azide was ground are arbitrary, as varying amounts of material were ground each time).

From the above results it is seen that reproducibility was obtained for lithium azide in both the powder and pellet forms. In the experiments performed above it was assumed that moisture and light would affect the decomposition and the azide was always handled in a dry-box under dry nitrogen and in the dark (red light). These assumptions were checked by exposing the pelleted material to sunlight prior to decomposition. The results of the thermal decomposition of such a pellet, composed to a pellet handled in dark conditions, are given in **FIGURE** 5.11 and **TABLE** 5.11. The reaction temperature was 190°**C**. It is seen that the induction period was shortened and the p/t curve was no longer sigmoid.

In an attempt to obviate the use of the drybox, lithium azide, pelleted and powder, was handled in the atmosphere until it became visibly moist, before thermal decomposition. The final pressure in the decomposition was lower than that for the same weight of material handled under dry conditions. For this reason, all further sample handling was performed under dry conditions. However, comparison of <u>normalised</u> runs at 210°**C** of pelleted lithium azide and powdered lithium azide at 195°**C**, shows no effect. These results are given in **TABLE** 5.12.

The effect of using an inert gas, dry argon, instead of dry nitrogen, in the drybox, was examined. This had no effect on the reproducibility or reaction rate of pelleted or powdered lithium azide. Similarly, no effect on the thermal decomposition of powdered azide was found, when dry air was allowed to come into contact with a sample in the decomposition line, prior to decomposition. After $3\frac{1}{2}$ hours, the line was pumped for 18 mins and the run done. The p/t results of this run and a blank run, (viz. material handled under dry nitrogen and the vacuum line and sample pumped for more than 12 hours), are presented in TABLE 5.13.

Thermal annealing in vacuum of the lithium azide was found to have no effect on the reproducibility or reaction rate. The thermal decomposition of powdered lithium azide annealed at 130°C for 1 hour, followed by ten hours pumping is shown graphically in **FIGURE** 5.12 and the results given in TABLE 5.14. It is seen that on comparing the p/t curve with a control run, there is no detectable effect.

The high vacuum apparatus was generally evacuated for more than 12 hours prior to a run and not longer than about 15 hours.

5.3 RESULTS

UNLESS OTHERWISE STATED, ALL MATERIAL USED IN THIS SECTION AND THE FOLLOWING SECTIONS (6,7,8,9) OF THE RESEARCH WILL BE TERMED (i) PELLETED LITHIUM AZIDE AND (ii) LITHIUM AZIDE POWDER. THE FORMER SHALL BE TAKEN AS GROUND LITHIUM AZIDE (VIBRATION MILL, 10 MINS) PELLETED UNDER A PRESSURE OF 1000 LBS/SQ.IN IN A 5mm DIE. THE LATTER SHALL BE TAKEN AS GROUND (GRINDEX, 30 SECS) PELLETED LITHIUM AZIDE, WHERE THE PELLETS WERE PREPARED AS FOR (i) ABOVE.

5.3.1 The effect of varying the temperature of decomposition

The mathematical equations applied and the relative constants determined in this section are discussed below, (5.3.2, 5.3.3).

In order to obtain the critical increments of the various chemical process(es) occurring in the thermal decomposition of both pelleted and powdered lithium azide, two methods were used, viz (1) Individual runs and (2) Split run methods.

(1) Individual runs

Separate decompositions carried to completion at a fixed temperature were done and are described as "individual runs".

(i) Pelleted lithium azide. Approximately 4.5 - 5.0 mg pellets were used in each run. The temperature range was 195° - 220°C. The p/t results are presented in TABLE 5.15. Rate constants were determined over the temperature range used and the acceleratory and decay period rate constants k_1 and k_3 (equations 5.2 and 5.3) and the duration of the induction periods (mins) are given in the table following 5.3.2. (The induction period was taken as the time for the decomposition to attain $\alpha = 0.006$). The effect of varying the temperature of decomposition is graphically illustrated in FIGURE 5.13.

(ii) Lithium azide powder. Approximately 5.4mg of specimen was used for each run. The temperature range was 185° - 205°C. The rate constants k_1 and k_3 (equations 5.2 and 5.3) were determined at each temperature and the duration of the induction period (mins) measured. A repeat series of the effect of varying the temperature of decomposition on the induction period was done using a different preparation. Only the pressure time readings to 4.0×10^{-2} torr and the p_a were noted in each run. The results of the varying temperature series are given in TABLE 5.16 and the rate constants and induction periods (mins) are presented in the table following 5.3.2 below.

(2) Split runs

The activation energy for the acceleratory and decay periods was determined using this method with pelleted lithium azide, while only the activation energy for the acceleratory period was determined for powdered lithium azide. The decomposition was allowed to proceed at the lowest temperature at which the first rate constant was to be calculated. After an appropriate time the run was interrupted by raising the bucket and allowing it to cool, while the furnace temperature was adjusted to the next higher temperature. It was shown (see below) that interruption of a run had no effect on the decomposition other than a small time lag due to the bucket and contents attaining thermal equilibrium. The run was then continued. Five or six rate constants were found in this manner for an acceleratory or decay period from a single decomposition. Fresh samples were used to obtain the rate constants for decay periods.

(i) Pelleted lithium azide. Approximately 4.5 - 5.5 mg single pellets were used for each activation energy determination. The results for the acceleratory period are given in TABLE 5.17 and the rate constants k_1 (equation 5.2) are listed in the table following 5.3.2 below. The temperature range was 160° - 190°C. The decay period results for a temperature range of 165° - 190°C also appear in TABLE 5.17. The rate constants k_3 (equation 5.3) also appear in the table below. A decomposition was taken to completion at a fixed temperature (195°C) to check the applicability of the mathematical analysis. The results of this run appear in TABLE 5.17.

(ii) Lithium azide powder. The acceleratory period was followed using the split run technique. 5.0mg of lithium azide was decomposed over the temperature range 165° - 185°C. The results of the decomposition, together with the results of an uninterrupted decomposition of the same material at 190°C to check the applicability of the mathematical analysis, are presented in TABLE 5.18. The rate constants k_1 (equation 5.2) appear in the table following 5.3.2 below.

5.3.2 Mathematical analysis of the results

(i) Pelleted lithium azide. A typical pressure-time curve showing the thermal decomposition of pelleted lithium azide at 215°C and the mathematical analysis appears in FIGURE 5.14. The p/t results appear in TABLE 5.15. The marked features are (i) a well defined induction period with no evolution of gas followed by (ii) a period of acceleration and (iii) a decay period. The inflexion point is at $\alpha = 0.58$ ($\alpha = {}^{p}/p_{f}$).

Since no gas was evolved during the induction period no mathematical analysis of this part of the decomposition was possible. For the determination of activation energies the lengths of the induction periods (mins) were used.

The acceleratory period was well described by the Avrami-Erofeyev equation with $n = 3$, i.e.

$$\left[- \log\left(1 - {}^{p}/p_{f}\right)\right]^{1/3} \quad = \quad k_1 t + c \quad \dots\dots\dots\dots\dots \quad (5.2)$$

The fit covered the whole of the acceleratory period and was found to be over the range $0.02 < \alpha < 0.58$. The plot of $\left[-\log(1 - {}^{p}/p_{f})\right]^{1/3}$ versus t (time in mins) is shown in FIGURE 5.14. In the same figure, the plot of the power law in the form $p^{1/3}$ versus t shows the extent of fit. The fit is not good, covering the range $0.02 < \alpha < 0.25$.

The decay reaction was well defined by the contracting sphere formula i.e.

$$1 - \left(1 - {}^{p}/p_{f}\right)^{1/3} \quad = \quad k_3 t \quad \dots\dots\dots\dots\dots\dots \quad (5.3)$$

The plot of $(1 - {}^{p}/p_{f})^{1/3}$ versus t is shown in FIGURE 5.14 and is seen to hold over the range $0.50 < \alpha < 0.95$.

The Avrami-Erofeyev equation with $n = 3$ and the contracting sphere equation were found to be applicable in the mathematical analysis of the acceleratory and decay periods respectively over the temperature range studied. The temperature range was 160° - 220°C.

(ii) <u>Lithium azide powder</u>. A typical pressure-time curve showing the thermal decomposition of powdered lithium azide at 185°C and the mathematical analysis is shown in FIGURE 5.15 and the results appear in TABLE 5.16.

The p/t plot is characterised by the same three features as found for the pelleted material (induction, acceleratory and decay periods. The inflexion point is at $\alpha = 0.52$.

As for the pelleted material, the lengths of the induction periods (mins) were used to determine an activation energy.

The acceleratory period was described by the Avrami-Erofeyev equation with $n = 3$ as found above. The extent of fit covered the acceleratory period from $0.09 < \alpha < 0.51$. The power law with $n = 3$ was found to hold over the same range as found above for pelleted lithium azide.

The decay period was fitted by the contracting sphere equation as was found above. The fit was over the range $0.49 < \alpha < 0.83$.

The plots of $\left[-\log(1 - {}^{p}/p_f)\right]^{1/3}$ and $(1 - {}^{p}/p_f)^{1/3}$ versus t (mins) are to be found in FIGURE 5.15.

The Avrami-Erofeyev with $n = 3$ and the contracting sphere equations were found to be applicable in the mathematical analysis of lithium azide powder over the temperature range studied. The temperature range was 165^{o} - 205^{o}C.

Equations 5.2 and 5.3 were found to fit the acceleratory and decay periods respectively irrespective of the method used to determine the rate constants (i.e. individual or split runs).

Specimen	Individual or Split runs	Temp. ^{o}C	Induction Period (mins)	k_1 (mins^{-1})	k_3 (mins^{-1})
Pellet	Indiv.	195.0	48	5.43×10^{-3}	4.18×10^{-3}
		200.0	37	6.91×10^{-3}	5.89×10^{-3}
		205.0	25	1.08×10^{-2}	7.30×10^{-3}
		210.0	19	1.26×10^{-2}	9.35×10^{-3}
		215.0	17	1.95×10^{-2}	1.61×10^{-2}
		220.0	12	2.86×10^{-2}	2.05×10^{-2}
Pellet	Split	160.0		1.01×10^{-3}	
		165.0		1.41×10^{-3}	
		170.0		2.78×10^{-3}	
		175.0		3.42×10^{-3}	
		180.0		5.10×10^{-3}	
		185.0		7.52×10^{-3}	
		190.0		8.85×10^{-3}	
Pellet	Split	166.0			7.41×10^{-4}
		170.0			9.03×10^{-4}
		175.0			1.22×10^{-3}
		180.0			2.49×10^{-3}
		185.0			3.69×10^{-3}
		190.0			3.77×10^{-3}
Powder	Indiv.	185.0	39	8.91×10^{-3}	6.94×10^{-3}
		190.0	30	1.12×10^{-2}	1.04×10^{-2}
		195.0	23	1.59×10^{-2}	1.19×10^{-2}
		200.0	18	2.82×10^{-2}	2.02×10^{-2}
		205.0	14	3.29×10^{-2}	2.21×10^{-2}

Specimen	Individual or Split runs	Temp. ^{o}C	Induction Period (mins)	k_1 (mins^{-1})	k_3 (mins^{-1})
Powder	Indiv.	180.0	64		
		185.0	52		
		190.0	38		
		195.0	29		
		200.0	23		
Powder	Split	165.0		1.97×10^{-3}	
		171.0		3.54×10^{-3}	
		175.0		4.94×10^{-3}	
		181.0		6.34×10^{-3}	
		186.0		8.20×10^{-3}	

5.3.3 Evaluation of the activation energies

The critical increment for the chemical process(es) occurring in the thermal decomposition of pelleted and powdered lithium azide was obtained by applying the Arrhenius equation.

For the determination of the activation energy for an induction period, the logarithms of the lengths of the induction periods were plotted against $1/T^{o}K$. T is the temperature of the decomposition in ^{o}K. The plot was a straight line from the slope of which an activation energy was calculated.

For the determination of the activation energies for the acceleratory and decay periods, log k_1 and log k_3 respectively were plotted against $1/T$. These plots were straight lines and were treated as above to obtain the activation energies. It is estimated that the error involved in the determination of the activation energies throughout the course of this research is ± 2 k.cals./mole.

The values of the activation energies calculated for the induction, acceleratory and decay periods for the thermal decomposition of pelleted and powdered lithium azide are tabulated below. The plots of log I.P., log k_1 and log k_3 against $1/T^oK$ for pelleted lithium azide using individual and split methods are to be found in FIGURES 5.16 and 5.17 respectively. FIGURE 5.18 shows the plots of log I.P. (duplicate), log k_1 and log k_3 against $1/T^oK$ for powdered lithium azide using the individual runs method. FIGURE 5.19 shows the plot of log k_1 against $1/T^oK$ for the latter azide, using the split run method.

ACTIVATION ENERGIES

Specimen	Individual or Split runs	Induction period Activation energy k.cals./mole	Acceleratory period Activation energy k.cals./mole	Decay period Activation energy k.cals./mole
Pellet	Individual	24	29	29
	Split		29	30
Powder	Individual	21 22	28	29
	Split		28	

5.3.4 Effect of interrupting a thermal decomposition

The effect of interrupting a decomposition by raising the bucket containing the sample out of the decomposition chamber was examined. The bucket was allowed to cool to ambient temperature and then lowered into the decomposition chamber after 15 mins. and the run continued as before at the same temperature.

(i) Pelleted lithium azide. Interruptions were done at the end of the induction period ($\alpha = 0.006$), at $\alpha = 0.06$ and $\alpha = 0.65$, at 190°C. The interruptions at $\alpha = 0.06$ and $\alpha = 0.65$ were in the acceleratory and decay periods. Apart from a small time lag (5-8 mins) during which the bucket and contents reached thermal equilibrium, there was no effect i.e. quenching during a decomposition produced no effect.

(ii) Powdered lithium azide. Interruptions were done at the end of the induction period, at $\alpha = 0.07$ and $\alpha = 0.41$ at 195°C. The interruptions were in the acceleratory period and at the inflexion point respectively. As found above, apart from a small time lag (3-5mins) there was no effect on resuming the decomposition.

The results for the pelleted and powdered lithium azide appear in TABLE 5.19.

5.3.5 The effect of admitting water vapour onto the salt in an interrupted decomposition

These runs are termed "water interruptions". The general technique followed has been described in 4.2.5. The partially decomposed sample of lithium azide was exposed to water vapour (17.0 torr pressure) for certain periods of time, after which the liquid nitrogen trap was replaced and the line pumped for 12 hours. The pump section was then isolated and the run continued at the same temperature as before.

All the results presented in this section (5.3.5) are not normalised to illustrate the effect of the water interruptions on the p_a . The azide, both pelleted and powdered, was exposed to water vapour for 30 secs. Several runs were done, however, using exposure times of 5 mins and these will be treated after each series receiving 30 secs. The method of determining the percentage decompositions is presented in 5.3.6.

(i) Pelleted lithium azide

30 secs exposure to water vapour. The effect of 30 secs exposure to water vapour at $\alpha = 0.03$, 0.13, 0.23 and 0.70 on the same pellet (5.6mg) of lithium azide at 190°C, was investigated. A blank run with interruptions, but no exposure to water vapour, was also done. For comparitive purposes the same weight of azide was used for the blank run.

It was found that the final pressure was reduced due to the water interruptions and the reaction rates on continuing the decomposition after an interruption were observed to be decreased. There was virtually no further decomposition after interruption in the decay period. The time taken for the reaction to resume after water interruptions, (12-14 mins), was slightly longer than for the blank run (3-7mins). These results are tabulated in TABLE 5.20 and the table below and the runs illustrated in FIGURE 5.20.

(b) <u>5 mins exposure to water vapour</u>. To investigate the presence of metallic nuclei at t = 0, pelleted lithium azide was exposed to water vapour for 5 mins to ensure the reaction between nuclei and the water vapour, as 30 secs exposures above did not appear to have an effect on the subsequent thermal decomposition.

5.6mg pellets were used for a blank uninterrupted run and a run exposed to 5 mins water vapour at t = 0 (i.e. prior to decomposition). The reaction temperature was 190°C. It was found that the only effect the water exposure had on the reaction, was to decrease the final pressure by approximately 30%. There was no significant change of the reaction rate or the length of the induction period, when these values were compared to those for the blank uninterrupted run.

Since 30 secs water interruption just after the induction period, in (i) (a) above, did not return the reaction to zero time, it was decided to observe the effect of 5 mins exposure to water vapour at this point. The reaction temperature was 190°C. On recommencing the reaction an induction period of 21 mins resulted, which was considerably shorter than that for the blank run (56 mins). A second interruption at the end of this induction period produced an induction period of 17 mins. A third interruption at this point produced a third induction period of 14 mins. At this stage the reaction was allowed to go to completion and it was seen that the percentage decomposition was 50% lower than that for the blank, as was the acceleratory period rate constant k_1 (equation 5.2).

The above results are tabulated in TABLE 5.20 and the table below.

(ii) Lithium azide powder

(a) 30 secs exposure to water vapour. Approximately 5.0mg of the azide were used for a run. Water interruptions were done at t = 0, 0.5 I.P., end of the I.P., $\alpha = 0.06$, inflexion point and $\alpha = 0.75$. A blank run with no interruptions was also done. The decomposition temperature was 195°C.

There was no change in the length of the induction period for the t = 0 interruption and the acceleratory period rate constant was not affected but a lowering of the percentage decomposition was observed. For interruptions at 0.5 I.P., end I.P. and $\alpha = 0.06$, new induction periods of equal length to the induction period for the uninterrupted run, were formed on resuming the decomposition. The rate constants k_1, for the end of the I.P. and the $\alpha = 0.06$ interruptions were lowered.

Interruption at the inflexion point and beyond virtually destroyed further decomposition.

Since interruption at the end of the induction period resulted in a new induction period, equal in duration to that of the blank run, the run was interrupted at the end of the second induction period and exposed to 30 secs water vapour. The run was allowed to continue and the process repeated, with the formation of an induction period after each interruption. After the fifth water interruption, the run was allowed to go to completion. It was observed that the acceleratory rate constant was lowered compared to that of the blank uninterrupted run and the percentage decomposition was only 46%.

It was observed that the final pressures were lower than that of the blank run in all the water interrupted runs.

The p/t values for these results appear in TABLE 5.20 and the table below contains the values for the rate constants k_1, lengths of the induction periods and percentage decomposition values. The results are graphically illustrated in FIGURE 5.21.

(b) 5 mins exposure to water vapour. Since 30 secs exposure to water vapour at t = 0 had no effect on the subsequent thermal decomposition, it was thought that 5 mins exposure at t=0 may have an effect.

Accordingly, two runs were done, one a blank run and the other was interrupted for 5 mins at t=0. The reaction temperature was 190°C. It was found, as above, that no effect on the reaction was observed other than a lowering of the percentage decomposition value. This was seen to have been lowered by 66%, as opposed to 30% for 30 secs exposure to water vapour. These results appear in TABLE 5.20 and the table below.

In all the above cases, for pelleted and powdered lithium azide, it was observed that the p_a was lowered after exposure to water vapour. Heating the end product(s) of the reaction to approximately 400°C for 15-25 mins in vacuo enabled recovery of a percentage (approx. 35-45%) of the "lost" gas.

Specimen	Exposure (mins)	Point of Interruption (α)	Acceleratory rate constant k_1 ($mins^{-1}$)	Induction period after interruption (mins)	Percentage Decomposition
Pellet	Blank	0.0	-	55	
"	"	0.01	-	7	
"	"	0.06	-	5	
"	"	0.65	-	3	102
"	0.5	0.0	-	58	
"	"	0.03	-	13	
"	"	0.13	-	12	
"	"	0.23	-	14	

Pellet	0.5	0.70	-	-	44
Pellet	Blank	0.0	1.22×10^{-2}	56	98
"	5	t=0	1.25×10^{-2}	54	68
"	"	Successive	-	21	
			-	17	
			0.71×10^{-2}	14	48
Powder	Blank	0.0	1.06×10^{-2}	35	96
"	0.5	t=0	1.05×10^{-2}	34	65
"	"	0.5 I.P.	1.08×10^{-2}	31	56
"	"	End I.P.	0.88×10^{-2}	39	73
"	"	0.06	0.53×10^{-2}	29	66
"	"	Inf. Pt.	No reaction	-	55
"	"	0.75	No reaction	-	78
"	"	Successive	-	42	
			-	34	
			-	34	
			-	40	
			0.70×10^{-2}	40	46
Powder	Blank	0.0	0.87×10^{-2}	43	93
"	5	t=0	0.88×10^{-2}	45	27

5.3.6 Percentage decomposition

This was calculated assuming the overall reaction was represented by:

$$2LiN_3 \rightarrow 2Li + 3N_2 \quad \ldots\ldots\ldots\ldots\ldots\ldots \quad (5.4)$$

In calculating the percentage decomposition, the volume of the particular decomposition section used was taken into account and ambient temperature was taken at 292°K. While performing the experiments, three lines were used having volumes 1.132, 1.334 and 1.557 litres.

It was observed that the error involved in weighing out the sample of lithium azide in the dry-box was considerable ($\pm$ 0.2 - 0.4mg in 5.0mg). This was the result of working in a restricted volume with the chemical balance in the drybox. Variations in the internal pressure of the drybox atmosphere (by movement of hands in the gloves) resulted in changes of the scale reading. The percentage decomposition figures can accordingly be taken as a rough estimate only.

The percentage decomposition of the decomposition runs reported above in the varying temperature series are as follows (decomposition temperature in brackets):

(i) Pelleted lithium azide: 70 (195°); 55 (200°); 100 (205°);
74 (210°); 96 (215°); 100 (220°); MEAN: 79%

(ii) Powdered lithium azide: 87 (185°); 83 (190°); 102 (195°);
82 (200°); 91 (205°); MEAN: 89%.

5.3.7 The effect of ageing on the thermal decomposition

Lithium azide powder was sealed in a baked evacuated Pyrex ampoule. This was blackened and stored for six months in a vacuum desiccator over P_2O_5. After this period of time the ampoule was opened and three runs done in the normal manner at 195°C. 5.0 - 6.0mg samples were used. Triplicate runs were done on the "fresh" and"aged" material. The p/t results appear in TABLE 5.21 and the rate constants k_1 (equation 5.2) for the normalised p/t plots, lengths of the induction periods and the percentage decomposition appear in the table below. The normalised pressure-time curves for "fresh" and "aged" samples are illustrated in FIGURE 5.22.

Specimen	Induction period (mins)	Rate constant k_1 (mins^{-1})	Percentage decomposition
Fresh	33	1.05×10^{-2}	123
"	33	0.96×10^{-2}	104
"	35	1.06×10^{-2}	112
Aged	35	1.02×10^{-2}	84

Aged	35	0.89×10^{-2}	72
"	34	0.95×10^{-2}	81

5.3.8 The effect of using Pyrex buckets for the decomposition

Normally a platinum bucket was used in the decomposition runs. For some runs, it was necessary to use a Pyrex container. Two runs were done using powdered lithium azide in Pyrex and platinum buckets at 195°C.

The resulting curves show no effect when different buckets are used. These results are presented in TABLE 5.22.

5.3.9 The effect of mixing lithium azide with the solid end product

The mixing was done by decomposing a sample of lithium azide and adding to it some fresh sample, under dry-box conditions.

(i) Pelleted lithium azide. Approximately 2mg of product was mixed with 5.3mg lithium azide powder and the mixture was then pelleted in the usual manner. A blank pellet, i.e. the same powdered lithium azide with no end product, was also used. The specimens were decomposed at 195°C and the results appear in TABLE 5.23 and FIGURE 5.23. It is seen that the induction period is reduced from 29 mins to 19 mins and the rate constants k_1 for the decompositions are 2.00×10^{-2} and 1.62×10^{-2} mins^{-1}, for the blank and the specimen with end product, respectively.

(ii) Lithium azide powder. A mixture of 5.3mg powdered salt and 1.9mg product were decomposed at 195°C. The induction periods for the "blank" and mixed specimens are 25 mins and 23 mins and the rate constants k_1 for the decompositions are 2.72×10^{-2} and 2.16×10^{-2} mins^{-1} respectively.

These results also appear in TABLE 5.23 and in FIGURE 5.23. From the results it is observed that the improved physical contact achieved through pelleting had a more pronounced effect on the subsequent chemical reaction, in that the induction period was reduced by 34% in the pelleted material and only 8% in the powdered azide. There is also a small decrease of the rate constants in both cases.

5.3.10 The effect of pelleting lithium azide powder

The effect of pelleting lithium azide was studied. It was found that no significant change in the rate of the subsequent thermal decomposition resulted, but that the induction period was increased slightly from 25 mins to 29 mins. The reaction temperature was 195°C.

The results for the p/t plots appear in the previous table (TABLE 5.23, Runs 2 and 4).

5.3.11 Visual observations

(i) After a water interruption when the water vapour was in contact with the undecomposed salt for 5 mins, the water in the trap (H) was refrozen, the vacuum broken and the trap removed. After melting the ice the liquid was tested with $FeCl_3$ (10% solution) but no positive results indicating the presence of the N_3^- ion were obtained. It was thought that hydrazoic acid due to hydrolytic reaction would be detectable in the water.

(ii) The brown reaction products after a decomposition were placed in a glass tube and a drop of water added. A vigorous reaction was observed with a flame and the product dissolved completely to yield a clear alkaline solution.

(iii) Examination of the pelleted material after complete decomposition showed the pellet to be dark grey-brown on the surface and generally patchy or of non-uniform colour. Examination of a cross-section of the product pellet showed the interior to be uniformly brown. More detailed observations appear in 5.3.12 when the pellet was observed at various stages of the decomposition using the hot-stage microscope.

Interruption (during the course of thermal decomposition) and low power microscope examination of the powdered azide exhibited the following features at the various points throughout a decomposition. The magnification used was 25X.

Point of interruption	Observations
(i) End of induction period.	The material was white. No visible change could be seen when the material was compared to the unreacted salt.
(ii) Immediately after the end of the induction period.	The material had turned a uniform light grey colour.
(iii) $\alpha = 0.28$.	The material was uniformly grey. No distinct nuclei could be observed on the particles.
(iv) Inflexion point.	The material was dark grey and uniformly decomposed as above. No distinct nuclei could be observed.
(v) $\alpha = 0.75$	Powder was a dark grey-brown colour at this stage, with dark grey particles admixed.
(vi) Completion of reaction	The material was dark reddish-brown and of uniform colour.

The percentage decomposition for the interruption (vi) above was 95%. It was generally found that for decomposition below this figure the product had a non-uniform colour and contained lumps and particles of dark grey material admixed in the dark brown product. For the lower percentage decompositions the end product contained more of the grey particles.

The above observations on the percentage decomposition applied to material given "water interruptions" and the end product after successive interruptions along the induction period varied from grey to dark grey and of uniform colour generally.

5.3.12 Photomicrography of pelleted lithium azide

Pelleted lithium azide was studied as poor thermal contact with the heating element and of the particles themselves gave erratic decompositions with the powdered salt.

The hot-stage microscope and illuminator used have been described in 4.1.2 and the sample handling and loading of the hot-stage have been described in 4.2.7. The method and details of the photographic techniques are also given in the latter section.

Initial attempts using a flat heating element with the thermocouple situated directly beneath this, gave unsatisfactory results. It was observed that to obtain the temperature of the heating element, the thermocouple bead had to be in thermal contact with the element. This was done throughout the course of the work using the hot-stage.

Tantalum metal was shaped into a box-like container with no lid initially and this used as a heating element and container for the pellet. The tantalum used was 0.010" thick and the box had dimensions 6 x 6 x 2.5mm. Using this heating element, erratic thermal decomposition of the lithium azide pellet was achieved, at ± 200°C. A lid was then placed so that this was in contact with the pellet and in electrical contact with two of the walls of the element. A 1.5mm hole in the lid permitted viewing of a section of the pellet surface.

Adjusting the temperature to an initial value of 195°C, values for the induction period of the salt at this temperature were in agreement with the values determined in the normal manner, but the reaction rate was well below the expected value. It was noticed however that the temperature dropped with increasing gas, (N_2), pressure and had fallen by more than 40°C during the course of a run. It was found that if the pumps were kept in the line, the temperature remained constant. The temperature was independent of the gas pressure, if this pressure was $< 2.5 \times 10^{-3}$ torr.

The "differential" method of recording the progress of the decomposition was therefore adopted and proved to be satisfactory and was used for all subsequent determinations. This method has been described in 4.2.7. Values of $^{dp}/dt$ were obtained and a $^{dp}/dt$ vs time graph plotted. A "blank" run done at the same temperature using the conventional decomposition chamber gave an inflexion point at 79-80 mins at 197°C. The hot-stage determination at the same temperature gave the inflexion point at 76-77 mins which was in good agreement.

When observing the progress of the thermal decomposition the 60 watt Ultropak illuminator was found to drastically affect the specimen. At 195°C with the illuminator at full intensity after 10 mins the section of pellet illuminated turned dark orange-brown in colour and the rate of the reaction was greatly enhanced. Trial runs showed that if the Ultropak was used at $^{2}/3$ the normal amperage (4 amps) and viewing was done for short intervals of time no effect of the light source was detected on a thermal decomposition.

The effect of illuminating a pellet of lithium azide for 1 hour with no heating, using the Ultropak at full intensity, is shown in FIGURE 5.24 and the results given in TABLE 5.24. The temperature for this run and a blank run, both done in the normal decomposition chamber was 195°C.

During the thermal decomposition of a pellet of the salt, $^{dp}/dt$ readings were recorded and photomicrographs taken at various stages during the reaction. The photomicrographs were taken with a 2 sec. exposure. Visual observations were also noted during the course of the reaction and the colours of the pellet and decomposition areas and nuclei noted.

Plate 1 shows the photomicrographs of the thermal decomposition of pelleted lithium azide, at 188 ± 2°C. Magnification was 65X. FIGURE 5.25 shows the differential plot and the arrows indicate where the photomicrographs were taken. TABLE 5.25 contains the results.

The series of photographs in plate 1 yield the following information (In brackets

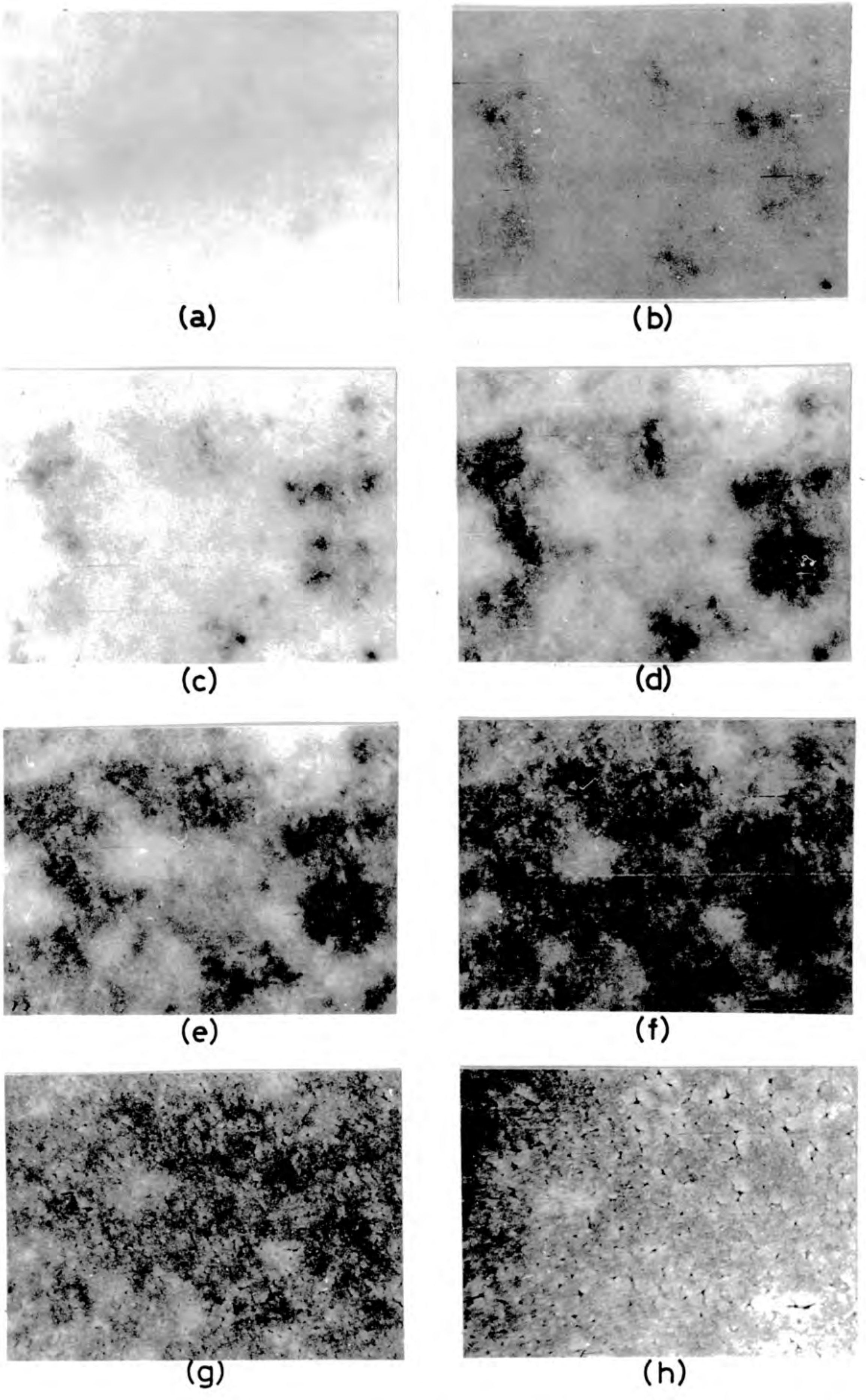

(a) (b)

(c) (d)

(e) (f)

(g) (h)

PLATE 1. THERMAL DECOMPOSITION OF PELLETED LITHIUM AZIDE. 188° C.

for comparitive purposes is the exposure time in secs, used to print the negative, at a constant light intensity from the enlarger, for the series. The time of exposure had to be reduced with progressive decomposition as contrast decreased on the negatives due to the diffuse dark background and dark nuclei).

(a) The photomicrograph shows the unreacted pellet surface viz $t = 0$. This was seen to be uniform and pure white in colour. (14)

(b) After 89 mins it is seen that the pellet has darkened generally to a grey colour with the appearance of dark grey-black centres of decomposition. The photomicrograph represents reaction shortly after the induction period. It was observed that no visible reaction occurred until this point, when the reaction progressed rapidly with the darkening of the pellet. (14)

(c) After 109 mins. when the reaction was in the acceleratory period, the surface had darkened considerably and although very few extra areas of decomposition could be discerned, those originally present were observed to have increased in size. Merging and overlap were noticed. (10)

(d) Mosaic pattern began to appear at 128 mins ($\sim \alpha = 0.35$) and the decomposition areas appear to have overlapped to a large extent. The diffuse areas (parts of the pellet surface which have generally turned a uniform grey) increased in size and intensity. (10)

(e) Extensive overlap of dark areas of decomposition and a further increase in the intensity of the background is seen. (10)

(f) The photomicrograph shows the reaction at the surface at the inflexion point, after 147 mins. and the surface is seen to be almost totally dark. (8)

(g) There was no increase in intensity of the surface colour, but complete reaction appears to have occurred at 165 mins. The mosaic structure is clearly visible. (8)

(h) The photomicrograph shows a higher magnification, (110X), of the mosaic structure at 180 mins i.e. well into the decay period. The surface was dark brown-black at this point and no further change in the surface was noticed during the remainder of the decomposition. (8)

5.4 DISCUSSION

The reproducibility of the isothermal decomposition of both pelleted and powdered unirradiated lithium azide was highly satisfactory. The p/t plots showed an initial period during which no gas evolution was detectable, followed by an acceleratory period described by the Avrami-Erofeyev equation with n = 3 and then finally a decay period conforming to the contracting sphere formula. The degree of fit of the mathematical equations was the same at all temperatures and there was little change in the value of α_i, the fractional decomposition corresponding to the inflexion point in the p/t plots.

In the study of the thermal decomposition of several azides(14,108,109) the power law has generally been used to describe the topochemistry of the decomposition. However, this equation, while describing centres of decomposition or growth nuclei, which are increasing in number according to a fixed power of time and growing 1, 2 or 3-dimensionally, takes no account of overlap of nuclei or ingestion of nuclei by each other. Avrami and Erofeyev(57,59) made such allowances and derived the equation which has previously been discussed namely:

$$\left[-\ln(1-\alpha)\right] = kt^n + C \quad \ldots\ldots\ldots\ldots\ldots (5.4.1)$$

where k, C and n are constants, the value of n being the sum of two integers, one relating the dimensional growth of the nuclei and the other the rate with which they are formed with time. The equation has been used in this work in the form:

$$[-\log(1-\alpha)]^{1/n} = kt + C \quad \ldots\ldots\ldots\ldots\ldots (5.4.2)$$

The integer n was found to assume the value 3 for the decomposition of both powdered and pelleted lithium azide, when the equation was applied to the acceleratory period. (For comparitive purposes when $n = 3$, the rate constant k has been numbered k_1 and when $n = 2$ (see Section 6,7,8) the rate constant was numbered k_2). The degree of fit using $n = 3$, was over the whole of the acceleratory period, namely $0.05 < \alpha < 0.50$.

For small values of α, $\ln(1-\alpha) \approx \alpha$ and thus $\alpha = kt^3$ can be expected to fit the early part of the main decomposition. The plot of $p^{1/3}$ versus t is a straight line over the range $0.02 < \alpha < 0.25$, indicating that overlap and ingestion are not significant up to $\alpha = 0.25$ (FIGURE 5.14).

The value of $n = 3$ in the Avrami-Erofeyev equation can be ascribed to one of the following types of nuclear formation and growth:

(i) one-dimensional growth of nuclei, increasing in number with the square of time,

(ii) two-dimensional growth of nuclei, increasing in number linearly with time,

(iii) three-dimensional growth of nuclei from a fixed number of centres.

It is proposed that the possibilities (i) and (ii) are unlikely and nuclear growth is considered to be two-dimensional, with the number of nuclei increasing linearly with time.

Possibility (i) is considered unlikely because of the relatively high value of α_i and the applicability of the contracting sphere formula in the decay region. The effect of interrupting the run before the decay period, destroying the surface nuclei by the admission of water vapour and then continuing the run was to reproduce the induction period and reduce the rate constant, k_1. These results contradict the possibility (iii) since destruction of the fixed number of nuclei at the time of interruption should destroy the reaction, or at least cause any new rate to be very different from the original value.

Metallic nuclei were not present at the commencement of heating since admission of water vapour (5 mins and 30 secs) at t = 0, on both the pelleted and powdered lithium azide, had no effect on the subsequent thermal decomposition other than lowering the final pressure. It is thought that this reduction in percentage decomposition was the result of partial hydrolysis of the azide. The effect of water vapour on the decomposition at any time after t = 0, indicates that the nuclei are metallic ones, as the reaction is returned to zero time. It is considered that the nuclei are surface ones, as are formed during the decomposition of U.V.-irradiated lithium azide, (Section 8). Similarities in the decay reactions for the unirradiated and U.V.-irradiated material indicate similar topochemistry of nucleation, which was conclusively shown to be largely confined to the surface of the decomposing particles of U.V.-irradiated lithium azide.

These are discrete nuclei in the initial stages of the acceleratory period, but as the reaction progresses independent growth of the individual reaction centres is no longer ensured and overlapping occurs as indicated by the use of the Avrami-Erofeyev equation, over the acceleratory period.

The fall in k_1, after interruption and admission of water vapour can be attributed to the de-activation of certain areas of the particle surface. The rate constant, k_1, is dependant on the number of nuclei at the start of the acceleration and a decrease in this number will reduce the value of k_1.

The decay period commences when the two-dimensional surface nuclei touch and the surfaces of the small particles are covered by reaction product. Reaction proceeds inwards with the reactant/product interface taking the form of a contracting envelope as shown by the fit of the appropriate equation.

Turning from the analysis of the topochemical nature of the decomposition to the mechanism of formation and growth of nuclei, the sites at which reaction commences must be considered. The decomposition of solids is governed by the formation and growth of nuclei and these have often been observed and photographed. They are generally formed on the external surfaces and to a lesser extent, within the crystal.

Clustering may be observed, or the distribution of the nuclei may suggest places where formation is preferred. These preferred positions are likely to be localities on the surface of the particle, such as surface cracks or lines of strain, where disorganisation or mechanical damage has taken place and where there is a higher thermodynamic instability and unsaturation of cohesive forces.

A theoretical treatment of the formation of nuclei at such sites in the thermal decomposition of barium azide, was put forward by Thomas and Tompkins(108). It was proposed that two adjacent azide groups on the surface are electronically excited by receipt of sufficient thermal energy and these decompose to give nitrogen.

An emergent edge dislocation, either isolated or in a grain boundary terminating at the surface will have a core near which the lattice is severely strained and thus a region favouring decomposition is present. The chemical potential and the stereochemical environment of ionic species in the immediate vicinity of the dislocation differ from those of similar species at "ideal" lattice sites. Thomas and Renshaw(1) have studied the preferential decomposition of calcium carbonate at regions of emergence of dislocations and Singh(6) has discussed decomposition at preferential sites on the surface of slowly decomposing mercury fulminate crystals. Bowden and McAuslan(5) have studied the slow surface decomposition of metallic azides using the scanning electron microscope. Jach(125) has also discussed decomposition along dislocation lines and Dreyfus and Levy(177) showed that decomposition of γ-irradiated potassium azide, occurred at preferential steps on heating, produced by subjecting the crystal to shock or strain. Such steps will contain a large number of dislocations.

The stresses induced in lithium azide during preparation (dehydration, pelleting and grinding) will have generated a large number of dislocations which will have grouped to form high angle grain boundaries. It is highly probable that a large number of incomplete planes of edge dislocations in an emergent grain boundary will contain only azide (N_3^-) or Li ions. The decomposition of two adjacent azide ions at the core of a dislocation will be favoured, particularly if they both lie on the surface.

Two adjacent azide ions on the surface decompose when these are electronically excited by receipt of sufficient thermal energy, to give nitrogen and two electrons. The ions are considered to be at points of strain on the surface, resulting from the method of sample preparation. The unsaturation of cohesive forces at these points facilitates the reaction and a slow surface decomposition results:

$$N_3^- + N_3^- \longrightarrow 3N_2 + 2e \quad \ldots\ldots\ldots\ldots\ldots\ldots\ldots \quad (5.4.3)$$

Lithium atoms will be formed as the lithium ions combine with the freed electrons. These Li atoms on the surface of the particle will be initially at the interatomic spacing in LiN_3, but after formation they will diffuse over the surface and, at a critical concentration, they will crystallise to form lithium metal, with the associated electronic properties of a metal. Work on the structure and properties of thin films of metals(178) indicates that the structure of a metal in a thin film is that of the bulk metal and that pseudomorphism is not shown except by elements with a high degree of homopolar bonding e.g. Bi and Ge. Films are formed by lateral growth of nuclei and may become continuous at thicknesses as low as 50Å. The character of the conductivity of such metal films corresponds very closely to that of the massive metal. Thus it will be possible for a very thin 2-dimensional metal nucleus with the electronic properties of the bulk metal to form on the surface of the particles at discrete centres.

Thus in the decomposition of lithium azide, the reaction is assumed to occur at strained areas and at points of damage on the crystal surface. With the pelleted material, which is regarded as a composite of crystallites, reaction will occur in the bulk of the pellet and on the external surface. The particles comprising the pellet behave as if they were isolated particles. The activation energy for the process of nuclear formation in pellets (24 k.cals/mole) was found to be slightly greater than that found for the powdered material (22 k.cals/mole). This difference may be due to the formation of pockets of nitrogen in the bulk of the pellet. Thus an activation energy of diffusion will exist in addition to that for the described reaction.

Pelleting powdered lithium azide was shown to lengthen the induction period from 25 to 29 mins., which also lend support to the theory that the nitrogen during this stage of the decomposition was hindered in escaping from the bulk of the pellet. The induction period was arbitrarily taken as the time for the reaction to give a gas pressure of 1 x 10^{-2} torr. It is also seen from the photomicrographs (Plate 1), that during the early stages of the reaction the pellet surface remained uniformly compact, while during the acceleratory period a "mosaic" pattern appeared as the surfaces of the particles constituting the pellet decomposed.

The failure to detect nitrogen during the induction period with the pressure gauges used, was probably due to absorption of the gas on the very large surface of the particles of powder or, as suggested by Torkar and Spath(33) in the case of barium azide, the sensitivity of the McLeod gauge used was not sufficient to record small pressure differences over the induction period.

For reasons considered later, the rate determining step over the induction period is proposed to be the diffusion of lithium atoms over the surface, to coalesce and form metal nuclei. The activation energy of 22 k.cals/mole, associated with the induction period correponds to that for this change in the powdered azide.

The mechanism for the formation of nuclei has been supported by the "water interruption" experiments. Exposure of both pellets and powdered lithium azide to water vapour at $t = 0$ had no effect on the subsequent thermal decomposition, indicating that at $t = 0$, no metallic nuclei or metal atoms were present at the start of the decomposition. Reitzner(179) found that the thermal decomposition of α-lead azide was affected by water vapour, due to deposition of a basic lead azide and the poisoning action of the water vapour on the autocatalytic lead nuclei. Young(180) has reported that hydrolysis followed by exposure to CO_2 was also responsible for nucleus-retardation in the thermal decomposition of α-lead azide.

It was observed that the final pressures were lower than was expected on exposing lithium azide to water vapour and this is attributed to partial hydrolysis of the azide. This was supported by exposing both powdered and pelleted lithium azide to water vapour for 5 mins at $t = 0$ when the final pressure was found to be lowered even further.

The deposition of hydrolysis product on the surface of the particles did not appear to create regions of strain or sites of preferential decomposition as no effect on the subsequent rate of thermal decomposition was observed. The fact that the induction period was repeated shows that the water vapour attacked <u>only</u> the metal atoms and did not affect the "thermal sites" (i.e. reaction initiating points), at which the reaction:

$$N_3^- + N_3^- \longrightarrow 3N_2 + 2e \qquad \text{....................} \qquad (5.4.3)$$

occurred.

Interruption at the end of the induction period, did not have the effect of repeating the induction period, in the case of pelleted azide. Increasing the time of exposure to water vapour, to 5 mins., had the effect of producing a longer induction period (21mins) than previously obtained, but this was still shorter than that for the uninterrupted run (58 mins). The water vapour largely destroyed nuclei situated on the surface of the pellet leaving a number in the bulk of the material intact. The increased exposure time to water vapour, allowed an increased amount of penetration into the pellet and it is observed that the length of the induction period after interruption at the end of the induction period was longer for the 5 mins. exposure to water vapour, when decomposition was resumed. The shorter induction period obtained with the pelleted azide on resuming reaction can be expected if a number of growth nuclei are still present in the bulk of the material and reaction commences immediately on heating but at fewer centres. After successive water interruptions along the induction period, the rate of the subsequent reaction was lowered significantly.

Successive water interruptions along the induction period, on powdered azide, had the effect of destroying the nuclei each time and so returning the reaction to zero time. It is therefore concluded that there must be a very large number of potential sites for nucleus formation. "True" induction periods were not found with the pelleted material however, for as explained above, the water only destroyed surface nuclei. These experiments clearly illustrated the vital role played by the lithium metal during the decomposition.

There was no effect on the duration of the induction period when powdered azide was decomposed after admixture with end products (Li metal, finely divided). This may be expected as the added metal was not incorporated in the matrix of the decomposing lithium azide. However, a 30% decrease in the duration of the induction period was observed when the end products were pelleted with azide and this decomposed. This may be expected as the physical contact is greatly increased.

From the proposed theory of the mechanism of nuclear formation, it would be expected that no colouration of the powdered or pelleted lithium azide should occur before the nuclei had formed as a result of the lithium atoms coalescing i.e. during the induction period. The photomicrography and visual observations showed this to be the case and no colouration was observed up to the end of the induction period. Immediately after this point, when gas was detectable at the commencement of the acceleratory period, the salt darkened and areas of decomposition were observed in the photomicrographs.

Interruption of the reaction during the induction period by cooling to room temperature, had no effect other than a small warm-up time indicating that no thermal energy chains were involved in the changes during the induction period.

At the end of the induction period growth of the nuclei commences and the reaction accelerates. During this period reaction occurs at a rapidly expanding metal/salt interface and at an increasing number of nuclei. Thus a measurable amount of nitrogen is evolved at the commencement of the acceleratory period and this is considered to result from a reaction involving the transfer of an electron from an azide ion, (N_3^-), into the lowest vacant level (conduction band) of the metal nucleus. This is analagous to the mechanism postulated for barium azide by Thomas and Tompkins(108), after modifying Mott's(74) original theory involving transfer of an electron to the conduction band of the crystal which is an energetically higher process. This transfer results in the formation of a positive hole (azide radical) which is stable to decomposition. This hole may then react with an adjacent azide ion when the latter receives sufficient thermal energy to raise one of its electrons to an excited state with the production of $3N_2$ according to the equation:

$$[N_3^-]^* + N_3 \longrightarrow 3N_2 + A + F \quad \ldots\ldots\ldots\ldots\ldots\ldots\ldots \quad (5.4.4)$$

where A is an anion vacancy and F an F-centre and $[N_3^-]^*$ is an excited anion. The F-centres combine to form an F-centre complex which is bound to the nucleus.

The rate determining step in the reaction is considered to be the elevation of the electron to the conduction band of the metal nucleus. The measured activation energy for growth (29 k.cals/mole for pelleted material and 28 k.cals/mole for powdered lithium azide) is proposed to be the activation energy of this reaction.

Thomas and Tompkins report a value of 29 k.cals/mole for this activation energy in their work on nucleus growth in barium azide and Prout and Moore(3) report a value of 27 k.cals/mole. The corresponding values for the decomposition of strontium and calcium azides are 25 k.cals/mole(139) and 27 k.cals/mole(48), respectively.

The importance of the metal nucleus during the acceleratory period (autocatalytic nature of the decomposition) has been illustrated by "water interruption" experiments. It was found that exposure to water vapour (30 secs) during the acceleratory period, destroyed the reaction and a new induction period of equal length as that found for the uninterrupted salt, resulted. The rate constant k_1 for the subsequent acceleratory period was seen to be lowered and this is considered to be due to the removal of potential nuclear sites by the water vapour, when already growing nuclei were destroyed.

Interruption at the inflexion point in the p/t plot and at greater values of α destroys all further reaction indicating that no new growth nuclei are possible after this point of the reaction. Reaction ceases when the lithium which totally covers the particle, is destroyed and even though a surface of azide at the original azide/metal interface is present, fresh nucleation cannot occur. From this it can be concluded that the original (potential) sites for the formation of nuclei are on the external surfaces and are at energetically highly favoured points which are not present at the new interface.

The photomicrographs of the decomposing pellet showed that a mosaic, "honeycomb-like" structure developed during the acceleratory period. A contraction in the size of the particles comprising the pellet would produce this effect and the reaction during the acceleratory period would be equivalent to the decomposition of the powdered material. The similarity found for the activation energies for the powdered and pelleted material is thus not unexpected.

Galwey and Jacobs(64) reported a change in the exponent from 4 to 3, in the Avrami-Erofeyev equation, when studying the thermal decomposition of powdered and pelleted ammonium perchlorate. They attribute this change to the fact that the particles are heavily compressed together so that the reaction can spread from particle to particle and nucleation is therefore relatively unimportant. They also report an increase in the activation energy for nucleus growth on pelleting, of 8 k.cals/mole. By analogy in the case of lithium azide, as no change in the activation energies or value of the exponent n was observed on pelleting, the assumption that the pellet consists of a mass of individual particles, decomposing independently of one another, is justified.

Interruption with water vapour in the acceleratory period resulted in short induction periods (12 - 14 mins) followed by a reaction, with k_1 reduced slightly, in the case of the pelleted material. This indicates that although the nuclei are destroyed, a considerable number are not affected by the water vapour and the ensuing reaction is due to these nuclei. The reduction in the number of nuclei would account for the lowering of the rate constant.

Here again the absence of any effect when the reaction is stopped by cooling to room temperature during the acceleratory and decay periods shows that no thermal energy chains are involved in the growth process in both powdered and pelleted lithium azide.

From photomicrographs and visual observations of the pelleted azide, it is seen that darkening of the pellet surface began in the early stages of the acceleratory period, indicating that metal centres are necessary before acceleration of the reaction begins. Particular centres were observed to grow and become darker. This is considered to be the result of very small nuclei overlapping and coalescing to form these darker regions. The magnification used (65X and 110X) was not high enough to distinguish individual nuclei. The areas of decomposition were observed to increase in number with time supporting the choice of (ii) earlier. The nuclei are also formed inside the pellet, consisent with the picture of the pellet consisting of particles pressed together and reaction occurring on the individual particles. At the point at which marked decay of the reaction occurs, there is considerable coverage of the pellet surface by product. No further change is observed from this point to the completion of the reaction.

The decay reaction commences when the surface nuclei touch and reaction takes place at the contracting interface. The mechanism here is similar to that occurring during the acceleratory period since the activation energies associated with these two processes are approximately the same, for both pelleted and powdered lithium azide (30 k.cals/mole and 29 k.cals/mole respectively). It is proposed that if nucleation occurs only on the surface of the particles in the powdered and pelleted azide, then in the decay stage of the reaction when the nuclei have so overlapped as to form a continuous interface with the salt, penetration of this interface into the particles occurs. It is expected that a mechanism of this nature would be described by the contracting sphere formula.

Several workers(7,20,89,181,182) have reported ageing effects in inorganic azides and other inorganic salts. Comparison of the normalised runs for the decomposition of fresh powdered lithium azide and aged (6 months) material of the same ground batch, showed no difference in the rate constants k_1 and k_3, for the acceleratory and decay periods respectively and the duration of the induction periods was the same in both cases. It was observed, however, that the final pressure was approximately 20% lower for the same weight of aged, as for the fresh material. Thermal annealing, under the conditions used, had no effect on the rate of the reaction or the percentage decomposition. These results on ageing indicate that changes do occur in the material over 6 months.

It is considered that physical ageing (dislocation and point defect movement) takes place and that the percentage decomposition which was 20% lower than normal, was the result of part of the LiN_3 not decomposing at the reaction temperature used because of the absence of nucleation.

Possible contributory factors to the high degree of irreproducibility of decomposition found with the newly prepared salt, were the presence of water vapour, oxygen and light. These were systematically eliminated with no improvement in the reproducibility. The decomposition was reproducible only when the technique of grinding, pelleting and then grinding, was adopted.

It is considered that the lithium azide as initially prepared and as ground material, was inhomogeneous with respect to physical imperfections and that pelleting and subsequent grinding had the effect of introducing large numbers of crystal defects homogeneously distributed in the powder. It is reasonable to presume that grinding and pelleting will be similar to cold-working of metals which produces a high concentration of vacancies(183,184) and increases the number of dislocations(185,186). There will also be the accumulation of dislocations to form new high angle grain boundaries. Steps will be formed at the surfaces of the particles and in general a highly damaged salt will be produced with a high concentration of point and line defects.

It was observed that when the reproducible powdered lithium azide was pelleted and then decomposed, no significant change in the reaction rates for the acceleratory and decay periods was observed, indicating that maximum damage had been achieved through one cycle of grinding, pelleting and then grinding. Similarly, several pelleting and grinding operations, maintaining a constancy in the conditions used, had no significant effect on the subsequent induction periods and rates of reaction.

It was observed that variation of the grinding <u>time</u>, after the initial pelleting, brought about a decrease in the rate constant during the acceleratory period and an increase in the length of the induction period. These results can be explained if it is assumed that the particle size before the first pelleting is not achieved again in subsequent grinding where the time of grinding is maintained constant. The particles may comprise agglomerates of the small particles, which will decompose as if the constituent particles were separated. Increasing the grinding time will result in smaller particles, the existence of which will produce the effects found if Mampel's theoretical analysis of nucleation with varying particle size is accepted. He showed(187) that theoretically the rate could be expected to pass through a maximum as the particle size decreased.

It was postulated that this happened because the acceleratory period only lasted until a short time after overlap of the growing surface nuclei and this happened sooner with smaller than with larger particles. This effect is balanced by the great increase in surface area as the particles decrease in size until a certain critical value is reached, when overlap occurs so quickly that the deceleratory part of the decomposition starts much sooner and the maximum rate then drops.

Such effects have been reported by other workers(182,188-190) when the reaction rate was observed to pass through a maximum as the particle size decreased. In the decomposition of lithium azide the absence of a steadily increasing rate with increasing grinding, prior to a fall in the rate, is attributed to the severe grinding of the lithium azide in 10 secs by the R.I.I.C. Grindex, so that rates were recorded approximately from the critical point in Mampel's theory, onwards. The results of this series of runs is good evidence in support of the theory.

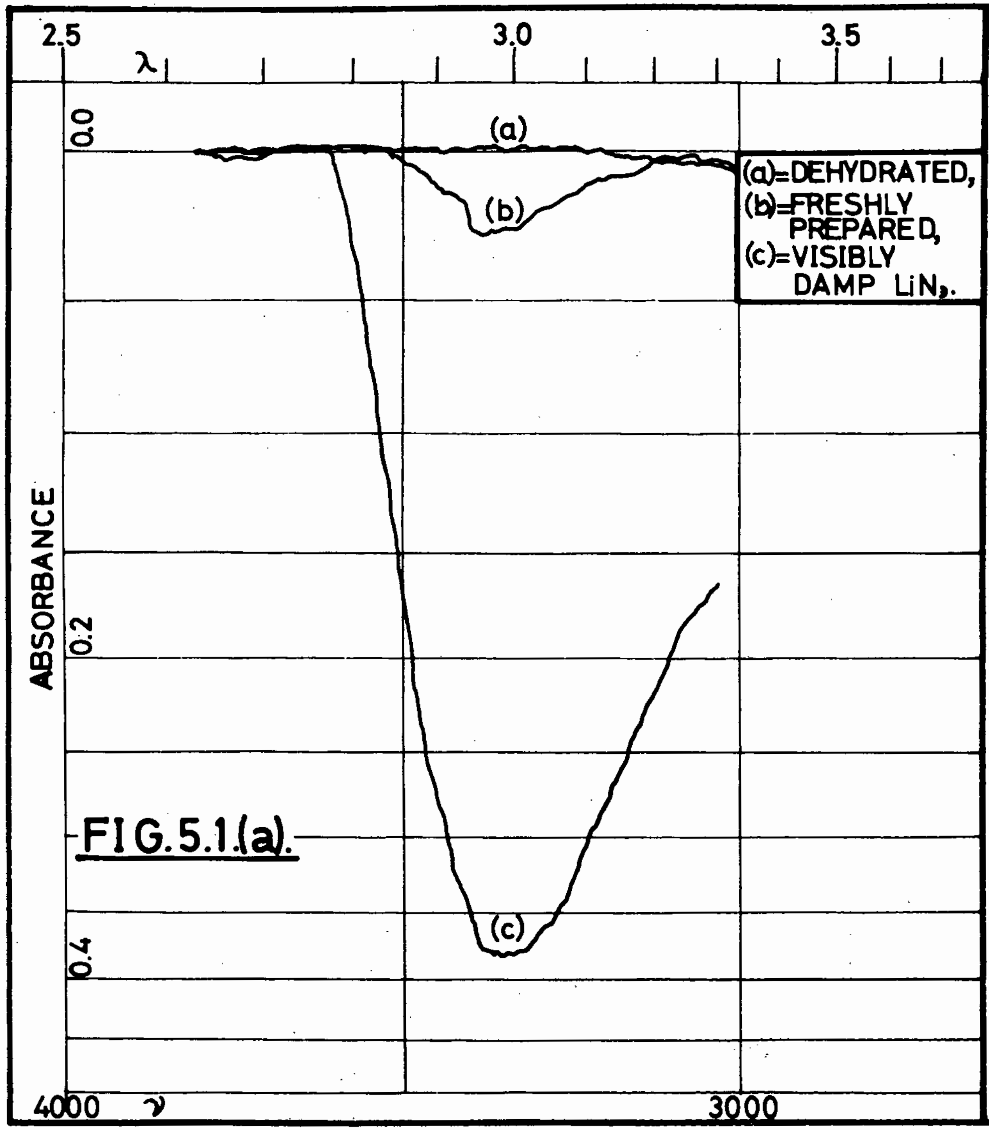

FIG. 5.1.(a).

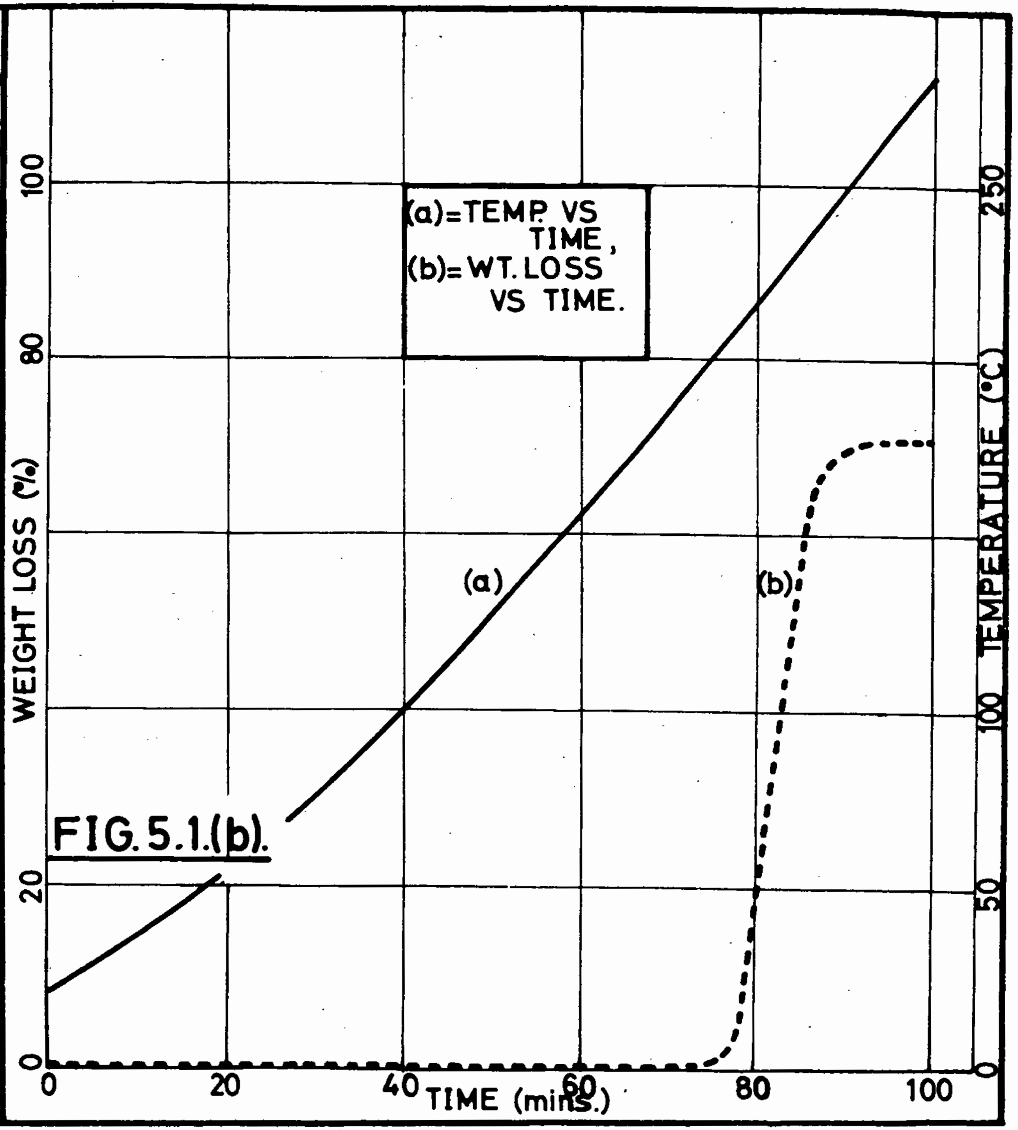

FIG. 5.1.(b).

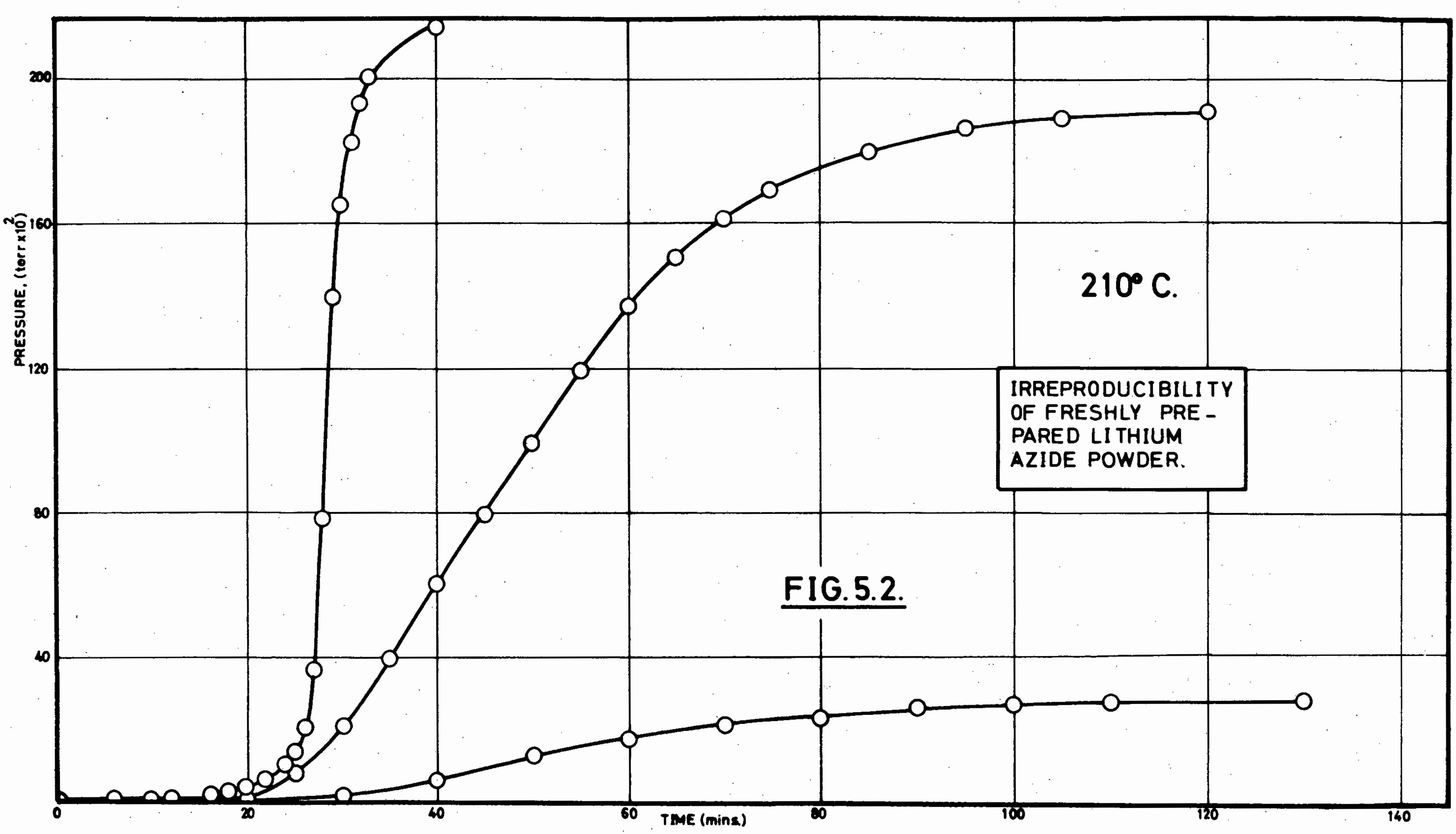

IRREPRODUCIBILITY OF FRESHLY PREPARED LITHIUM AZIDE POWDER.

FIG. 5.2.

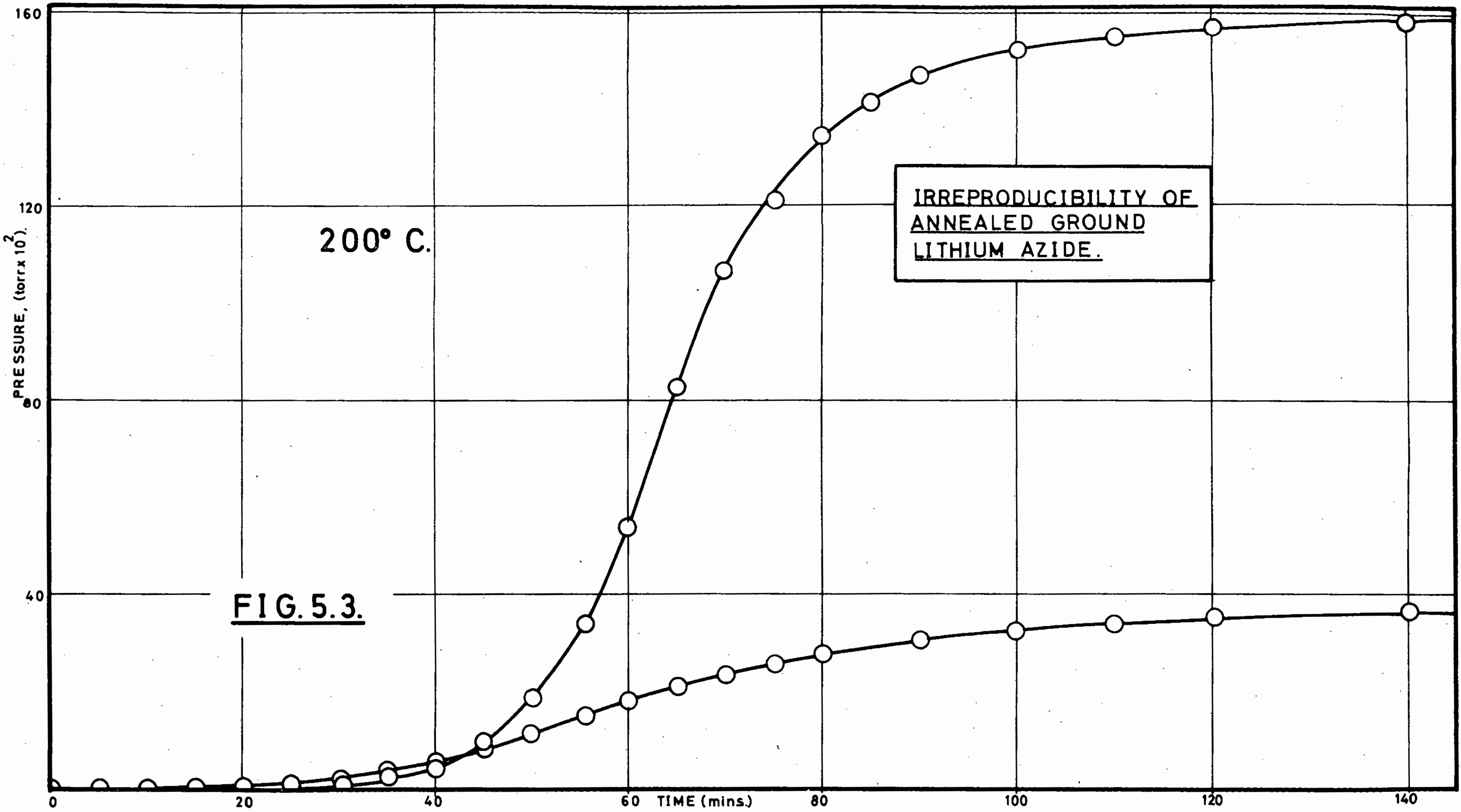
IRREPRODUCIBILITY OF ANNEALED GROUND LITHIUM AZIDE.
200° C.
PRESSURE, (torr x 10^{2}).
160
120
80
40
0
20
40
60
TIME (mins.)
80
100
120
140

FIG. 5.3.

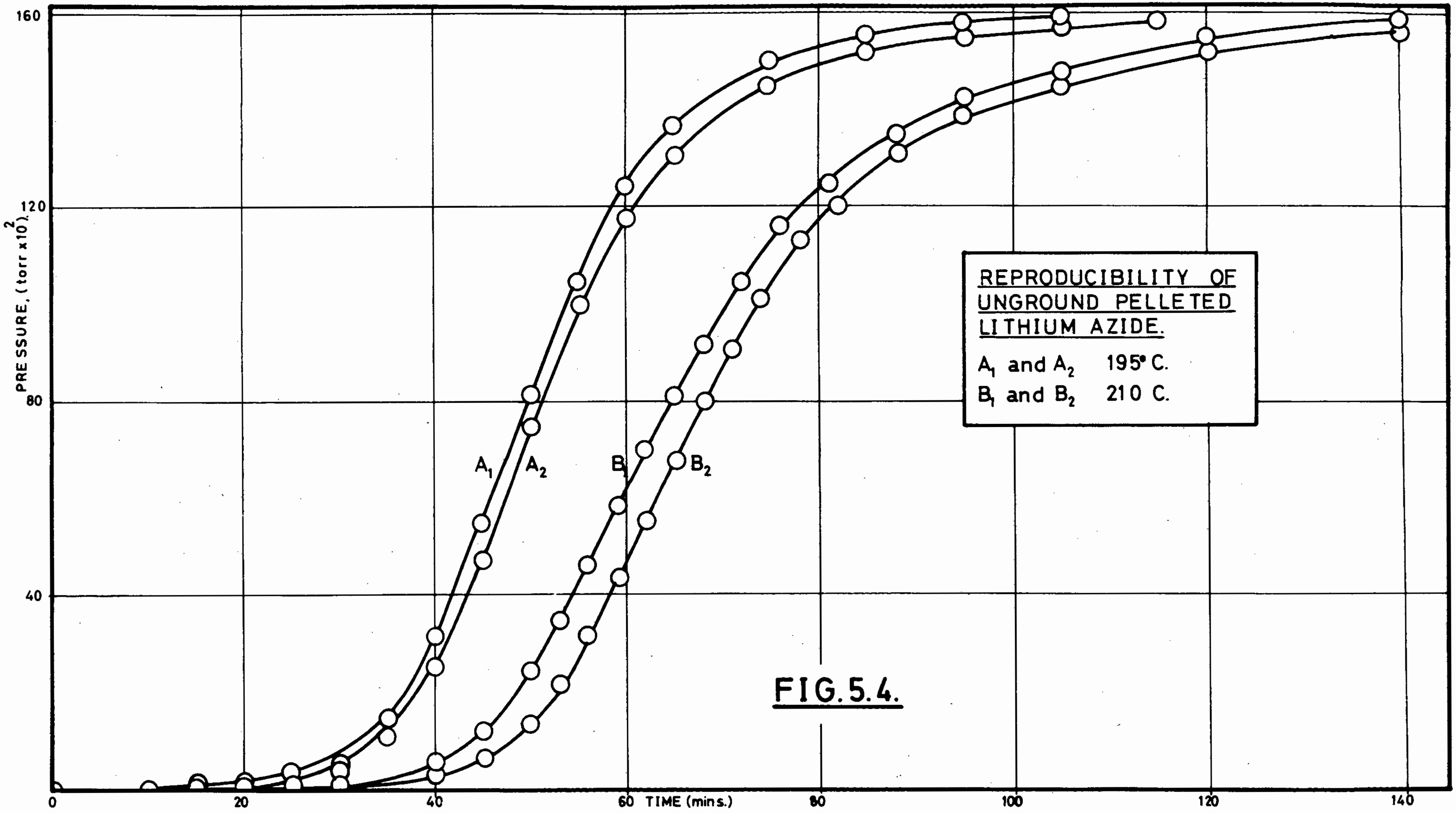

REPRODUCIBILITY OF UNGROUND PELLETED LITHIUM AZIDE.

FIG.5.4.

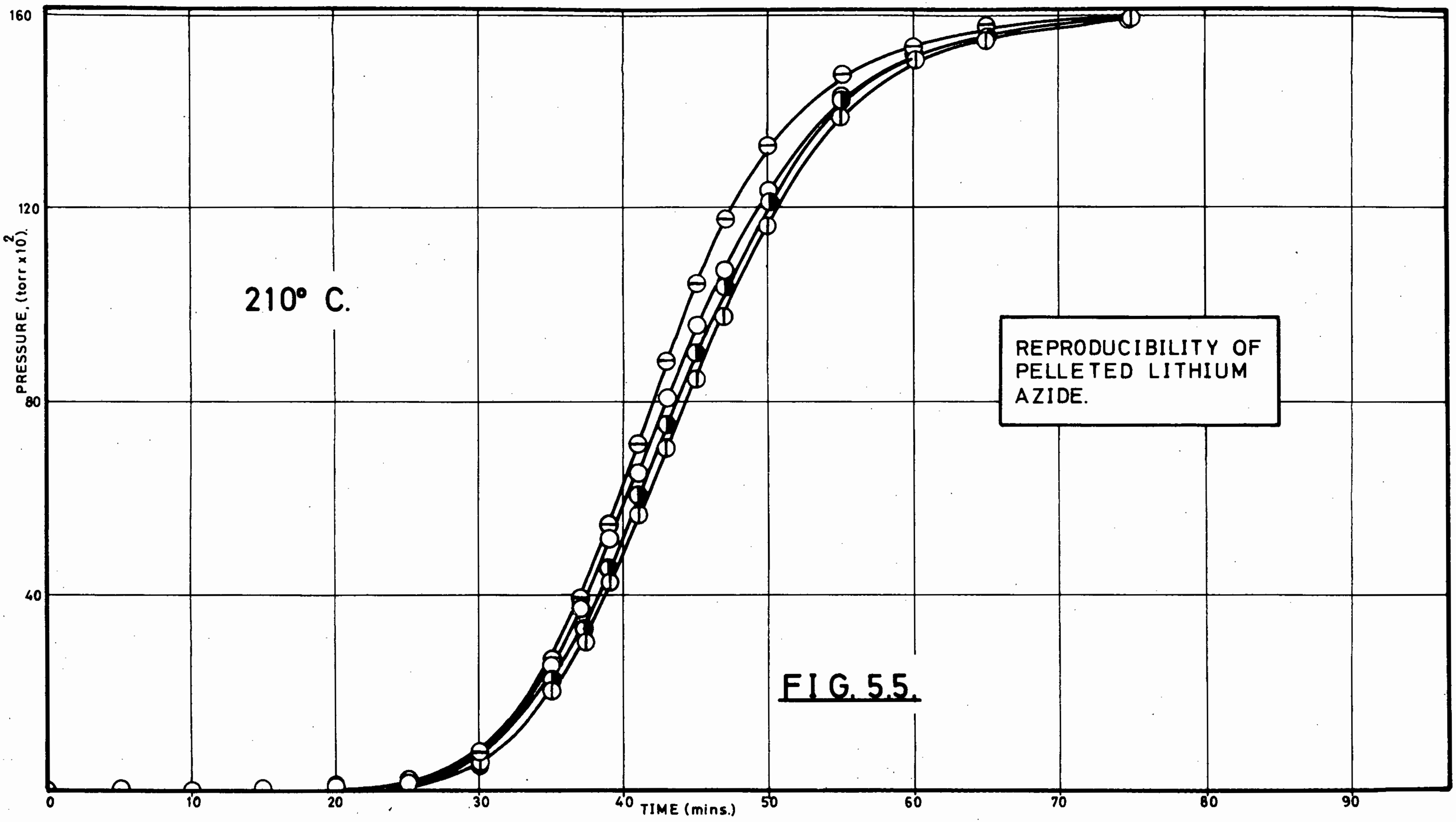

REPRODUCIBILITY OF PELLETED LITHIUM AZIDE.

FIG. 5.5.

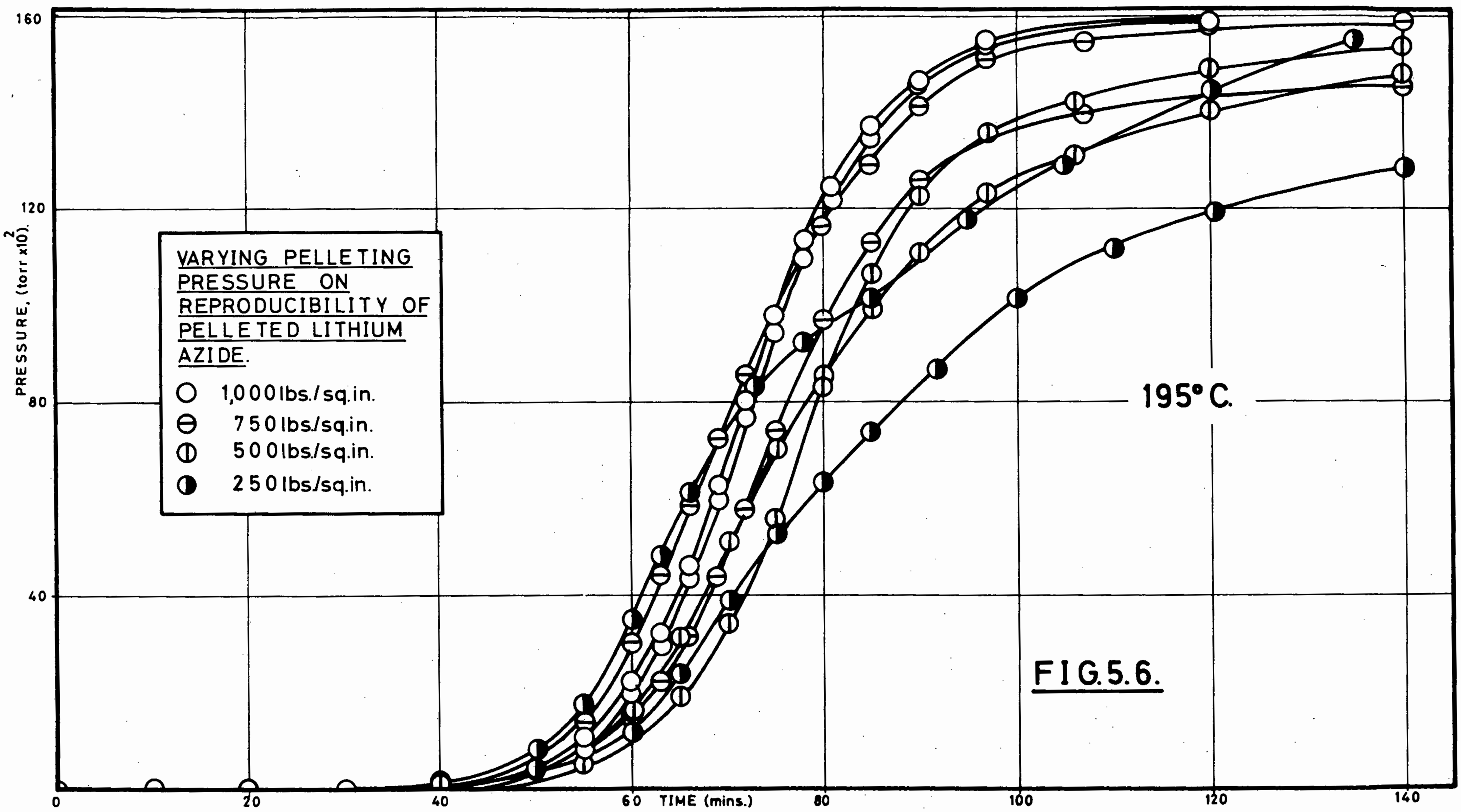

VARYING PELLETING PRESSURE ON REPRODUCIBILITY OF PELLETED LITHIUM AZIDE.
○ 1,000 lbs./sq.in.
⊖ 750 lbs./sq.in.
⦶ 500 lbs./sq.in.
◐ 250 lbs./sq.in.
195° C.
PRESSURE, (torr x10^2).
TIME (mins.)
160
120
80
40
0
20
40
60
80
100
120
140

FIG.5.6.

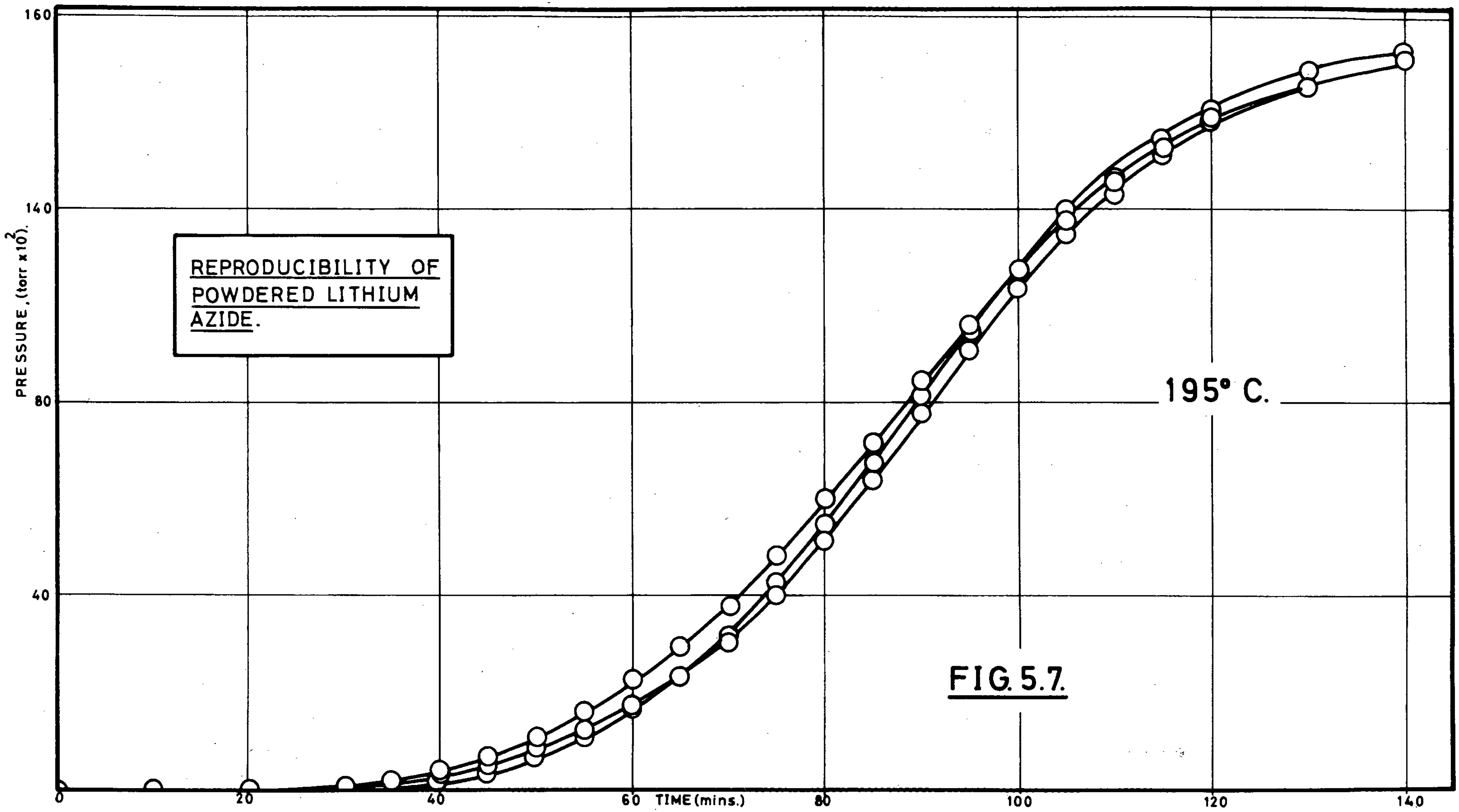
REPRODUCIBILITY OF POWDERED LITHIUM AZIDE.
195° C.
PRESSURE, (torr x 10^2).
160
140
80
40
0
20
40
60
TIME (mins.)
80
100
120
140

FIG. 5.7.

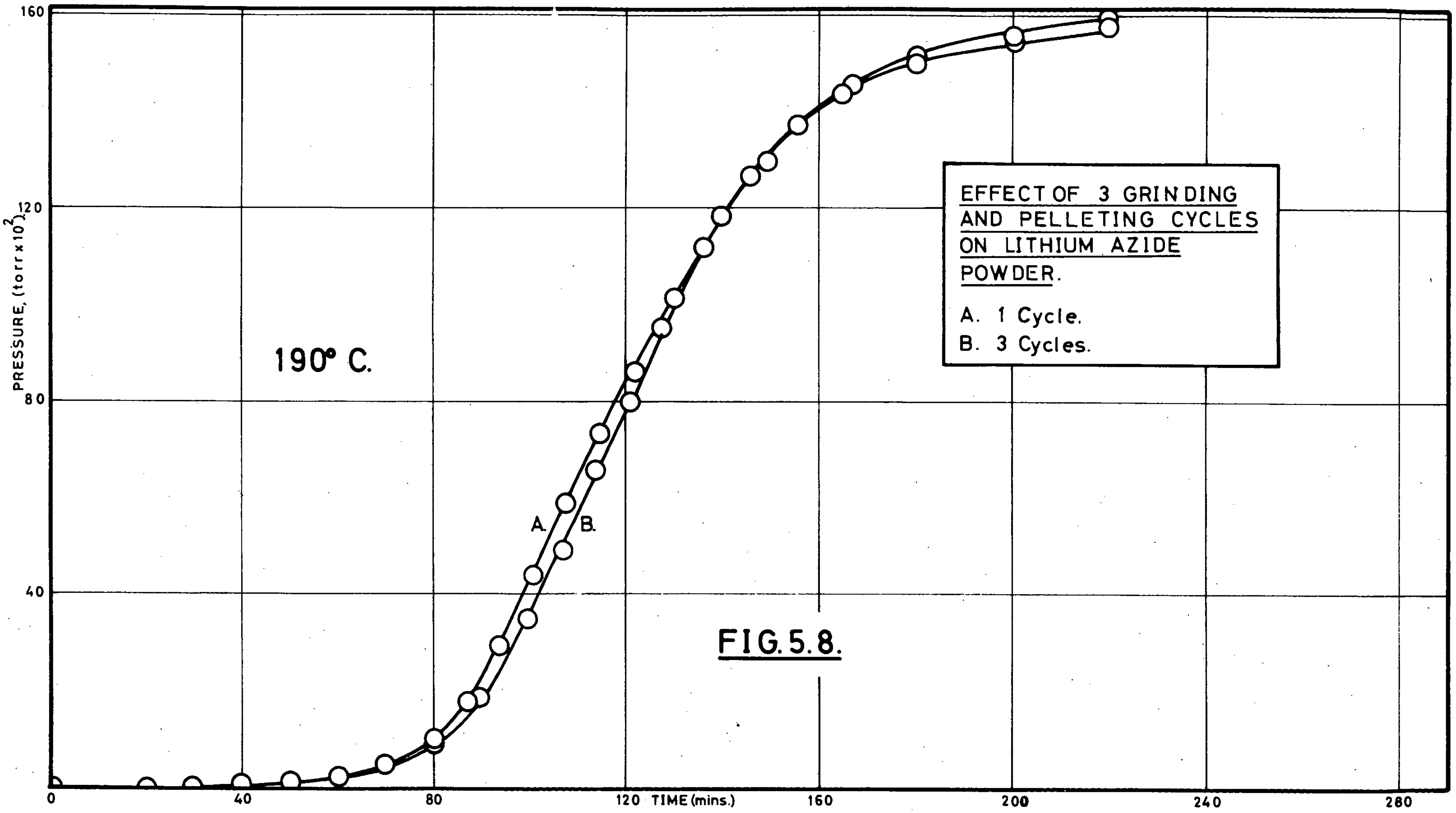
PRESSURE, (torr x 10^2)
160
120
80
40
0
40
80
120 TIME (mins.)
160
200
240
280
190° C.
A.
B.
EFFECT OF 3 GRINDING AND PELLETING CYCLES ON LITHIUM AZIDE POWDER.
A. 1 Cycle.
B. 3 Cycles.

FIG. 5.8.

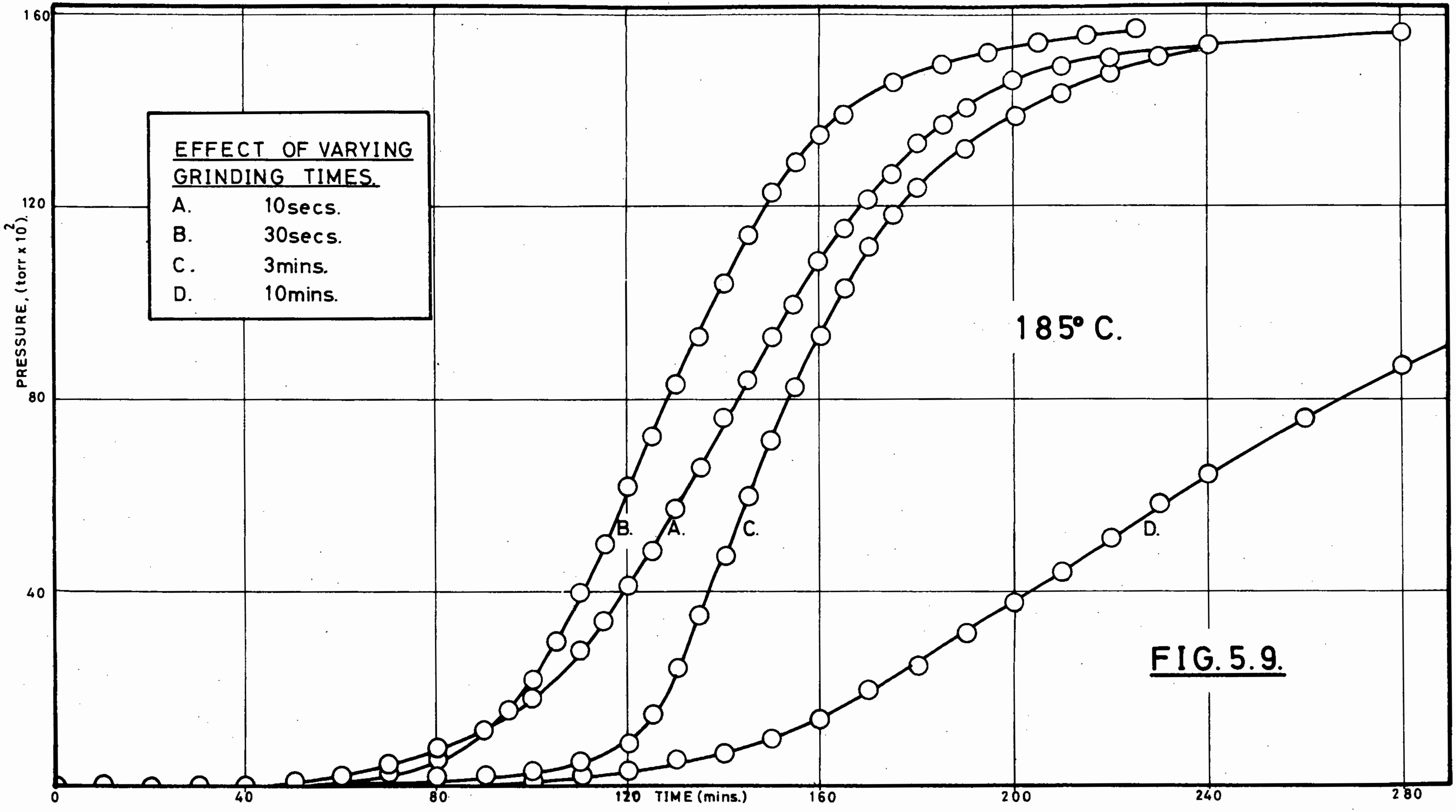
EFFECT OF VARYING GRINDING TIMES.
A. 10secs.
B. 30secs.
C. 3mins.
D. 10mins.
185° C.
PRESSURE, (torr x 10^2).
TIME (mins.)
0
40
80
120
160
200
240
280
40
80
120
160
B.
A.
C.
D.

FIG. 5.9.

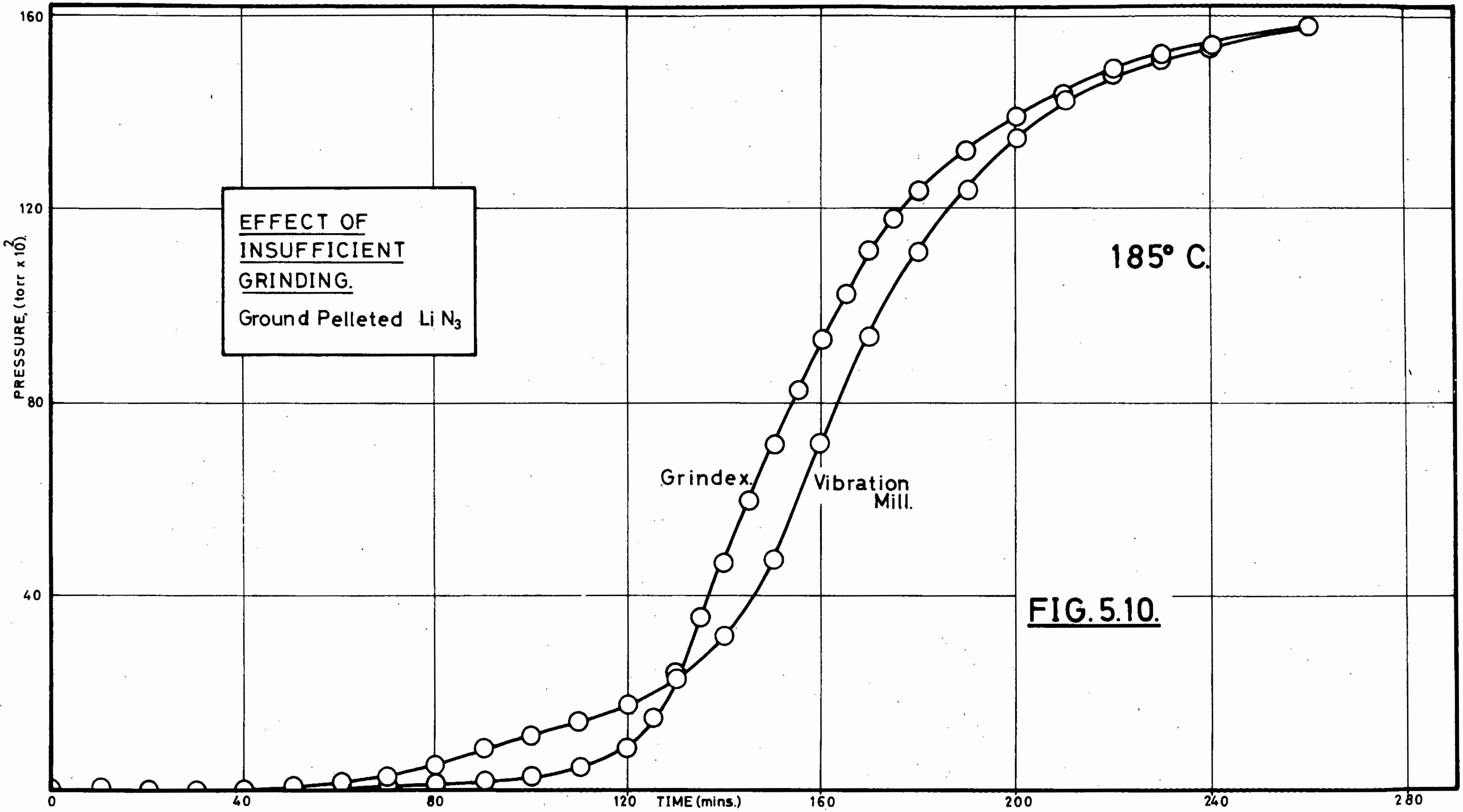
EFFECT OF INSUFFICIENT GRINDING.
Ground Pelleted Li N_3
185° C.
Grindex.
Vibration Mill.
PRESSURE, (torr x 10^2).
TIME (mins.)
0
40
80
120
160
200
240
280
40
80
120
160

FIG. 5.10.

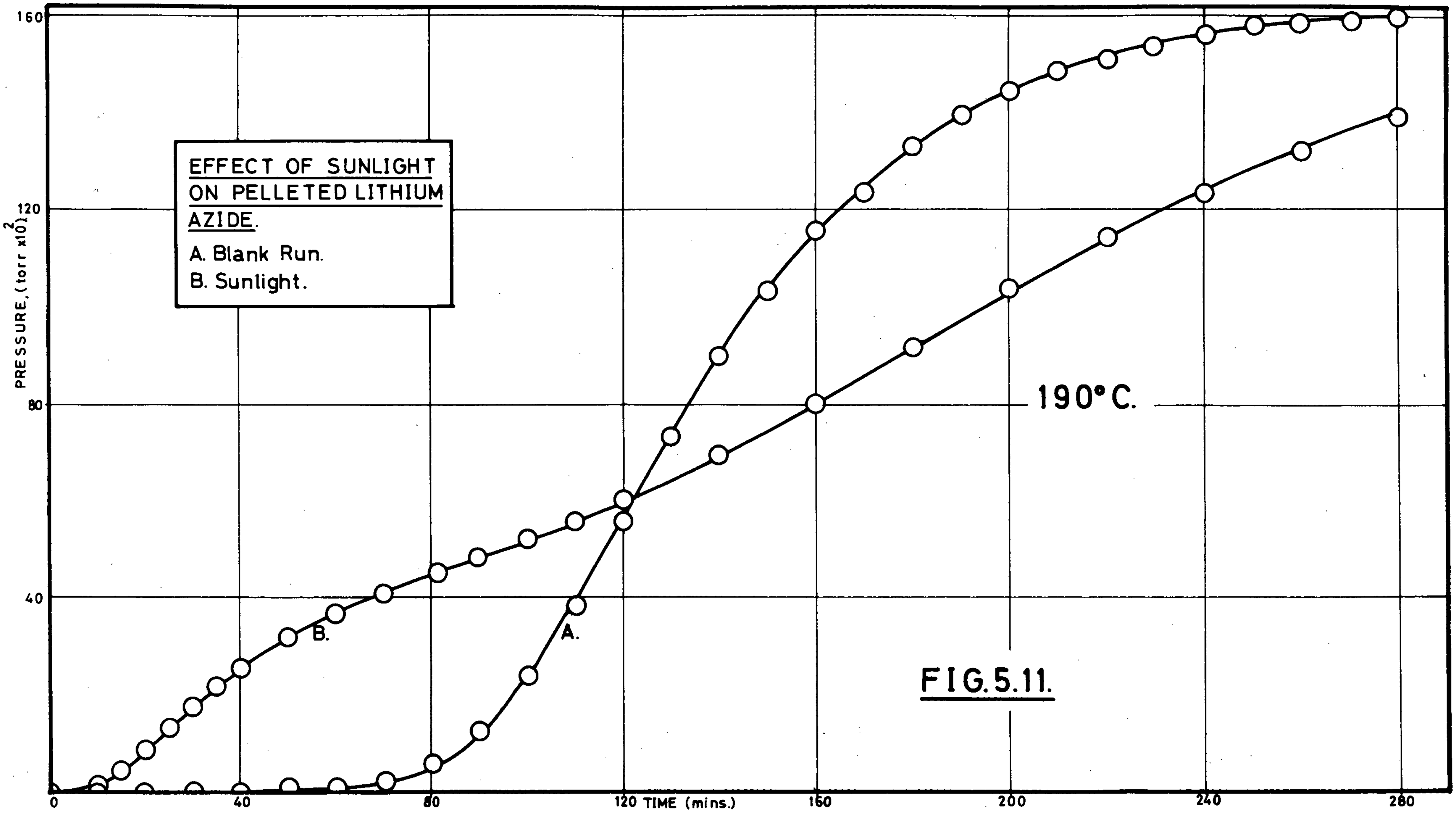

FIG. 5.11.

EFFECT OF SUNLIGHT ON PELLETED LITHIUM AZIDE.

A. Blank Run.

B. Sunlight.

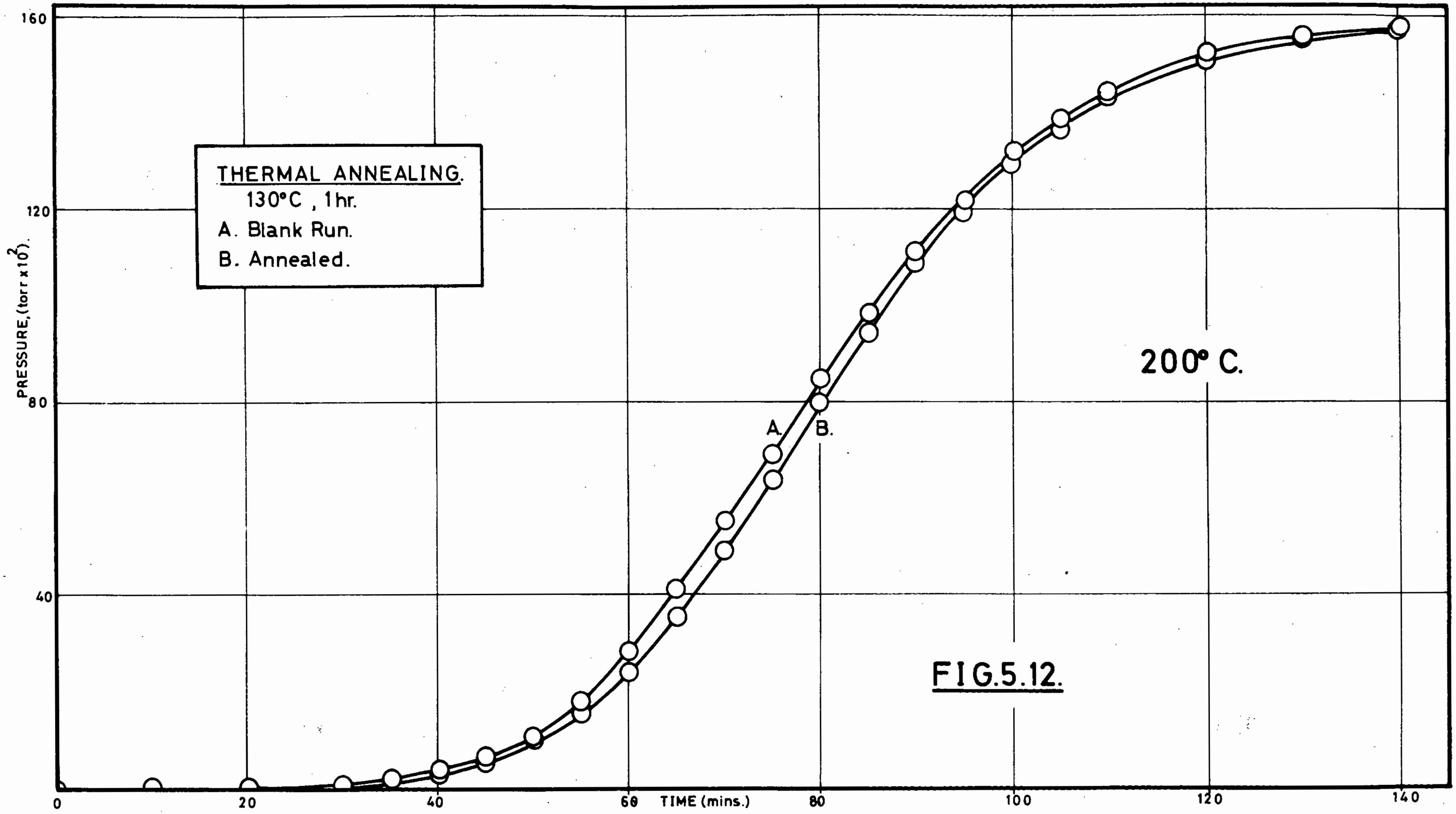
THERMAL ANNEALING.
130°C , 1 hr.
A. Blank Run.
B. Annealed.
200° C.
PRESSURE, (torr x 10^2).
TIME (mins.)
0
20
40
60
80
100
120
140
40
80
120
160
A.
B.

FIG.5.12.

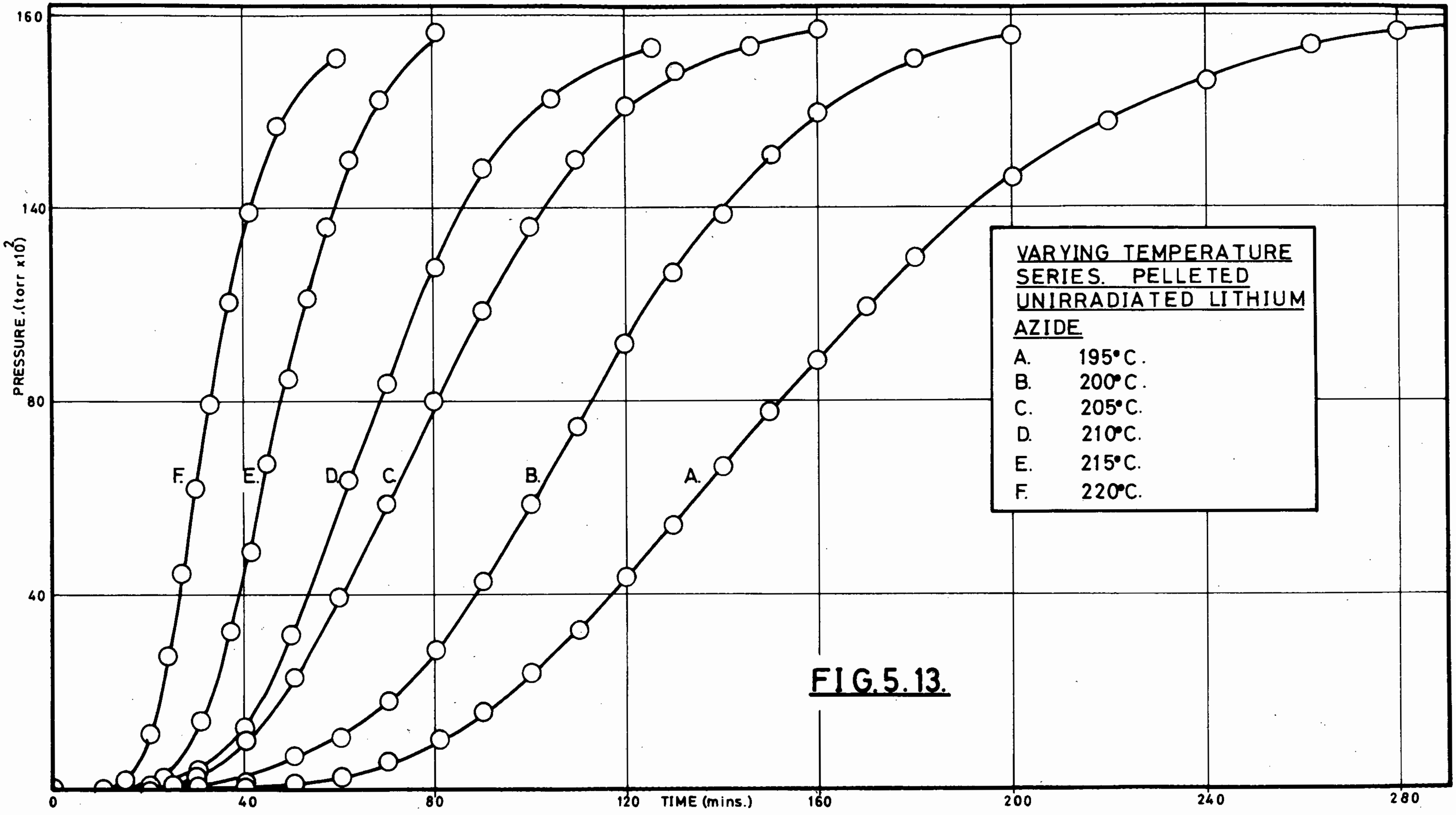
PRESSURE.(torr x10^2)
160
140
80
40
0
40
80
120
TIME (mins.)
160
200
240
280
F.
E.
D.
C.
B.
A.
VARYING TEMPERATURE SERIES. PELLETED UNIRRADIATED LITHIUM AZIDE
A. 195°C.
B. 200°C.
C. 205°C.
D. 210°C.
E. 215°C.
F. 220°C.

FIG.5.13.

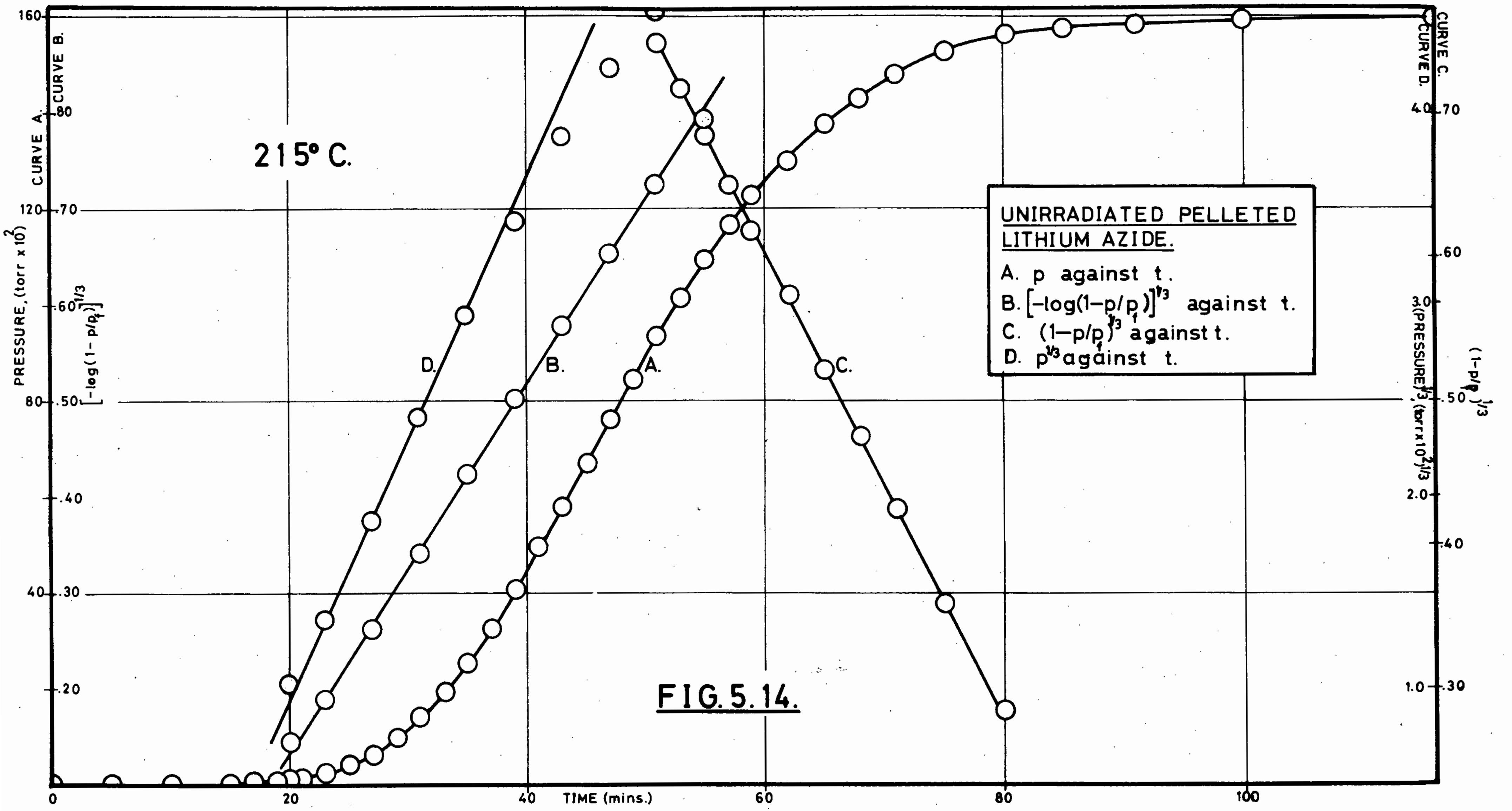
215° C.
UNIRRADIATED PELLETED LITHIUM AZIDE.
A. p against t.
B. $[-\log(1-p/p_f)]^{1/3}$ against t.
C. $(1-p/p_f)^{1/3}$ against t.
D. $p^{1/3}$ against t.
D.
B.
A.
C.
CURVE A.
CURVE B.
PRESSURE, (torr x 10^2)
$[-\log(1-p/p_f)]^{1/3}$
160
120
80
40
.80
.70
.60
.50
.40
.30
.20
CURVE C.
CURVE D.
(PRESSURE)$^{1/3}$, (torr x 10^2)$^{1/3}$
$(1-p/p_f)^{1/3}$
4.0
3.0
2.0
1.0
.70
.60
.50
.40
.30
TIME (mins.)
0
20
40
60
80
100

FIG. 5.14.

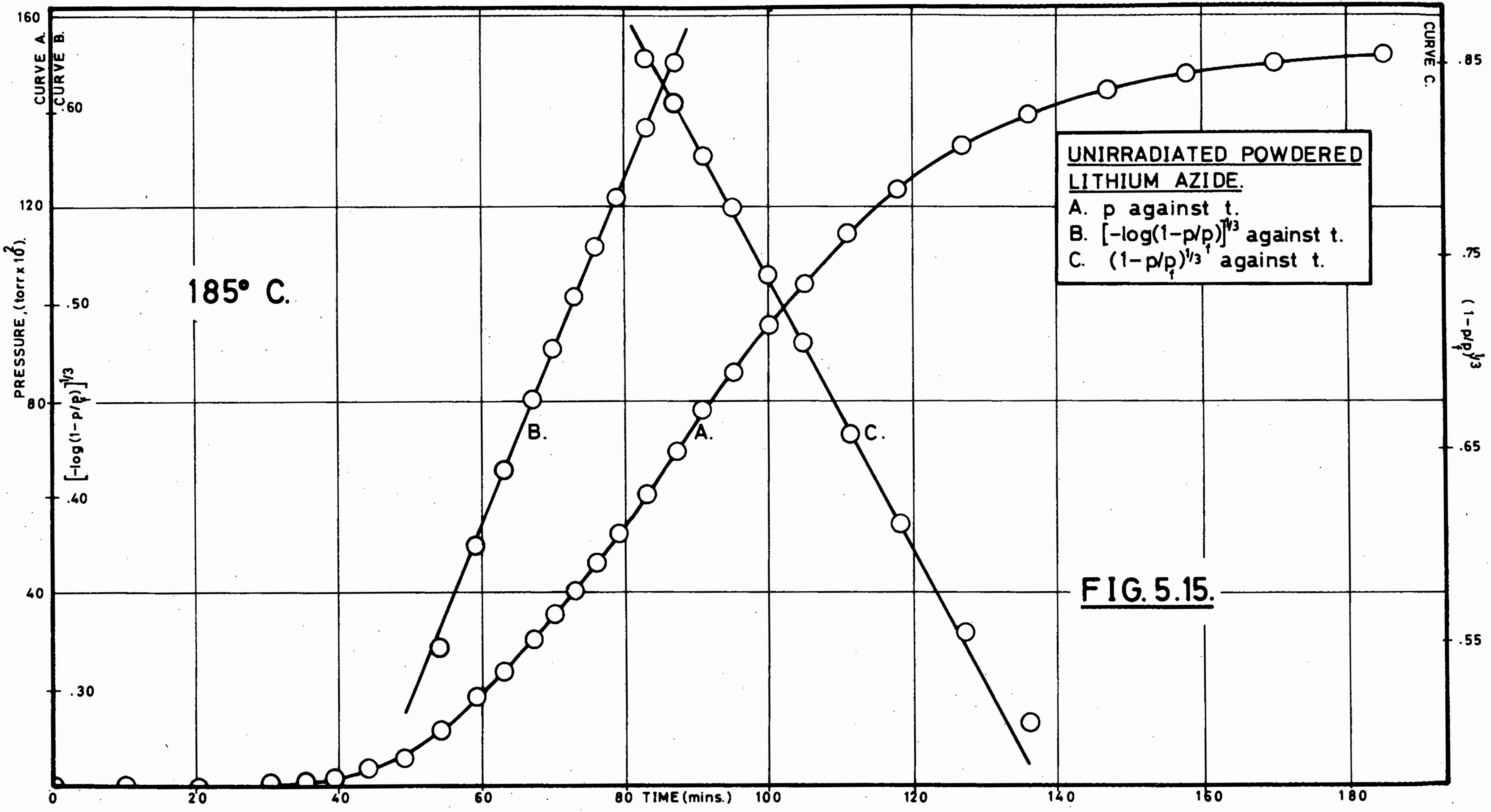
UNIRRADIATED POWDERED LITHIUM AZIDE.
A. p against t.
B. $[-\log(1-p/p_f)]^{1/3}$ against t.
C. $(1-p/p_f)^{1/3}$ against t.
185° C.
CURVE A.
CURVE B.
CURVE C.
PRESSURE, (torr x 10^2).
$[-\log(1-p/p_f)]^{1/3}$
$(1-p/p_f)^{1/3}$
160
120
80
40
.60
.50
.40
.30
.85
.75
.65
.55
0
20
40
60
80
TIME (mins.)
100
120
140
160
180
A.
B.
C.

FIG. 5.15.

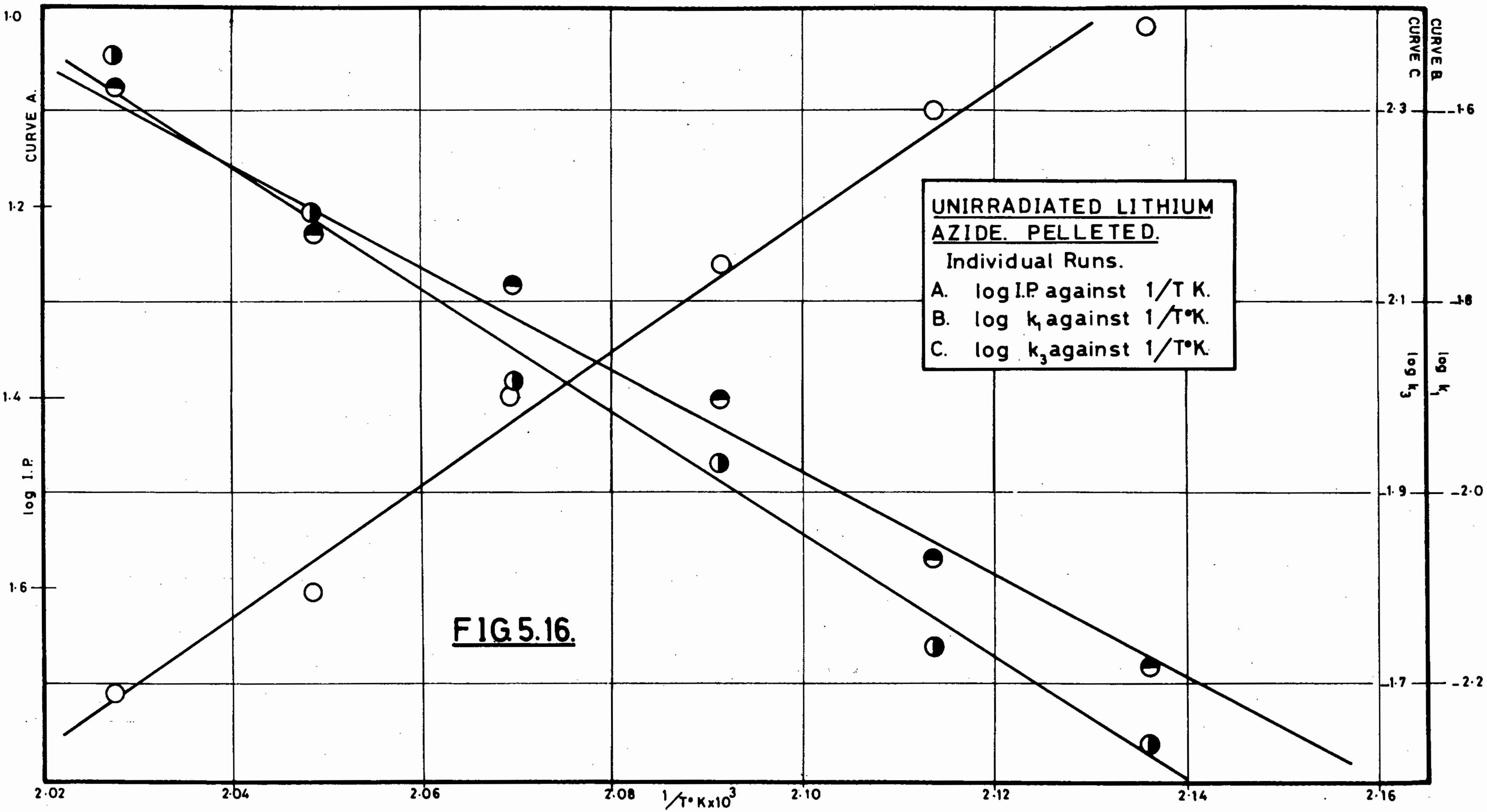
UNIRRADIATED LITHIUM AZIDE. PELLETED.
Individual Runs.
A. log I.P. against 1/T K.
B. log k₁ against 1/T°K.
C. log k₃ against 1/T°K.
CURVE A.
log I.P.
1·0
1·2
1·4
1·6
CURVE C
CURVE B
log k₃
log k₁
2·3
2·1
1·9
1·7
1·6
1·8
2·0
2·2
2·02
2·04
2·06
2·08
2·10
2·12
2·14
2·16
1/T° K×10³

FIG. 5.16.

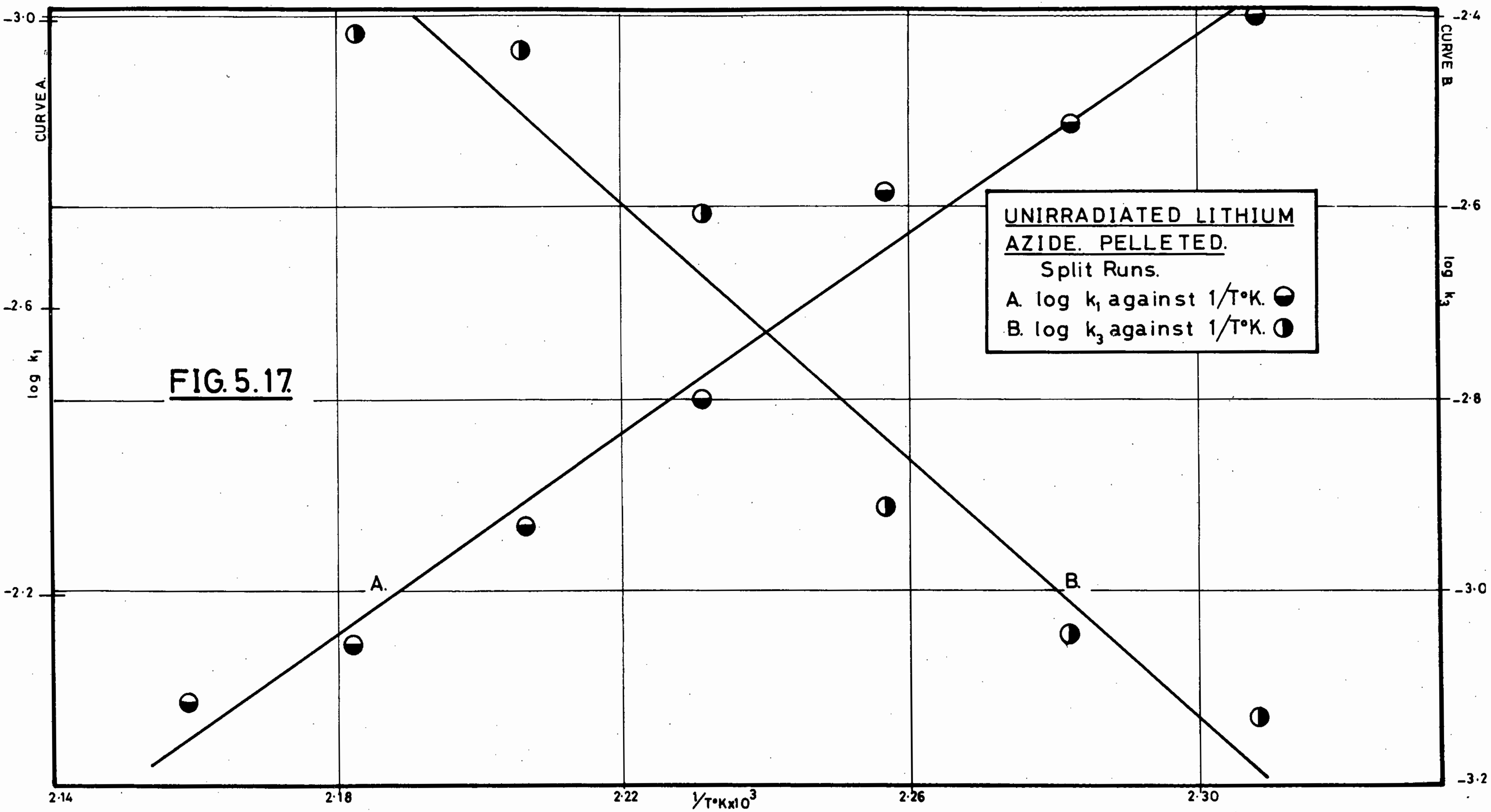
UNIRRADIATED LITHIUM AZIDE. PELLETED.
Split Runs.
A. log k_1 against 1/T°K. ◒
B. log k_3 against 1/T°K. ◑
CURVE A.
log k_1
CURVE B.
log k_3
-3·0
-2·6
-2·2
-2·4
-2·6
-2·8
-3·0
-3·2
2·14
2·18
2·22
2·26
2·30
1/T°K x 10^3
A.
B.

FIG. 5.17

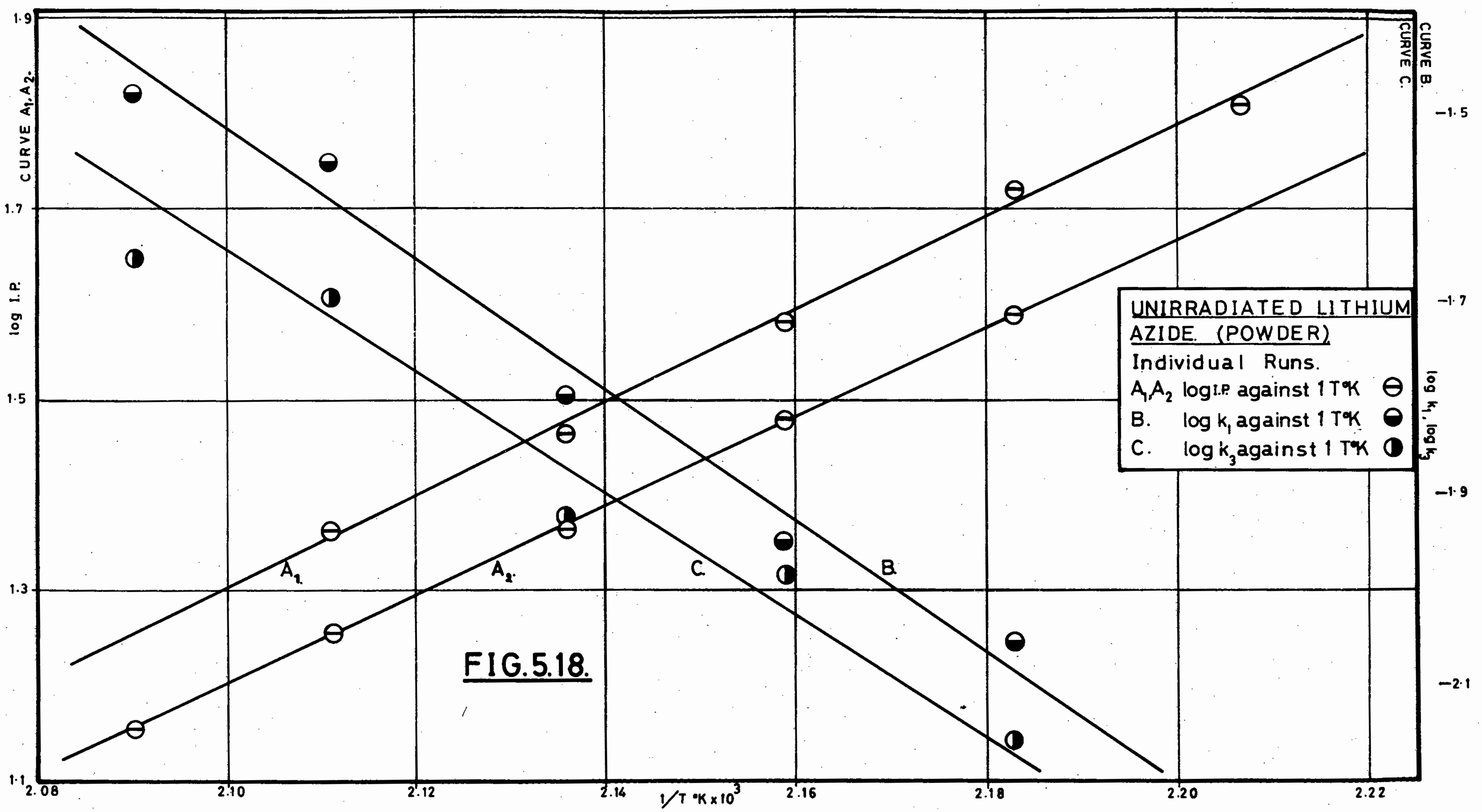
UNIRRADIATED LITHIUM AZIDE (POWDER)
Individual Runs.
A_1, A_2 log I.P. against 1/T °K ⊖
B. log k_1 against 1/T °K ⬓
C. log k_3 against 1/T °K ◐
CURVE A_1, A_2.
log I.P.
CURVE B.
CURVE C.
log k_1, log k_3
1·9
1·7
1·5
1·3
1·1
−1·5
−1·7
−1·9
−2·1
2.08
2.10
2.12
2.14
2.16
2.18
2.20
2.22
1/T °K x 10^3
A_1
A_2.
C.
B.

FIG.5.18.

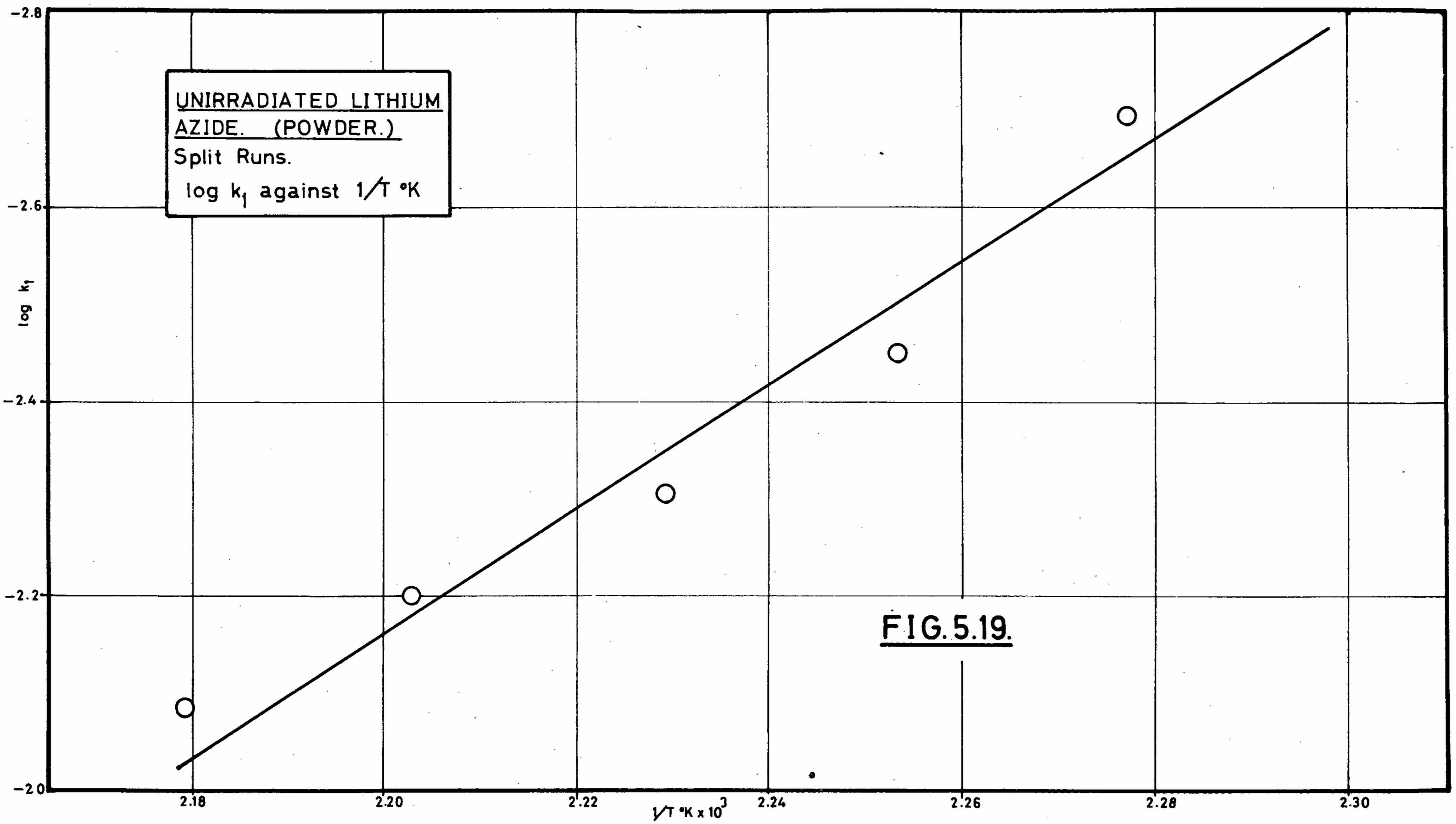
UNIRRADIATED LITHIUM AZIDE. (POWDER.)
Split Runs.
log k_1 against 1/T °K
log k_1
−2.8
−2.6
−2.4
−2.2
−2.0
2.18
2.20
2.22
2.24
2.26
2.28
2.30
1/T °K x 10^3

FIG. 5.19.

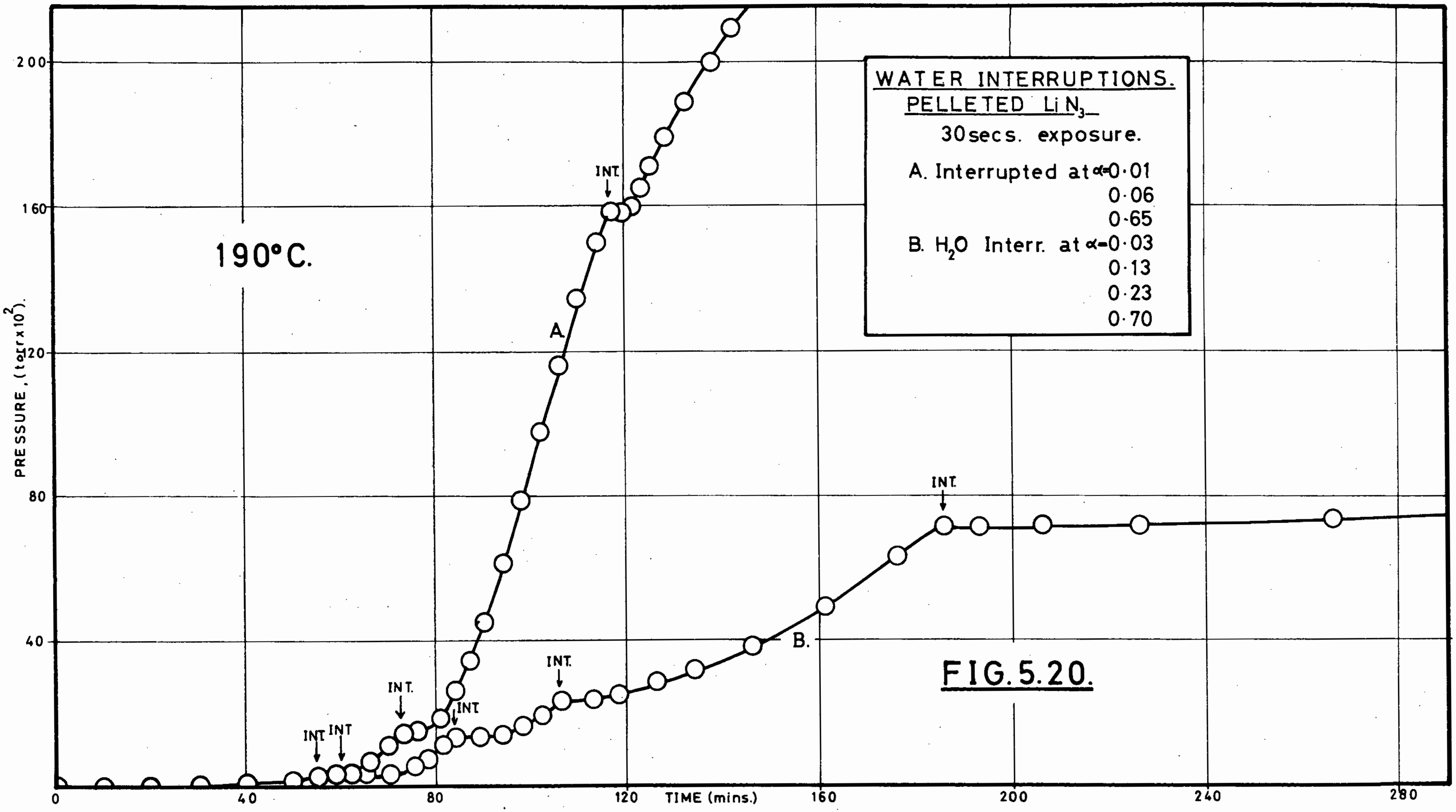
WATER INTERRUPTIONS.
PELLETED LiN_3
30secs. exposure.
A. Interrupted at α=0·01
0·06
0·65
B. H_2O Interr. at α=0·03
0·13
0·23
0·70
190°C.
A.
B.
INT.
INT
INT
INT.
INT
INT.
INT.
INT.
PRESSURE, (torr x 10^2).
200
160
120
80
40
TIME (mins.)
0
40
80
120
160
200
240
280

FIG. 5.20.

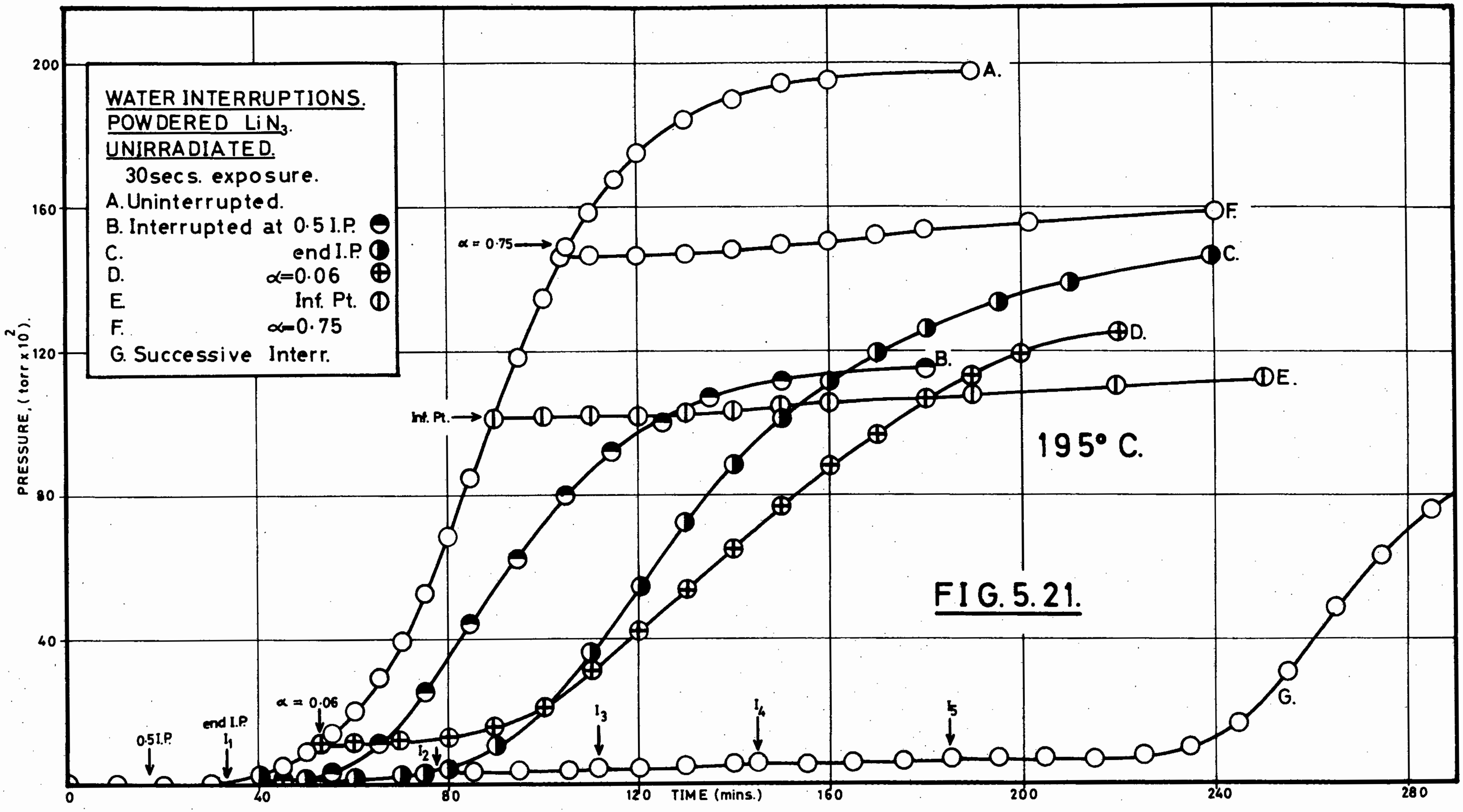
WATER INTERRUPTIONS.
POWDERED LiN3.
UNIRRADIATED.
30secs. exposure.
A. Uninterrupted.
B. Interrupted at 0·5 I.P. ◒
C. end I.P. ◐
D. α=0·06 ⊕
E. Inf. Pt. ⦶
F. α=0·75
G. Successive Interr.
195° C.
PRESSURE, (torr x 10²).
TIME (mins.)
0
40
80
120
160
200
240
280
200
160
120
80
40
A.
B.
C.
D.
E.
F.
G.
α = 0·75
Inf. Pt.
α = 0·06
0·5 I.P.
end I.P.
I1
I2
I3
I4
I5

FIG. 5.21.

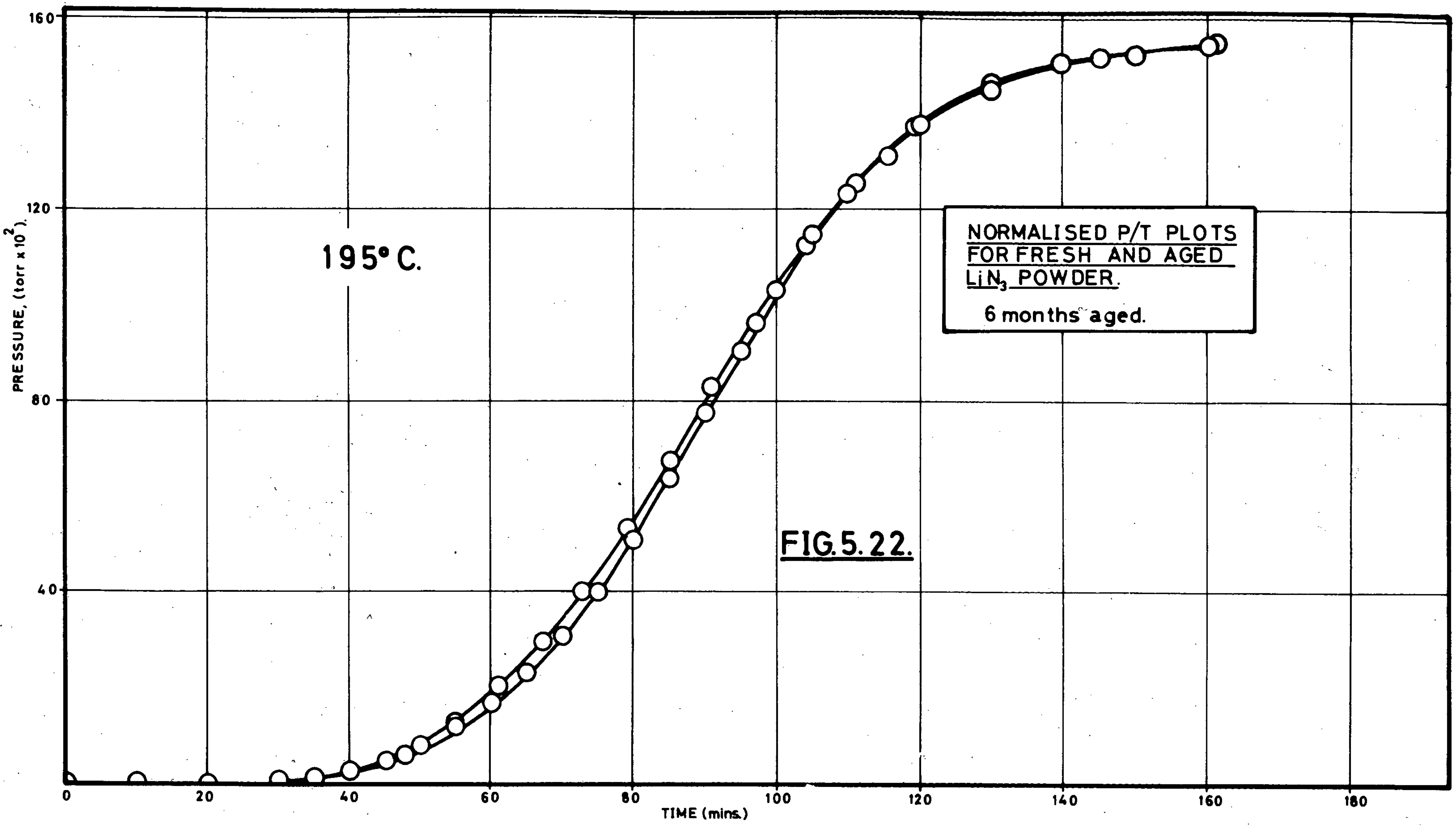

160
120
80
40
PRESSURE, (torr x 10^2).
0
20
40
60
80
100
120
140
160
180
TIME (mins.)
195° C.
NORMALISED P/T PLOTS FOR FRESH AND AGED LiN_3 POWDER.
6 months aged.

FIG. 5. 22.

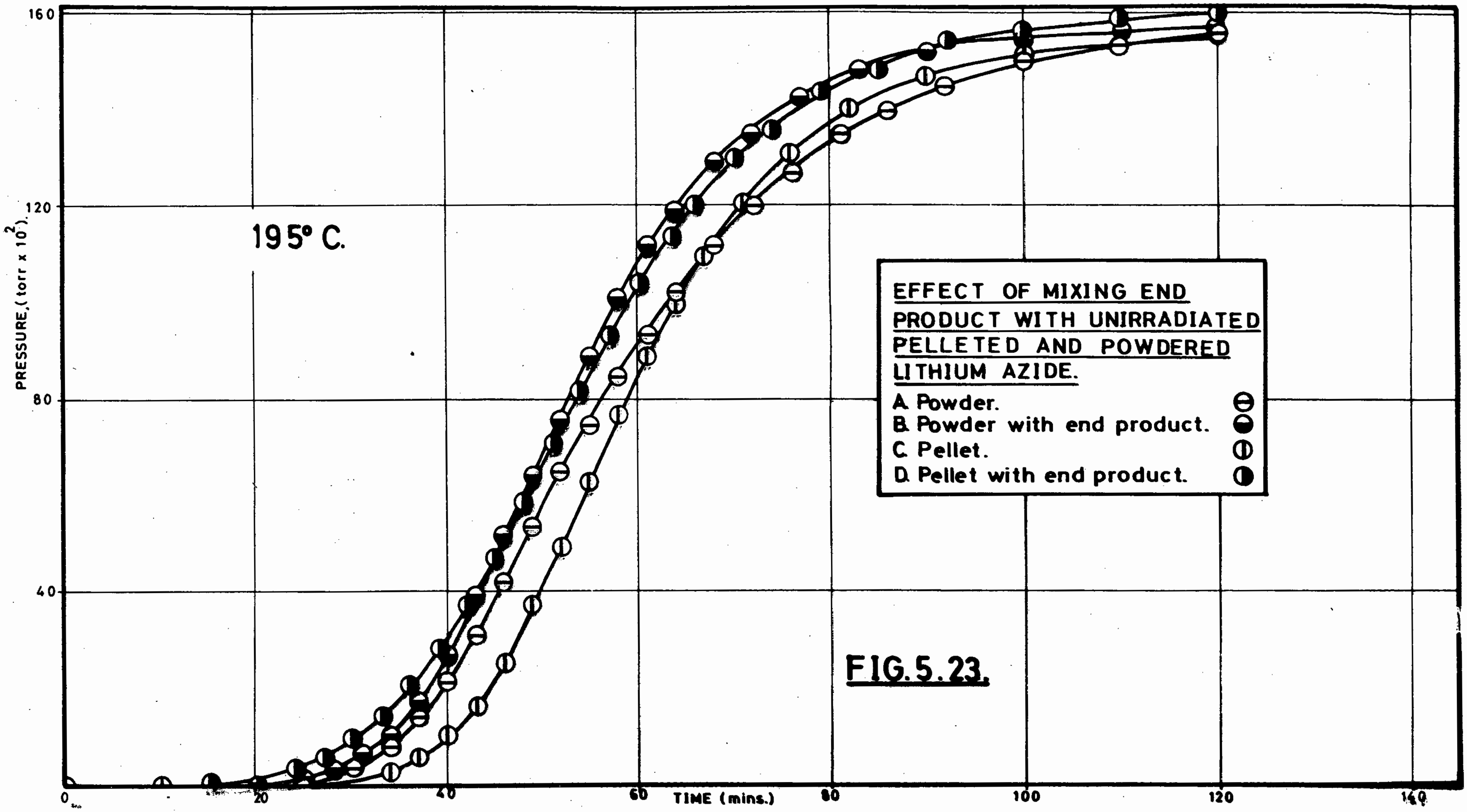

FIG. 5.23.

EFFECT OF MIXING END PRODUCT WITH UNIRRADIATED PELLETED AND POWDERED LITHIUM AZIDE.

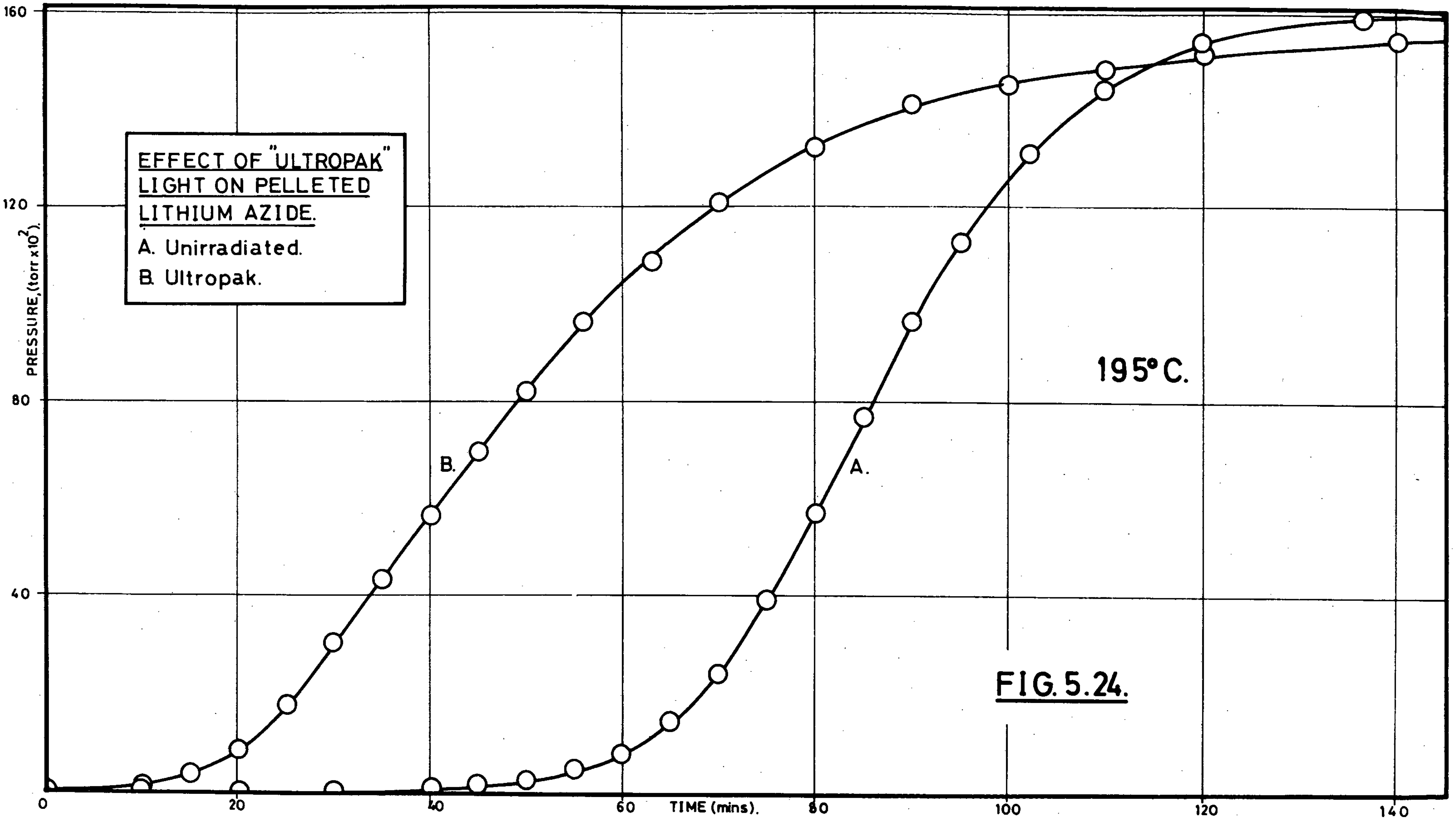
EFFECT OF "ULTROPAK" LIGHT ON PELLETED LITHIUM AZIDE.
A. Unirradiated.
B. Ultropak.
195° C.
B.
A.
PRESSURE, (torr x 10^2).
160
120
80
40
0
20
40
60
80
100
120
140
TIME (mins).

FIG. 5.24.

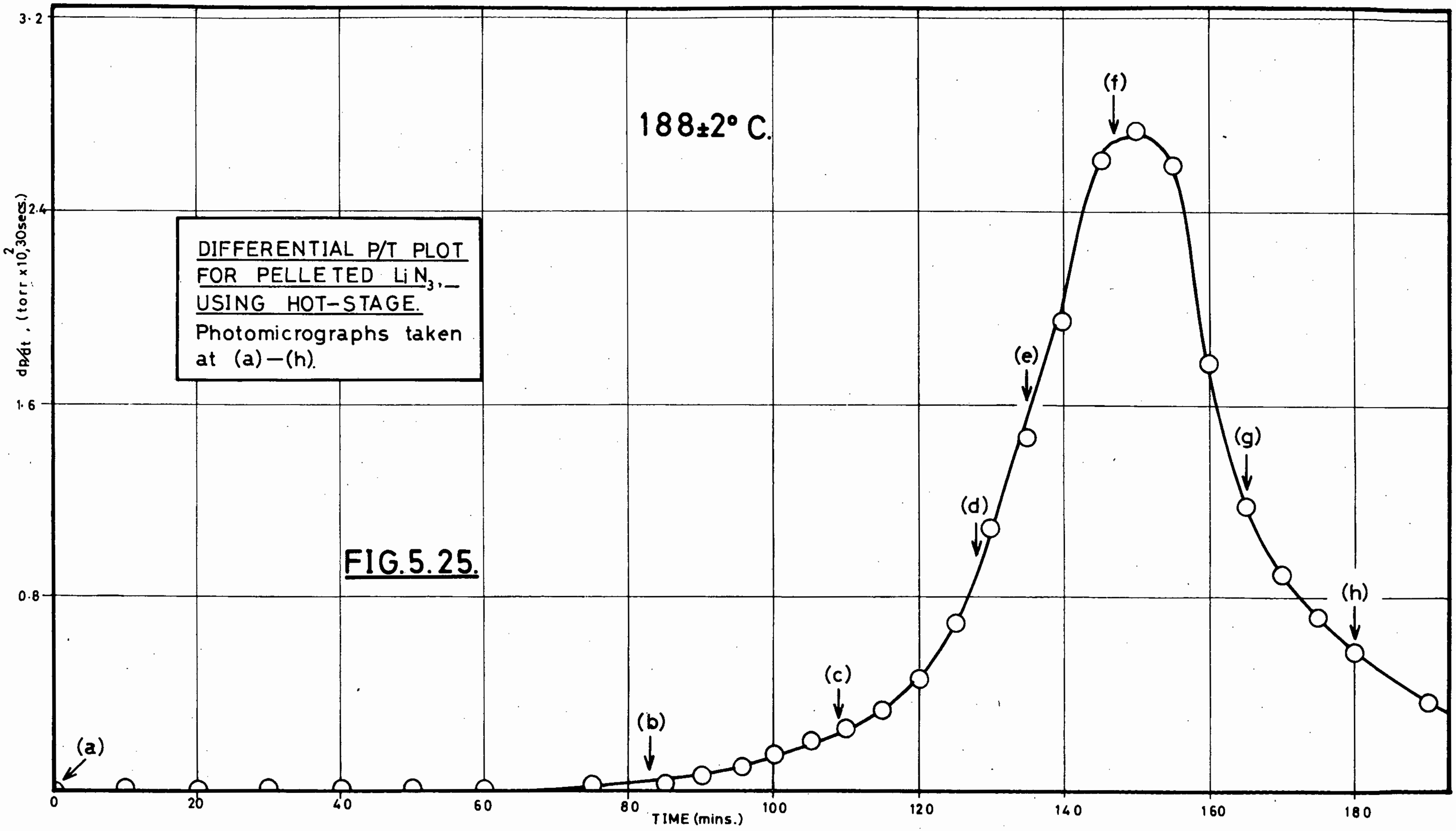

FIG. 5.25.

DIFFERENTIAL P/T PLOT FOR PELLETED LiN_3, USING HOT-STAGE.

Photomicrographs taken at (a)–(h).

6. THERMAL DECOMPOSITION OF LITHIUM AZIDE PRE-IRRADIATED WITH γ-RAYS

6.1 PRELIMINARY INVESTIGATIONS

6.1.1 Pelleted lithium azide

Irradiations were done in sealed, blackened and evacuated Pyrex ampoules as has been described in 4.1.4 and 4.2.3. Initial irradiations with doses of 1.0 and 5.0 roentgens (1 M roentgens = 10^6 roentgens), (characteristic doses for previous studies on the effects of γ-preirradiation on the alkali metal azides), proved to be too large and even at temperatures 30°C lower than the lowest temperature (170°C) used for unirradiated decompositions, the reaction was too fast. The induction period was completely eliminated and rapid decomposition, virtually explosion, occurred at t=1-2 mins. The p/t plot for the thermal decomposition of pelleted lithium azide (pre-irradiated with 5.0 M roentgens) at a low temperature (110°C) is illustrated in FIGURE 6.18. The induction period for the unirradiated material at this temperature was found by extrapolation of the plot of log I.P. against 1/T (°K), (FIGURE 5.16), to be approximately 13 days. The induction period for the run at 110°C of pelleted azide pre-irradiated with a γ-ray dose of 5.0 M roentgens was found to be 25 mins.

The effect of 500 roentgens γ-rays on pelleted material is illustrated in FIGURE 6.1. The reaction temperature was 190°C. The p/t plots show a marked decrease in the length of the induction period followed by the introduction of a sigmoid reaction and a secondary acceleratory and decay stage. The "initial" reaction was of short duration compared to the time for the decomposition to go to completion at the reaction temperature used. The same material that was pre-irradiated with 500 roentgens was used as a blank run for comparative purposes. These results appear in TABLE 6.1.

6.1.2 Powdered lithium azide

As seen in 6.1.1, doses of the order of M roentgens proved unsuitable. Accordingly, powdered lithium azide as was used throughout Section 5, was irradiated with a γ-ray dose of 15000 roentgens. The effects of pre-irradiation with this dose of γ-rays on the subsequent thermal decomposition of lithium azide, together with a blank unirradiated run, appear in FIGURE 6.2 and the results are tabulated in TABLE 6.1. The reaction temperature was 190°C and approximately 5.0mg samples were used.

It is seen that pre-irradiation with 15000 roentgens at the reaction temperature used, drastically affected the thermal decomposition of powdered lithium azide. Pre-irradiation had the effect of eliminating the induction period and greatly increasing the rate of the reaction. The p/t plot was observed to be sigmoid, as was found for unirradiated pelleted and powdered lithium azide in Section 5.

6.2 REPRODUCIBILITY

6.2.1 Pelleted lithium azide

Pelleted lithium azide as used throughout Section 5 was irradiated with a γ-ray dose of 15000 roentgens. The p/t plots for two runs at 175°C are shown in FIGURE 6.3 and the results are tabulated in TABLE 6.2. Approximately 4.6mg pellets were used.

The reproducibility which was found with this type of unirradiated material, was not found. It was observed that double-sigmoid curves as reported above in 6.1.1 were obtained.

In an attempt to overcome this irreproducibility the material used for pelleting, i.e. ground lithium azide (Vibration Mill, 10 mins), was irradiated with a dose of 5000 roentgens and this material then pelleted in the method described previously.

Two runs at 190°C are illustrated in **FIGURE** 6.4 and the results presented in **TABLE** 6.2. The runs were not reproducibile. One pressure-time plot is seen to have the two pronounced acceleratory periods characteristic of the irradiated, pelleted lithium azide described in 6.1.1, while the other p/t plot does not.

It was decided to abandon attempts to obtain reproducible results with γ-irradiated pelleted lithium azide.

6.2.2 Powdered lithium azide

The powdered lithium azide used was the same as was used throughout Section 5. Irradiation of the salt with a dose of 15000 roentgens γ-rays yielded reproducible results for the thermal decomposition.

This was particularly satisfying as this enabled comparison with the previous work on azides where only powdered material had been used.

Four runs at 170°C are shown in **FIGURE** 6.5 and the results presented in **TABLE** 6.2. The pressure-time plots are seen to be smooth and sigmoidal. The induction periods were found to be 9,9,8 and 8 mins in duration. The rate constants k_1 (equation 5.2) for the acceleratory period were calculated to be as follows:

Acceleratory period: 2.07×10^{-2}; 1.98×10^{-2};

2.04×10^{-2} and 2.08×10^{-2}/min respectively.

6.3 RESULTS (POWDERED LITHIUM AZIDE)

ON ACCOUNT OF THE IRREPRODUCIBLE NATURE OF IRRADIATED PELLETED LITHIUM AZIDE, IT WAS DECIDED TO CONFINE THE INVESTIGATIONS OF THE EFFECTS OF γ-RADIATION ON THE THERMAL DECOMPOSITION TO POWDERED LITHIUM AZIDE. SOME INVESTIGATIONS OF THE UNUSUAL P/T PLOT OBTAINED WITH IRRADIATED PELLETED AZIDE WERE INVESTIGATED HOWEVER AND THESE RESULTS ARE REPORTED IN 6.4.

6.3.1 The effect of varying doses of γ-irradiation

The effect of an increasing dose of γ-rays on the subsequent thermal decomposition of lithium azide is illustrated in **FIGURE** 6.6 and the p/t values appear in **TABLE** 6.3. The decomposition temperature was lowered to 170°C (from 190°C - 195°C at which most of the previous runs were done on unirradiated lithium azide) due to the extreme sensitivity of the azide to γ-irradiation. The decomposition temperature (170°C) was constant throughout the series. The γ-ray doses used were 10, 50, 250, 500, 1500, 5000, 15000 and 700000 roentgens.

A marked decrease and virtual elimination of the induction period was observed for large doses. The inflexion point was at $\alpha = 0.35$ approximately throughout the irradiated series. The acceleratory and decay rates increased with increasing dose.

The acceleratory rate constants k_1 (equation 5.2) together with the decay period rate constants k_3 (equation 5.3) and the induction periods (mins) for the various pre-irradiation doses are given in the table below. The rate constants for the decomposition of the unirradiated salt at this temperature were obtained by extrapolation of the unirradiated activation energy plots.

DOSE (roentgens)	INDUCTION PERIOD (mins)	ACCELERATORY RATE CONSTANT, k_1, (mins^{-1})	DECAY RATE CONSTANT, k_3, (mins^{-1})
0	120	2.34×10^{-3}	2.19×10^{-3}
10	86	2.51×10^{-3}	2.27×10^{-3}
50	61	3.66×10^{-3}	2.85×10^{-3}
250	33	8.25×10^{-3}	3.95×10^{-3}
500	25	1.15×10^{-2}	6.35×10^{-3}
1500	12	1.39×10^{-2}	1.25×10^{-2}

5000	9	1.62×10^{-2}	2.06×10^{-2}
15000	7	2.55×10^{-2}	4.44×10^{-2}
700000	2	-	-

6.3.2 The effect of varying the temperature of decomposition

The mathematical equations applied and the rate constants derived in this part of the work are discussed below in 6.3.3 and 6.3.4.

The critical increments for the chemical process(es) occurring in lithium azide pre-irradiated with a γ-ray dose of 15000 roentgens were determined using the individual and split-run techniques.

The activation energies associated with the acceleratory and decay periods were determined using the individual runs method, while the split-run technique was used as an additional method of estimating the activation energy for the acceleratory period. The rate constants k_1 and k_3 (equations 5.2 and 5.3) were determined over the temperature range 140° - 170°C in the former method and the rate constant k_1 in the latter case was determined over the temperature range 145° - 165°C.

As a preliminary to this study it was shown that no effect was observed on interrupting the decomposition of γ-irradiated lithium azide (see below 6.3.5).

Approximately 4.5 - 5.5 mg of the salt pre-irradiated with a γ-ray dose of 15000 roentgens, were used for the decomposition runs.

Even at 140°C the duration of the induction period was only 20 mins and accordingly a series of runs over a lower temperature range than that used above was necessary to determine the effect of varying the temperature of decomposition. The length of the induction period was examined over the range 121° - 144°C and was found to be 65 - 17 mins. The method employed for recording the induction period in a series of runs in this manner was to allow the decomposition to proceed to 4 x 10^{-2} torr at a particular temperature, after which the temperature was raised to 215°C for 1½ hours to obtain the p_a.

The p/t results for the above runs appear in TABLE 6.4. The derived rate constants k_1 and k_3 (equations 5.2 and 5.3) and the lengths of the induction periods appear in the table below.

INDIVIDUAL or SPLIT RUNS	TEMP. °C	INDUCTION PERIOD (mins)	k_1 (mins^{-1})	k_3 (mins^{-1})
Indiv.	121.3	65	-	-
	126.0	49	-	-
	130.1	37	-	-
	135.3	29	-	-
	140.1	21	-	-
	144.4	17	-	-
Indiv.	140.8	-	4.30 x 10^{-3}	4.90 x 10^{-3}
	145.0	-	5.18 x 10^{-3}	5.85 x 10^{-3}
	150.3	-	6.83 x 10^{-3}	8.85 x 10^{-3}
	155.0	-	9.54 x 10^{-3}	1.48 x 10^{-2}
	160.0	-	1.57 x 10^{-3}	2.31 x 10^{-2}
	170.0	-	2.76 x 10^{-3}	4.44 x 10^{-2}
Split	144.9	-	2.19 x 10^{-3}	-
	150.5	-	3.66 x 10^{-3}	-
	154.8	-	4.70 x 10^{-3}	-
	159.5	-	6.56 x 10^{-3}	-
	165.0	-	8.42 x 10^{-3}	-

6.3.3 Mathematical analysis of the results

Typical p/t plots of lithium azide pre-irradiated with a γ-ray dose of 15000 and 0.7 M roentgens at 170°C and 130°C respectively, appear in FIGURE 6.7 and 6.8. The mathematical analysis is shown. The p/t results appear in TABLE 6.5. The main features of the curves are similar to those found for the p/t plots of unirradiated lithium azide. The inflexion points are at $\alpha = 0.38$ and $\alpha = 0.34$ respectively.

Evaluation of the activation energy associated with the induction period for material pre-irradiated with a γ-ray dose of 15000 roentgens was done using the lengths of the induction periods at various temperatures as rate constants.

The acceleratory period is defined by the Avrami-Erofeyev equation with the exponent n taking the value 3 for γ-ray doses up to and including 15000 roentgens, i.e.:

$$\left[-\log\left(1 - {}^{p}/_{p_f}\right)\right]^{1/3} = k_1 t + C \quad \ldots\ldots\ldots\ldots\ldots (5.2)$$

For pre-irradiation with γ-ray doses of greater than 0.7 M roentgens the integer n is 2 i.e.:

$$\left[-\log\left(1 - {}^{p}/_{p_f}\right)\right]^{1/2} = k_2 t + C \quad \ldots\ldots\ldots\ldots\ldots (6.1)$$

The fit for lithium azide pre-irradiated with a dose of 15000 roentgens (equation 5.2) is over the range $0.01 < \alpha < 0.39$.

The decay period is described by the contracting sphere equation (equation 5.3) over the whole range of γ-ray doses. The equation was found to hold from the inflexion point of the pressure-time plot ($\alpha = 0.38$ for 15000 roentgens) to $\alpha = 0.74 - 0.84$.

The Avrami-Erofeyev equation (for the doses studied) and the contracting sphere equation were found to be applicable in the mathematical analysis of γ-irradiated lithium azide over the temperature range 115° - 190°C.

6.3.4 Evaluation of the activation energies

The critical increments for the chemical process(es) occurring in the thermal decomposition of lithium azide pre-irradiated with a γ-ray dose of 15000 roentgens were obtained by applying the Arrhenius equation. For the determination of the activation energy for the induction period, the logarithms of the lengths of the induction periods were plotted against $1/T$ ($^{\circ}K$) as described before in Section 5.3.3.

The values of the activation energies and the methods of determination of rate constants are as follows:

(i) Induction period: 20 k.cals/mole (Individual)
(ii) Acceleratory period: 26 k.cals/mole (Individual)
24 k.cals/mole (Split-run)
(iii) Decay period : 28 k.cals/mole (Individual)

The plots of log I.P., log k_1 and log k_3 against $1/T$ ($^{\circ}K$) are to be found in FIGURE 6.9 and FIGURE 6.10.

6.3.5 The effect of interrupting a thermal decomposition

The decomposition of lithium azide pre-irradiated with a γ-ray dose of 15000 roentgens showed no effect on continuing the run after interruption for 30mins at the end of the induction period, in the acceleratory period and in the decay period. A small time lag of 2 - 3 mins, due to the bucket and contents attaining reaction temperature, was observed.

6.3.6 The effect of interrupting a thermal decomposition and irradiating the salt

The method used and the preparations taken in performing this type of experiment have been described in 4.2.6. A platinum bucket was generally employed for all the decompositions, but for the interruption and irradiation of the salt it was necessary to use Pyrex buckets. Two runs done at 170°C using lithium azide pre-irradiated with 15000 roentgens γ-rays and using platinum and Pyrex buckets, showed no effect on the subsequent thermal decomposition. These results appear in **TABLE** 6.6.

On account of the extreme shortening of the induction period of unirradiated lithium azide on irradiating with γ-rays, it was not possible to arrange experimental conditions so that a blank irradiated decomposition at a reaction temperature of 175°C would have an induction period of length $>$ 30 mins and a maximum reaction rate significantly greater than that for unirradiated lithium azide at the same temperature. Accordingly, two γ-ray doses were chosen so that (i) at 175° the p/t plot of the irradiated salt would have a significant induction period and (ii) that at 175° the rate of the irradiated decomposition would be considerably greater than the rate of reaction for unirradiated azide. The γ-ray doses used were (i) 200 and (ii) 1000 roentgens.

(i) <u>Interruption followed by γ-irradiation (200 roentgens)</u>. The thermal decomposition of approximately 5.0mg unirradiated lithium azide was interrupted at $\alpha = 0.23$ and the salt irradiated with γ-rays (200 roentgens). On continuing the decomposition an induction period of duration approximately 17 - 18 mins was observed, after which time the reaction accelerated at an enhanced rate. Blank runs of the same material pre-irradiated with γ-rays (200 roentgens) and unirradiated were also done. The blank run using pre-irradiated azide, showed the salt to have an induction period of 40 mins.

The p/t values for these runs appear in **TABLE** 6.7 and the runs are graphically illustrated in **FIGURE** 6.11.

(ii) <u>Interruption followed by γ-irradiation (1000 roentgens)</u>. Approximately 5.0mg specimens were used for a decomposition run. The decomposition was interrupted at various stages of the reaction and the sample irradiated with γ-rays (1000 roentgens). Interruptions were made at 0.5 I.P., at the end of the I.P. (induction period), at $\alpha = 0.18$, 0.37, 0.47 and 0.78. Blank runs were done at the same temperature (175°) using the same unirradiated and irradiated lithium azide.

At points on the p/t plot up to and including the inflexion point of the unirradiated blank run, interruption followed by irradiation of the azide resulted in a new, short induction period (10 - 12 mins) followed by a period of rapid and increased acceleration. Interruption and irradiation after the inflexion point at $\alpha = 0.50$ (i.e. in the decay period) had virtually no effect on the subsequent thermal decomposition.

These results appear in TABLE 6.7. At the point of interruption and irradiation of the salt, the word "Interruption" is written in the table. The results are graphically presented in FIGURE 6.12.

6.3.7 The effect of admitting water vapour onto the salt in an interrupted decomposition

The general technique followed in the "water interruption" runs has been described in 4.2.5. All the results presented in this section (6.3.7) are not normalised to illustrate the effects of the water interruptions on the p_a.

The effects of exposure to water vapour for 30 secs on the thermal decomposition of γ-irradiated lithium azide (15000 roentgens), was investigated.

The effect of longer exposure (5 mins) at $t = 0$ and re-irradiation of lithium azide was also investigated.

(i) 30 secs exposure to water vapour. Approximately 5.0mg of lithium azide was used for a decomposition run. The reaction temperature was 165°C. Water interruptions (30 secs) were done at t = 0, at 0.5 I.P., at the end of the I.P., at $\alpha = 0.24$, 0.47 and 0.66 on lithium azide pre-irradiated with γ-rays (15000 roentgens). A blank run using the irradiated material, with no interruption, was also done.

There was no change of the p/t plot for 30 secs. exposure at t = 0 and the rate constant for the acceleratory period was not affected. For interruptions at 0.5 I.P. and beyond new induction periods were formed. The rate constant k_1 (equation 5.2) was observed to decrease for all interruptions beyond t = 0. After water interruption at $\alpha = 0.50$, virtually no decomposition was observed on continuing the run.

Since interruption at the end of the induction period resulted in a new induction period, the run was interrupted at the end of the second induction period and the sample again exposed to water vapour. A further induction period was formed on continuing the decomposition and at the end of this induction period, a further water interruption was done. The procedure of decomposition followed by interruption and exposure to water vapour (30 secs) was done for the fourth time and the reaction then allowed to proceed to completion. The p_a was found to be low at 165°C, but on raising the temperature to 215°C for 2 hours, the value doubled. The p_a obtained after this procedure was approximately 100×10^{-2} torr, which is 66% of the final pressure value obtained using a blank irradiated run.

The final pressures (p_a) in all the interrupted runs were lower than for the blank decomposition. Heating to 400°C enabled recovery of a percentage (35-45%) of the lost gas.

The p/t results appear in TABLE 6.8 and are graphically illustrated in FIGURE 6.13. The lengths of the induction periods, values of the derived rate constants and p_a values appear in the table below.

(ii) 5 mins exposure to water vapour. The effect of interrupting the thermal decomposition of γ-irradiated lithium azide (15000 roentgens) at $t = 0$ (i.e. prior to the thermal decomposition) and exposing the specimen to water vapour for 5 mins, was studied. The sample was then decomposed after pumping for 10 hours, at 180°C. Approximately 5.0mg of the salt was used for this run and for a blank, uninterrupted unirradiated decomposition.

The effect of interrupting the run was to introduce an induction period of the same duration, (73 mins), as found for unirradiated lithium azide at the same at the same temperature. The rate constant for the acceleratory reaction was lower than that for the unirradiated salt and the Avrami-Erofeyev equation with $n = 3$ was applicable, as previously found. The percentage decomposition was observed to be lower than after exposure for 30 secs at $t = 0$, above.

These results are graphically illustrated in **FIGURE** 6.14 and the p/t values for the runs appear in **TABLE** 6.8. The results are not normalised, as mentioned above.

Since 5 mins exposure to water vapour at $t = 0$ appeared to destroy the irradiation effect, the interrupted irradiated lithium azide which had been exposed to water vapour (5 mins) at $t = 0$, was re-irradiated with γ-rays (15000 roentgens). Decomposition of this material showed the p/t plot to exhibit the features of the normal decomposition characteristics of pre-irradiated lithium azide. Interruption and exposure to water vapour at $t = 0$ (5 mins) of another specimen of the re-irradiated material, followed by thermal decomposition, resulted once again in the formation of an induction period of approximately the same duration as that for unirradiated lithium azide (29 mins) at the same temperature.

A specimen of the material that had been re-irradiated and interrupted at $t = 0$, was irradiated with a further dose of γ-rays (15000 roentgens) and the subsequent thermal decomposition displayed a p/t plot with similar features as found for the previous irradiated specimens and interruption of a specimen of this material at $t = 0$ (5 mins) once again showed the irradiation effects to be destroyed when the thermal decomposition was carried out. The p/t plot approximated that of the unirradiated material. When a specimen of this material, which had been taken through three cycles of irradiation followed by 5 mins exposure to water vapour at $t = 0$, was irradiated for the fourth time (15000 roentgens) and interrupted at $t = 0$ (5 mins), similar p/t plots as found previously were obtained for the irradiated and the interrupted specimens.

The reaction temperature for these runs was 195°C and approximately 4.6 - 5.0 mg specimens were used for a decomposition run. These p/t results and those for a blank unirradiated run appear in TABLE 6.8 and the values of the derived rate constants k_1 (equation 5.2) for the acceleratory period after water interruption, the percentage decomposition and lengths of the induction periods appear in the table below.

Specimen	Exposure (mins)	Temp °C	Point of Interruption	Induction Period after interruption (mins)	k_1 (mins^{-1})	Percent Decomp.
Irradiated (15000r)	Blank	165	-	10	2.44×10^{-2}	81
"	0.5	"	t=0	10	2.38×10^{-2}	74
"	"	"	0.5 I.P.	23	1.55×10^{-2}	49
"	"	"	End I.P.	29	1.09×10^{-2}	52
"	"	"	$\alpha = 0.24$	31	1.11×10^{-2}	50
"	"	"	$\alpha = 0.47$	-	-	58
"	"	"	$\alpha = 0.66$	-	-	53
"	"	"	Successive	34 54		

Specimen	Exposure (mins)	Temp ^{o}C	Point of Interruption	Induction period after interruption (mins)	k_1 (mins^{-1})	Percent. Decomp.
				103 150	-	58
Unirrad.	Blank	180	-	71	$6.94x10^{-3}$	90
Irradiated	5	"	t = 0	73	$4.72x10^{-3}$	57

Specimen	Induction Period after interruption (mins)	k_1 (mins^{-1})	Percentage Decomposition
Blank (unirradiated)	29	1.38×10^{-2}	102
1st t = 0 interruption	35	6.80×10^{-3}	89
2nd t = 0 interruption	34	7.21×10^{-3}	79
3rd t = 0 interruption	21	7.66×10^{-3}	74
4th t = 0 interruption	36	8.16×10^{-3}	17

6.3.8 The effect of thermal annealing

Lithium azide pre-irradiated with γ-rays (15000 roentgens) was thermally annealed at 125^{o}C for 3/4 hour in the vacuum line with the pumps in operation. The specimen was further pumped for ten hours, the temperature raised and the run done in the normal manner at 165^{o}C. No change was observed in the normal decomposition, after thermal annealing of the pre-irradiated azide.

6.3.9 Percentage decomposition

The percentage decomposition as described in 5.3.6 of the runs used for the varying temperature series of γ-irradiated lithium azide was found to be as follows:

(i) Results from varying temperature series, (temperature in brackets):

86 (140°); 103 (145°); 115 (150°); 99 (155°); 68 (160°);
85 (170°); **MEAN:** 93%

(ii) Series for induction period determination:

64 (121°); 83 (126°); 109 (130°); 100 (135°); 82 (140°);
93 (144°); **MEAN:** 91%

The percentage decomposition of lithium azide, pre-irradiated with a γ-ray dose of 0.7 M roentgens was found to be as follows:

88, 80, 85 (130°C) **MEAN:** 84%

6.3.10 Visual observations

As for the unirradiated salt, these observations centred upon the colour of the salt at various stages of the decomposition.

(i) It was observed that for doses used in this work (≯15000 roentgens) no colour change resulted from pre-irradiation with γ-rays. However, for larger doses (0.7 M roentgens) a light buff colouration was observed.

(ii) The powdered lithium azide displayed similar colour changes during the course of the thermal decomposition, as found for the unirradiated salt, Up to the end of the induction period the material was white but immediately past this point, the material turned grey. From the inflexion point onwards the material changed in colour to an increasing dark red-brown.

6.4 RESULTS (PELLETED LITHIUM AZIDE)

6.4.1 The effect of varying doses of γ-irradiation

The effect of an increasing dose of γ-rays on the thermal decomposition of pelleted lithium azide is illustrated in FIGURE 6.15 and the p/t results appear in TABLE 6.9. γ-ray doses of 0, 50, 250, 500, 5000, 15000 and 1.0 M roentgens were used. A marked decrease in the induction period followed by the introduction of a sigmoid character and the second acceleratory and decay periods was observed for doses greater than 50 roentgens. The large dose (1.0 M roentgens) eliminated the initial reaction and the p/t plot shows the reaction to commence at nearly maximum rate. Approximately 5.0mg pellets were used. The reaction temperature was 190°C.

The rate of the initial reaction was observed to increase with increasing dose up to 15000 roentgens. The inflexion point ($\alpha = 0.13$) for the initial reaction was approximately the same for the 500 and 15000 roentgens runs.

6.4.2 The effect of interrupting a thermal decomposition

The decomposition of pelleted lithium azide pre-irradiated with 15000 roentgens γ-rays, showed no effect on continuing the reaction after interruption for 30 mins at the end of the induction period, in the 1st acceleratory period and in the 2nd decay period. A small time lag as described earlier (6.3.5), was observed.

6.4.3 The effect of varying the temperature of decomposition

The rate constants for the acceleratory and decay periods of the γ-irradiated pelleted azide were obtained by the split run technique on account of the irreproducibility of decomposition using separate pellets. This method has been described earlier in 5.3.1 (2). The activation energies for the induction period were obtained by the individual runs method. The decomposition was allowed to proceed to 4×10^{-2} torr at a particular temperature, after which the temperature was raised to 215°C for 1½ hours to obtain the p_a.

Such studies were made on pelleted azide, pre-irraidated with γ-ray doses of 50 and 15000 roentgens.

(a) 50 roentgens. Approximately 4.8 - 6.4mg pellets were used for the individual runs to determine the temperature effect on the induction period over the temperature range 165° - 185°C. An 11.0mg pellet was used to determine the activation energy of the acceleratory period by the split-run technique. The temperature range was 161° - 185°C. A 4.4mg pellet was used to determine the activation energy of the decay period by the split run technique over the temperature range 157° - 182°C.

A complete decomposition at a fixed temperature was analysed to check the applicability of the mathematical analyses. The reaction temperature was 190°C. The p/t results for this run appear in TABLE 6.9 (varying dose series).

(b) 15000 roentgens. The pressure-time curves for lithium azide pre-irradiated with a γ-ray dose of 15000 roentgens exhibited a double sigmoid character, as mentioned in 6.1.1. For the determination by individual runs of the effect of varying temperature on the induction period over the range 126° - 146°C, approximately 4.4 - 6.9mg pellets were used.

A decomposition where the reaction was taken to completion at a fixed temperature, 175°C, was done to check the applicability of the mathematical analyses in the split runs used in the following series.

For the determination of the critical increment for the acceleratory period an 11.0mg pellet was used and rate constants were determined for each temperature over the range 115° - 130°C. The first decay and second acceleratory periods could not be satisfactorily examined by the split-run technique because of the overlap of these reactions and the difficulty involved in obtaining a reliable estimate of the p_a for the initial reaction.

The results for the second decay period (over the temperature range 160° - 190°) were obtained using a 5.0mg pellet.

The p/t results for the above runs (50 and 15000 roentgens) appear in TABLE 6.10 and the lengths of the induction periods and the derived rate constants k_2 and k_3 (equations 5.2, 6.1 and 5.3) for the acceleratory and decay periods respectively, appear in the table below.

Specimen	Individual or Split runs	Temp. °C	Induction period (mins)	k_1 (mins^{-1})	k_3 (mins^{-1})
50r	Indiv.	165.0	39	-	-
		170.0	28	-	-
		175.0	23	-	-
		180.0	17	-	-
		185.0	13	-	-
50r	Split	160.4	-	4.96×10^{-4}	-
		170.0	-	1.50×10^{-3}	-
		175.3	-	2.43 X 10^{-3}	-
		185.0	-	4.64×10^{-3}	-
50r	Split	157.0	-	-	7.08×10^{-4}
		162.0	-	-	1.06×10^{-3}
		167.0	-	-	1.49×10^{-3}
		172.0	-	-	2.41×10^{-3}
		182.0	-	-	3.10×10^{-3}
15000r	Indiv.	126.0	55	-	-
		131.7	41	-	-
		135.7	30	-	-

Specimen	Individual or Split runs	Temp. °C	Induction period (mins)	k_1 (mins^{-1})	k_3 (mins^{-1})
15000r	Indiv.	140.4	23	-	-
		145.5	18	-	-
15000r	Split	114.7	-	5.18×10^{-4}	-
		120.7	-	8.43×10^{-4}	-
		125.0	-	1.28×10^{-3}	-
		130.0	-	1.53×10^{-3}	-
15000r	Split	160.0	-	-	2.04×10^{-2}
		170.0	-	-	4.44×10^{-2}
		180.0	-	-	7.91×10^{-2}
		190.0	-	-	1.38×10^{-1}

6.4.4 Mathematical analysis of the results

(a) 50 roentgens. A typical p/t plot of the decomposition of pelleted lithium azide, pre-irradiated with a γ-ray dose of 50 roentgens showing the extent of fit of the mathematical analyses appears in FIGURE 6.16 and the p/t results appear in TABLE 6.9. The inflexion point was at $\alpha = 0.35$.

The marked features of this plot are the same as those for the unirradiated lithium azide pelleted material i.e. (i) a well defined induction period with no evolution of gas, followed by (ii) an acceleratory period and (iii) a decay period.

As was found for unirradiated lithium azide, no mathematical analysis of the induction period was possible since no gas was evolved. For evaluation of the activation energy associated with the induction period, the duration of the induction periods at various decomposition temperatures were used.

The acceleratory period was well described by the Avrami-Erofeyev equation (equation 5.2) with $n = 3$. The degree of fit was such that the whole of the acceleratory period over the range $0.05 < \alpha < 0.35$ was described by the equation.

The decay period was well defined by the contracting sphere equation (equation 5.3). The extent of fit was over the range $0.30 < \alpha < 0.80$.

(b) <u>15000 roentgens</u>. A typical pressure-time plot for the decomposition of pelleted lithium azide, pre-irradiated with a γ-ray dose of 15000 roentgens showing the extent of fit of the mathematical analyses, is given in FIGURE 6.17 and the p/t results appear in TABLE 6.10. The reaction temperature was 175°C.

The main features of the curve are (i) no induction period at the reaction temperature 175°C, other than a small heating lag, (ii) a marked acceleratory period (iii) a decay period (iv) a second acceleratory period and (v) a well defined decay period. The two inflexion points are at $\alpha = 0.13$ and $\alpha = 0.53$. When the reaction temperature was lowered a measurable induction period was obtained. Hence a value of the activation energy associated with the induction period was obtained, as above, by using the duration of the induction periods at various decomposition temperatures.

The first acceleratory period was described by the Avrami-Erofeyev equation with $n = 2$ (equation 6.1). The extent of fit was over the range $0.02 < \alpha < 0.14$.

The first decay period was fitted with the two-dimensional contracting growth equation:

$$(1 - {}^{p}/p_{f})^{\frac{1}{2}} = k_4 \, t \quad \ldots\ldots\ldots\ldots\ldots\ldots\ldots\ldots \quad (6.2)$$

The final pressure associated with the initial reaction was estimated to be 54×10^{-2} torr. A reasonably good plot was found.

The contracting sphere formula (equation 5.3) as found above, fitted the second decay period. The equation was found to hold for the range $0.46 < \alpha < 0.94$.

(c) <u>5.0 M roentgens</u>. A typical p/t plot for the decomposition of pelleted lithium azide pre-irradiated with a γ-ray dose of 5.0 M roentgens, showing the extent of fit of the mathematical analysis appears in **FIGURE** 6.18 and the p/t values appear in **TABLE** 6.10. The reaction temperature was 110°C. A 4.6mg pellet was used.

It is observed that for the large dose used, the p/t curve is sigmoid. The inflexion point is at $\alpha = 0.32$. The induction period is 25 runs in duration. The acceleratory period was described by the Avrami-Erofeyev equation (equation 6.1) with n = 2 and the extent of fit was over the entire acceleratory period ($0.02 < \alpha < 0.40$). As previously found, the decay period was described by the contracting sphere formula (equation 5.3).

6.4.5 Evaluation of the activation energies

The critical increments for the chemical process(es) occurring in the thermal decomposition of pelleted lithium azide pre-irradiated with γ-ray doses of 50 and 15000 roentgens were obtained by applying the Arrhenius equation. For the determination of the activation energy for the induction period, the logarithms of the lengths of the induction periods were plotted against 1/T ($^{\circ}$K), as described before in 5.3.3. The values of the activation energies and the methods of determination of the rate constants are tabulated below. The plots of log. I.P., log k_1 and log k_2, and log k_3 against 1/T ($^{\circ}$K) appear in **FIGURES** 6.19 and 6.20.

Dose (roentgens)	Individual or Split runs	Activation energy for Induction period k.cals/mole	Activation energy for Acceleratory period k.cals/mole	Activation energy for Decay period k.cals/mole
50	Individual	22		
"	Split		29	28
15000	Individual	19		
"	Split		25	27

6.4.6 The effect of varying pellet weight on the initial reaction

The effect of varying the weight of the pellet of lithium azide on the initial reaction during thermal decomposition, after pre-irradiation with γ-rays (15000 roentgens), was examined. Thermal decomposition of two pellets, 4.4 and 11.0mg, pre-irradiated with γ-rays (15000 roentgens), showed the initial reaction to be dependant upon the weight of the pellet. For more than twice the weight of material an initial reaction of more than twice the magnitude was obtained. These results appear in TABLE 6.10 and the p/t plots for a reaction temperature of 185°C appear in FIGURE 6.21. The values are not normalised for comparative purposes.

6.4.7 Comparison of pre-irradiated pelleted and powdered lithium azide and pelleted irradiated lithium azide

The effect of pelleting powdered lithium azide, pre-irradiated with a dose of 15000 roentgens, compared to pelleted and powdered material pre-irradiated with the same γ-ray dose, is illustrated in FIGURE 6.22. The reaction temperature was 165°C. The p/t results appear in TABLE 6.11.

It was seen that the pelleted irradiated material has a longer induction period and the double-sigmoid character of the irradiated pelleted material was observed to appear. However, this was not as pronounced as for the latter. The dotted section of curve B is the estimated reaction after subtracting the "initial reaction".

6.4.8 The effect of thermal annealing

Thermal annealing of pelleted lithium azide, pre-irradiated with γ-rays (15000 roentgens), at 115°C for $^3/4$ hour in the vacuum line followed by 10 hours pumping and thermal decomposition at 185°C, showed no effect on the subsequent p/t plot. The p/t plot was compared with a blank run handled under similar conditions, but no annealing.

6.4.9 Percentage decomposition

The percentage decompositions (as described in 5.3.6) of the runs used in the varying temperature series to determine the activation energies associated with the induction periods of pelleted lithium azide pre-irradiated with 50 and 15000 roentgens, were found to be as follows:
(decomposition temperatures in brackets)

(a) 50 roentgens

93 (165°); 84 (170°); 85 (175°); 87 (180°); 77 (185°).

MEAN: 85%

(b) 15000 roentgens

82 (126°); 87 (132°); 82 (136°); 89 (140°); 85 (146°)

MEAN: 85%

6.4.10 Visual observations

Examination of the changes undergone by the irradiated pelleted material showed that the sequence of colour changes during decomposition was the same as found for the unirradiated pelleted azide. It was found that at the inflexion point of the first (initial) reaction the pellet was grey on the outside with darker patches or areas and the inside was dark red-brown. Examination of the pellet surfaces at the point when photograph (e) was taken (6.4.11) showed that reaction commenced at both faces simultaneously. More detailed observations during thermal decomposition appear in 6.4.11 when the surface of the pellet was viewed at various stages, using the optical microscope.

No colour change was observed for doses up to 15000 roentgens γ-rays. However, larger doses, (as found for the powdered salt) turned the pelleted material a faint buff colour.

6.4.11 Photomicrography

Only pelleted material was studied, for reasons given in 5.3.12. The pellets had been pre-irradiated with a γ-ray dose of 15000 roentgens.

Details of the apparatus and experimental procedures have been given in 4.1.2, 4.2.7 and 5.3.12.

PLATE 2 shows the thermal decomposition of γ-irradiated pelleted lithium azide, at 160° ± 2°C. Magnification was 65X. The $^{dp}/_{dt}$ results appear in **TABLE** 6.12 and **FIGURE** 6.23. The arrows indicate where the photomicrographs were taken.

The series of photomicrographs show the following features:
(Figures in brackets are exposure times used in printing the photographs, as explained in 5.3.12).

(a) The photomicrograph shows the surface of the pellet shortly after the end of the induction period. Decomposition was observed to start from one half of the viewed surface and diffuse grey particles appeared. The photomicrograph was taken after 10 mins. (12)

(b) The early stages of the first acceleratory period again appear in the photomicrograph at t = 18 mins. The grey areas darkened in colour but no new dark areas of decomposition are seen. (12)

(c) After 30 mins, further decomposition was observed in the dark areas, now grey-brown in colour. (12)

(d) At 36 mins, just before the inflexion point, nearly one half of the observed area was covered with product, with the remaining area becoming increasingly darker. (10)

(e) At the inflexion point at 41 mins, further decomposition was observed. (10)

(f), (g) and (h). These photomicrographs taken at 51, 65 and 100 mins respectively,

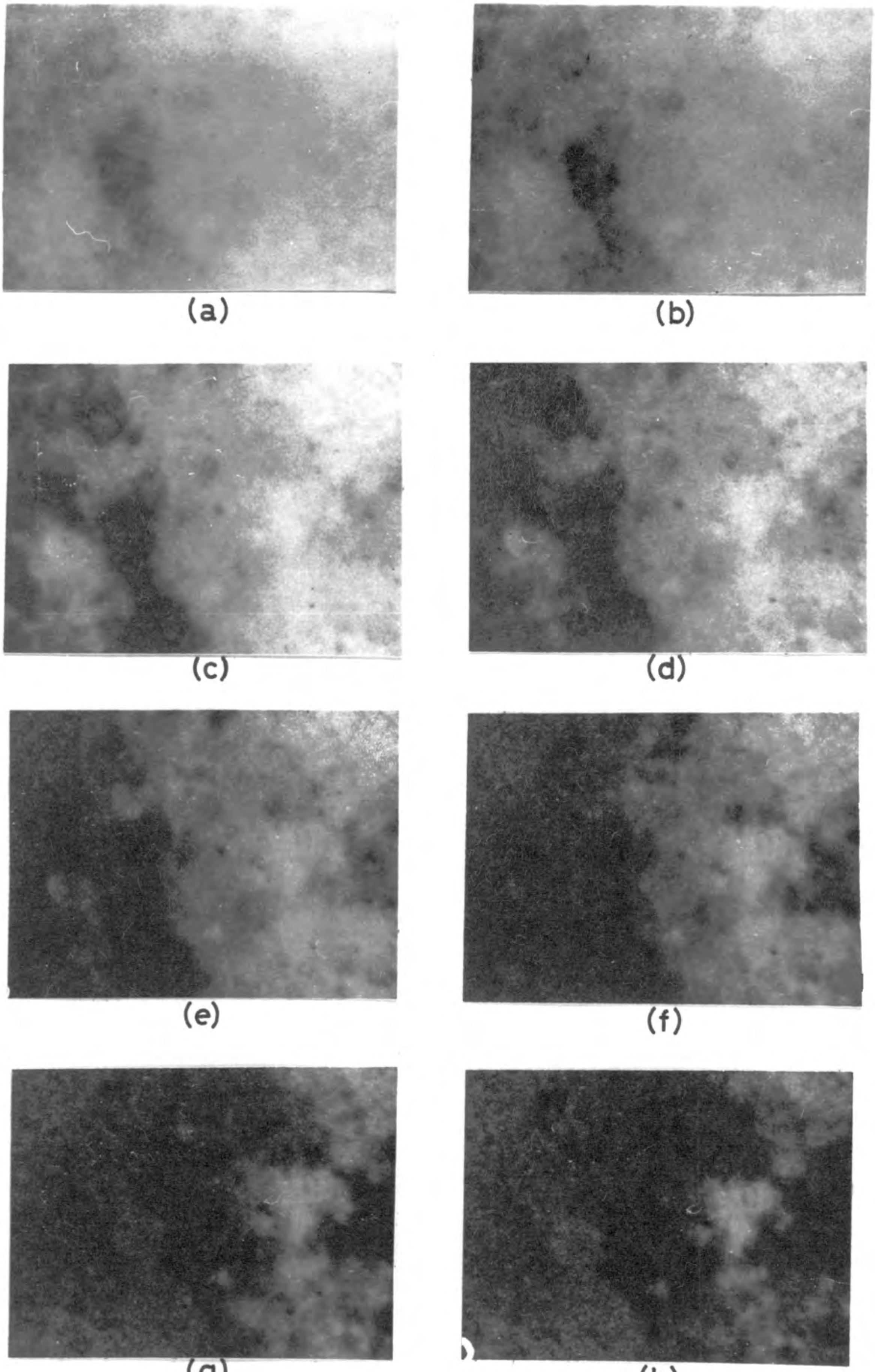

(a) (b) (c) (d) (e) (f) (g) (h)

PLATE 2. THE THERMAL DECOMPOSITION OF γ-IRRADIATED PELLETED LITHIUM AZIDE. 160°C.

in the decay period of the initial reaction show progressive darkening of the viewed surface, until the surface was completely covered with red-brown reaction product. This marked the end of the initial reaction and during the second reaction, no further changes were observed on the pellet surface.

(10, 10 and 10)

6.5 DISCUSSION

Irradiation with γ-rays has definite advantages compared with radiation by nuclear particles. The γ-rays are absorbed only slightly and therefore effects produced by γ-rays take place practically uniformly throughout the entire thickness of the irradiated crystal(191). No local heating of the crystal (formation of thermal spikes) occurs with γ-rays, as is found with heavy particles.

The attenuation of the intensity of γ-radiation in its passage through a solid is due chiefly to three effects:

(i) the photoelectric effect,
(ii) the Compton effect,
(iii) pair formation.

As a consequence of these processes, electrons and electron-position pairs are liberated in the irradiated material and this may be seen to be in effect an "internal electron (β-ray) bombardment". These electrons may vary in velocity from very fast to very slow and the possible reactions in the solid are numerous.

It has been calculated(192) that atomic displacements following internal irradiation by Compton electrons as a result of irradiation with ^{60}Co γ-rays, may be expected to be a maximum for atoms of low atomic number, with the effect decreasing as this value increases. Besides elastic scattering of Compton electrons by atoms resulting in displaced atoms, the elastic scattering of photoelectrons can also be shown to bring about displacement of atoms, although the cross-section for displacement by photo-electrons is considerably less than that for Compton electrons. Galavonov(191) has calculated that Frenkel defects (interstitial-vacancy pairs) formed in germanium when this is irradiated with 1.25 MeV γ-rays are the result of the Compton effect. This is contrary to earlier investigations by Cleland and others(193) who stated that the photoelectric effect and the Compton effect make equal contributions to the process of formation of defects in Ge. The probability of displacement of an atom by elastic scattering at the nucleus of the γ-rays has been shown by calculation to be extremely small and is not considered as a factor in the displacement of atoms in a solid when irradiated with γ-rays.

γ-, (and short wavelength X-irradiation) then in effect transfers part of its energy to the release of electrons by (i), (ii) and (iii) above, which in turn bombard the crystal lattice.

In addition to displacement of atoms to interstitial positions, colour-centre formation occurs when electrons, resulting from the interaction of γ-rays with the solid, are trapped at suitable sites in the crystal.

The overall damage is distributed uniformly throughout the lattice since absorption of the γ-rays is small enough to ensure this.

Seitz(194) has proposed that excitons (bound positive hole-electron entities) may be produced, which are mobile and diffuse through the crystal lattice until they encounter a lattice irregularity at which point the energy is discharged producing a local "hot spot". Jogs at dislocation lines are likely points and the release of energy at a jog can induce dislocation climb, as vacancies are "boiled off". Also, migration of point defects away from their centre of origin may be caused by further absorption of excitons on the defects.

A further mode of interaction of γ-rays with ionic solids characterised by a high degree of ionic bonding, has been proposed by Varley(149-151). He proposed that multiple ionization of an anion to form an unstable positively charged ion was possible, with the electrons diffusing away. Ejection of the ion and recapture of the electrons resulted in a Frenkel defect. In addition an F-centre could be created if a diffusing electron were trapped by the newly formed anion vacancy.

A mechanism combining those of Varley and Seitz has been proposed(195), where the interstitials are formed near dislocation lines, causing the dislocation core to climb.

The effects of irradiation are illustrated generally in the changes in the physical properties of the solid(196) whether it be a metal, a semi-conductor or an insulator (e.g. ionic solids). Changes may be observed in the extrinsic semi-conductivity, photoconductivity, optical absorption bands, paramagnetism contributing to the susceptibility and paramagnetic resonance, scattering of conduction electrons, gravimetric density, deformation behaviour, self-diffusion, thermal conductivity or on certain occasions, lattice structure.

In the light of the above discussion it is likely that irradiation of solids by γ-rays may produce damage which may influence the rate of the subsequent thermal decomposition of the solid, as artificial centres and areas of lowered chemical potential are formed. The reaction may thus be expected to proceed at an enhanced rate in certain favourable cases e.g. the permanganates(197).

6.5.1 Powdered lithium azide

The effects of pre-irradiation on the pressure-time plot for the thermal decomposition of lithium azide were observed to be:

(i) a drastic reduction in the length of the induction period,

(ii) an increase in the rate constant for the acceleratory period,

(iii) an increase in the rate constant for the decay period.

The effects of progressively increasing the γ-ray dose on the subsequent thermal decomposition were to steadily (i) shorten the length of the induction period, and (ii) increase the acceleratory and decay rate constants. No colouration of the salt was observed for γ-ray doses normally used (15000 roentgens), but for a dose of 0.7 M roentgens the salt turned a light buff-cream colour.

The activation energies for the process(es)occurring during the thermal decomposition were found to be:

(i)	Induction period:	20 k.cals/mole	
(ii)	Acceleratory period:	26 k.cals/mole	(Individual runs)
		24 k.cals/mole	(Split run)
(iii)	Decay period:	28 k.cals/mole	

The difference in the values of the activation energies associated with the acceleratory period using the individual and split runs methods may be attributed to the inaccuracies involved in the latter method. Pressure-time measurements are taken over small pressure differences at a particular temperature and the kinetic analysis is then performed over a fragment of the acceleratory period, using only a few values. It is considered in view of the experimental difficulties involved in split- run determinations that the value of 26 k.cals/mole is the closer estimation of the activation energy associated with the acceleratory period.

The nuclei are considered to form largely inside the lithium azide particles. In addition, some form on the external surfaces. The same kinetic expression was found to hold (contracting sphere formula) for the decay period for the irradiated material, as for the unirradiated salt and the values of the activation energy associated with the process was similar (28 k.cals/mole). These facts indicate that the same decay mechanism is operative in the irradiated salt, but that the reactant product interface at the commencement of the decay reaction is much larger in the irradiated salt which would be the case if internal nucleation occurred.

Thus it is assumed that internal nucleation along dislocations and along grain boundaries (both high and low angle) occurs on decomposition, thus separating the particle into mosaic blocks at the start of the decay reaction. This pictures a large number of "contracting envelopes" which satisfy the application of the contracting sphere formula and account for the enhanced decay rate constant after γ-irradiation. With increasing irradiation doses, the number of nuclei and hence the number of decomposing blocks of solid, increases, leading to increased decay rate constants.

The acceleratory period was found to be described by the Avrami-Erofeyev equation with n = 3, as found for the decomposition of unirradiated lithium azide, although the plots of $\left[-\log (1 - \alpha)\right]^{1/3}$ against time were not as good as those for the unirradiated salt. As proposed for the unirradiated material, it is considered that the nuclei form and grow 2-dimensionally, increasing in number linearly with time. "Water interruption" experiments (FIGURE 6.13) indicate that 1- or 3-dimensional nuclei are not possible. The p/t plots for the decomposition of lithium azide pre-irradiated with a large dose(0.7 M roentgens) of γ-rays, were found to be well described by the Avrami-Erofeyev equation with the exponent n = 2. In this case it is proposed that 2-dimensional nuclei are formed and grow, but that these form such large numbers that the effect is almost as if reaction occurs from a fixed number of nuclei. Overlap and decay of the nuclei are thus the predominating features of the decomposition.

As stated above, γ-irradiation of a solid is, in effect, an internal bombardment by electrons varying in velocity from very fast to very slow and the possible reactions in the solid are numerous. The following changes are considered possible when lithium azide is pre-irradiated with high energy (~1.3 MeV) γ-rays:

$$N_3^- \rightarrow N_3 + e \quad \ldots\ldots\ldots\ldots\ldots\ldots \quad (6.5.1)$$

$$N_3 + e \rightarrow N_3^- \quad \ldots\ldots\ldots\ldots\ldots\ldots \quad (6.5.2)$$

$$N_3^- \rightarrow N_3^{-*} \quad \ldots\ldots\ldots\ldots\ldots\ldots \quad (6.5.3)$$

$$N_3^{-*} + N_3 \rightarrow 3N_2 + A + F \quad \ldots\ldots\ldots\ldots\ldots\ldots \quad (6.5.4)$$

$$A + e \rightarrow F \quad \ldots\ldots\ldots\ldots\ldots\ldots \quad (6.5.5)$$

$$N_3 + F \rightarrow N_3^- + A \quad \ldots\ldots\ldots\ldots\ldots\ldots \quad (6.5.6)$$

$$N_3 + C + N_3 \rightarrow 3N_2 + C + 2A \quad \ldots\ldots\ldots\ldots\ldots\ldots \quad (6.5.7)$$

where A = anion vacancy, C = cation vacancy, F = F-centre and N_3^{-*} is an exciton (described previously). These reactions may be expected to occur uniformly throughout the solid as the γ-ray absorption is low enough to permit this (cf. X-ray absorption observations). In addition, the formation of Frenkel defects is also thought to occur but to a minor degree compared to the formation of F-centres.

Significant formation of interstitial ion/vacancy pairs by displacement reactions is discounted because of the similarity of the effects of γ-irradiation on the thermal decomposition of barium, strontium and calcium azides(3,137,139) and lithium azide. The cross-section for displacement is extremely small (negligible) in the alkaline earth azides and the radiation effect is attributed to the formation of electronic defects.

Thus the LiN_3 after irradiation may contain N_2, cation and anion vacancies and F-centres, as the main irradiation products. Although colouration of the salt was not observed for doses up to 15000 roentgens, it was noticed that the salt turned a pale buff-cream colour on irradiating with larger doses.

The irradiation effects are considered to occur, in the main, along grain boundaries, at dislocation pile-ups and along dislocations within the azide particle. In addition, some irradiation effects will be produced on the external surface. The effect of irradiation on the subsequent thermal decomposition is considered to be associated with the F-centres produced at these places. These aggregate at suitable traps by thermal diffusion at room temperature. This aggregation will occur in grain boundaries and on external surfaces at points at which the Coulombic distortion is sufficiently large to trap migrating F-centres.

It has been shown(4) by spectroscopic measurements that on warming potassium azide, irradiated at -78°C, to room temperature, the large spectral band attributed to F-centres diminishes and disappears with the simultaneous formation of another band, attributed to the formation of clusters of F-centres. The F-centres became mobile around -20°C and at room temperature the mobility was very high. It was also found that irradiation at room temperature produced similar results, when the F-centres formed diffused to grain boundaries.

On reaching a critical size during the early stages of the induction period in the decomposition of lithium azide, the aggregations of F-centres will collapse and lithium atoms will be formed as:

$$Li^+ + e \rightarrow Li \quad \ldots\ldots\ldots\ldots\ldots\ldots\ldots \quad (6.5.8)$$

The crystallisation of the lithium atoms marks the end of the induction period, after which point nuclear growth commences.

The lithium atoms can diffuse away from their points of formation on the external surface and migrate along the channels of emergent edge dislocations as well as diffusing along the grain boundaries and over the external surface, during the induction period. The analagous migration of silver atoms during the thermal decomposition of silver azide has been observed using the electron microscope(198), coupled with electron diffraction studies to observe change in the atomic arrangement. The results indicated that the formation of crystalline silver was preceded by the migration of silver atoms into the lattice. It was also indicated that silver was deposited internally at defects in the crystals. Scanning electron microscope observations of the thermal decomposition of lead and cadmium azides(122) showed that single crystals of these salts broke up into small blocklets and it was suggested that the reaction in these cases occurred preferentially at defects

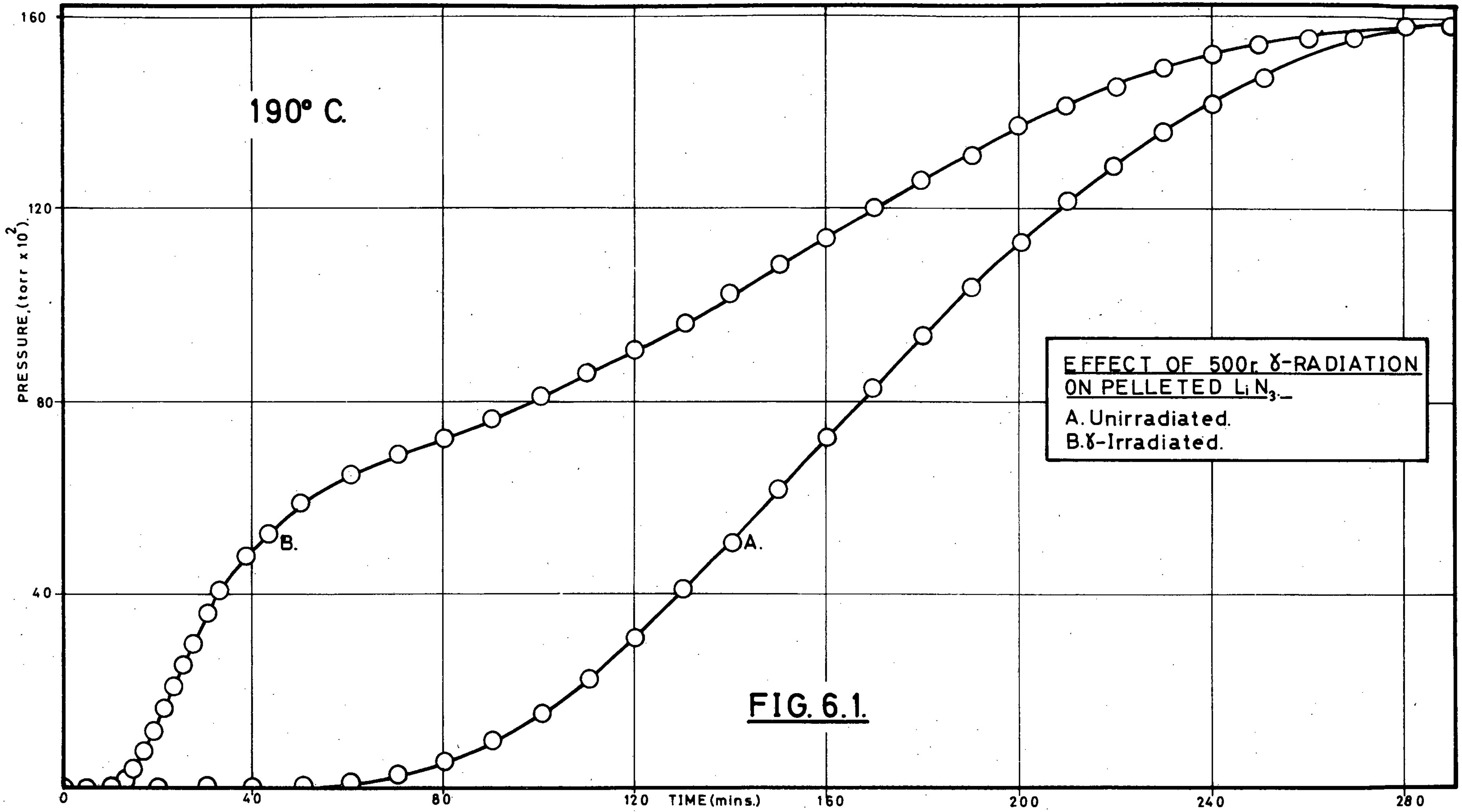
190° C.
PRESSURE, (torr x 10^2).
160
120
80
40
0
40
80
120
TIME (mins.)
160
200
240
280
B.
A.
EFFECT OF 500r γ-RADIATION ON PELLETED LiN_3.
A. Unirradiated.
B. γ-Irradiated.

FIG. 6.1.

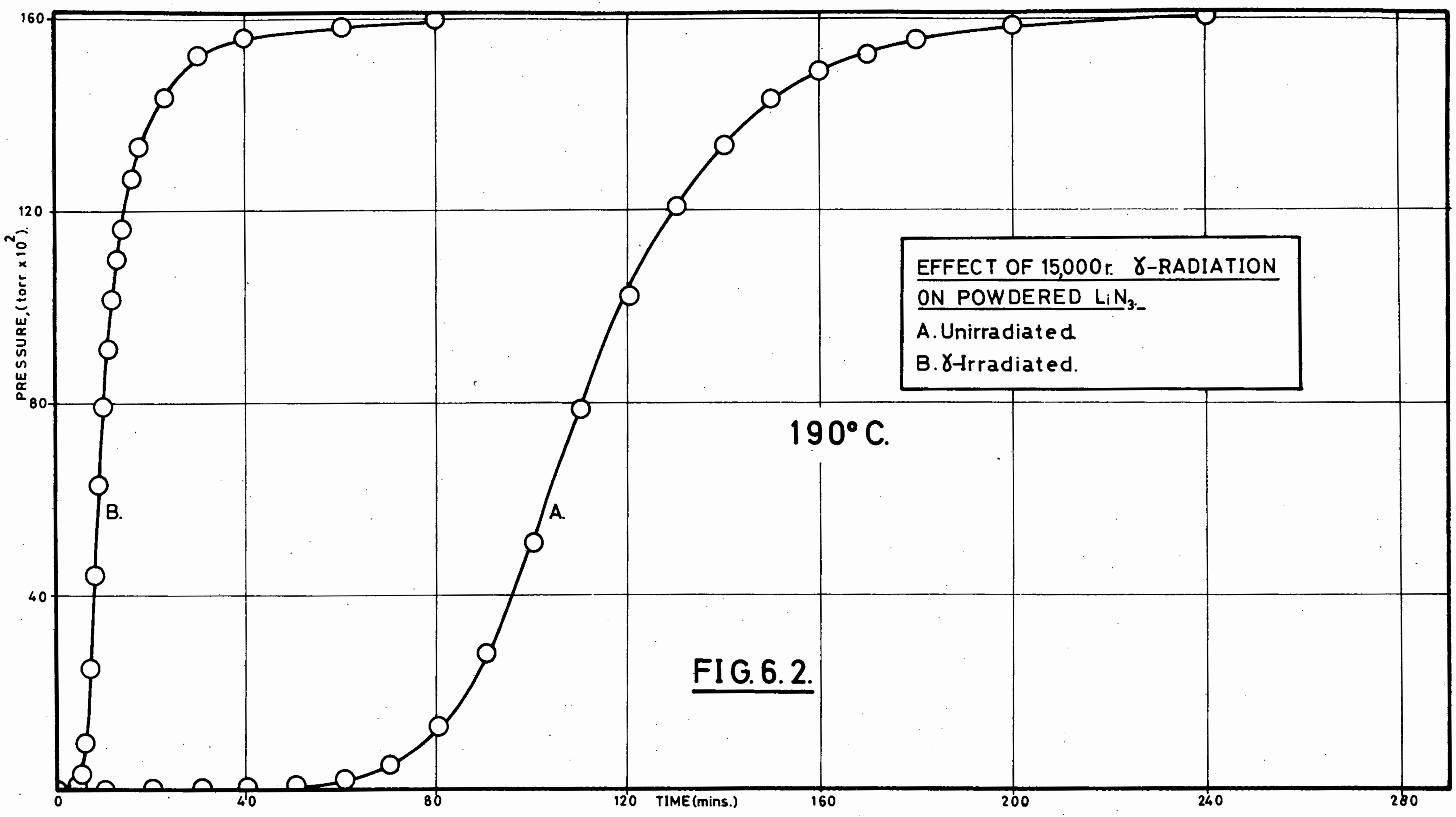
EFFECT OF 15,000r. γ-RADIATION ON POWDERED LiN_3.
A. Unirradiated.
B. γ-Irradiated.
190° C.
PRESSURE, (torr x 10^2).
160
120
80
40
0
40
80
120
TIME (mins.)
160
200
240
280
A.
B.

FIG. 6. 2.

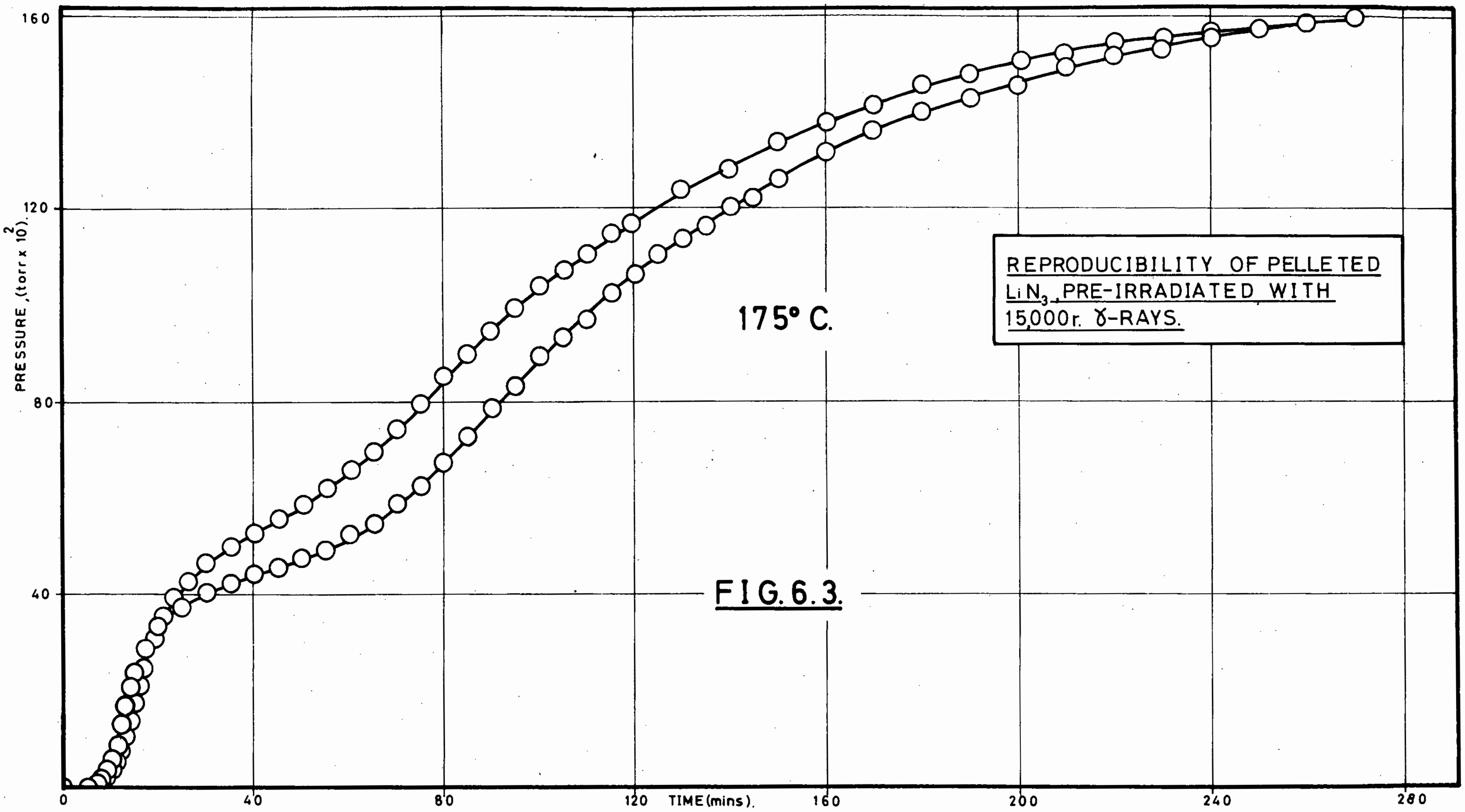
160
120
80
40
PRESSURE, (torr x 10^2).
0
40
80
120
TIME (mins).
160
200
240
280
175° C.
REPRODUCIBILITY OF PELLETED
LiN$_3$, PRE-IRRADIATED WITH
15,000r. γ-RAYS.

FIG. 6.3.

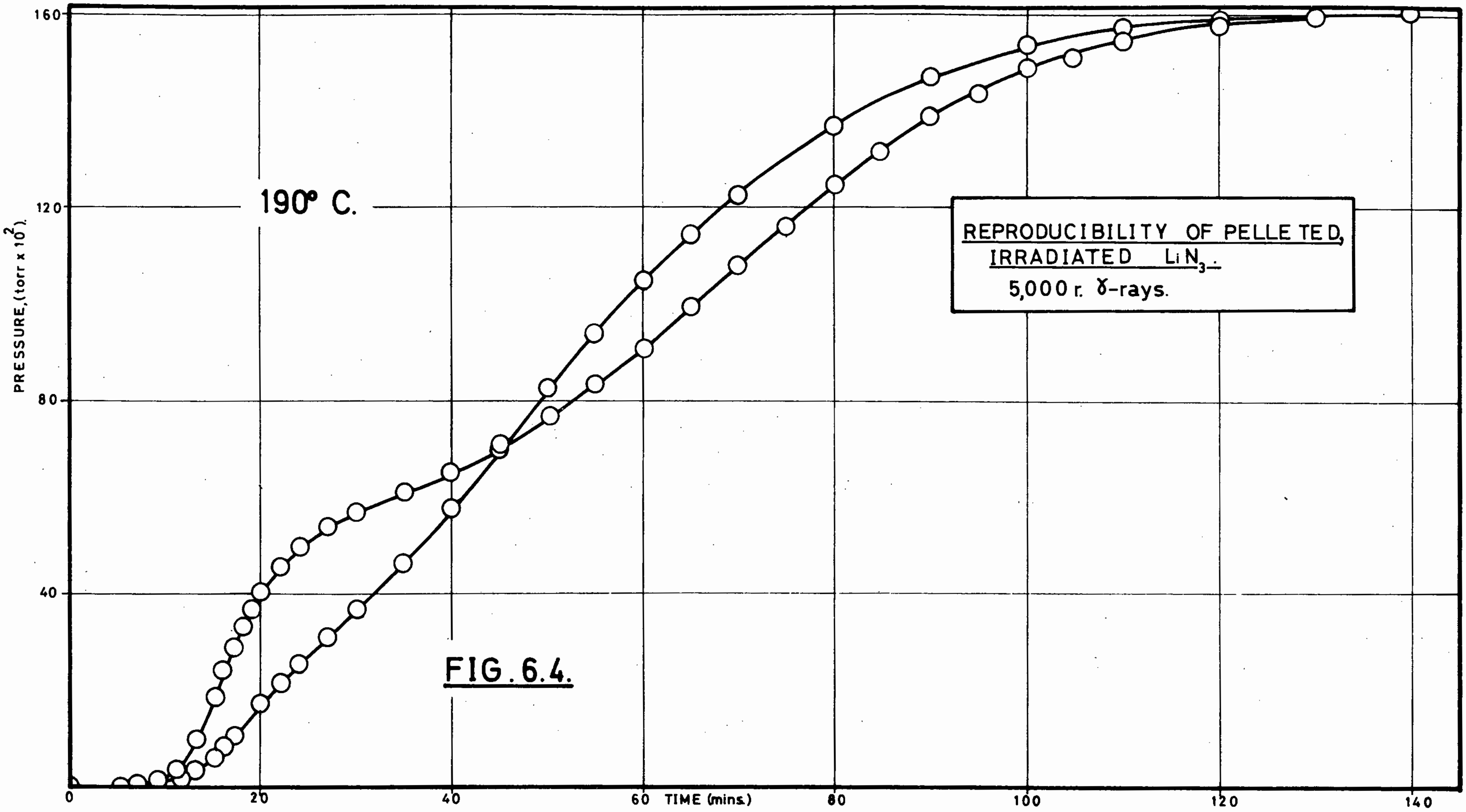

REPRODUCIBILITY OF PELLETED, IRRADIATED LiN_3.
5,000 r. γ-rays.

FIG. 6.4.

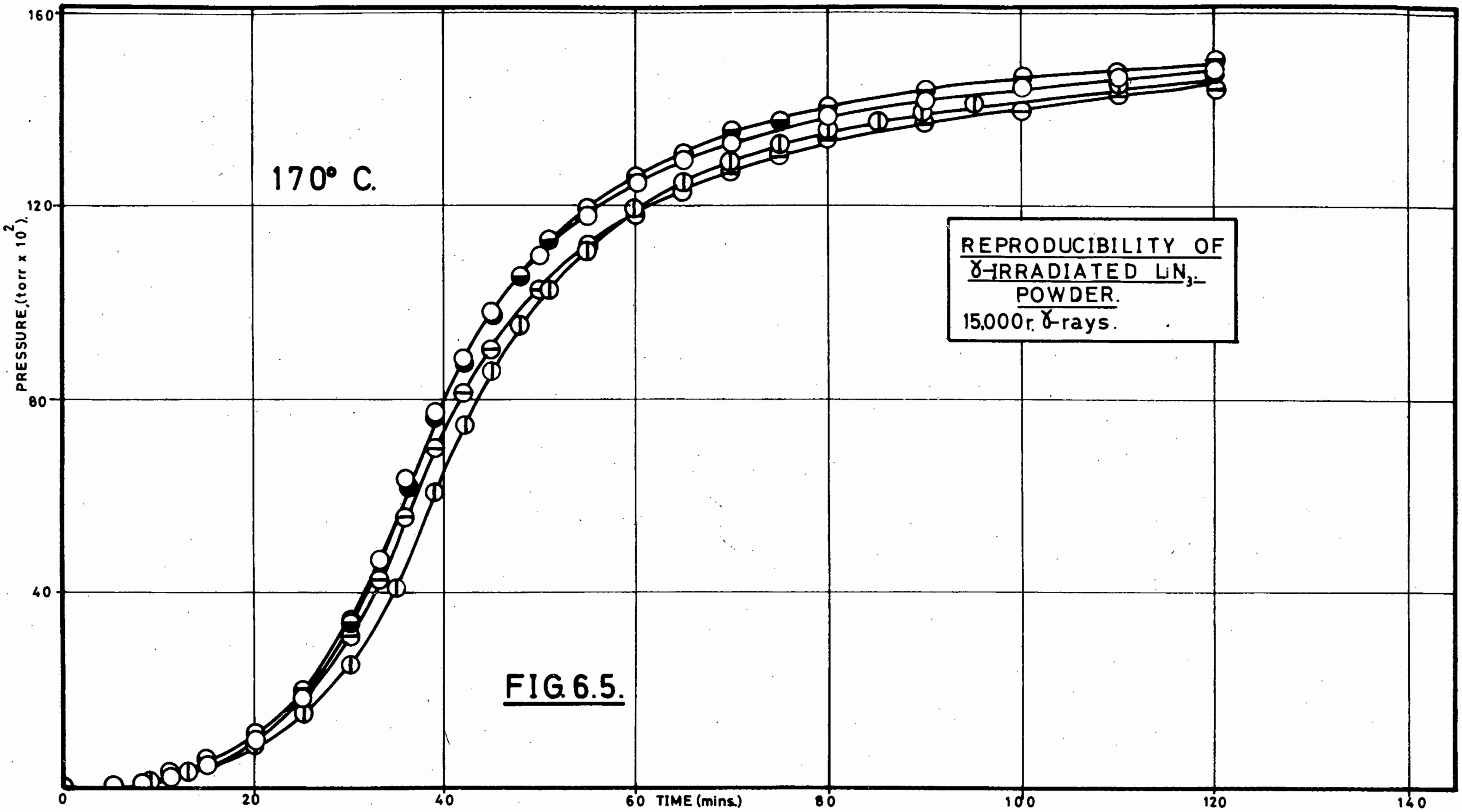
170° C.
REPRODUCIBILITY OF
γ-IRRADIATED LiN_3:-
POWDER.
15,000r. γ-rays.
PRESSURE, (torr x 10^2).
TIME (mins.)
0
20
40
60
80
100
120
140
40
80
120
160

FIG. 6.5.

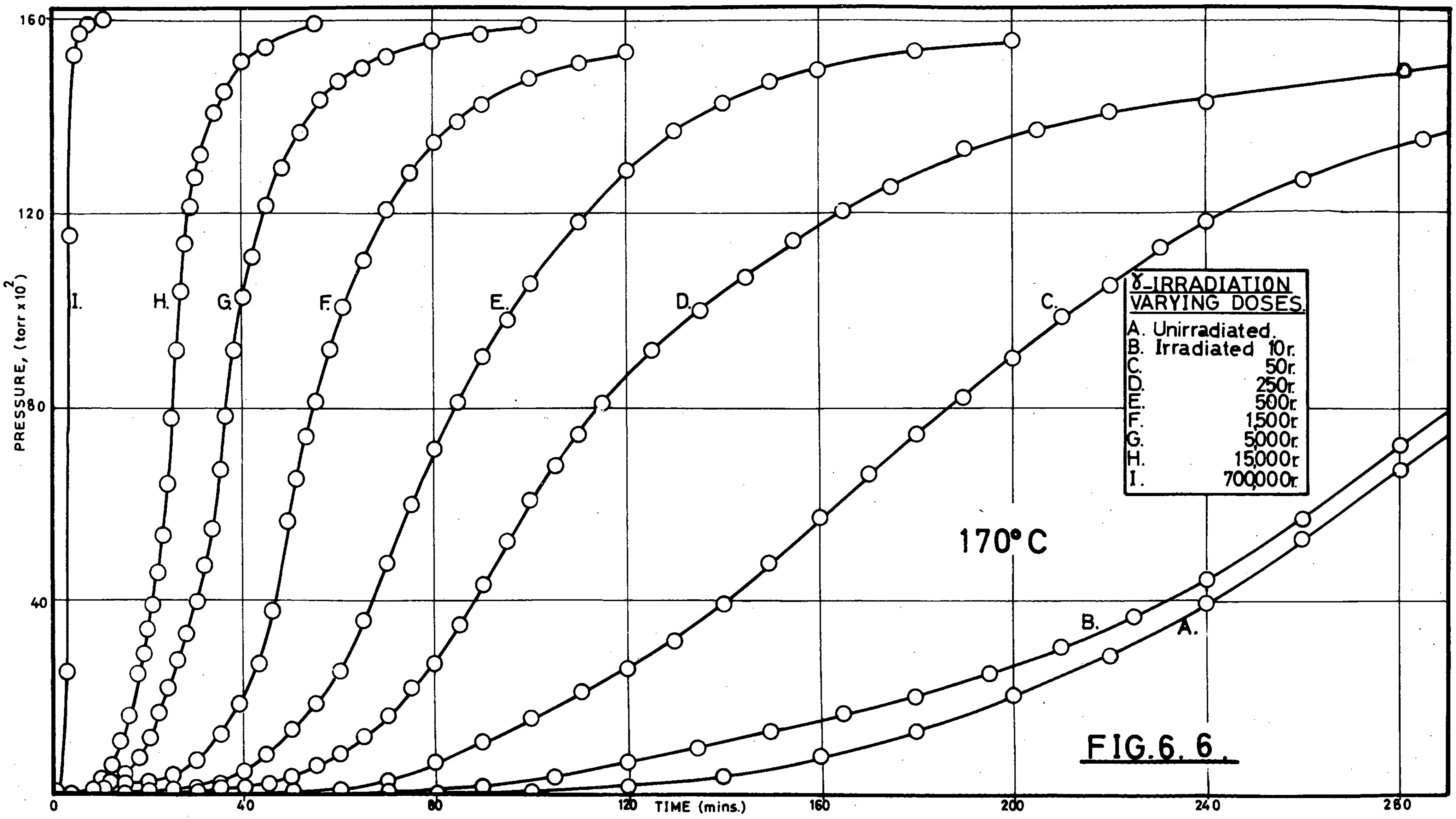

160
120
80
40
0
PRESSURE, (torr x 10^2)
0
40
80
120
160
200
240
280
TIME (mins.)
I.
H.
G.
F.
E.
D.
C.
B.
A.
γ-IRRADIATION
VARYING DOSES.
A. Unirradiated.
B. Irradiated 10r.
C. 50r.
D. 250r.
E. 500r.
F. 1,500r.
G. 5,000r.
H. 15,000r.
I. 700,000r.
170° C

FIG. 6. 6.

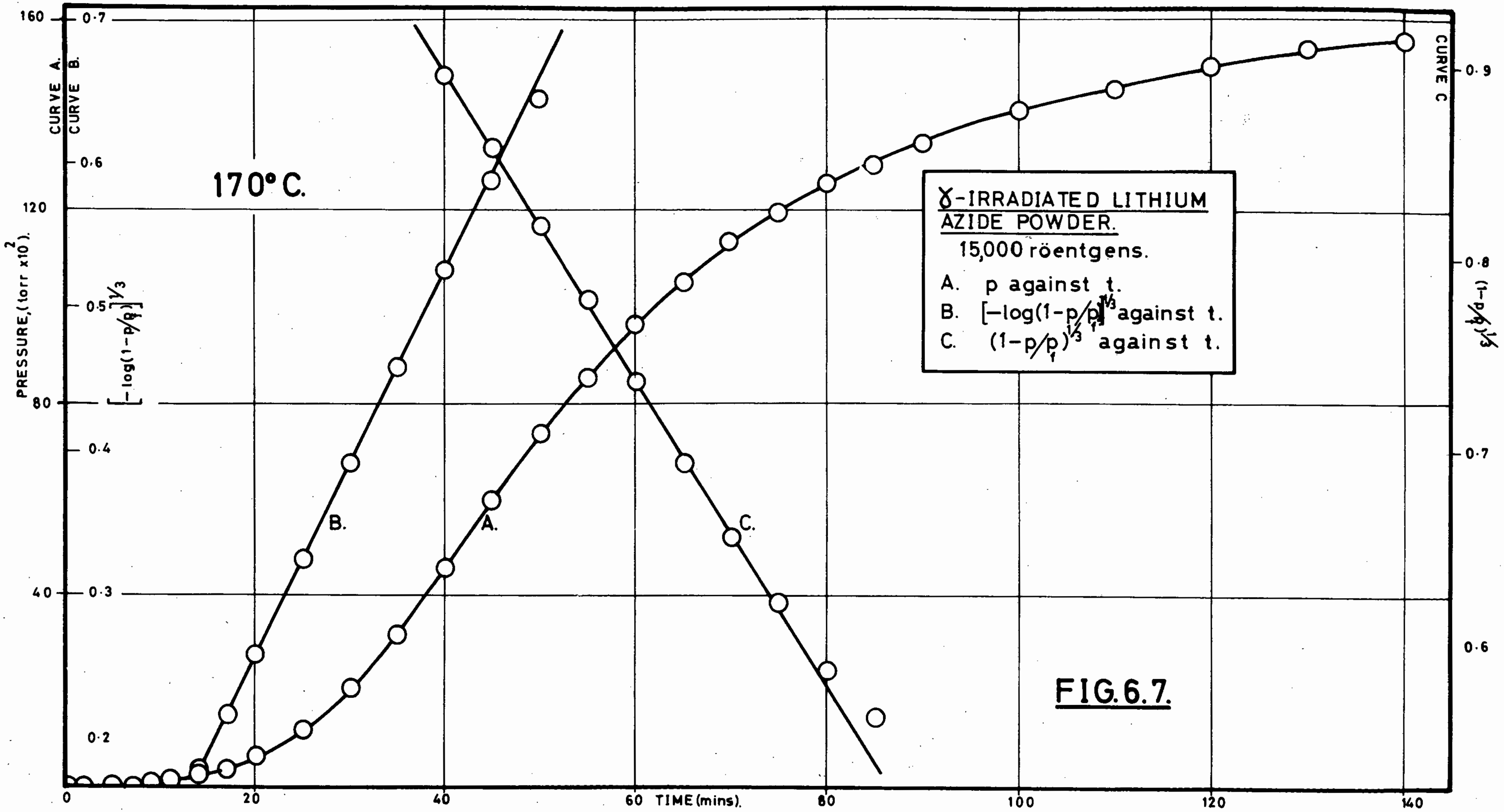
170° C.
γ-IRRADIATED LITHIUM AZIDE POWDER.
15,000 röentgens.
A. p against t.
B. $[-\log(1-p/p_f)]^{1/3}$ against t.
C. $(1-p/p_f)^{1/3}$ against t.
CURVE A.
CURVE B.
CURVE C
PRESSURE, (torr x10^2).
$[-\log(1-p/p_f)]^{1/3}$
$(1-p/p_f)^{1/3}$
TIME (mins).
160
120
80
40
0·7
0·6
0·5
0·4
0·3
0·2
0·9
0·8
0·7
0·6
0
20
40
60
80
100
120
140
A.
B.
C.

FIG.6.7.

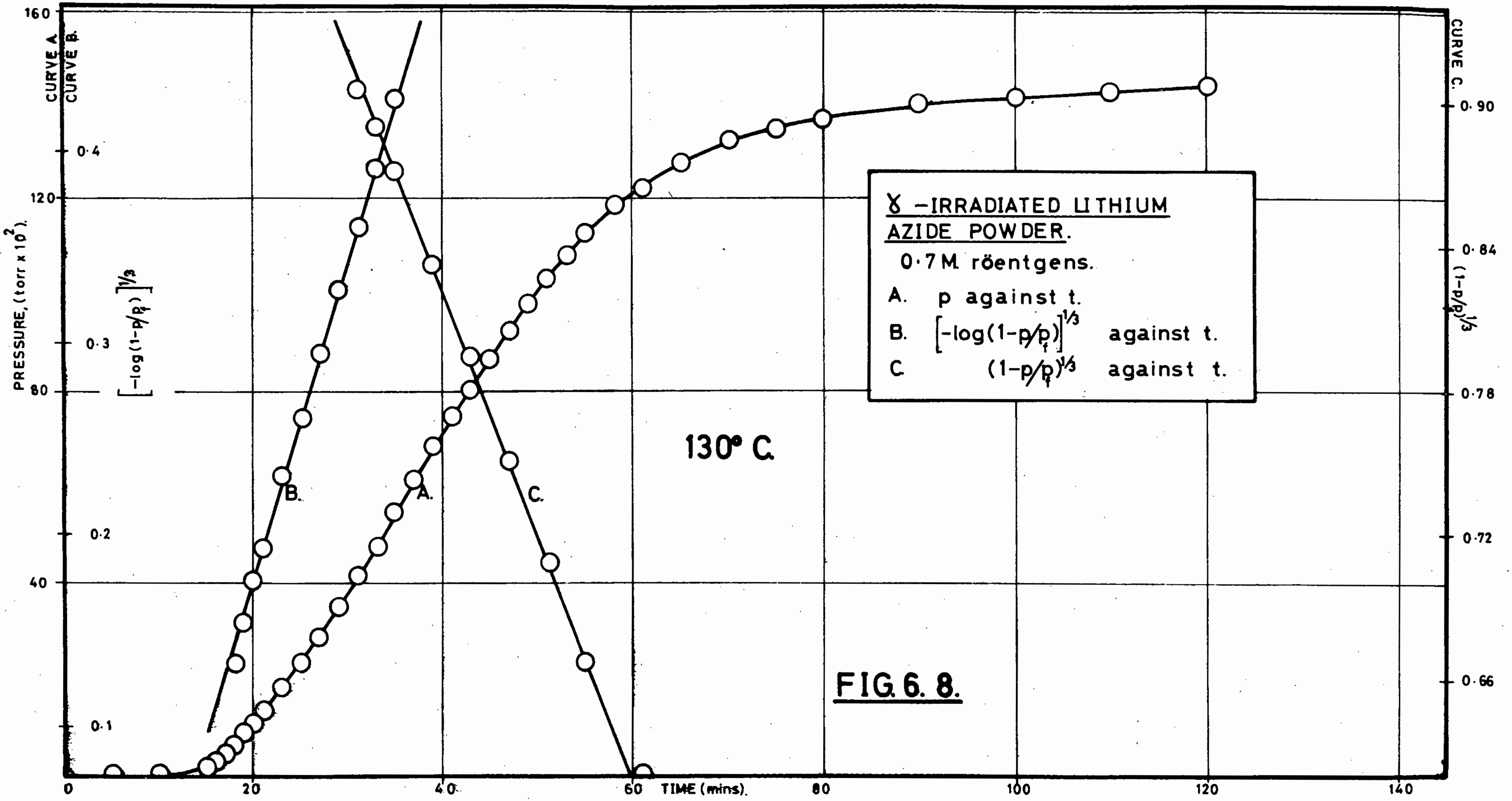
γ -IRRADIATED LITHIUM AZIDE POWDER.
0·7M röentgens.
A. p against t.
B. $[-\log(1-p/p_f)]^{1/3}$ against t.
C. $(1-p/p_f)^{1/3}$ against t.
130° C.
PRESSURE, (torr x 10^2).
CURVE A
CURVE B.
$[-\log(1-p/p_f)]^{1/3}$
CURVE C.
$(1-p/p_f)^{1/3}$
TIME (mins).
160
120
80
40
0·4
0·3
0·2
0·1
0·90
0·84
0·78
0·72
0·66
0
20
40
60
80
100
120
140
A.
B.
C.

FIG. 6. 8.

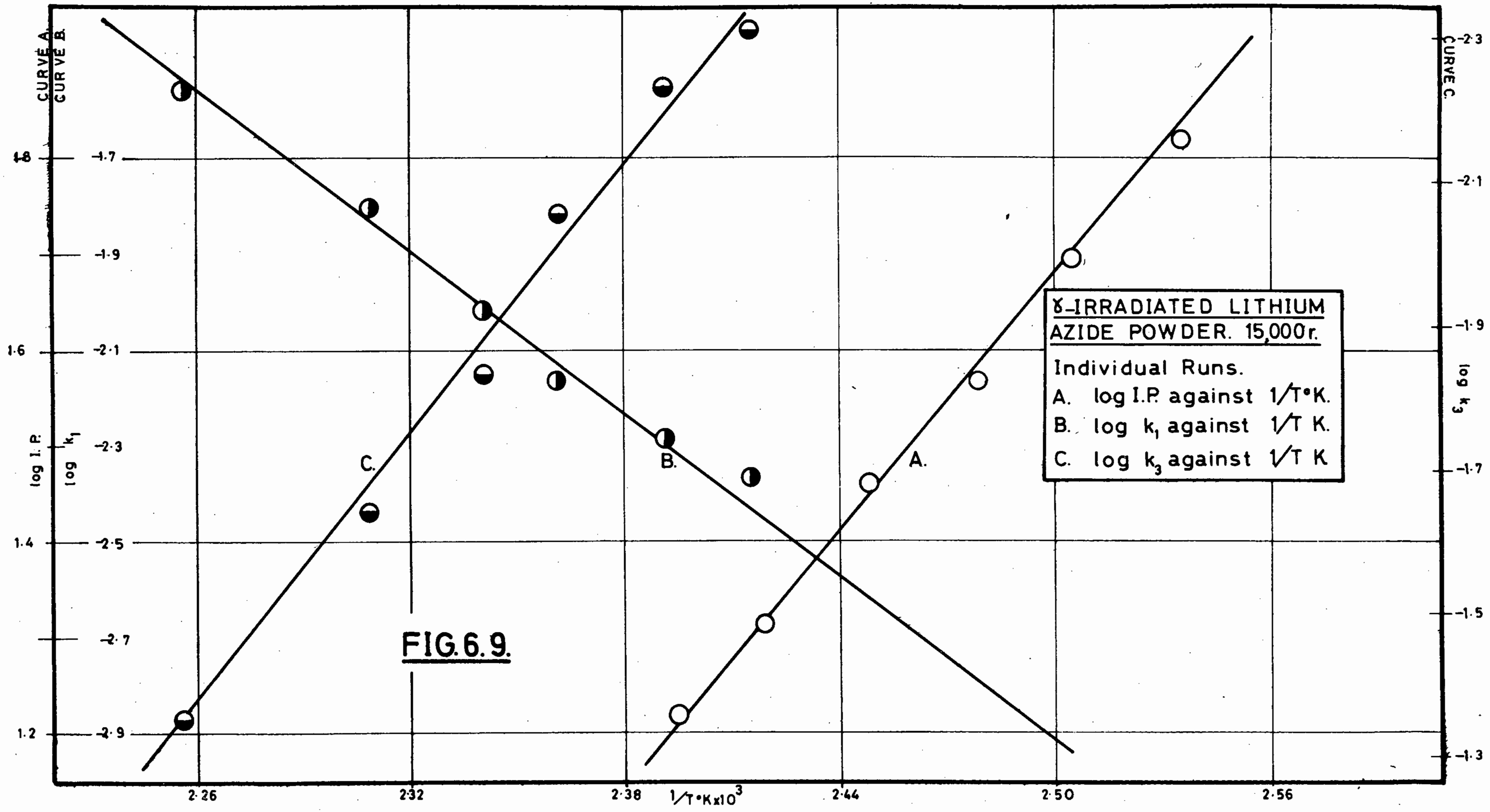
CURVE A.
CURVE B.
log I.P.
log k_1
1·8
1·6
1·4
1·2
-1·7
-1·9
-2·1
-2·3
-2·5
-2·7
-2·9
CURVE C.
log k_3
-2·3
-2·1
-1·9
-1·7
-1·5
-1·3
2·26
2·32
2·38
$1/T°K \times 10^3$
2·44
2·50
2·56
A.
B.
C.
γ-IRRADIATED LITHIUM AZIDE POWDER. 15,000r.
Individual Runs.
A. log I.P. against 1/T°K.
B. log k_1 against 1/T K.
C. log k_3 against 1/T K.

FIG. 6.9.

within the crystal.

The slow, or rate-determining step for the process associated with the induction period is proposed to be the diffusion of lithium atoms over the surfaces, external and internal, to coagulate to form metal nuclei as mentioned earlier for the unirradiated salt. There is thus a common factor for changes during the induction period of unirradiated and γ-irradiated material i.e. the diffusion of lithium atoms and trapping at appropriate sites. From the agreement of the activation energies it appears that this common process is the slow step in both reactions and one is led to postulate that the activation energies are associated with the formation of lithium metal. The activation energy for the migration of barium atoms in barium azide has been estimated at 20 to 25 k.cals/mole(74) which is in agreement with the observed activation energy for the process in γ-irradiated lithium azide (20 k.cals/mole).

The essential difference between nuclear formation in the unirradiated and γ-irradiated material is that the metal nuclei are formed only on the surface of the particles in the former case, while they are formed in addition along internal grain boundaries and dislocations, in the latter case.

It is considered that the process of nuclear formation in lithium azide is analagous to the formation of the latent image in silver bromide crystals, followed by separation of silver in the crystals by chemical development(199-201). Pre-irradiation of lithium azide powder is considered to be analagous to the formation of the latent image in silver bromide, while heating during the induction period when the lithium atoms coalesce to form nuclei along grain boundaries and surfaces is analagous to the chemical development of the latent image when silver is precipitated along the dislocation network in silver bromide.

Hedges and Mitchell(199,200) studied the formation of silver in polygonised, (strained), crystals of silver bromide. The polygonised crystals (achieved by straining, and annealing and quenching) were exposed to light. The latent image formed in the silver bromide crystals was then chemically developed and silver was observed (using the optical microscope) to have precipitated internally along what these workers termed "sub-boundaries", (the grain boundaries discussed above) separating the crystal in effect into "mosaic" blocks. Experimental work in both large single crystals and in microcrystals showed that internal silver separated at structural imperfections and that the localised separation which is observed was due to the localised nature of the imperfections. On prolonged exposures to light, chemical development was not necessary, and visible silver was always observed to separate as discrete particles internally along dislocation lines of the grain boundaries, making them visible. These results are illustrated in the photomicrographs taken by Hedges and Mitchell(199), reprinted in PLATE 2(a). The magnification was 1200X.

Photomicrograph (a) was obtained after a visible image was produced and the single crystal then developed, while in (b) the latent image produced was developed after dissolving away the surface layer of silver bromide. The latter photograph was another part of the same crystal used for (a). The photomicrographs clearly illustrate the sub-structure comprising dislocations and grain boundaries, existing internally in Ag Br.

The effect of depositing a thin film of silver on the surface of a crystal of silver bromide and then storing the crystal in vacuo for a period, was that the silver diffused freely over the external surface and into the internal grain boundaries of the crystal. It was stated that silver spread by thermal diffusion at room temperature over the internal grain boundaries of the crystals, which were defined as being arrays and networks of dislocation lines separating small volume elements of relatively perfect material.

Amelinckx and others(202) have also demonstrated interior dislocation patterns

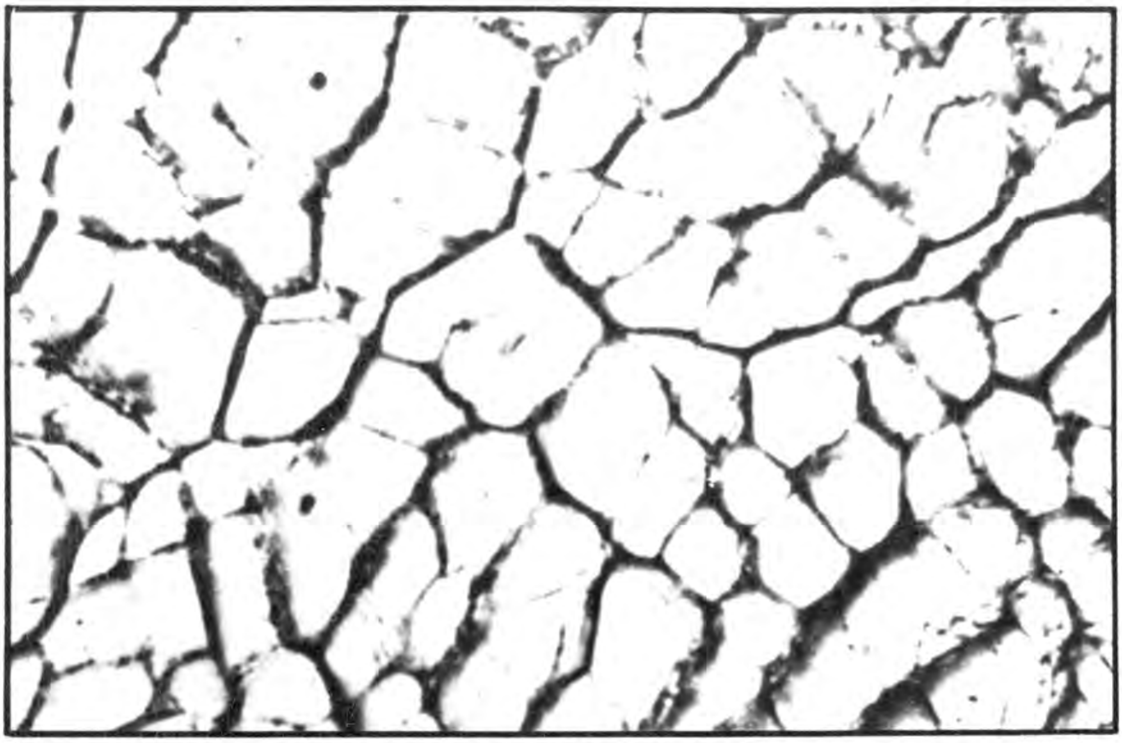

(a). Silver bromide crystal exposed until visible image produced due to separation of Ag in grain boundaries, and then developed.

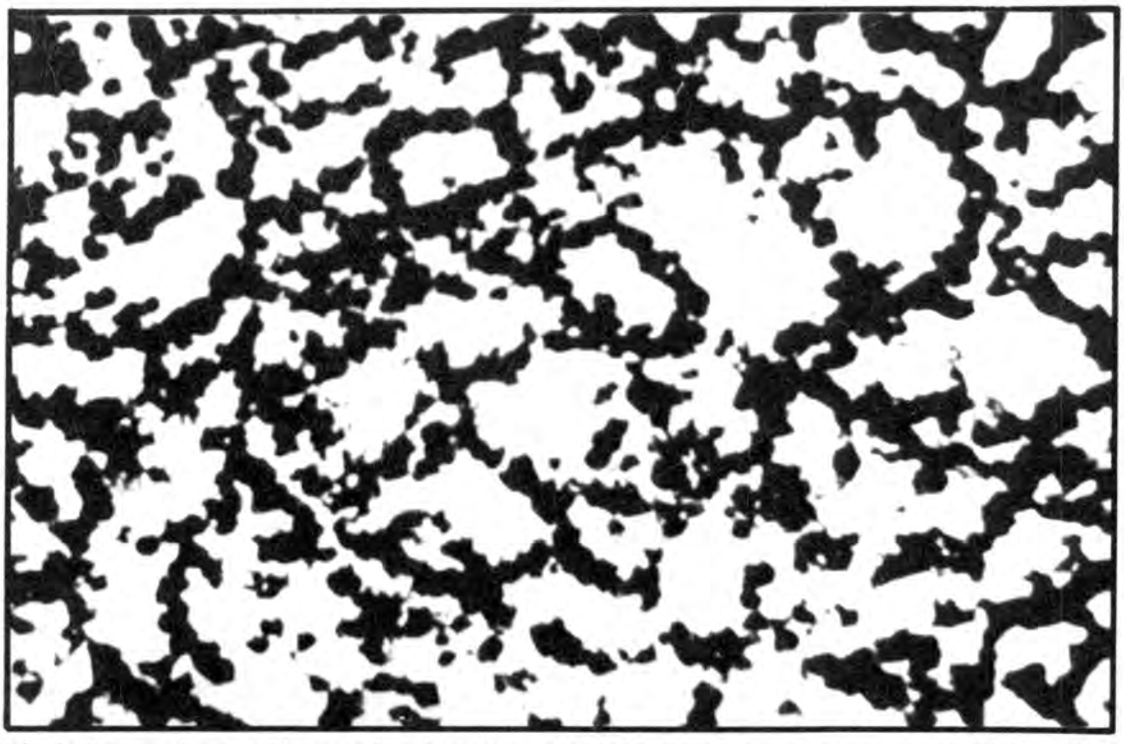

(b). Adjacent section of above crystal exposed for shorter period and developed after dissolving away surface layers.

(Hedges and Mitchell: Phil. Mag., 7, 357 (1953).)

PLATE 2(a). PHOTOMICROGRAPHS SHOWING THE SUB-STRUCTURE OF AgBr.

when polygonised sodium chloride crystals after heat treatment with sodium metal, were viewed and observed to contain networks of lines. These were suggested to be sets of dislocation lines forming internal grain boundaries, which were effective traps for the precipitation of sodium in the interior of the crystals. Tompkins and Young(4) have similarly reported that heating potassium azide coloured with ultra-violet light resulted in the formation of colloidal centres of potassium. These centres were thought to form by diffusion of potassium atoms along dislocations to diffusional jogs and crossing points, which acted as deep traps for the potassium atoms.

Thus, it is considered that heating irradiated lithium azide leads to specks or nuclei of lithium metal along grain boundaries and on the external surface. From this point, nuclear growth commences and the reaction enters the acceleratory phase.

The mechanism for nuclear growth during the acceleratory period is considered to be the same as that occurring during the same phase of the decomposition of unirradiated lithium azide. This mechanism involves the elevation of an electron from an azide ion to the conduction band of the lithium metal formed during the induction period, followed by reaction between the positive hole so formed and an adjacent azide ion, on receipt of sufficient thermal energy for the reaction to proceed. The rate determining step is considered to be the same as that for the unirradiated salt i.e. the elevation of the electron to the metal. The activation energy for this process (26 k.cals/mole) is in agreement with the value found for the unirradiated azide (28 k.cals/mole and 29 k.cals/mole for powder and pelleted material respectively). Reaction between an adjacent azide ion and positive hole can be expected to be effected more easily during the decomposition of the irradiated salt, due to strain along the internal grain boundaries. The thermodynamic instability of the azide ion in the region of a grain boundary leads to the belief that the reaction of azide ion and positive hole will be relatively easy and rapid, so that the slow step will be as proposed above:

$$N_3^- \rightarrow N_3 + e \quad \ldots\ldots\ldots\ldots\ldots\ldots\ldots\ldots (6.5.9)$$

Interruption with water vapour (5 mins) at t = 0, i.e. prior to thermal decomposition, was observed to completely destroy the irradiation effect and an induction period of the same duration as found for the decomposition of the unirradiated material, resulted. The rate constant k_1 was reduced to a small extent. It is considered that the water vapour penetrated into the grain boundaries and the radiation effect was completely destroyed. It is not unlikely that the water vapour can diffuse into the grain boundaries internally in the particle, as in the example of silver bromide the bromine formed readily diffused to the surface and escaped$^{(200)}$. Also, in the case of the decomposition of γ-irradiated pelleted lithium azide when large volumes of nitrogen escaped into the reaction container, no explosion or disintegration of the pellet occurred, illustrating the relative case with which the nitrogen escaped.

It is thought that two possibilities exist for the removal of the radiation damage by water vapour (5 mins exposure). These are:

(i) direct attack on F-centre aggregates,

(ii) attack on trapping sites and subsequent collapse of F-centre aggregates.

It is also possible that (i) and (ii) above may occur, however, it is thought that (ii) is the more likely process. The experimental results obtained can be explained if one assumes that the water vapour destroys the traps by hydrolytic reaction and the F-centres aggregated at them to form lithium atoms which would react with the water vapour. If the new centres formed were still capable of trapping F-centres then fresh irradiation by γ-rays should regenerate the irradiation effect which was removed by exposure to water vapour. The reason that 30 secs exposure to water vapour at $t = 0$ had no effect on the subsequent reaction is thought to be that this exposure time was insufficient to produce the effect that the longer exposure time did. The water vapour penetrates the interior of the crystal (as is supported by the fact that 0.5 I.P. and end of the induction period 30 sec exposures produced a new reaction, after destroying the lithium atoms present along the grain boundaries) but does not effect hydrolysis of the trapping sites.

Interruption of the decomposition (30 secs exposure) at $\alpha = 0.24$ destroyed the metal nuclei but not any radiation species ($t = 0$, 30 secs has no effect). During the new induction period the changes are the same as those taking place during the induction period of the decomposition of the irradiated salt. The new induction period is longer than that for the normal decomposition of the irradiated salt. This is to be expected as the number of lithium atoms formed is only a fraction of the number formed during the original induction period. The smaller number of nuclei account for the slower rate.

In all the water interruption runs it was observed that the final pressure was lower than that expected, indicating partial hydrolysis of the azide.

It can be assumed from the series (FIGURE 6.12) involving interruption followed by irradiation (1000 roentgens) that internal nucleation due to the radiation damage always results on resuming the decomposition, as interruption and irradiation even at $\alpha = 0.47$ (at the inflexion point) when the surfaces of the particles are covered by "contracting envelopes", results in an increased rate on resuming decomposition. The fact that on resuming reaction the p/t plots did not follow the original p/t plot (unirradiated) until nucleation along grain boundaries had occurred is probably due to destruction of some of the thermal nuclei by water vapour during sealing the sample in the ampoule and during irradiation. An increasing initial reaction (i.e. no true induction period) indicating a reduced number of thermal nuclei preceeds the subsequent enhanced acceleratory rate, due to nuclear growth along grain boundaries, as mentioned previously.

The supposition that water vapour destroys some of the thermal nuclei during sealing and irradiation is probably correct because with a similar run, along with an irradiated blank run (200 roentgens) exhibiting a well marked induction period, the same effect was obtained to a greater degree, since the subsequent rate was closer to the unirradiated curve, (FIGURE 6.11).

It is assumed that thermal energy chains are not operative since interruption of the decomposition produced no effect in the decomposition of irradiated material.

Annealing the γ-irradiated material produced no change in the state of radiation damage.

At the commencement of the decay reaction and into this period, the reaction mechanism is assumed to be similar to that occurring during the decomposition of unirradiated lithium azide, namely blocks of material are enveloped by a layer of lithium and reaction occurs at the steadily contracting metal/salt interface. This type of mechanism leads to the decay portion of the p/t plot being described by the contracting sphere formula. This phase of the decomposition was found to have an activation energy of 28 k.cals/mole which is the same value as that found for the similar phase of the decomposition with the unirradiated salt (29k.cals/mole).

Accordingly it is proposed that as for the unirradiated material, the rate determining step is the combination of a positive hole and an adjacent azide ion:

$$N_3 + N_3^- \rightarrow 3N_2 + e \quad \ldots\ldots\ldots\ldots\ldots\ldots \quad (6.5.10)$$

In the decay region, the material is considered to consist of blocks of unirradiated material. Interruption and irradiation well into the decay period produced no effect on the subsequent decay reaction indicating that the trapping sites in the crystals had been destroyed at this stage.

The percentage decomposition of the γ-irradiated powder was found on the average to be 91%, this value being slightly higher than that found for unirradiated lithium azide powder.

6.5.2 Pelleted lithium azide

The p/t plots for the decomposition of γ-irradiated pelleted lithium azide are characterised by a double-sigmoid plot, as illustrated in FIGURES 6.1 and 6.3. There is marked reduction in the length of the induction period, as found for the γ-irradiated powder. The induction period is followed by short acceleratory and decay periods, which are in turn followed by a second sigmoid reaction. The p/t plot obtained when γ-irradiated lithium azide powder was pelleted and then decomposed, exhibited the same features as found for the irradiated pelleted material. However, the initial reaction (i.e. first acceleratory and decay periods) was not as pronounced as in the latter case.

The runs using irradiated pelleted material exhibited irreproducibility and the activation energies associated with the first acceleratory period and second decay period were accordingly attempted by the split-run technique. Values obtained for these stages of the reaction were 25 and 27 k.cals/mole respectively. For reasons mentioned below, it is thought that a certain amount of experimental error was involved in these determinations.

Successful analysis of the initial acceleratory reaction using the Avrami-Erofeyev equation, with the exponent $n = 2$, for material irradiated with a γ-ray dose of 15000 roentgens gives rise to two possibilities for nuclear formation and growth,

(i) one-dimensional nuclei, increasing in number linearly with time,

(ii) two-dimensional nuclei, growing from a fixed number of sites.

The results obtained can be accounted for if (ii) is assumed to be the nuclear process.

As a result of the pelleting process there will be extreme disorganisation of the surfaces of the particles as they are pressed together, to form new "internal surfaces". These regions are considered to be likely ones for the formation of F-centres. In addition, some F-centres will also form as before at the grain boundaries in the individual particles, but it is assumed that the concentration of centres in the new "internal surfaces" is very high. Both sets will contribute to the reaction but the first acceleratory and decay reactions are considered to be associated with reaction at the new "internal surfaces".

On pelleting the <u>irradiated material</u>, it is suggested that a number of the F-centre aggregates present in the material diffuse to the "internal surface". Seitz(194) favours the diffusion of the more mobile aggregates but does not preclude the mobility of F-centres in crystals.

Thus the pelleted material in both cases will represent the same physical condition at the commencement of heating, except that aggregation of F-centres and the number of aggregates already formed at the "internal surface" by thermal diffusion at room temperature will be higher in the case of the irradiated pellet.

When heating commences the F-centre aggregates at the "internal surfaces" collapse to form Li atoms which then crystallise to form metal nuclei. Reaction then occurs at a fixed number of nuclei which grow two-dimensionally. There will also be reaction in the grain boundaries of the particles but this is considered to be less significant than the one at the "internal surfaces" at this stage of the decomposition. This process is considered to account for the first or initial reaction during the decomposition of pelleted irradiated or irradiated pelleted lithium azide.

The proposed mechanism will also account for the fit of the two-dimensional contracting growth law to the first decay i.e. the rate of reaction falls off as the two-dimensional nuclei overlap. The activation energies associated with the first acceleratory and decay reactions and for the powdered irradiated material, should be the same. It was not possible to obtain a reliable estimate of the first decay activation energy due to the irreproducible nature of the pelleted material and to the overlap occurring during this phase. The value of the activation energy for the first acceleratory period (25 k.cals/mole) is considered within the experimental errors involved in the split run technique, to be in agreement with the value obtained for the acceleratory process in the irradiated lithium azide powder (26 k.cals/mole).

On completion of the reaction at the "internal surfaces", the normal reaction along grain boundaries in the individual particles which comprised the pellet predominates and the second acceleration and decay in the p/t plot are due to this change. The activation energy for the second decay reaction (27 k.cals/mole) was determined by the split-run method. The decay mechanism is assumed to be contracting sphere mechanism previously reported for the decay period of the irradiated powdered material (28 k.cals/mole).

It is considered that the same mechanisms apply in the case of the decomposition of lightly irradiated (50 roentgens) pelleted azide, as in the decomposition of unirradiated pelleted lithium azide. The activation energies for the induction, acceleratory and decay periods for the lightly irradiated pelleted material (22, 29 and 28 k.cals/mole respectively) are in agreement with those for similar processes in the pelleted unirradiated azide (24, 29 and 30 k.cals/mole respectively). This would also explain why a sigmoid curve (p/t plot) and not a double-sigmoid plot was obtained for the thermal decomposition.

Visual observations and the photomicrographs indicate that extensive external decomposition has occurred at the end of the first decay reaction as the pellet was covered with reaction product and the interior of the pellet was uniformly brown at this stage indicating large surface coverage of the constituent particles of the pellet. Reaction had commenced throughout the pellet as evident from visual observations of a cross-section of the pellet at the inflexion point of the first reaction.

The effect of increasing the pellet weight increased the extent of the initial reaction indicating that this reaction in the decomposition of the pelleted lithium azide irradiated with γ-rays was not dependant on the external surface area of the pellet, but on the quantity of material.

The average percentage decomposition for the pelleted lithium azide pre-irradiated with 15000 roentgens γ-rays was found to be slightly higher (85%) than that for the unirradiated pelleted azide (79%). A similar trend was observed on irradiating lithium azide powder.

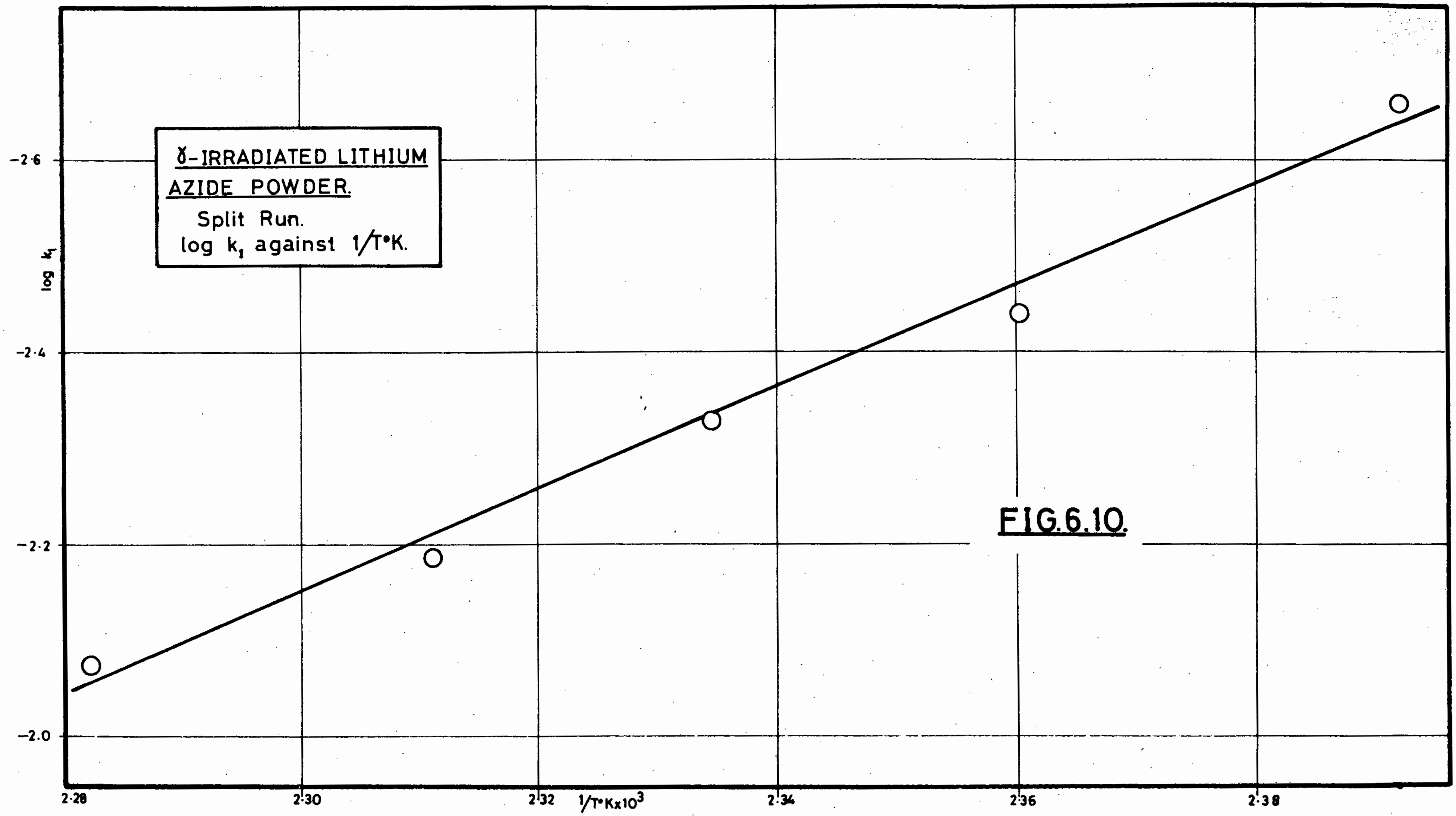
γ-IRRADIATED LITHIUM AZIDE POWDER.
Split Run.
log k₁ against 1/T°K.
log k₁
−2·6
−2·4
−2·2
−2.0
2·28
2·30
2·32
1/T°K x 10³
2·34
2·36
2·38

FIG.6.10.

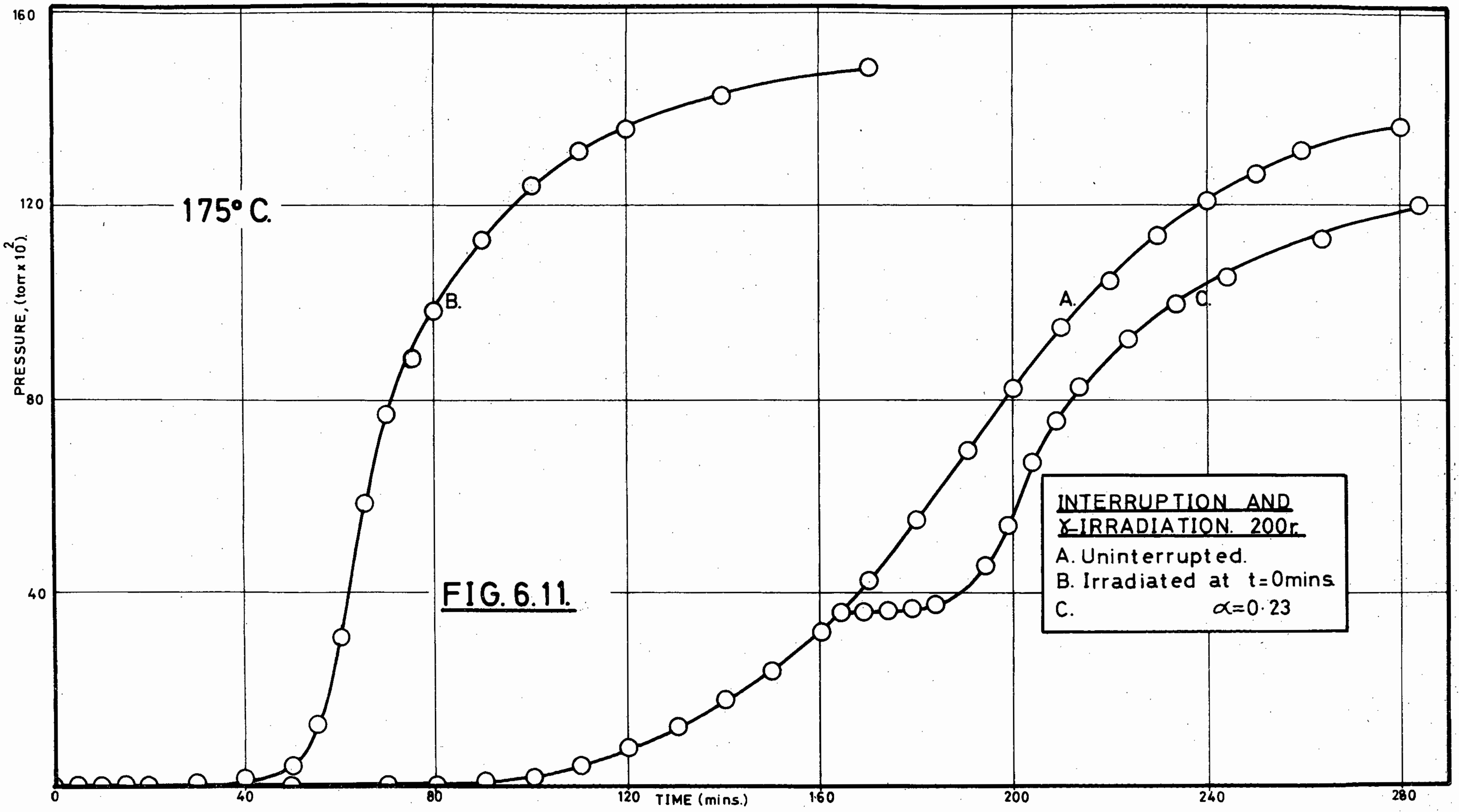
160
120
80
40
0
PRESSURE, (torr x 10^2).
0
40
80
120
TIME (mins.)
160
200
240
280
175° C.
B.
A.
C.
INTERRUPTION AND
γ-IRRADIATION. 200r.
A. Uninterrupted.
B. Irradiated at t=0mins.
C. α=0·23

FIG. 6.11.

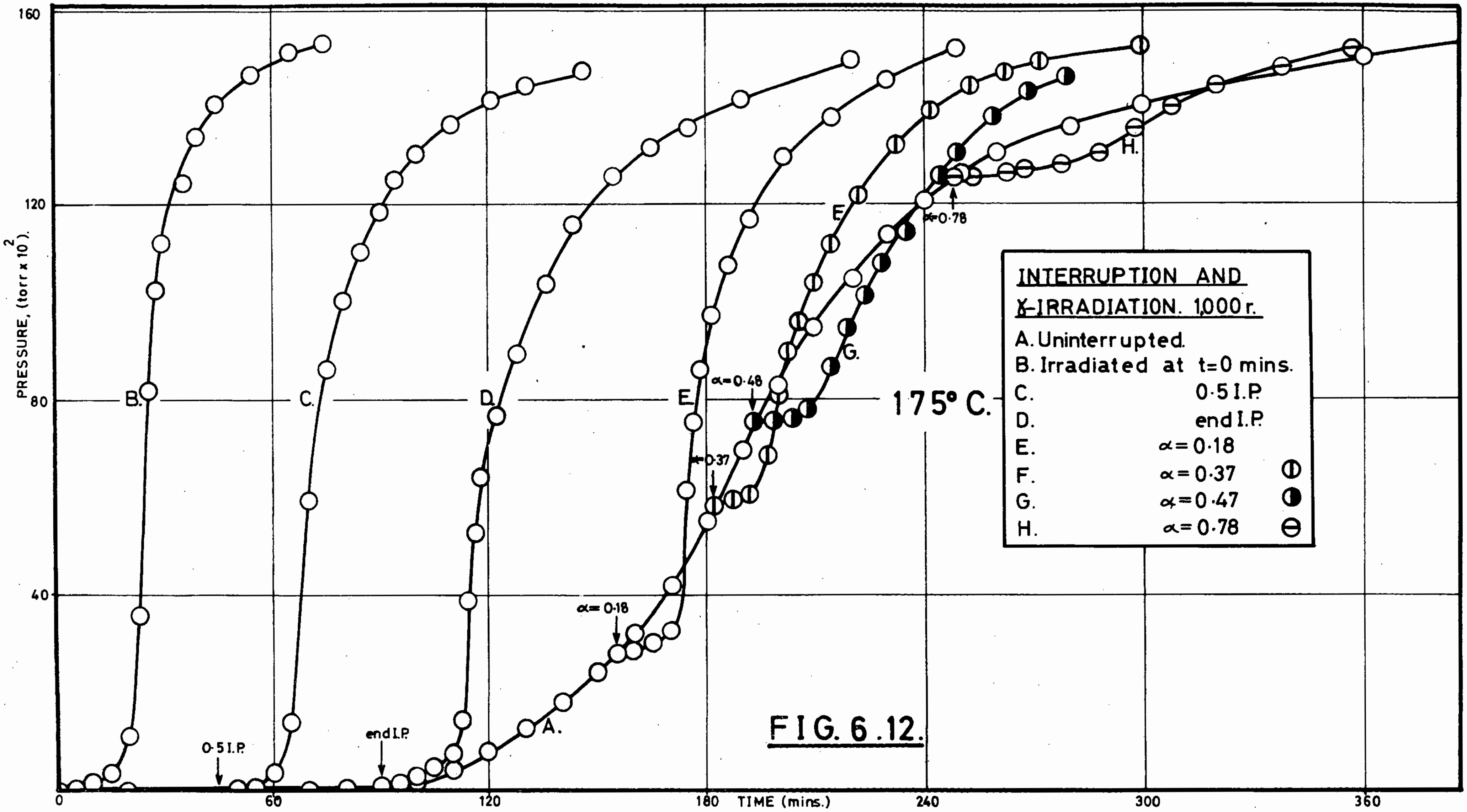

INTERRUPTION AND
γ-IRRADIATION. 1,000 r.
A. Uninterrupted.
B. Irradiated at t=0 mins.
C. 0·5 I.P.
D. end I.P.
E. α = 0·18
F. α = 0·37 ⦶
G. α = 0·47 ◑
H. α = 0·78 ⊖
175° C.
PRESSURE, (torr x 10^2).
TIME (mins.)
160
120
80
40
0
60
120
180
240
300
360
A.
B.
C.
D.
E.
E.
G.
H.
0·5 I.P.
end I.P.
α= 0·18
α=0·37
α=0·48
α=0·78

FIG. 6.12.

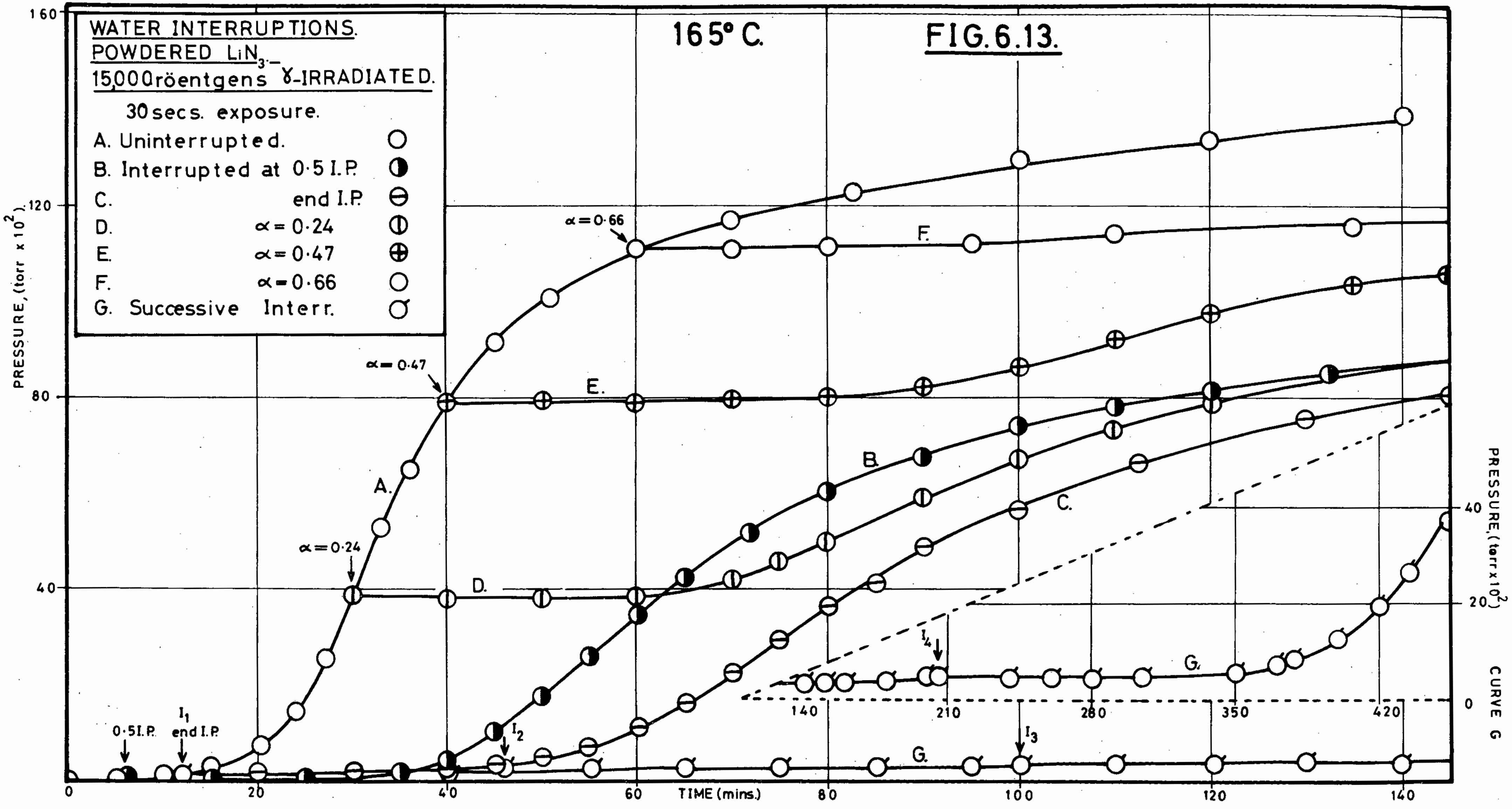

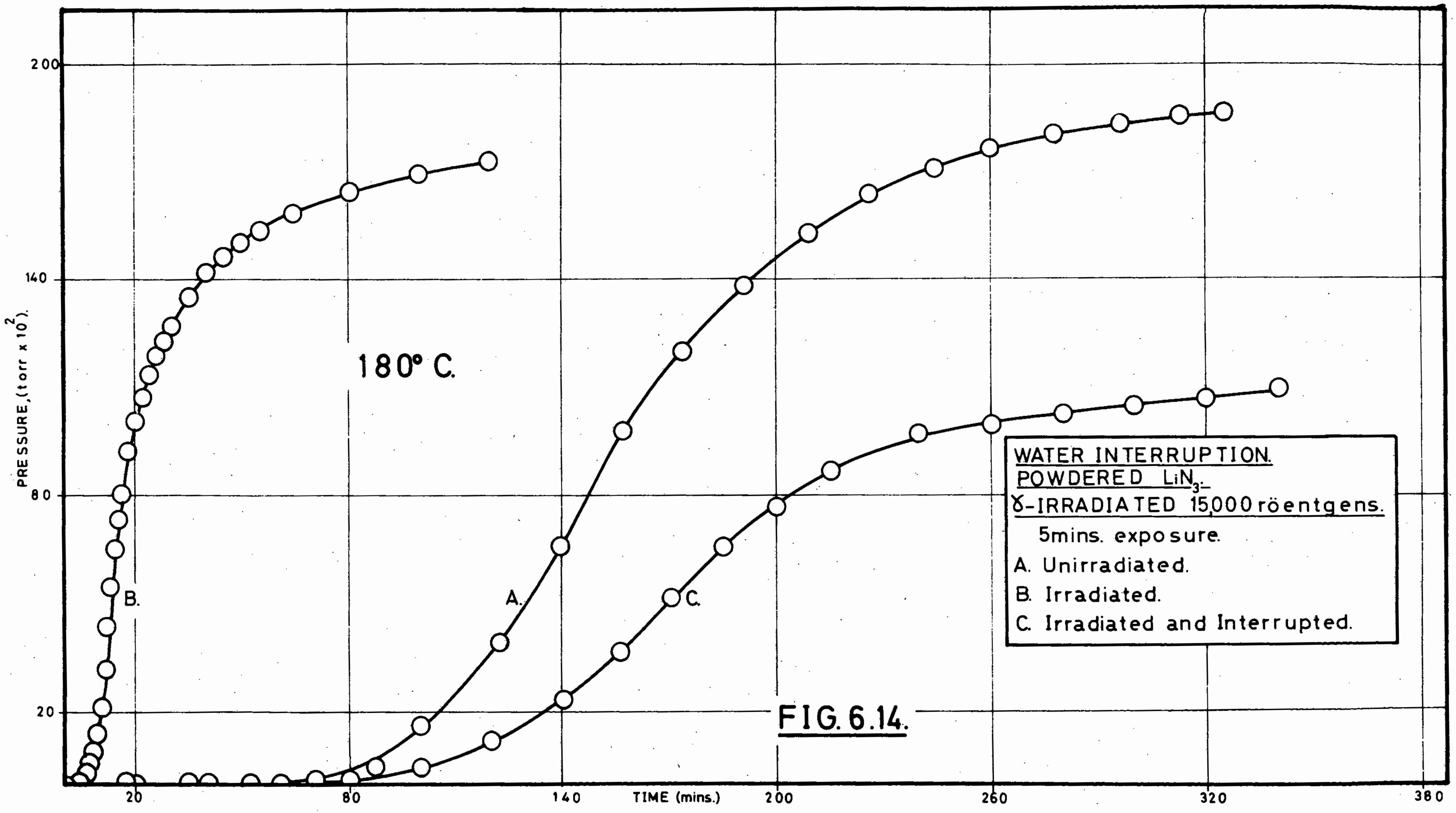
PRESSURE, (torr x 10^2).
200
140
80
20
TIME (mins.)
20
80
140
200
260
320
380
180° C.
A.
B.
C.
WATER INTERRUPTION.
POWDERED LiN_3.
γ-IRRADIATED 15,000 röentgens.
5mins. exposure.
A. Unirradiated.
B. Irradiated.
C. Irradiated and Interrupted.

FIG. 6.14.

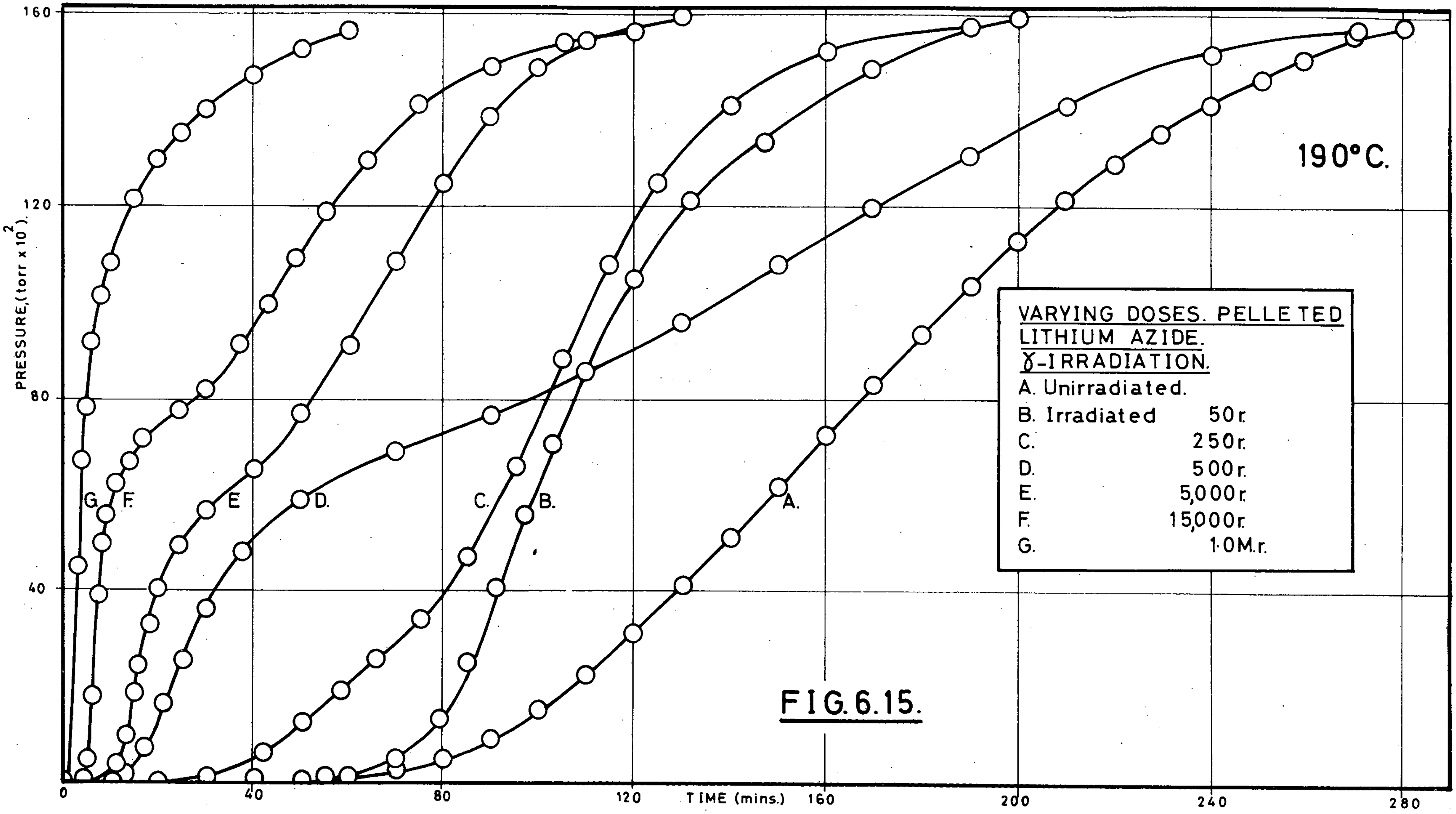
PRESSURE, (torr x 10^2).
160
120
80
40
0
40
80
120
TIME (mins.)
160
200
240
280
190°C.
G
F.
E
D.
C.
B.
A.
VARYING DOSES. PELLETED LITHIUM AZIDE.
γ-IRRADIATION.
A. Unirradiated.
B. Irradiated 50r.
C. 250r.
D. 500r.
E. 5,000r.
F. 15,000r.
G. 1·0M.r.

FIG. 6.15.

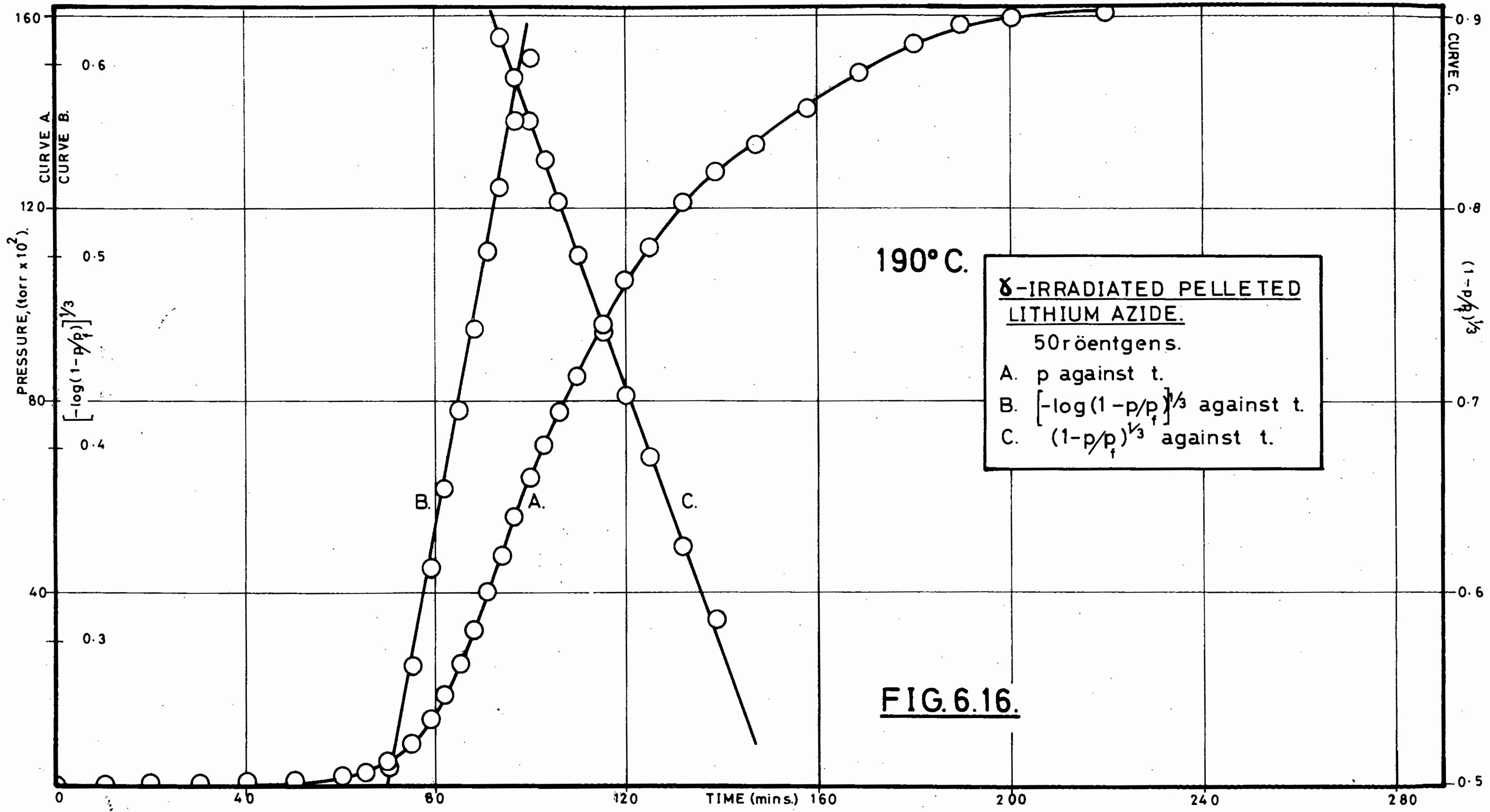

FIG. 6.16.

190° C.
γ-IRRADIATED PELLETED LITHIUM AZIDE.
50 röentgens.
A. p against t.
B. $[-\log(1-p/p_f)]^{1/3}$ against t.
C. $(1-p/p_f)^{1/3}$ against t.
B.
A.
C.
PRESSURE, (torr x 10^2). CURVE A.
$[-\log(1-p/p_f)]^{1/3}$ CURVE B.
$(1-p/p_f)^{1/3}$ CURVE C.
TIME (mins.)
0
40
80
120
160
200
240
280
160
120
80
40
0·6
0·5
0·4
0·3
0·9
0·8
0·7
0·6
0·5

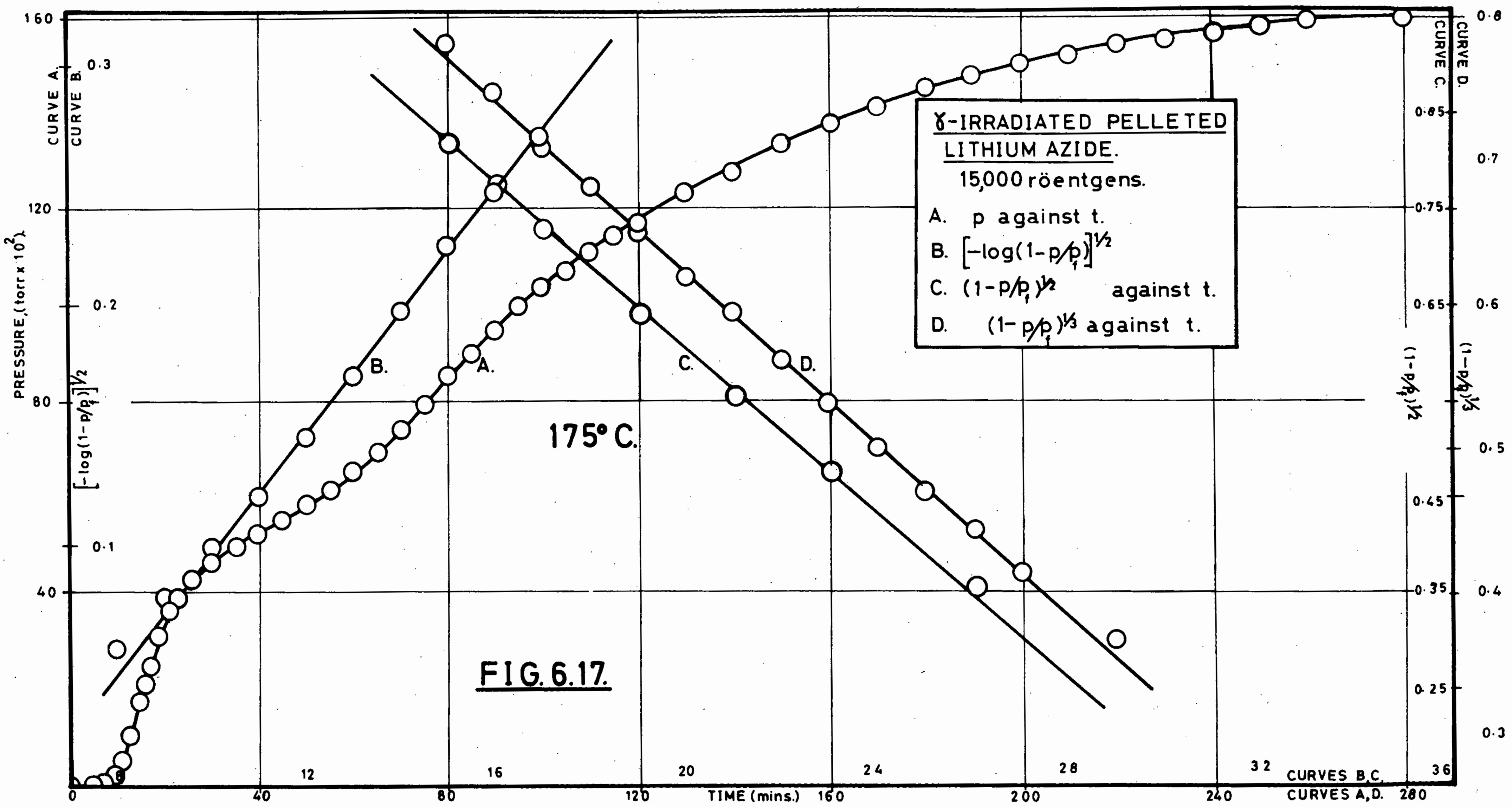

γ-IRRADIATED PELLETED
LITHIUM AZIDE.
15,000 röentgens.
A. p against t.
B. $[-\log(1-p/p_f)]^{1/2}$
C. $(1-p/p_f)^{1/2}$ against t.
D. $(1-p/p_f)^{1/3}$ against t.
175° C.
PRESSURE, (torr x 10^2)
CURVE A.
CURVE B.
$[-\log(1-p/p_f)]^{1/2}$
CURVE C.
CURVE D.
$(1-p/p_f)^{1/2}$
$(1-p/p_f)^{1/3}$
B.
A.
C.
D.
160
120
80
40
0.3
0.2
0.1
0.8
0.7
0.6
0.5
0.4
0.3
0.85
0.75
0.65
0.45
0.35
0.25
0
40
80
120
160
200
240
280
8
12
16
20
24
28
32
36
TIME (mins.)
CURVES B,C.
CURVES A,D.

FIG. 6.17.

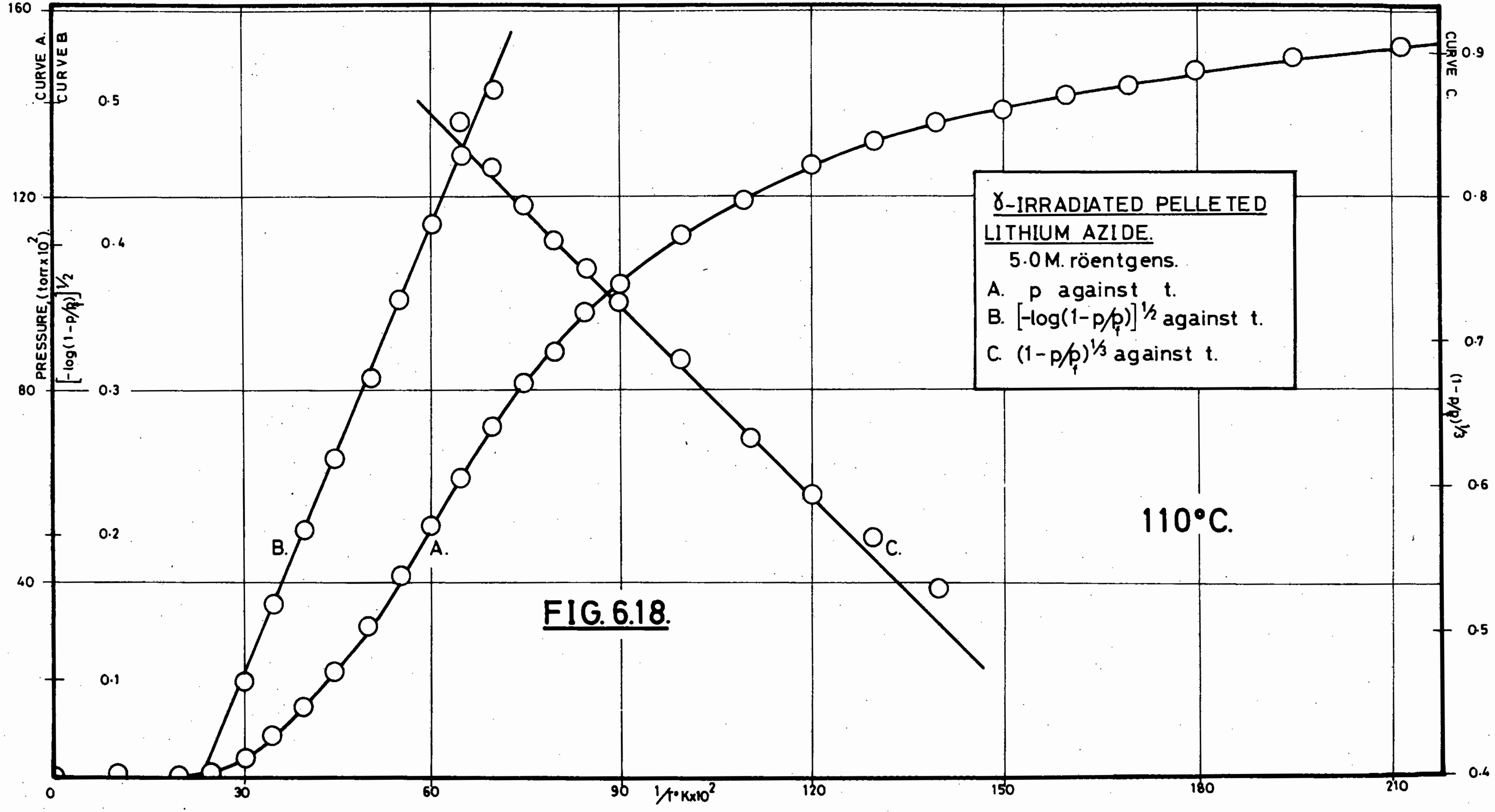
160
120
80
40
0
0·5
0·4
0·3
0·2
0·1
CURVE A.
CURVE B
PRESSURE, (torr x 10^2).
$[-\log(1-p/p_f)]^{1/2}$
0
30
60
90
$1/t$ °K x 10^2
120
150
180
210
CURVE C.
0·9
0·8
0·7
0·6
0·5
0·4
$(1-p/p_f)^{1/3}$
B.
A.
C.
γ-IRRADIATED PELLETED LITHIUM AZIDE.
5·0 M. röentgens.
A. p against t.
B. $[-\log(1-p/p_f)]^{1/2}$ against t.
C. $(1-p/p_f)^{1/3}$ against t.
110°C.

FIG. 6.18.

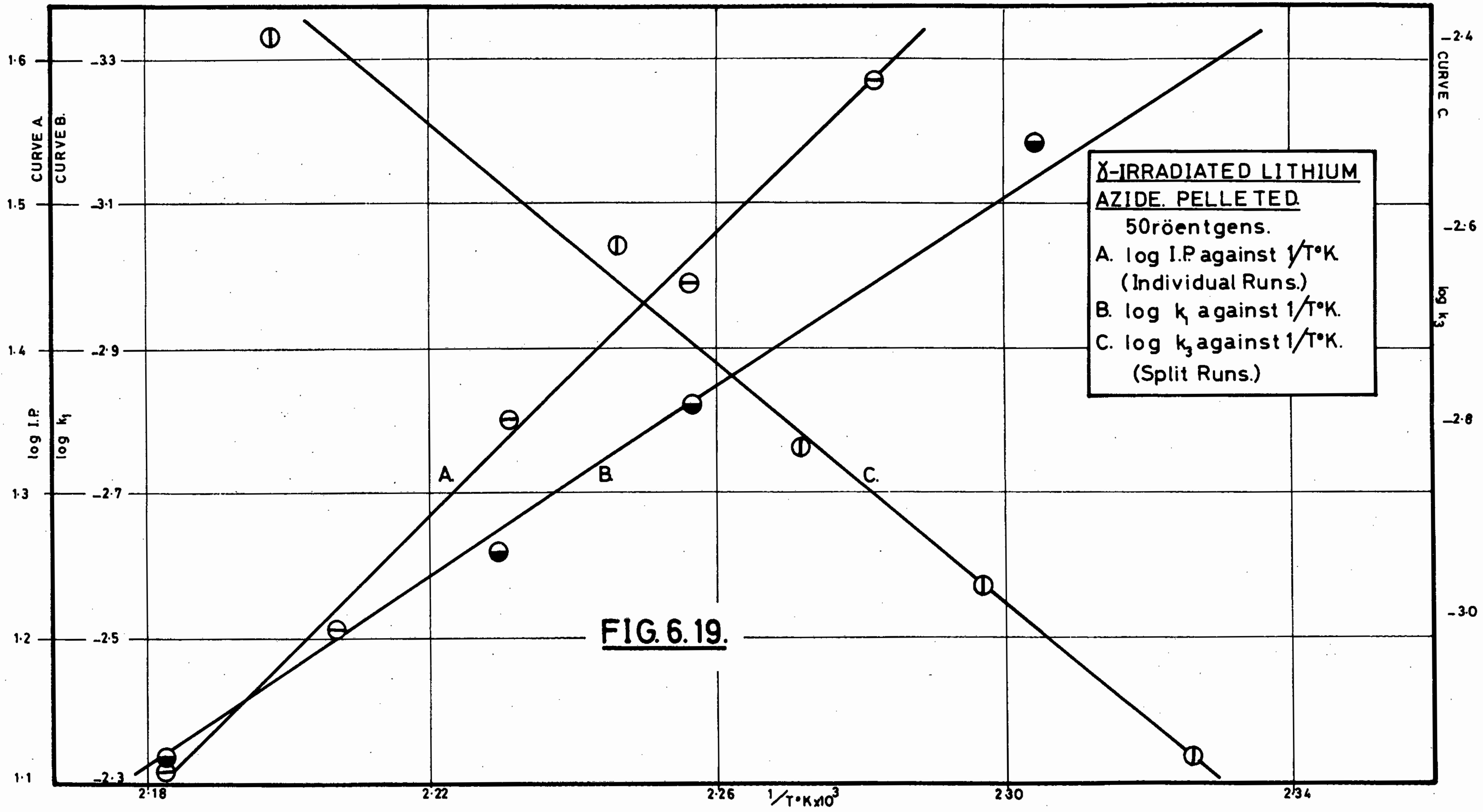

CURVE A
CURVE B.
log I.P.
log k_1
1·6
1·5
1·4
1·3
1·2
1·1
-3·3
-3·1
-2·9
-2·7
-2·5
-2·3
CURVE C
log k_3
-2·4
-2·6
-2·8
-3·0
2·18
2·22
2·26
2·30
2·34
1/T°K×10^3
A.
B.
C.
γ-IRRADIATED LITHIUM AZIDE. PELLETED.
50röentgens.
A. log I.P against 1/T°K.
(Individual Runs.)
B. log k_1 against 1/T°K.
C. log k_3 against 1/T°K.
(Split Runs.)

FIG. 6. 19.

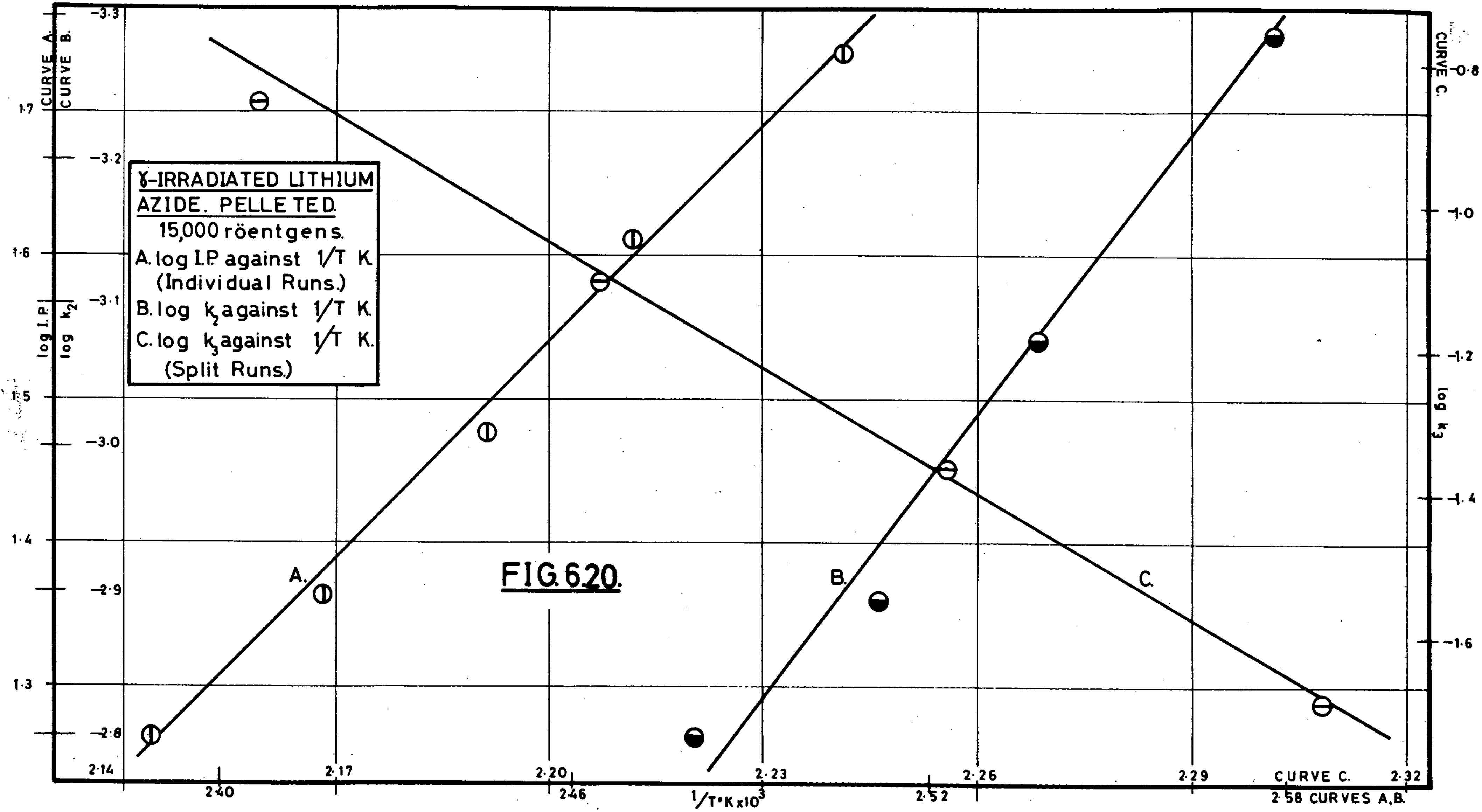
γ-IRRADIATED LITHIUM AZIDE. PELLETED.
15,000 röentgens.
A. log I.P. against 1/T K.
(Individual Runs.)
B. log k₂ against 1/T K.
C. log k₃ against 1/T K.
(Split Runs.)
CURVE A.
CURVE B.
log I.P.
log k₂
1·7
1·6
1·5
1·4
1·3
−3·3
−3·2
−3·1
−3·0
−2·9
−2·8
CURVE C.
log k₃
−0·8
−1·0
−1·2
−1·4
−1·6
A.
B.
C.
2·14
2·17
2·20
2·23
2·26
2·29
2·32
CURVE C.
2·40
2·46
2·52
2·58 CURVES A, B.
1/T°K x10³

FIG. 6.20.

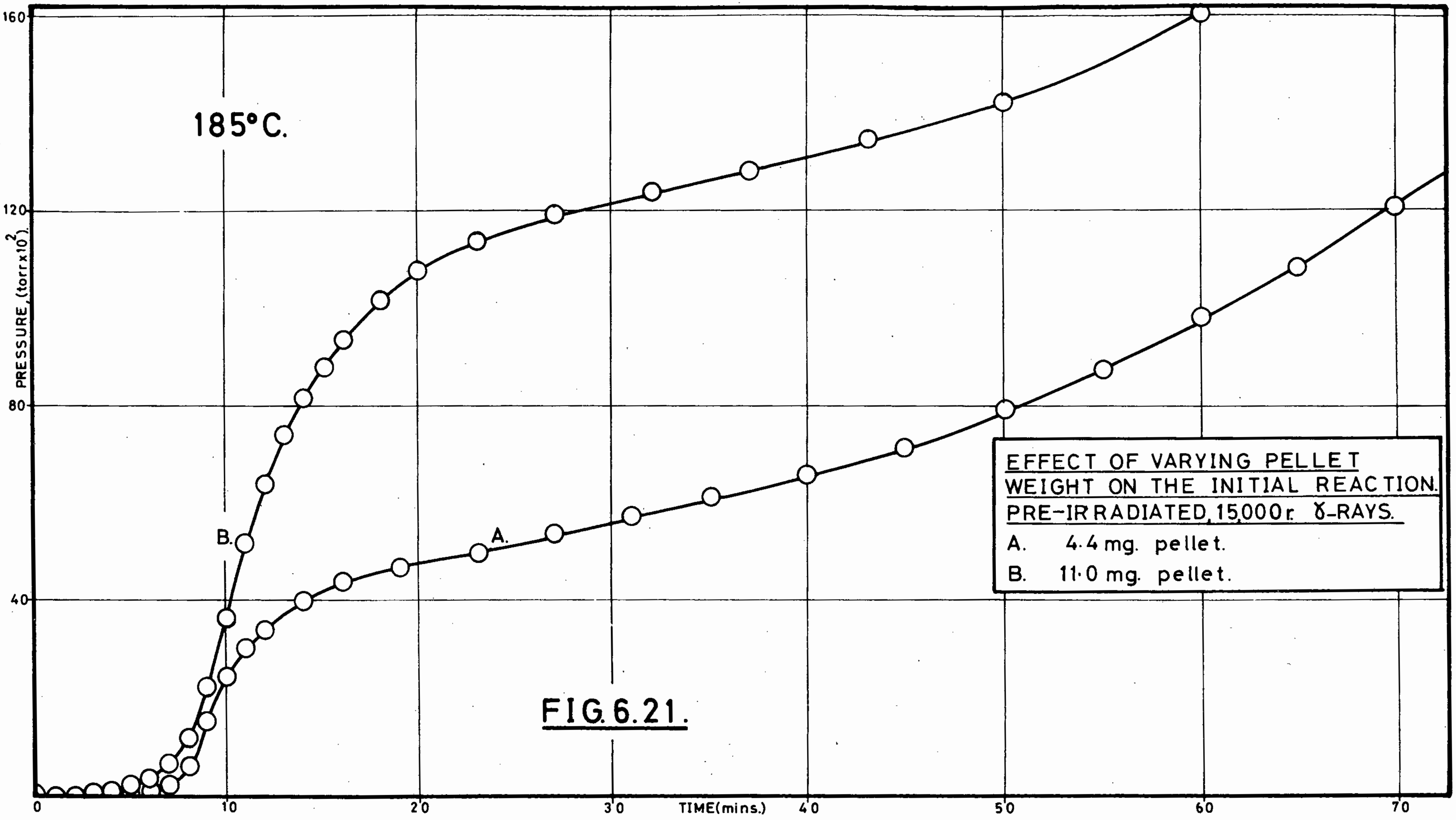

EFFECT OF VARYING PELLET WEIGHT ON THE INITIAL REACTION. PRE-IRRADIATED, 15,000 r. γ-RAYS.

FIG. 6.21.

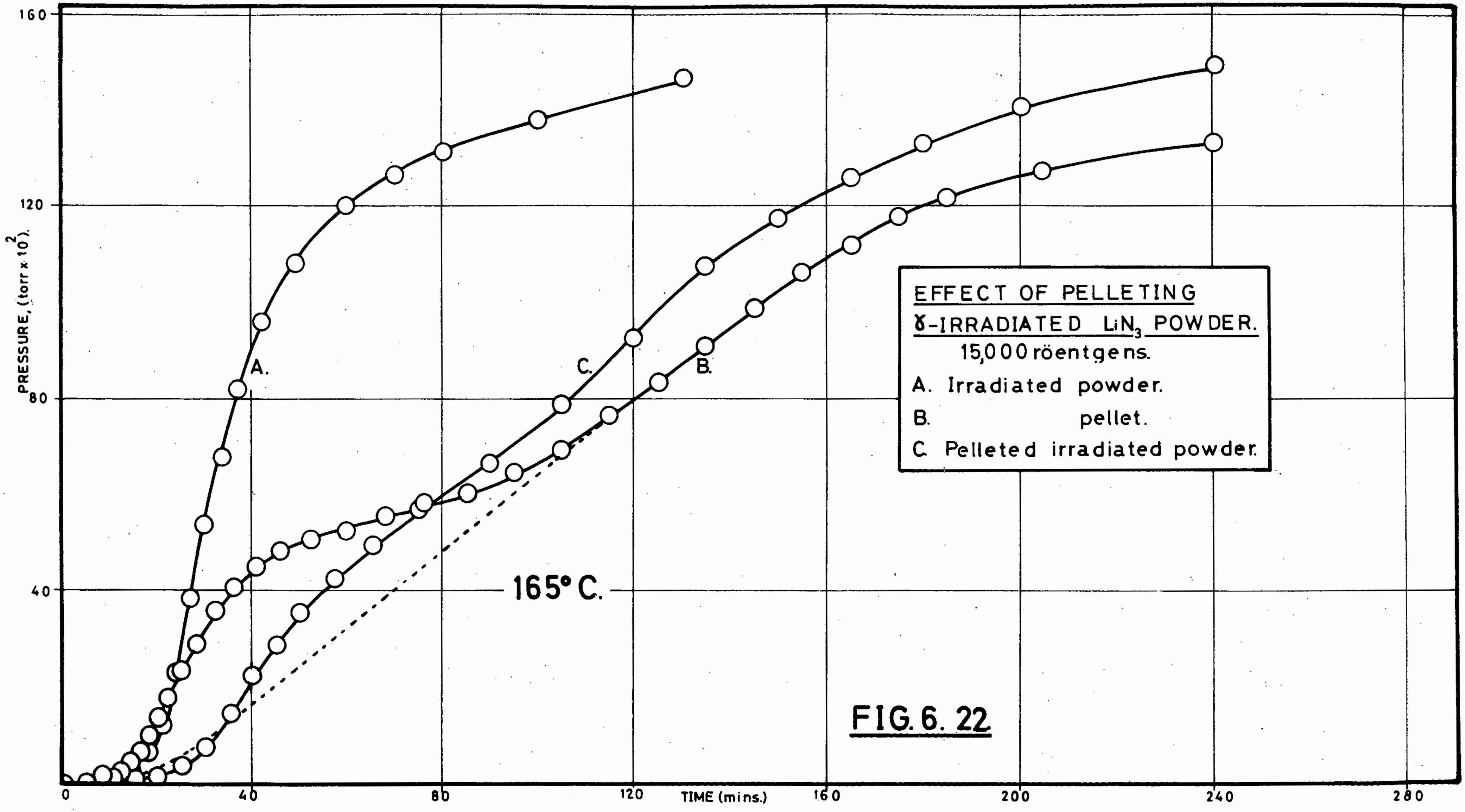
EFFECT OF PELLETING
γ-IRRADIATED LiN_3 POWDER.
15,000 röentgens.
A. Irradiated powder.
B. pellet.
C. Pelleted irradiated powder.
165° C.
A.
B.
C.
PRESSURE, (torr x 10^2).
TIME (mins.)
0
40
80
120
160
200
240
280
40
80
120
160

FIG. 6. 22

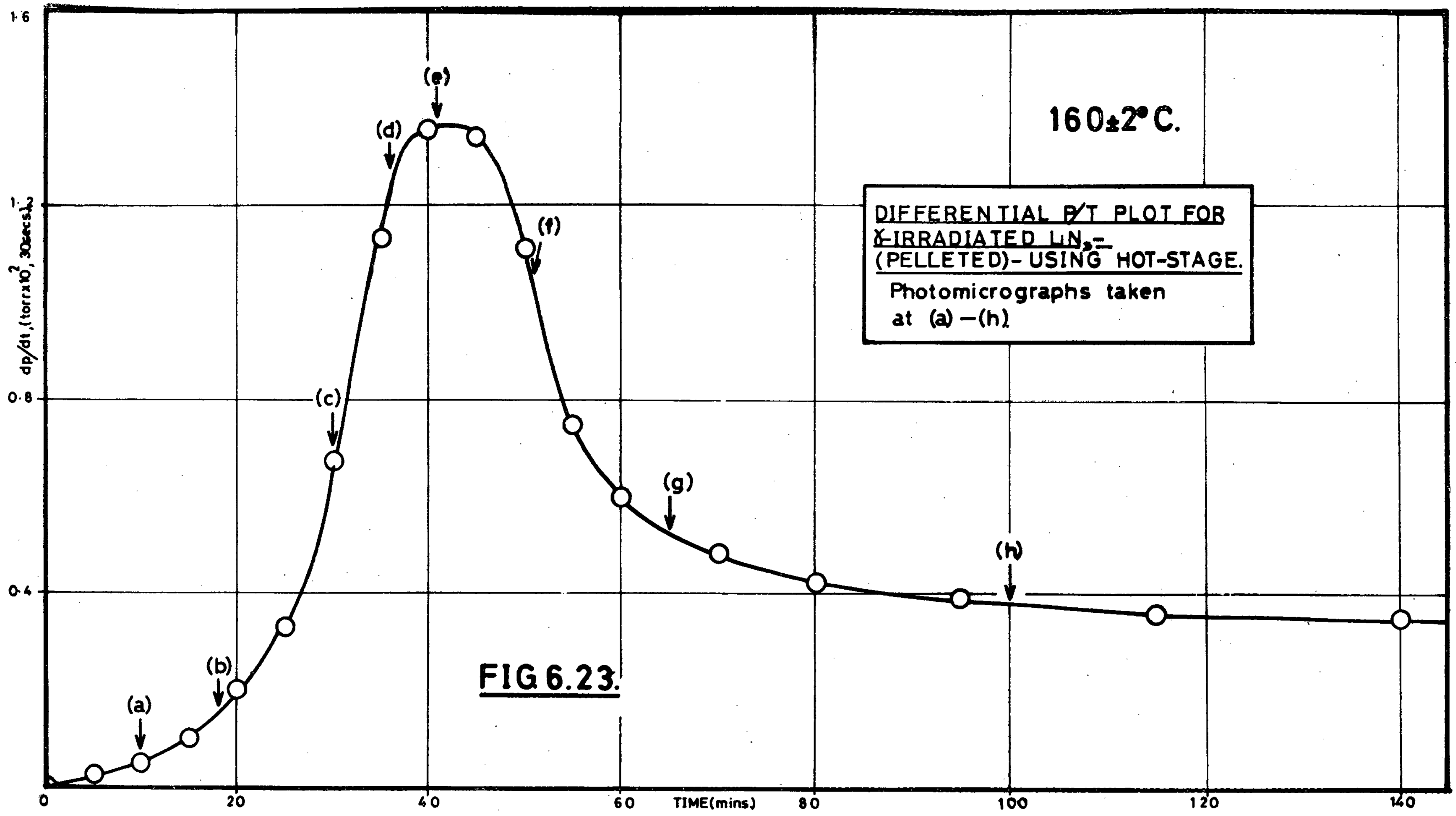
1·6
1·2
0·8
0·4
0
20
40
60
TIME(mins.)
80
100
120
140
dp/dt,(torr x10^2, 30secs)
(a)
(b)
(c)
(d)
(e)
(f)
(g)
(h)
160±2°C.
DIFFERENTIAL P/T PLOT FOR γ-IRRADIATED LiN3-(PELLETED)- USING HOT-STAGE.
Photomicrographs taken at (a)-(h).

FIG 6.23.

7. THE THERMAL DECOMPOSITION OF LITHIUM AZIDE PRE-IRRADIATED WITH X-RAYS

7.1 PRELIMINARY INVESTIGATIONS

7.1.1 Pelleted lithium azide

On account of the sensitivity shown by lithium azide to pre-irradiation with γ-rays, low generator settings were used initially for the X-irradiations. The material was irradiated with a tube voltage of 10 kV and a tube current of 5mA.

Examination of the effect of X-irradiation on the thermal decomposition of pelleted lithium azide showed that a double-sigmoid pressure-time plot was obtained. The p/t plot was similar to those obtained for the thermal decomposition of pelleted material pre-irradiated with γ-rays. No colour change was observed as the result of X-irradiation for two hours (10 kV, 5 mA). The p/t curves for the thermal decomposition of pelleted lithium azide pre-irradiated with X-rays for two hours and a blank run, appear in FIGURE 7.1 and the p/t results are tabulated in TABLE 7.1. The reaction temperature was 195°C. It is seen that the induction period was reduced from 45 to 8 mins.

7.1.2 Powdered lithium azide

Irradiation of powdered lithium azide (prepared as in 5.3 and as used in previous work on the powdered salt) for 30 mins (10 kV, 5 mA) followed by thermal decomposition of 5.0mg of the salt at 175°C in the usual manner, showed the induction period to be reduced from 79 to 25 mins. The reaction rate was observed to have increased and the inflexion point was lowered to $\alpha = 0.26$. No colour change was observed to occur as a result of the irradiation of the powdered lithium azide.

The p/t plots of the decomposition of X-irradiated powdered lithium azide and a blank unirradiated run appear in FIGURE 7.2 and the results are tabulated in TABLE 7.1.

7.2 REPRODUCIBILITY

7.2.1 Pelleted lithium azide

As was found in 6.2.1 with γ-irradiated pelleted lithium azide, X-irradiation of pelleted azide resulted in irreproducible pressure-time plots. It was also observed that interruption of a decomposition had an irreproducible effect on the subsequent thermal decomposition, making investigation of the activation energies for the various chemical processes, by the split-run technique, impossible.

Accordingly, it was decided to confine the investigation of the effects of pre-irradiation with X-rays to the powdered salt.

7.2.2 Powdered lithium azide

Powdered lithium azide was pre-irradiated with X-rays (10 kV, 5 mA), as has been described in 4.2.3 (b). The equipment used has been described in 4.1.4 (b). Approximately 4.4 - 5.5mg of the sample of pre-irradiated salt were used for a decomposition. Decomposition was carried out in vacuo in the manner described previously, at 175°C. The material was pre-irradiated for 30 mins. Reproducibility was found to be of a high order. The lengths of the induction periods were found to be 32, 31 and 31 mins.

The results appear in TABLE 7.2 and the p/t plots are graphically illustrated in FIGURE 7.3. The derived rate constants k_2 and k_3 (equations 6.1 and 5.3) for the acceleratory and decay periods respectively were found to be as follows:

(i) Acceleratory period: 1.05×10^{-2}; 1.03×10^{-2}; and 1.06×10^{-2} min^{-1} respectively.

(ii) Decay period: 3.98×10^{-3}; 4.08×10^{-3}; and 4.16×10^{-3} min^{-1} respectively.

Reproducibility was found to be good when the samples were drawn from a bulk of irradiated lithium azide but p/t plots were different for different batches of lithium azide irradiated under "identical" conditions, (30 mins; 10 kV, 5 mA; 100 - 200 mg. LiN_3). This effect is illustrated in FIGURE 7.4 and the results appear in TABLES 7.2 and 7.3, for two runs done at 175°C. The same kinetic equations were applicable for these runs although the rate constants differed.

7.3 RESULTS (POWDERED LITHIUM AZIDE)

FOR REASONS GIVEN IN 7.2.1, ONLY THE PRE-IRRADIATED POWDERED AZIDE WAS INVESTIGATED.

7.3.1 The effect of varying doses of X-irradiation

The effect of an increasing dose of X-rays on the thermal decomposition of lithium azide using a tube voltage of 10 kV and tube current of 5 mA throughout the series, is graphically illustrated in FIGURE 7.5. The reaction temperature was 175°C and approximately 5.0mg of material were used for a decomposition run. The p/t results appear in TABLE 7.4.

The azide was exposed to the X-ray beam for 2,5,10, 15 and 30 mins, and 1, 3 and 16 hours.

There was a decrease in the length of the induction period and this effect became more pronounced with the increasing dose. The subsequent p/t plot after the induction period was sigmoid throughout the series and the acceleratory and decay rate constants increased with increasing dose. The increase in the decay rate constant, however, was negligible compared to the corresponding increase following γ-preirradiation.

After decreasing from $\alpha = 0.46$ to $\alpha = 0.38$ the inflexion point was observed to remain approximately constant, but a noticeable decrease for the material irradiated for 16 hours was observed. The inflexion point for the latter run was $\alpha = 0.16$. After 16 hours exposure to X-rays the salt was observed to be a light grey colour and a low p_a was recorded for the weight of material used in the decomposition. No visible change in the material was observed for lesser doses than 16 hours.

The lengths of the induction periods (mins) and the acceleratory and decay periods derived rate constants k_2 and k_3 for the X-irradiated varying dose series and for a blank unirradiated run, appear in the table below.

DOSE (mins)	INDUCTION PERIOD (mins)	INFLEXION POINT (α)	k_1, k_2 (mins^{-1})	k_3 (mins^{-1})
0	75	0.46	7.25×10^{-3} (k_1)	4.70×10^{-3}
2	52	0.38	6.54×10^{-3} (k_2)	3.50×10^{-3}
5	42	0.36	8.75×10^{-3}	3.85×10^{-3}
10	36	0.34	8.81×10^{-3}	3.80×10^{-3}
15	31	0.28	1.03×10^{-2}	4.08×10^{-3}
30	25	0.31	1.23×10^{-2}	4.80×10^{-3}
60	16	0.28	1.83×10^{-2}	7.65×10^{-3}
180	10	0.32	2.50×10^{-2}	9.20×10^{-3}
960	7	0.16	2.86×10^{-2}	1.02×10^{-2}

7.3.2 The effect of varying the temperature of decomposition

The mathematical equations applied and the rate constants derived in this section are discussed below in 7.3.3.

The critical increments for the chemical process(es) occurring in the thermal decomposition of powdered lithium azide pre-irradiated with X-rays for 30 mins (10 kV, 5 mA) were determined using the individual runs method. Approximately 5.0 mg samples were used for a thermal decomposition. The temperature range was 165° - 185°C.

The effect of varying the decomposition temperature on the length of the induction period was repeated using a different ground batch, irradiated separately from the material used in the varying temperature series in this section. The temperature range was 150° - 180°C. Reaction was allowed to proceed to approximately 4×10^{-2} torr at a particular temperature and the temperature was then raised to 215°C for 2 hours to obtain the p_a.

The rate constants k_2 and k_3 (equation 6.1 and 5.3) and the duration of the induction periods (mins) appear in the table below. The p/t values for the decompositions are given in **TABLE** 7.5. The effect of varying the temperature of decomposition is shown in **FIGURE** 7.6.

Temperature (°C)	Induction period (mins)	k_2 (mins^{-1})	k_3 (mins^{-1})
150.0	53	-	-
155.0	44	-	-
161.0	33	-	-
165.0	27	-	-
170.0	19	-	-
175.0	16	-	-
180.0	13	-	-

Temperature (^{o}C)	Induction Period (mins)	k_2 (mins $^{-1}$)	k_3 (mins $^{-1}$)
165.0	27	6.73×10^{-3}	1.65×10^{-3}
170.0	22	9.60×10^{-3}	2.66×10^{-3}
175.0	18	1.21×10^{-2}	3.91×10^{-3}
180.0	13	1.74×10^{-2}	4.05×10^{-3}
185.0	11	2.34×10^{-2}	5.93×10^{-3}
190.0	-	2.74×10^{-2}	8.89×10^{-3}

7.3.3 Mathematical analysis of the results

A typical p/t plot of the thermal decomposition of powdered lithium azide, pre-irradiated with X-rays for 30 mins (10 kV, 5 mA), at 185°C showing the extent of fit of the mathematical analyses, appears in FIGURE 7.7. The inflexion point is at $\alpha = 0.20$. The p/t results appear in TABLE 7.5. The main features of the curve are (i) a short, well-defined induction period with no evolution of gas followed by (ii) a short acceleratory period and (iii) a long decay period occupying approximately 80% of the reaction time.

As found for the unirradiated and γ-irradiated lithium azide no mathematical analysis of the induction period was possible since no gas was evolved. The duration of the induction periods at various temperatures were used as before, to obtain a value for the activation energy.

The acceleratory period was well defined by the Avrami-Erofeyev equation (equation 6.1) with n = 2. The fit covered the whole of the acceleratory period and was found to hold over the range $0.03 < \alpha < 0.20$. The Avrami-Erofeyev equation with n = 2 was found applicable to all p/t plots for X-irradiated lithium azide, throughout the dose range examined and over the temperature range 145° - 190°C.

The decay period was described by the contracting sphere formula (equation 5.3) and the fit was for the range $0.20 < \alpha < 0.65 - 0.75$. The contracting sphere equation was found applicable over the temperature range studied, ($145^{\circ} - 190^{\circ}C$).

7.3.4 Evaluation of the activation energies

The critical increments for the chemical process(es) occurring in the thermal decomposition of powdered lithium azide pre-irradiated with X-rays for 30 mins (10 kV, 5mA) were obtained by applying the Arrhenius equation.

The activation energy for the induction period was found as described in 5.3.3 by plotting the logarithms of the lengths of the induction periods against 1/T (°K), where T is the decomposition temperature in °K.

The activation energies for the acceleratory and decay periods were obtained by plotting log k_2 and log k_3 (equations 6.1 and 5.3) against 1/T (°K).

The above plots were straight lines from the slopes of which the activation energies were obtained. The plots of log I.P., log k_2 and log k_3 against 1/T (°K) appear in FIGURE 7.8. The values of the activation energies calculated for the induction, acceleratory and decay periods for the thermal decomposition of X-irradiated lithium azide are as follows:

(i)	Induction period:	22 k.cals/mole
		19 k.cals/mole
(ii)	Acceleratory period:	25 k.cals/mole
(iii)	Decay period:	28 k.cals/mole

7.3.5 The effect of interrupting a decomposition

Interruption of a thermal decomposition has been described previously in 5.3.4. No effect other than a small time lag (4 - 6 mins) was observed when a decomposition run of lithium azide, pre-irradiated for 30 mins with X-rays, (10 kV, 5mA), was interrupted. Interruptions were at the end of the induction period, at $\alpha = 0.10$, 0.28 and in the decay period at $\alpha = 0.55$. The reaction temperature was 180°C. These results appear in TABLE 7.6.

7.3.6 The effect of interrupting a thermal decomposition and irradiating the salt

The method used and the precautions taken in performing this type of experiment have been described in 4.2.6. The thermal decomposition of unirradiated lithium azide was interrupted at various stages during the course of the reaction and the partially decomposed salt irradiated with X-rays for two hours at 10 kV and 5mA. Approximately 5.0mg of the salt were used for a run. The decomposition temperature was 175°C.

Interruptions were done at $t = 0$, (prior to decomposition), at the end of the induction period, at $\alpha = 0.25$, at the inflexion point ($\alpha = 0.48$) and in the decay period at $\alpha = 0.80$. It was observed that an increase in the reaction rate on commencing decomposition resulted for interruptions up to and including the inflexion point. No new induction periods were formed, other than a small time lag during which the bucket and contents attained thermal equilibrium. Interruption in the decay period had no effect on the subsequent thermal decomposition.

The p/t values for these runs are presented in TABLE 7.7 and the results are graphically illustrated in FIGURE 7.9.

7.3.7 The effect of admitting water vapour onto the salt in an interrupted decomposition

The general technique used for the "water interruptions" series has been described in 4.2.5. All the results presented in this section (7.3.7) are not normalised to illustrate the effect of water interruptions on the p_a.

The effects of exposure to water vapour (30 secs) on the thermal decomposition of X-irradiated lithium azide powder (30 mins, 10 kV, 5mA), were investigated.

The effect of longer exposure, (5 mins), at t = 0 was also investigated.

(i) <u>30 secs exposure to water vapour</u>. Approximately 5.0mg lithium azide, preirradiated with X-rays were used for a decomposition. Water interruptions were done at t = 0, 0.5 I.P., at the end of the I.P., at $\alpha = 0.15$, 0.25 and in the decay period at $\alpha = 0.50$.

The effect of water vapour at t = 0 was to reduce the percentage decomposition, with no effect on the length of the induction period or the value of the rate constant, k_2. Interruption at 0.5 I.P. and at the end of the induction period resulted in a new induction period. In the former case, (0.5 I.P.), k_2 was reduced and for interruption at the end of the I.P. the Avrami-Erofeyev equation with n = 3 was found to be applicable.

For water interruptions at $\alpha = 0.15$ and beyond there was virtually no further decomposition. The p_a in all the water interrupted runs was lower than for the blank decomposition. Heating to 400°C enabled recovery of some of the (35 - 50%) lost gas.

The p/t plot after water interruption at the end of the induction period was so reduced that it was felt that it was of no value to carry out successive interruptions along the induction period. The difficulty involved in obtaining even an approximate value for the length of the induction period after interruption made the investigation impossible.

(ii) <u>5 mins. exposure to water vapour</u>. X-irradiated lithium azide was exposed to water vapour for 5 mins at t = 0, and the sample and vacuum line evacuated for 12 hours, in the normal manner. A blank run, as well as an unirradiated blank run were also done. Approximately 5.0 - 5.5mg of the azide were used for a decomposition.

It was observed that the length of the induction period after exposure to water vapour (162 mins) approached that found for the unirradiated run, (220 mins). The percentage decomposition for the run exposed to water vapour was found to be 42% lower than that for the blank irradiated run.

The Avrami-Erofeyev equation with n = 3 was applicable in the analysis of the acceleratory period for the thermal decomposition of the interrupted run. The rate constant, k_1, was higher than that found for the unirradiated run.

The lengths of the induction periods, the acceleratory period associated rate constants (k_1 and k_2, equations 5.2 and 6.1) and the percentage decomposition for all the runs done above appear in the table below and the p/t values appear in TABLE 7.8. The plots are graphically illustrated in FIGURE 7.10.

Specimen	Exposure (mins)	Temp. ^{o}C	Point of Interruption	Induction period after interruption (mins)	Acceleratory period rate constant $(mins)^{-1}$	Percentage decomposition
Irradiated	Blank	165	-	37	7.40×10^{-3} (k_2)	96
"	0.5	"	t = 0	40	7.47×10^{-3}	75
"	"	"	0.5 I.P.	39	5.01×10^{-3}	67
"	"	"	End I.P.	42	7.35×10^{-3} (k_1)	80
"	"	"	$\alpha = 0.15$	-	-	65

Specimen	Exposure (mins)	Temp °C	Point of Interruption	Induction period after interruption (mins)	Acceleratory period rate constant $(\mathrm{mins})^{-1}$	Percentage decomposition
Irradiated	0.5	165	$\alpha = 0.25$	-	-	51
"	"	"	$\alpha = 0.50$	-	-	78
Unirradiated	Blank	165	-	220	1.94×10^{-3} (k_1)	98
Irradiated	Blank	"	-	37	7.40×10^{-3} (k_2)	96
"	5	"	t = 0	162	3.42×10^{-3} (k_1)	54

7.3.8 The effect of thermal annealing

Powdered lithium azide pre-irradiated with X-rays for 30 mins (10 kV, 5 mA) was thermally annealed at 110°C for 45 mins in the vacuum line and the run then carried out at 175°C. The vacuum line was open to the pump section during the annealing and after the annealing the line was pumped for a further 10 hours. A blank run was done for comparative purposes with no annealing. Comparison of the normalised plots showed that thermal annealing had no effect on the decomposition of lithium azide, pre-irradiated with X-rays.

7.3.9 Percentage decomposition

The percentage decomposition as described in 5.3.6 for the runs used for the varying temperature series of X-irradiated lithium azide powder, pre-irradiated for 30 mins (10 kV, 5mA) was found to be as follows (decomposition temperature in brackets):

96 (165°); 100 (175°); 104 (180°); 89 (185°); 100 (190°);

MEAN: 98%

The percentage decomposition for the runs used in the varying dose series was found to be as follows (irradiation time using X-rays (10 kV, 5 mA) in brackets):

97 (unirr.); 78 (2 mins); 97 (5 mins); 102 (10 mins);
100 (15 mins); 96 (30 mins); 98 (1 hour); 104 (3 hours);
93 (16 hours). MEAN: 96%

7.3.10 Visual observations

Similar observations as reported for γ-irradiated lithium azide, 6.3.10, can be reported for X-irradiated LiN_3. It was noticed however that the salt turned a faint grey colour after prolonged exposure (16 hours) to the X-ray beam. Similar changes in colour during thermal decomposition were observed, there being no change in colour until the end of the induction period when the salt turned grey.

7.4 RESULTS (PELLETED LITHIUM AZIDE)

7.4.1 Activation energies

As mentioned previously in 7.2.1, it was not possible to obtain values for the activation energies of the processes occurring in the thermal decomposition of X-irradiated pelleted lithium azide due to the irreproducibility of the material and difficulty in obtaining rate constants using the split-run technique.

However some qualitative work was done in an attempt to understand the reasons for the double-sigmoid pressure-time plot. These investigations are reported below.

7.4.2 The effect of varying pellet weight on the initial reaction

The effect of varying the weight of the pelleted azide pre-irradiated with X-rays for 2 hours (10 kV, 5mA) showed the initial reaction to be dependant upon the weight of the pellet as found previously in 6.4.6 for the effect of γ-irradiation on pelleted material (cf. FIGURE 6.21).

7.4.3 Comparison of pre-irradiated pelleted and powdered lithium azide and pelleted irradiated lithium azide

In attempting to determine the reasons for the initial reaction observed when pre-irradiated pelleted lithium azide was thermally decomposed, pre-irradiated powdered azide was pelleted and the subsequent thermal decomposition showed a double-sigmoid character. This effect was not as pronounced as for the irradiated pelleted salt. The pelleted irradiated azide had a longer induction period than those of the powdered and pelleted lithium azide, pre-irradiated with the same X-ray dose. All the specimens were pre-irradiated for 30 mins (10 kV, 5 mA) and the reaction temperature was 175°C. The p/t results appear in TABLE 7.9 and FIGURE 7.11.

7.4.4 The effect of irradiating lithium azide using various supports

The procedure describing the irradiation technique in 4.2.3 (b) mentioned the reasons for irradiating the lithium azide on a brass plate. The effects of using a glass surface was investigated. Pellets were made from the same ground batch and pre-irradiated for two hours with X-rays (10 kV, 5 mA), using brass and glass supports. The reaction temperature was 195°C.

It was observed that when the pelleted lithium azide was irradiated on glass and brass, the extent of the first acceleratory reaction was less for glass than for brass. There was small change in the lengths of the induction periods.

The derived rate constants for the initial acceleratory period were found as follows (k_2, equation 6.1):

(i) Irradiation on brass: 7.60×10^{-2} mins^{-1}

(ii) Irradiation on glass: 1.83×10^{-2} mins^{-1}

The tabulated results appear in TABLE 7.10 and the p/t plots including a blank run of unirradiated pelleted azide, are graphically shown in FIGURE 7.12.

7.4.5 Visual observations

As found for the powdered material, no colour change on irradiation was observed for the X-ray doses used in the above study. Examination of the irradiated pelleted material showed that decomposition commenced on both surfaces simultaneously (as for γ-irradiated pelleted azide) and at the inflexion point of the initial reaction the interior of the pellet was dark red-brown, while the faces were predominantly dark grey, with brown distinct areas of product. More detailed observations, however, appear in 7.4.7 when photomicrographic studies were carried out.

7.4.6 The effect of thermal annealing

No effect was found on the subsequent thermal decomposition when pelleted lithium azide, pre-irradiated for 2 hours with X-rays (10 kV, 5 mA), was thermally annealed in vacuo for $^3/4$ hour at 120°C.

The reaction temperature for the decomposition was 190°C.

7.4.7 Photomicrography

Only the thermal decomposition of pelleted lithium azide, pre-irradiated with X-rays for two hours, (10 kV, 5 mA) was studied, for reasons given in 5.3.12.

PLATE 3 shows the thermal decomposition of X-irradiated lithium azide at 164° ± 2°C. Magnification was 65X. FIGURE 7.13 illustrates the dp/dt plot and the arrows indicate where the photomicrographs were taken. The results appear in TABLE 7.11.

(The figures in brackets are exposure times in printing the photographs, as previously explained in 5.3.12).

(a) The photomicrograph shows the pellet at t = 0 (prior to decomposition). The striations are due to the piston used in the die when the pellet was made. The surface was white and uniform. (17)

(b) The photomicrograph was taken in the early stages of the first acceleratory period as may be seen from the illustrated differential plot. Darkening of the viewed surface occurred. (17)

(c) After 85 mins, just before the inflexion point, the surface is seen to have darkened further, with signs of concentrated regions of decomposition appearing. (17)

(d) Dark areas of product are seen to have formed out of the diffuse background at the inflexion point of the first reaction. (15)

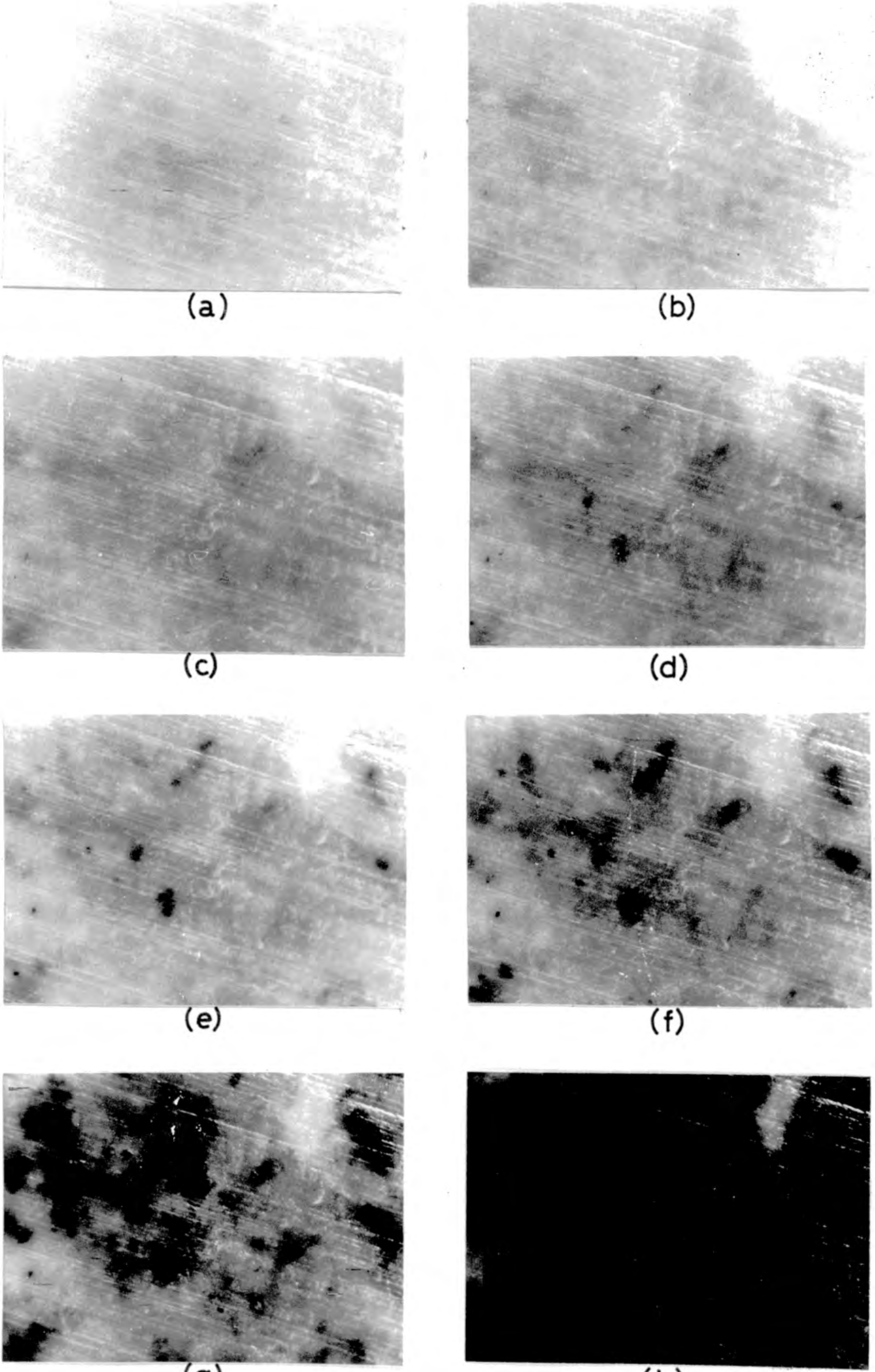

(a) (b) (c) (d) (e) (f) (g) (h)

PLATE 3. THE THERMAL DECOMPOSITION OF X-IRRADIATED PELLETED LITHIUM AZIDE. 164° C.

(e) Although not many more of the distinct areas of decomposition have appeared after 135 mins, those previously formed grew darker and more intense. The background was observed to be grey while the dark areas varied from dark grey to brown in colour. (13)

(f) After 155 mins, in the decay reaction of the initial reaction, the dark centres of decomposition are seen to have increased in size and number. (13)

(g) The photomicrograph shows the overlap, growth and formation of further areas of decomposition. The picture was taken after 210 mins, before the onset of the second reaction. (11)

(h) Just prior to complete surface cover at 210 mins before the onset of the second acceleratory period. The surface was covered with dark grey-brown product. (10)

7.5 DISCUSSION

The effects of X-rays on ionic solids are similar to those discussed for γ-rays, but with the exception that the irradiation damage can be expected to be the consequence of internal electron bombardment, with displacements unlikely. The effects of X-rays on solids and in particular on the alkali halides, have been discussed in detail by Seitz(194,203,204) and studies of the effects on azides have been made by several workers(89,142,143,205).

Irradiation at room temperature has been shown to result largely in the production of F-centres, produced by the combination of anion vacancies and electrons. The electrons may result from dissociation of excitons formed during irradiation or may be secondary electrons resulting from the photoelectric effect(194). In the latter case secondary electrons and holes are produced as units which can wander around until they recombine or are trapped, after which the self-trapped electrons diffuse and ultimately come to rest at vacancies.

The F-centres produced may be situated at imperfections (dislocations, grain boundaries) as in sodium azide or within the lattice as found in potassium azide(89).

V-centres (combination of positive holes and cation vacancies) and aggregates of F-centres and V-centres have also been discussed(194) and are generally present as a consequence of the formation of F-centres.

7.5.1 Powdered lithium azide

The effects of pre-irradiation by X-rays and γ-rays on the thermal decomposition of lithium azide were similar, but with the notable exceptions that the rate constant k_3 for the decay reaction did not change significantly after irradiation in the former case and also the value of α_i, (the fractional decomposition at onset of the decay reaction), decreased with increasing X-ray dose.

In the series of varying doses of X-rays on the thermal decomposition of lithium azide (FIGURE 7.5), the decay period rate constant was found to change from 4.70×10^{-3} mins^{-1} (unirradiated) to 9.20×10^{-3} mins^{-1} (180 mins X-rays, 10 kV, 5 mA). The corresponding change observed for lithium azide pre-irradiated with varying doses of γ-rays prior to thermal decomposition was 2.19×10^{-3} mins^{-1} (unirradiated) to 44.4×10^{-3} mins^{-1} (15000 roentgens).

The inflexion point in the p/t plots was observed to fall with increasing doses of X-rays and for very heavy doses it occurred at $\alpha = 0.16$.

The acceleratory period for the decomposition of X-irradiated azide was found to be described by the Avrami-Erofeyev equation with the exponent n taking the value

2 for all X-ray doses studied. Such a value is consistent with the growth of two dimensional nuclei, growth occurring from a fixed number of nuclei. The irradiation effect is very pronounced indeed and it is likely that even if there was a linear increase in the number of the nuclei with time during the acceleratory period, this effect could be swamped by the very large number of nuclei formed at the end of the short induction period.

The fall in the inflexion point in the p/t plot as the X-ray dose increases is probably due to the fact that radiolysis occurs at high doses so that the surface is partly covered with lithium hydroxide. Thus, when the nuclei cease growing over the surface a smaller fraction of the salt will have been decomposed than with the unirradiated salt.

The decay reaction was analysed using the contracting sphere formula. A significant feature of the decay reaction, as mentioned above, was that the decay rate constant k_3 displayed negligible dependance on the X-ray dose. From this observation it can be concluded that the topochemistry of this stage of the reaction must be similar to that in the decomposition of the unirradiated material and that after surface nucleation growth and coverage, the product/reactant interface moves inwards on the particles of the powder. Also, irradiation after interruption during the decomposition of the unirradiated salt is effective only when the expected time of acceleration due to the X-ray effect is less than the time at which the decay reaction commences (FIGURE 7.9). This also indicates that the nuclei are primarily surface ones.

It is considered that large numbers of F-centres are formed on exposing the salt to X-irradiation. The primary act of irradiation is to strip electrons from the azide ions:

$$N_3^- \rightarrow N_3 + e \quad \ldots\ldots\ldots\ldots\ldots\ldots\ldots (7.5.1)$$

These electrons then combine with (i) the positive holes (N_3), or (ii) are trapped at vacant anion sites present on the surfaces of the particles.

The effects of X-irradiation on the subsequent thermal decomposition of sodium(92) and lead(123) azides have been reported to be the result of radiolytic decomposition of the material. Heal(142) has reported that sodium azide irradiated with X-rays at room temperature contains large numbers of trapped electron centres. It was stated that positive holes and electrons result on irradiating the azide, which then yields molecular nitrogen and electrons:

$$2N_3^- \rightarrow 3N_2 + 2e + 2A \quad \ldots\ldots\ldots\ldots\ldots\ldots\ldots\ldots (7.5.2)$$

$$2N_3 \rightarrow 3N_2 + 2A \quad \ldots\ldots\ldots\ldots\ldots\ldots\ldots\ldots (7.5.3)$$

$$N_3^- + N_3 \rightarrow 3N_2 + e + 2A \quad \ldots\ldots\ldots\ldots\ldots\ldots\ldots\ldots (7.5.4)$$

The electrons and holes are then trapped at suitable trapping centres.

A similar mechanism can also be expected to apply in lithium azide, with the formation of F-centres on X-irradiation. A number of anion vacancies will result from 7.5.2 - 7.5.4, which after trapping at suitable sites will in turn trap mobile electrons yielding F-centres in addition to those formed as a consequence of 7.5.1 above. The F-centres aggregate due to thermal diffusion at the irradiation temperature (room temperature), as mentioned previously for γ-irradiated lithium azide.

On heating the irradiated lithium azide the F-centres collapse and produce lithium atoms and finally lithium metal centres, during the short induction period.

During the decomposition of irradiated lithium azide, the nuclei are formed rapidly and in large numbers. It is considered that at the end of the induction period these are present in virtually a saturation amount and that during the acceleratory period further formation is "swamped", leading to the value 2 for n in the Avrami-Erofeyev equation.

Further support for the view that reaction occurs only on the surface of the particle is found when comparing the results for X-irradiated and U.V. irradiated lithium azide. It is conclusively shown (cf. 8.5) that the U.V. reaction is entirely a surface one. The close similarity in the results for the X- and U.V.-irradiated azide confirm the reaction to thus be a surface one in the former case as well.

This view that nuclei grow two-dimensionally on the surface and increase in number fractionally with time, is supported by the series of "water interruption" runs. It was observed that exposure to water vapour (30 secs) at $t = 0$ (i.e. prior to decomposition) had no effect on the subsequent thermal decomposition, indicating the absence of lithium atoms or nuclei at that point and the absence of interaction between the F-centre aggregates and water vapour. However, the same exposure at points halfway and at the end of the induction period resulted in the formation of an induction period of length approximately equal to the induction period for the decomposition of the uninterrupted irradiated azide, followed by a slower evolution of gas which passes into the type of gas evolution one would expect with unirradiated material at this point and at the reaction temperature used.

These acceleratory periods were best described by the Avrami-Erofeyev equation with $n = 3$, for interruption at the end of the induction period and $n = 2$ for interruption at a point halfway along the induction period. These results indicate that the reaction is returned effectively to that of the decomposition of unirradiated salt.

Interruption after the induction period resulted in virtual destruction of the subsequent reaction. The slow reaction is attributed to the thermal decomposition of unirradiated azide.

Exposure to water vapour (5mins) at $t = 0$ had the effect of destroying the trapping sites and at the same time the F-centre aggregates (as described previously for the γ-irradiated material). The length of the induction period was found to approach the value for that of unirradiated material. The acceleratory period was fitted with n = 3 in the Avrami-Erofeyev equation, as found for the decomposition of unirradiated lithium azide i.e. the irradiation effect was removed.

In all the water interruption runs the percentage decomposition was lowered presumably due to hydrolysis. Exposure to 5 mins water vapour had a greater lowering effect on the percentage decomposition.

It is proposed that the rate determining steps during the induction period is the same as that postulated for the γ-irradiated azide. This step is the diffusion over the surface of lithium atoms to crystallise and form a metal nucleus. The activation energy associated with this process (21 k.cals/mole) is, within the limits of experimental error, the same as that found for γ-irradiated and unirradiated material (20 k.cals/mole and 22 k.cals/mole respectively).

The mechanism for the growth is considered to be similar to that for the γ-irradiated salt as a consequence of similarity in the activation energies (25 k.cals/mole for X-rays, 26 k.cals/mole for γ-rays) within the limits of experimental error. The rate determining step during the acceleratory period is proposed to be that postulated for γ-irradiated lithium azide. This step is the elevation of an electron from an azide ion to the conduction band of the lithium metal nucleus with the formation of an azide radical:

$$N_3^- \rightarrow N_3 + e \quad \ldots\ldots\ldots\ldots\ldots\ldots\ldots \quad (7.5.5)$$

This nucleation process proposed for lithium azide is analagous to the surface nucleation postulated for the thermal decomposition of unirradiated and U.V.-irradiated calcium and strontium azides(109). Nucleation was considered to occur at the point of emergence of dislocations on the surface of the crystals. These were thought to be mainly spiral dislocations and the discontinuities associated with the mosaic structure (cf. Hedges and Mitchell(199) and PLATE 2(a))

During the decay reaction when the envelopes of product contract and the interface moves inwards on blocks of unirradiated material the contracting sphere equation holds, as for the decomposition of unirradiated and γ-irradiated lithium azide. The reaction mechanism in this case is considered to be the same. The activation energy for this process was found to be 28 k.cals/mole as found for the decay process in γ-irradiated lithium azide.

No effect was observed when X-irradiated material was annealed under the conditions employed, as previously found for unirradiated and γ-irradiated lithium azide.

The mean percentage decomposition was observed to be higher (97%) than that for the unirradiated material (89%). This increase in the percentage decomposition was observed with the γ-irradiated material as well.

7.5.2 Pelleted lithium azide

No reliable values were obtained for the activation energies associated with the first acceleratory and decay reactions, observed during the thermal decomposition of X-irradiated lithium azide. This was due to the irreproducible nature of the thermal decomposition and the difficulty associated with estimating a reliable "final" pressure for the first reaction.

As for γ-rays, it is considered that the initial reaction was due to a surface reaction at points on the "internal surfaces". The fit of the Avrami-Erofeyev equation with $n = 2$ indicates two-dimensional growth from a large, fixed number of nuclei. These nuclei take the form of contracting two-dimensional centres during the first decay region.

The photomicrographs show (Plate 3) the formation of dark areas of product against a background of diffuse darkening grey. These dark areas increase in number and size as the initial reaction proceeded, until the viewed surface was completely covered by reaction product at the end of the initial reaction.

It was noted that if the pellet was irradiated on a glass support instead of the brass plate used throughout the X-irradiations, the initial reaction was reduced in magnitude and the overall effect is equivalent to irradiating the material with a smaller dose of X-rays. The enhanced effect obtained when irradiating on a brass support is probably due to the bombardment of the pellet by photoelectrons emitted from the brass. The electronic work function of brass is several thousand times less than the energy of the incident X-radiation and consequently a "shower" of electrons from the brass surface results. It was found that lithium azide in the amounts used, was transparent to the X-ray beam as no image of the material was recorded on a sensitive screen placed behind the irradiated material. Thus electrons were emitted from the brass at the point of contact of the azide with the support.

A similar enhanced reaction due to the emission of photoelectrons has been reported by Cunningham and Tompkins(89), during a study of the spectra of ultra-violet irradiated sodium and potassium azides. It was found that the formation of colour centres (F-centres) was enhanced by a factor of 4 in the case of KN_3 and by a factor of 50 in the case of NaN_3, when these azides were irradiated on aluminium, instead of quartz. The enhanced effect was attributed to the release of photoelectrons from the aluminium, which were then transferred to the conduction band of the azides and subsequently trapped at anion vacancies, the neutrality of the crystal being maintained by the formation of surface azide radicals which transfer the electron of an (excited) surface azide ion to the metal.

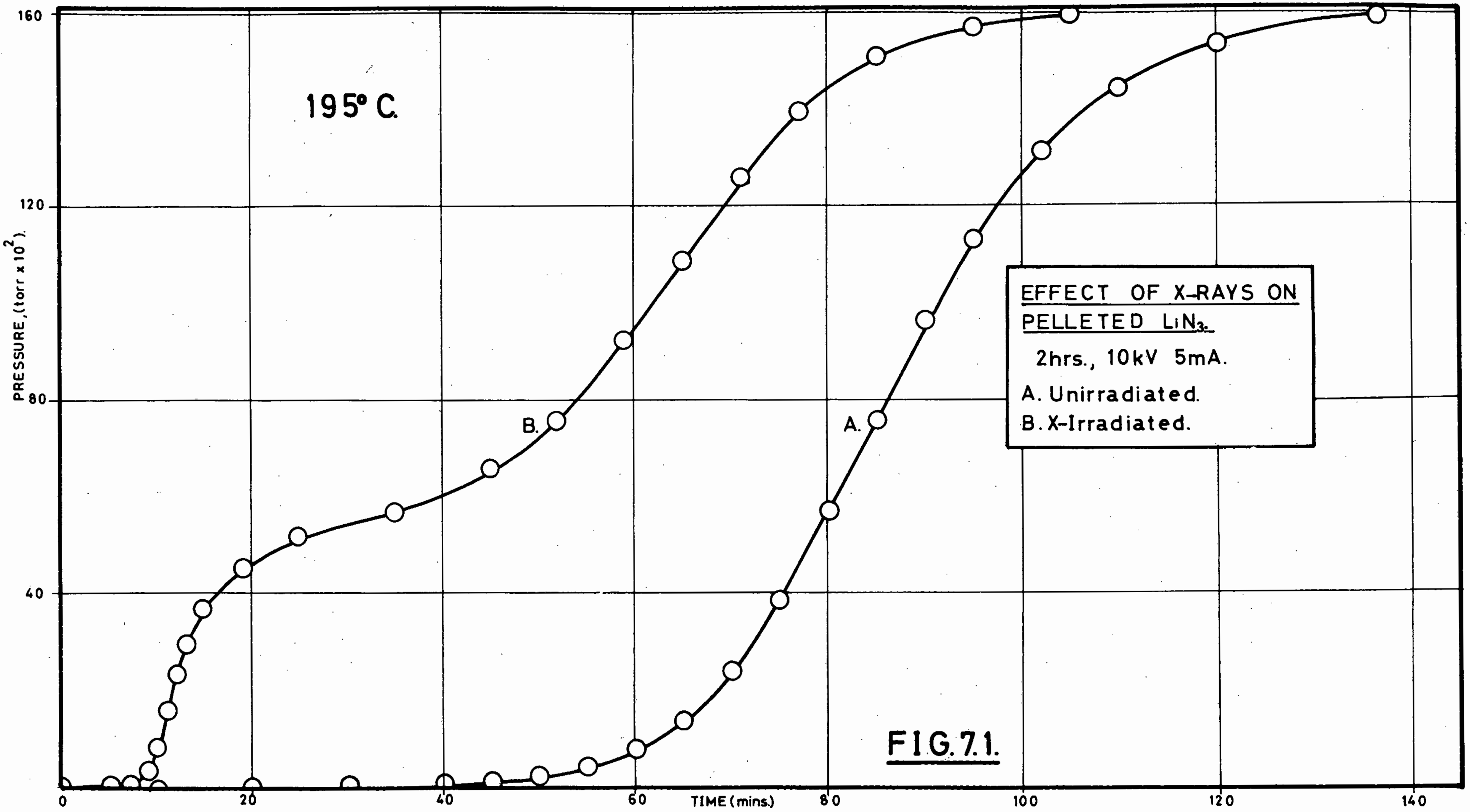
195° C.
EFFECT OF X-RAYS ON PELLETED LiN_3.
2hrs., 10kV 5mA.
A. Unirradiated.
B. X-Irradiated.
A.
B.
PRESSURE, (torr x 10^2).
160
120
80
40
0
20
40
60
80
100
120
140
TIME (mins.)

FIG. 7.1.

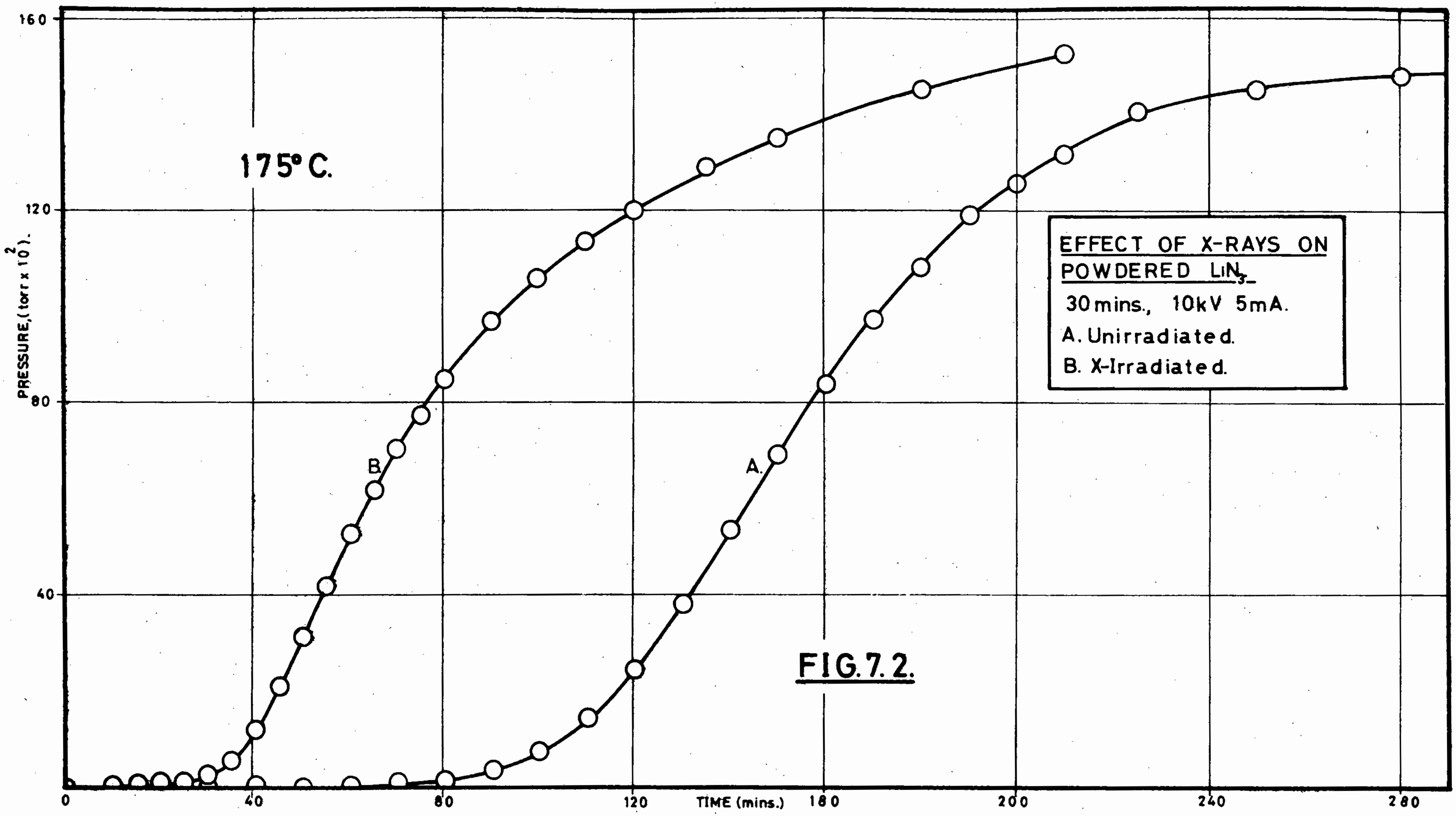
175°C.
EFFECT OF X-RAYS ON POWDERED LiN3
30 mins., 10kV 5mA.
A. Unirradiated.
B. X-Irradiated.
A.
B.
PRESSURE, (torr x 10²).
160
120
80
40
0
40
80
120
TIME (mins.)
180
200
240
280

FIG. 7.2.

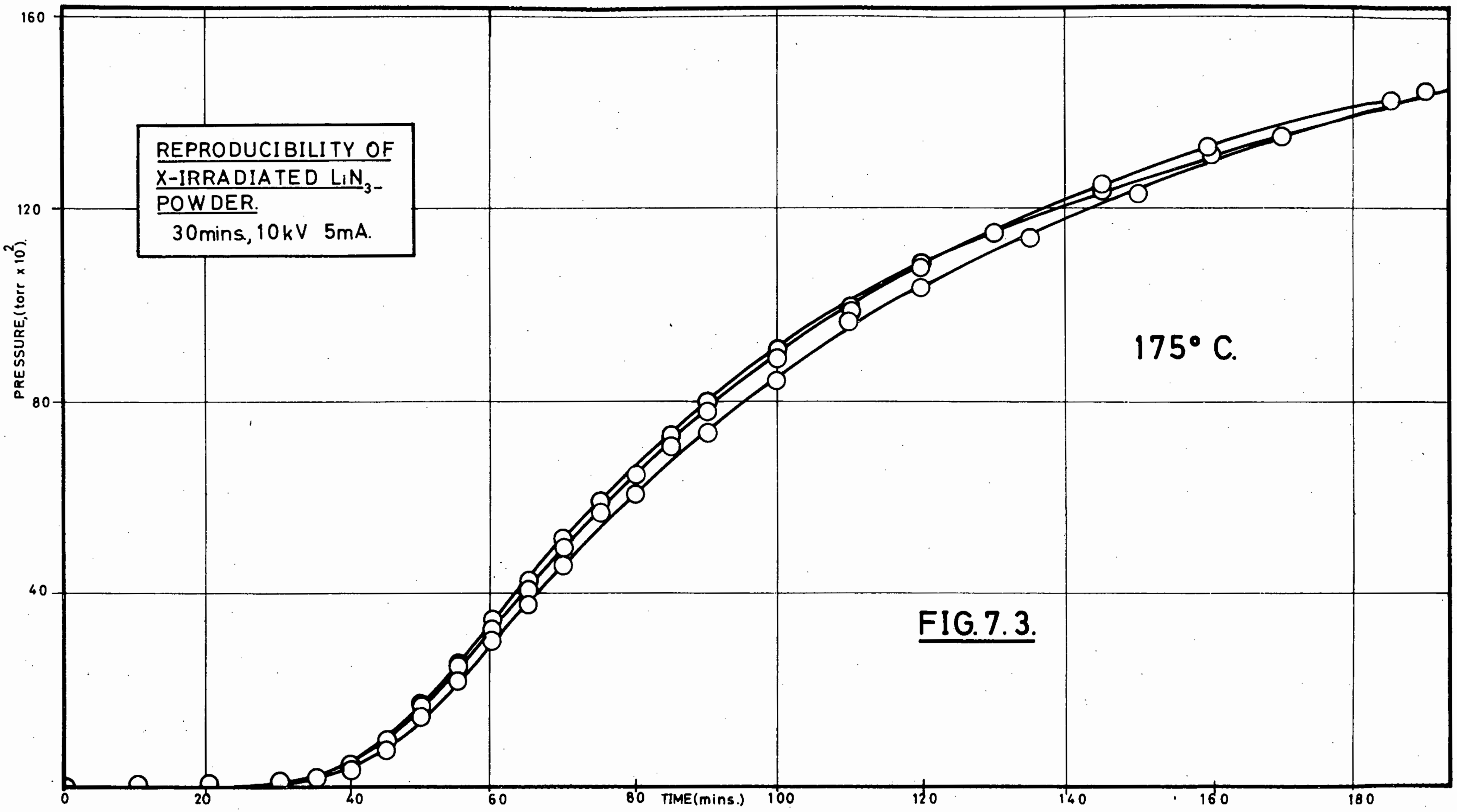

REPRODUCIBILITY OF X-IRRADIATED LiN_3- POWDER.
30mins., 10kV 5mA.
175° C.
PRESSURE, (torr x 10^2).
160
120
80
40
0
20
40
60
80
TIME(mins.)
100
120
140
160
180

FIG. 7. 3.

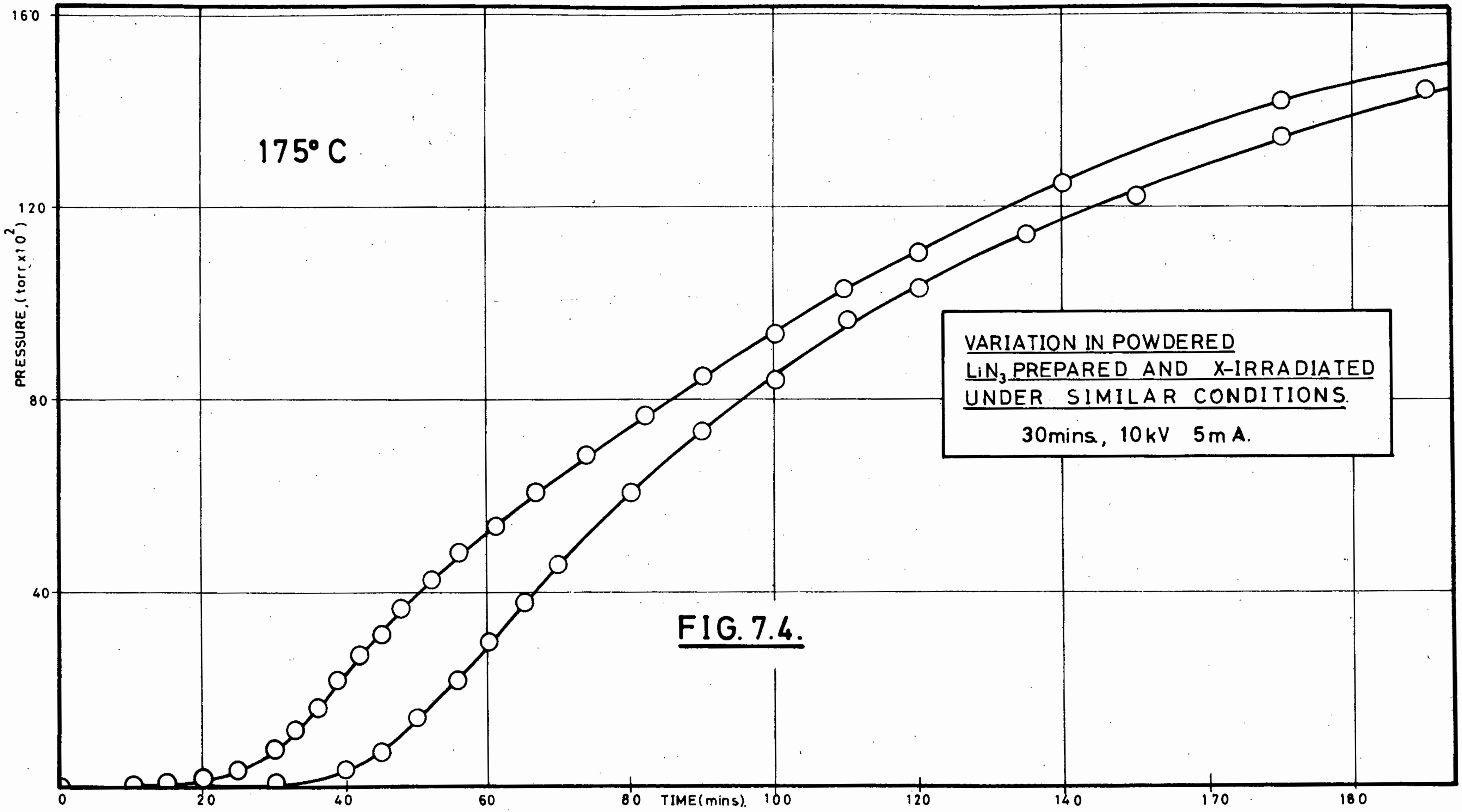
175° C
VARIATION IN POWDERED LiN_3 PREPARED AND X-IRRADIATED UNDER SIMILAR CONDITIONS.
30mins., 10kV 5mA.
PRESSURE, (torr x 10^2)
160
120
80
40
0
20
40
60
80
TIME(mins).
100
120
140
170
180

FIG. 7.4.

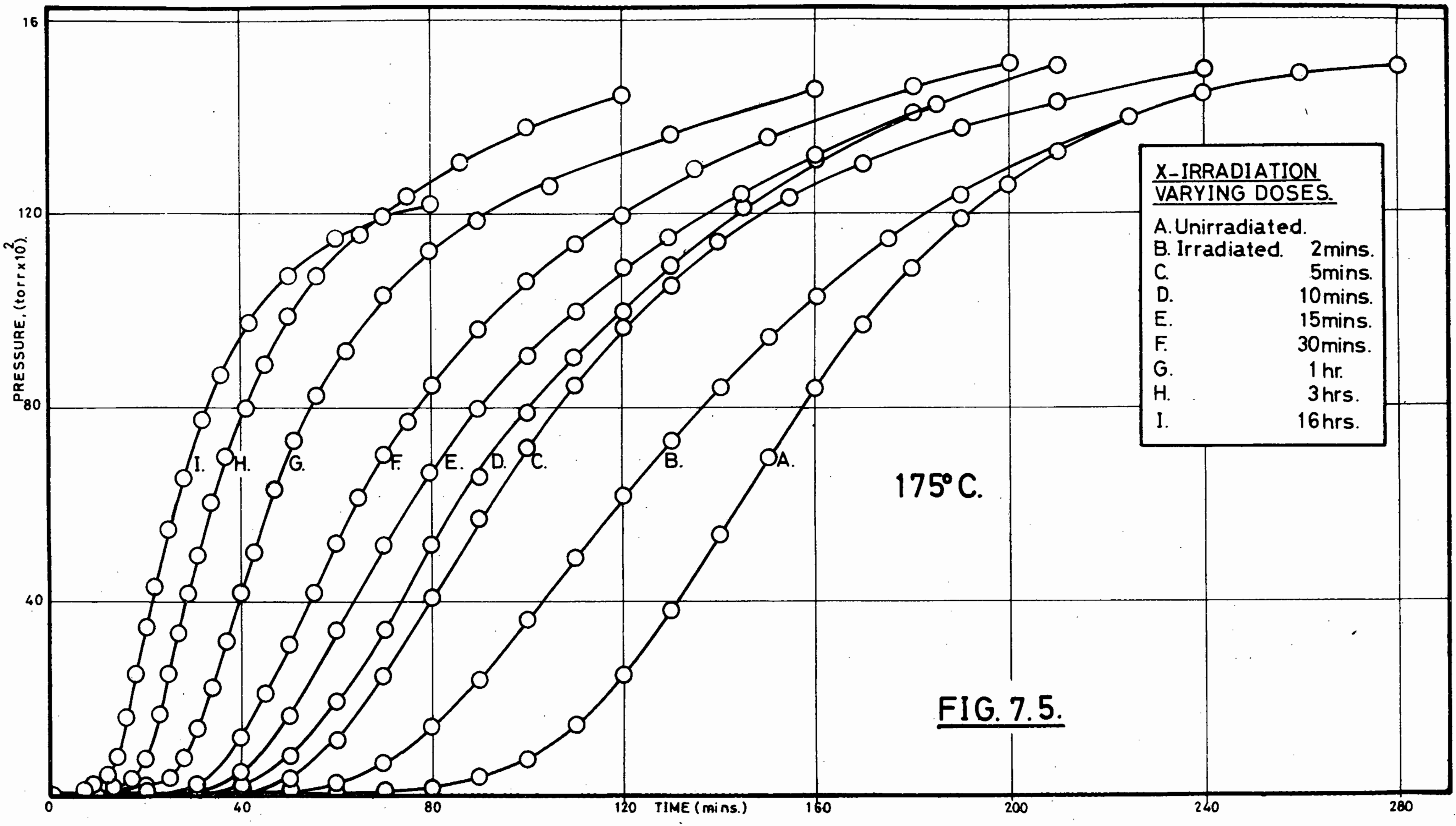
PRESSURE, (torr x 10²).
16
120
80
40
0
40
80
120
TIME (mins.)
160
200
240
280
I.
H.
G.
F.
E.
D.
C.
B.
A.
175°C.
X-IRRADIATION VARYING DOSES.
A. Unirradiated.
B. Irradiated. 2mins.
C. 5mins.
D. 10mins.
E. 15mins.
F. 30mins.
G. 1 hr.
H. 3hrs.
I. 16hrs.

FIG. 7.5.

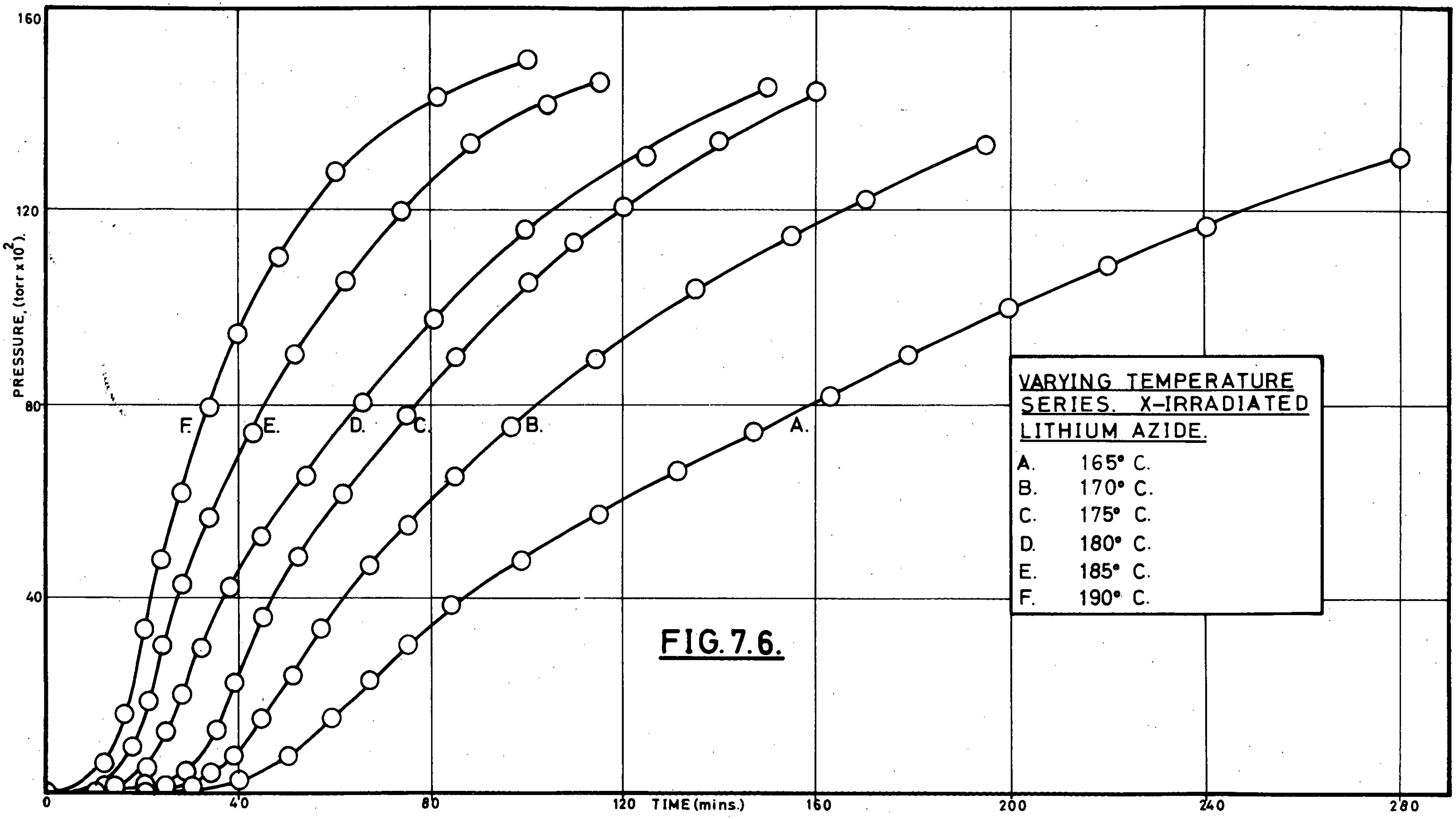

PRESSURE, (torr x 10^2).
160
120
80
40
0
40
80
120
TIME (mins.)
160
200
240
280
F.
E.
D.
C.
B.
A.
VARYING TEMPERATURE SERIES. X-IRRADIATED LITHIUM AZIDE.
A. 165° C.
B. 170° C.
C. 175° C.
D. 180° C.
E. 185° C.
F. 190° C.

FIG. 7.6.

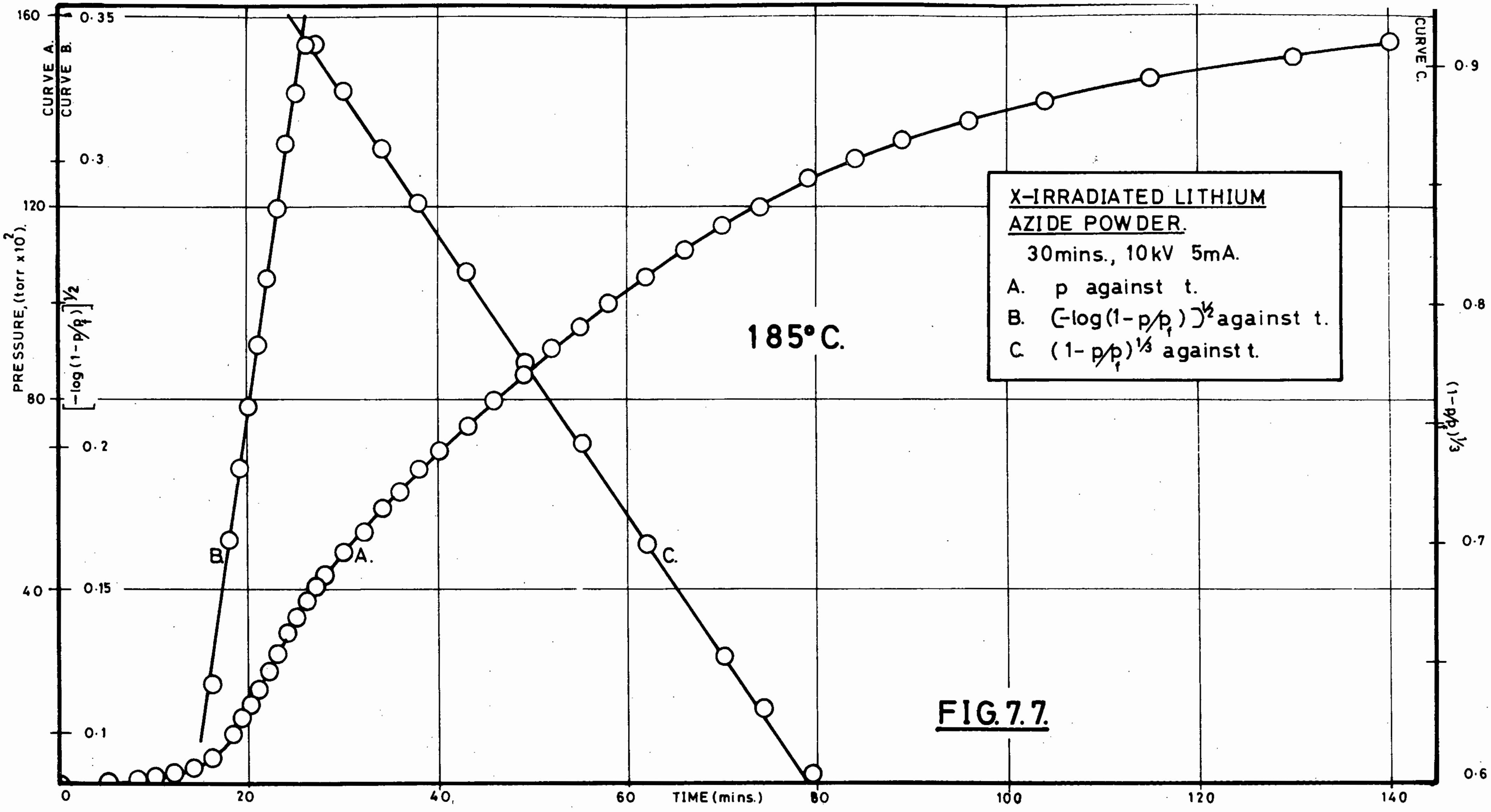
X–IRRADIATED LITHIUM AZIDE POWDER.
30mins., 10kV 5mA.
A. p against t.
B. $[-\log(1-p/p_f)]^{1/2}$ against t.
C. $(1-p/p_f)^{1/3}$ against t.
185° C.
CURVE A.
CURVE B.
PRESSURE, (torr x10^2).
$[-\log(1-p/p_f)]^{1/2}$
160
120
80
40
0·35
0·3
0·2
0·15
0·1
CURVE C.
$(1-p/p_f)^{1/3}$
0·9
0·8
0·7
0·6
0
20
40
60
80
100
120
140
TIME (mins.)
A.
B.
C.

FIG. 7.7.

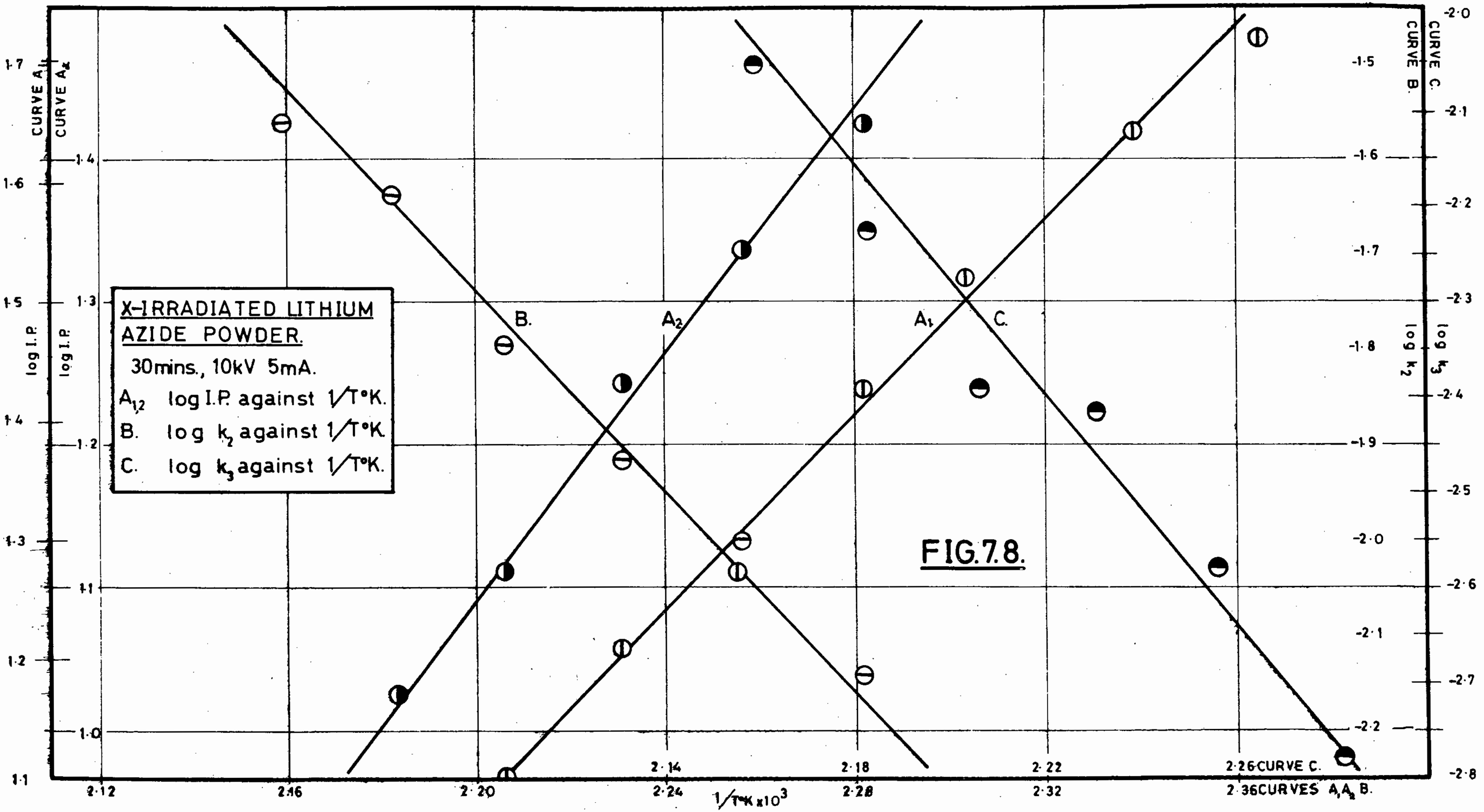
X-IRRADIATED LITHIUM AZIDE POWDER.
30mins., 10kV 5mA.
$A_{1,2}$ log I.P. against 1/T°K.
B. log k_2 against 1/T°K.
C. log k_3 against 1/T°K.
B.
A_2
A_1
C.
CURVE A_1
CURVE A_2
log I.P.
log I.P.
1·7
1·6
1·5
1·4
1·3
1·2
1·1
1·4
1·3
1·2
1·1
1·0
CURVE B.
CURVE C.
log k_2
log k_3
-1·5
-1·6
-1·7
-1·8
-1·9
-2·0
-2·1
-2·2
-2·0
-2·1
-2·2
-2·3
-2·4
-2·5
-2·6
-2·7
-2·8
2·14
2·18
2·22
2·26 CURVE C.
2·12
2·16
2·20
2·24
2·28
2·32
2·36 CURVES A_1A_2 B.
$1/T°K \times 10^3$

FIG.7.8.

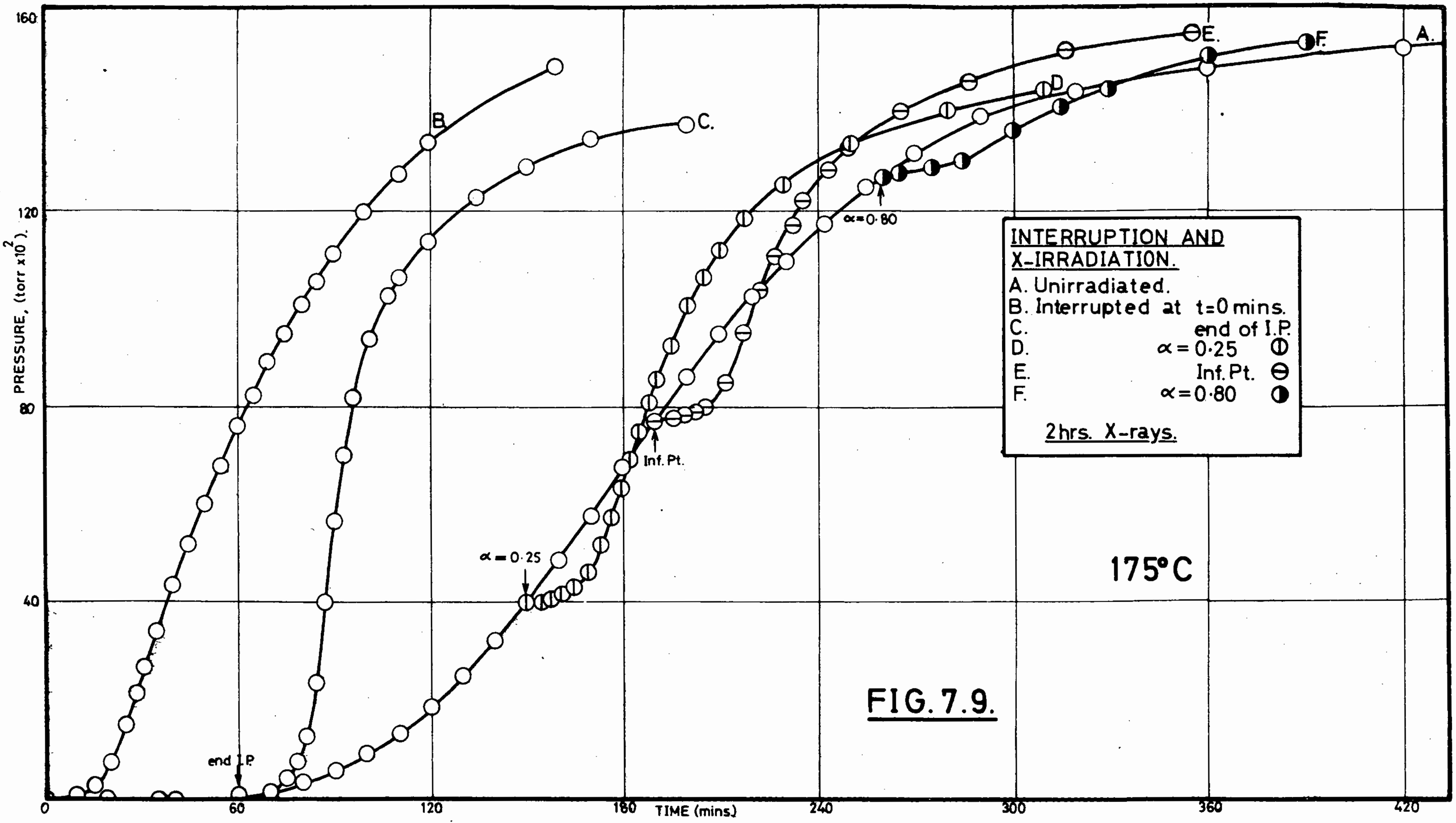
160
120
80
40
PRESSURE, (torr x10^{2}).
0
60
120
180
240
300
360
420
TIME (mins)
B.
C.
D.
E.
F.
A.
end I.P.
α = 0·25
Inf. Pt.
α = 0·80
INTERRUPTION AND X-IRRADIATION.
A. Unirradiated.
B. Interrupted at t=0 mins.
C. end of I.P.
D. α = 0·25 ⦶
E. Inf. Pt. ⊖
F. α = 0·80 ◑
2hrs. X-rays.
175°C

FIG. 7.9.

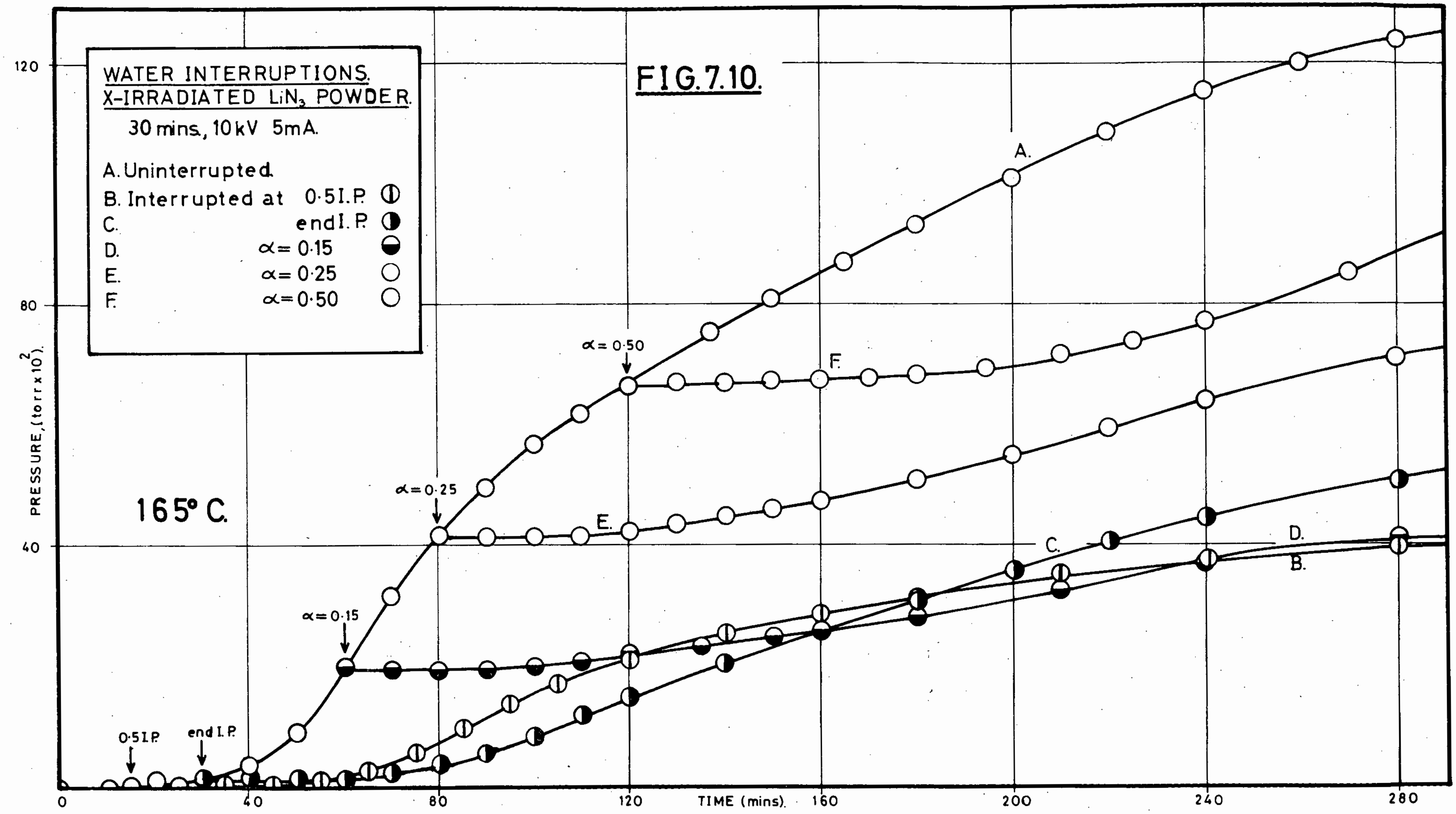

FIG. 7.10.

WATER INTERRUPTIONS.
X-IRRADIATED LiN_3 POWDER.
30 mins., 10 kV 5 mA.
A. Uninterrupted.
B. Interrupted at 0·5 I.P. ◐
C. end I.P. ◐
D. α = 0·15 ◒
E. α = 0·25 ○
F. α = 0·50 ○
165° C.
α = 0·50
α = 0·25
α = 0·15
0·5 I.P.
end I.P.
A.
B.
C.
D.
E.
F.
PRESSURE, (torr x 10^2).
TIME (mins).
0
40
80
120
160
200
240
280
40
80
120

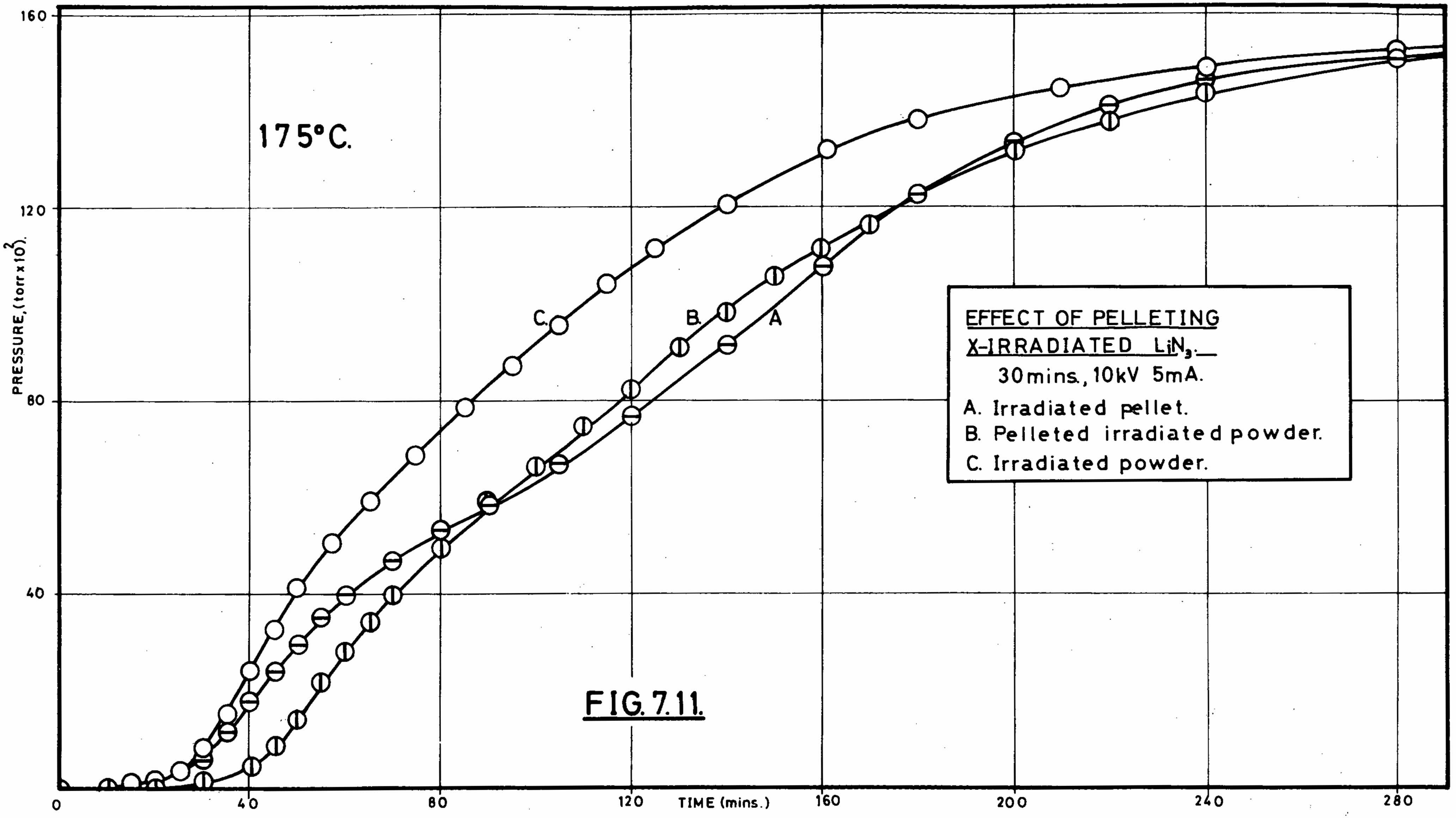
175°C.
EFFECT OF PELLETING
X-IRRADIATED LiN_3.
30 mins., 10kV 5mA.
A. Irradiated pellet.
B. Pelleted irradiated powder.
C. Irradiated powder.
A
B.
C.
PRESSURE, (torr x 10^2).
160
120
80
40
0
40
80
120
160
200
240
280
TIME (mins.)

FIG. 7.11.

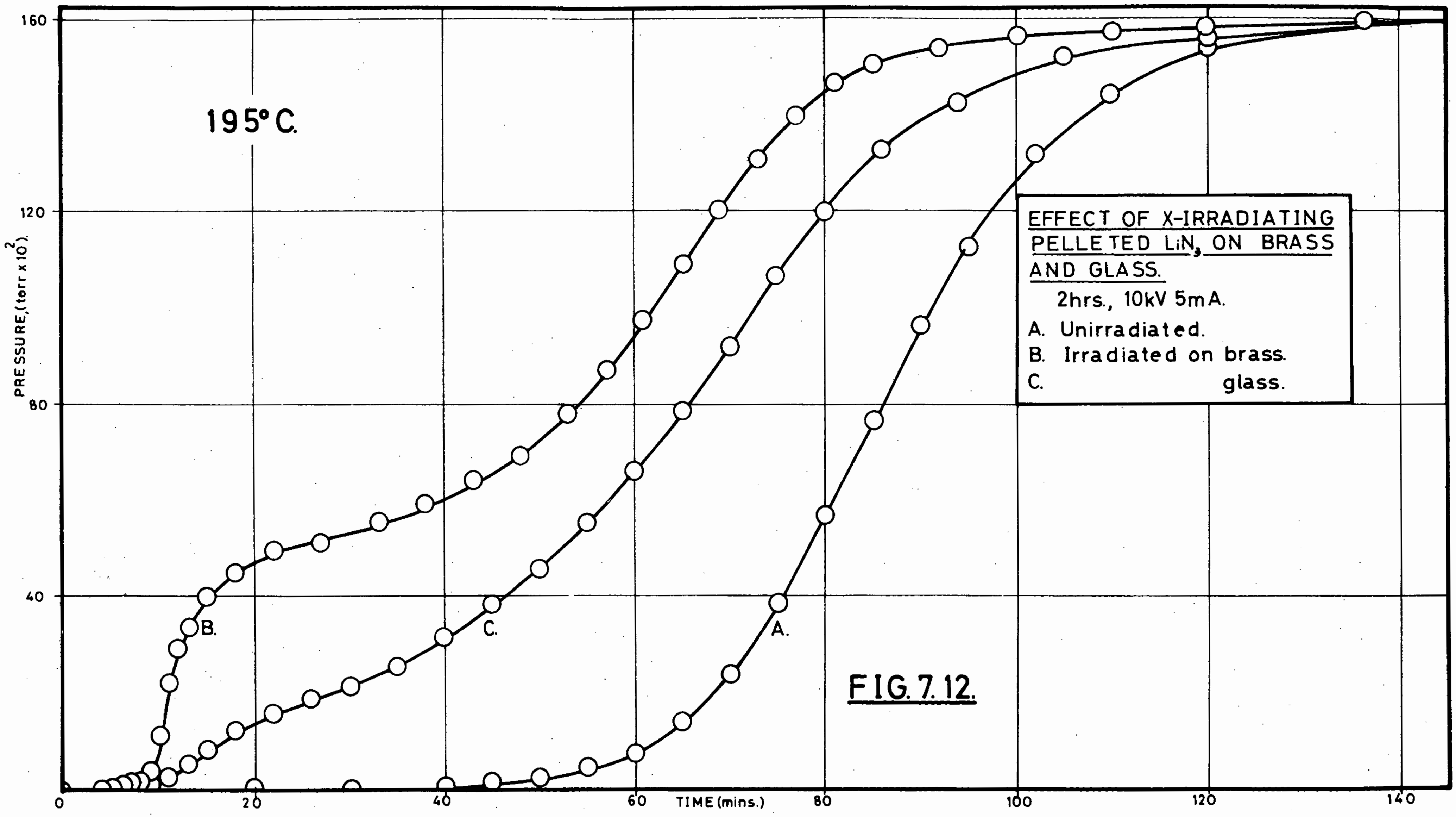

195°C.
EFFECT OF X-IRRADIATING PELLETED LiN3 ON BRASS AND GLASS.
2hrs., 10kV 5mA.
A. Unirradiated.
B. Irradiated on brass.
C. glass.
A.
B.
C.
PRESSURE, (terr x 10^2).
160
120
80
40
0
20
40
60
80
100
120
140
TIME (mins.)

FIG. 7.12.

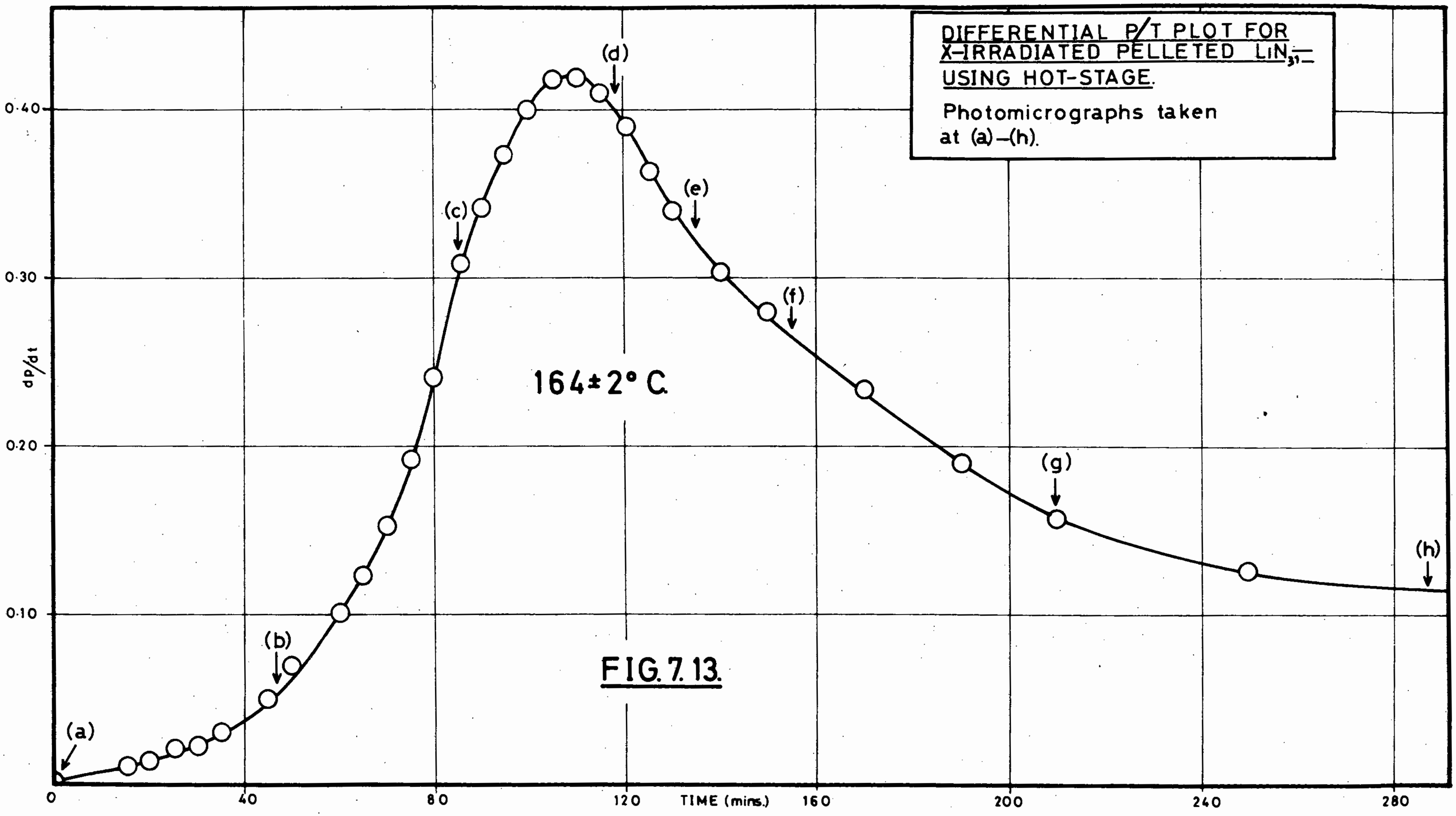

DIFFERENTIAL P/T PLOT FOR X-IRRADIATED PELLETED LiN$_3$ — USING HOT-STAGE.

Photomicrographs taken at (a)–(h).

FIG. 7.13.

8. THE THERMAL DECOMPOSITION OF LITHIUM AZIDE PRE-IRRADIATED WITH ULTRA-VIOLET RADIATION

8.1 PRELIMINARY INVESTIGATIONS

8.1.1 Pelleted lithium azide

The effect of irradiating pelleted lithium azide was investigated initially, to ascertain the shape of the p/t plot. Pelleted lithium azide was pre-irradiated for 2 hours using (i) the low intensity and (ii) the high intensity ultra-violet lamps, following procedure described in 4.2.3(c). The pellets were irradiated on one face only at a distance of 6 cm. beneath the lamps. The lamps used have been described in 4.1.4(c). The pelleted material was decomposed in vacuo in the usual manner, at 190°C. It was observed that the induction period was reduced from 65 mins to 4 mins for the material irradiated with the low intensity lamp. The azide pre-irradiated with the high intensity lamp had no induction period. Both irradiated p/t plots showed small initial reactions, this being slightly more pronounced in the case of the material irradiated with the high intensity lamp. After the initial burst of gas the plots assumed a sigmoid character.

It was observed that the pellet irradiated with the high intensity lamp had turned yellow-brown on the irradiated face only, while no colour change was observed in the other irradiated pellet. These results appear in TABLE 8.1 and the p/t plots are illustrated in FIGURE 8.1.

8.1.2 Powdered lithium azide

Powdered lithium azide was pre-irradiated with ultra-violet radiation using the low intensity lamp at a distance of 6.5cm beneath the tube for 15 mins. The azide was stirred every three minutes. Approximately 5 mg. of the material were decomposed at 195°C and a blank run using unirradiated material at the same temperature was done for comparative purposes. It was observed that the induction period was virtually eliminated and the reaction appeared to start at maximum rate. This was followed by a decay reaction. The results appear in TABLE 8.2 and the p/t plots are illustrated in FIGURE 8.2.

8.2 REPRODUCIBILITY

8.2.1 Pelleted lithium azide

Pelleted lithium azide, pre-irradiated with ultra-violet radiation gave p/t plots with good reproducibility. Pelleted material irradiated for $1\frac{1}{2}$ hours at a distance of 6.5cm below the low intensity lamp was decomposed at 198°C. The results for two runs using pellets of approximately 4.6mg are given in TABLE 8.3 and the p/t plots illustrated in FIGURE 8.3. It is seen that for this dose there was no induction period at 190°C, and the reaction commenced at maximum rate.

8.2.2 Powdered lithium azide

Powdered lithium azide as described in 5.3 was irradiated for 15 mins, 6.5cm beneath the low intensity lamp. The irradiation was done in an atmosphere of dry nitrogen as previously described in 4.2.3(c) and the powder was stirred every 3 mins. Approximately 5.0mg were used for a decomposition. The specimens were decomposed in vacuo in the normal manner, at a reaction temperature of 175°C.

The reproducibility was of a high order, as may be seen from FIGURE 8.4. The p/t values for the runs appear in TABLE 8.3.

8.3 RESULTS (POWDERED LITHIUM AZIDE)

It was found (8.4.1) that the initial reaction observed in the decomposition of ultra-violet light pre-irradiated pelleted lithium azide was not amenable to mathematical analysis. Accordingly, as was done with γ- and X-rays, the investigations of the effects of pre-irradiation with ultra-violet radiation were largely confined to powdered lithium azide. Some investigations using pelleted azide, pre-irradiated with ultra-violet light are reported in 8.4.

UNLESS OTHERWISE STATED ALL IRRADIATIONS IN THIS SECTION (8.3) WERE CARRIED OUT USING THE LOW INTENSITY ULTRA-VIOLET LAMP AT A DISTANCE OF 26cm BELOW THE U.V. TUBE.

8.3.1 The effect of varying doses on the thermal decomposition

The effect of an increasing dose of ultra-violet irradiation on the thermal decomposition of powdered lithium azide at 175°C was studied. The specimen was irradiated in the normal manner under dry nitrogen with frequent stirring. The specimen was placed 26cm beneath the tube. Approximately 5.0mg specimens were used for a decomposition run.

The azide was irradiated for 2, 10 and 80 seconds and 6 and 32 hours.

There was a decrease in the length of the induction period and exposure to U.V.-radiation for 2 secs halved the induction period. For larger doses ($>$ 80secs) the induction period was virtually eliminated. The reaction following the induction period was sigmoid throughout the series with increasing reaction rate. The inflexion point was observed to decrease with increasing exposure to U.V., while small change in the decay rate was observed.

The lengths of the induction periods, the acceleratory and decay period rate constants and the inflexion points appear in the table below, for the U.V.-irradiated varying dose series and for a blank unirradiated run. The series is illustrated in FIGURE 8.5. The p/t values for the decomposition runs appear in TABLE 8.4. The changes in the mathematical analysis of the p/t plots as the dose is increased is discussed below in 8.3.3.

Dose	Inflexion point	Induction period (mins)	Acceleratory period rate constant (mins^{-1})	k_3 (mins^{-1})
0	0.40	95	3.26×10^{-3} (k_1)	1.80×10^{-3}
2 secs	0.36	45	3.78×10^{-3}	2.72×10^{-3}
10 secs	0.34	26	4.90×10^{-3} (k_2)	2.61×10^{-3}
80 secs	0.31	12	8.50×10^{-3}	3.58×10^{-3}
6 hrs	0.14	4	-	4.10×10^{-3}
32 hrs	0.14	3	-	4.06×10^{-3}

8.3.2 The effect of varying the temperature of decomposition

The critical increments for the chemical process(es) occurring during the thermal decomposition of lithium azide, pre-irradiated with ultra-violet radiation for 15 secs, were determined using the individual runs method. Approximately 5.0mg of the irradiated azide were used for a decomposition. The temperature range was 170° - 195°C.

Rate constants were determined over the temperature range chosen and the duration of the induction periods noted (induction period was the time taken for the reaction to reach $\alpha = 0.006$). The derived rate constants for the acceleratory and decay periods, k_2 and k_3 respectively, (equations 6.1 and 5.3), and the lengths of the induction periods appear in the table below. The p/t values for the decompositions are to be seen in TABLE 8.5.

Specimen	Temp. ^{o}C	Induction period (mins)	k_2 (mins^{-1})	k_3 (mins^{-1})
U.V.-irradiated for 15 secs.	170.0	34	-	-
"	175.0	24	5.17×10^{-3}	2.64×10^{-3}
"	180.0	20	7.08×10^{-3}	3.16×10^{-3}
"	185.0	15	9.90×10^{-3}	4.50×10^{-3}
"	190.0	11	1.32×10^{-2}	6.33×10^{-3}
"	195.0	-	1.68×10^{-2}	8.42×10^{-3}

8.3.3 Mathematical analysis of the results

A typical plot of the decomposition of lithium azide pre-irradiated for 15 secs with U.V.-radiation at $185^{o}C$ showing the extent of fit of the mathematical analyses, appears in FIGURE 8.6 and the p/t results in TABLE 8.5. The marked features of the p/t plot are similar to those found for material pre-irradiated with X- and γ-rays. These are (i) a short induction period with no evolution of gas followed by (ii) a short acceleratory period and (iii) a decay period. The inflexion point was at $\alpha = 0.27$.

As previously found, no mathematical analysis of the induction period was possible since no gas was evolved. The lengths of the induction periods at various temperatures were used as before to obtain a value for the activation energy.

The acceleratory period was well defined by the Avrami-Erofeyev equation (equation 6.1) with n = 2. The fit was such that the whole of the acceleratory period was described by the equation. The degree of fit was over the range $0.02 < \alpha < 0.28$. The Avrami-Erofeyev equation in the above form was found to hold for ultra-violet doses of greater than two seconds and less than 30 mins. For exposures to U.V.-radiation for two seconds or less, the Avrami-Erofeyev equation with n = 3 as for the unirradiated material was found to be applicable. For doses above 30 mins the reaction commenced at maximum rate over the temperature range studied and no acceleratory period analysis was possible.

The decay period was fitted by the contracting sphere equation (equation 5.3) as previously found. The degree of fit was over the range $0.25 < \alpha < 0.85$.

The above mathematical analysis was found to be applicable over the temperature range studied. This range was $165^{\circ} - 195^{\circ}$C.

8.3.4 Evaluation of the activation energies

The critical increments of the chemical process(es) occurring in the thermal decomposition of ultra-violet pre-irradiated lithium azide (15 secs) were obtained by applying the Arrhenius equation.

The activation energy for the induction period was found as described in 5.3.3 by plotting the logarithms of the lengths of the induction periods against $1/T$ ($^{\circ}$K), where T is the reaction temperature in $^{\circ}$K.

The activation energies for the acceleratory and decay periods were obtained by plotting the logarithms of the derived rate constants k_2 and k_3 against $1/T$ ($^{\circ}$K).

The above plots were straight lines, from the slopes of which the activation energies were obtained.

The plots of log I.P., log k_2 and log k_3 against 1/T appear in FIGURE 8.7. The values for the activation energies calculated for the induction, acceleratory and decay periods for the thermal decomposition of U.V.-irradiated lithium azide are as follows:

(i)	Induction period :	21 k.cals/mole
(ii)	Acceleratory period :	25 k.cals/mole
(iii)	Decay period :	27 k.cals/mole

8.3.5 The effect of interrupting a thermal decomposition

Interruption of a thermal decomposition has been described previously in 5.3.4. Two runs were done with U.V.-preirradiated lithium azide powder, at 185°C. The material was irradiated for 15 secs as described earlier. One run was interrupted at 0.5 I.P. and at the inflexion point and the other run was interrupted at $\alpha = 0.2$ and in the decay period at $\alpha = 0.7$. No effect on the subsequent thermal decomposition on resuming the reaction was observed, other than a short time lag during which the bucket and contents attained thermal equilibrium. These results are graphically presented in FIGURE 8.8 and the p/t values appear in TABLE 8.6.

8.3.6 The effect of interrupting a thermal decomposition and irradiating the salt

The method used and the precautions taken in performing this type of experiment have been described in 4.2.6. The decomposition was interrupted at various points during the decompositions and the specimen irradiated for 8 mins at 26 cm beneath the ultra-violet tube. The reaction temperature was 185°C. Approximately 3.0 - 5.0mg of azide were used for each run.

Interruptions were done at six points during the course of the thermal decomposition. These were at t = 0 (prior to decomposition), 0.5 I.P., at the end of the induction period at $\alpha = 0.15$, at $\alpha = 0.48$ and in the decay period at $\alpha = 0.78$.

A large exposure to ultra-violet radiation was used in order to observe the effect of the U.V. on the subsequent reaction rate. A characteristic of the U.V. runs was a drastic shortening of the induction period for a small change in the rate, for lower exposure times.

It was observed that there was an increase in reaction rate after interruption, up to $\alpha = 0.15$. Interruption and irradiation at the inflexion point and beyond produced no change in the decomposition rate, on resuming the reaction. The results for the p/t values for these runs and a blank unirradiated run appear in TABLE 8.7 and the derived rate constants k_1 and k_2 for the acceleratory periods appear in the table below. The p/t plots are illustrated in FIGURE 8.9.

Specimen	Point of Interruption	Acceleratory period rate constant (mins^{-1})
Powder	Blank	7.05×10^{-3} (k_1)
	t = 0	3.13×10^{-2} (k_2)
	0.5 I.P.	3.50×10^{-2}
	End I.P.	3.32×10^{-2}
	$\alpha = 0.15$	3.04×10^{-2}
	$\alpha = 0.48$	-
	$\alpha = 0.78$	-

8.3.7 The effect of admitting water vapour onto the salt in an interrupted decomposition

The general technique used for the "water interruption" series has been described in 4.2.5. Unless otherwise stated the results presented are not normalised to illustrate the reduction of the p_a.

Exposure to water vapour for 30 secs was investigated. The effect of 5 mins exposure to water vapour at t = 0 on the subsequent thermal decomposition was also studied.

(i) 30 secs exposure to water vapour. Approximately 5.0mg of powdered lithium azide, pre-irradiated with ultra-violet radiation for 15 secs at a distance of 26cms beneath the U.V. tube were used for each decomposition. The decompositions were interrupted at various stages and the specimen exposed to water vapour for 30 secs. Interruptions were made at t = 0, 0.5 I.P., end I.P., $\alpha = 0.11$, at the inflexion point and in the decay period at $\alpha = 0.60$. Blank runs were also done using the same irradiated material and the same unirradiated material. The reaction temperature was 185°C.

As previously found for the γ- and X-irradiated lithium azide, interruption at t = 0 had no effect on the subsequent thermal decomposition, other than lowering the percentage decomposition.

Exposure at all points up to and including the inflexion point resulted in the formation of a new induction period (33 - 45 mins in duration) on resuming decomposition. The new induction periods were longer than that for the uninterrupted irradiated run and less than that for unirradiated azide (48 mins). The Avrami-Erofeyev equation with n = 2, (equation 6.1), was found to be applicable in the analysis of the acceleratory period for runs interrupted at t = 0 and 0.5 I.P. The Avrami-Erofeyev equation with n = 3 (equation 5.2) was found to be applicable in the analysis of the acceleratory period for runs interrupted at the end of the induction period and beyond.

The rate constants (k_1) for the runs interrupted after 0.5 I.P. are seen to be less than that for the unirradiated decomposition.

Since interruption at the end of the induction period resulted in a new induction period, a second interruption at the end of the new induction period was done. The process of exposing the specimen to water vapour at the end of the new induction period for 30 secs was repeated five times and the reaction was then allowed to proceed in the normal manner after the fifth exposure. The p_a was lowered, as found above, and the Avrami-Erofeyev equation with $n = 3$ was found to be applicable in the mathematical analysis of the acceleratory period. The lengths of the induction periods are seen to be similar to that found for the unirradiated blank run.
These results are graphically illustrated in FIGURE 8.10.

(ii) <u>5 mins exposure to water vapour</u>. Powdered lithium azide, pre-irradiated with ultra-violet light for 80 secs at a distance of 26 cms below the U.V. tube, was exposed to water vapour for 5 mins at $t = 0$. After pumping the sample and vacuum line in the normal manner for 12 hours, the material was decomposed at 185°C.

It was found that the length of the induction period for the interrupted run (5 mins) was slightly longer than that found for the decomposition of the unirradiated material (48 mins). The exponent n changed from 2 to 3 (Avrami-Erofeyev equation) in the analysis of the acceleratory period for the interrupted decomposition. The rate constant, k_1 (equation 5.2), is seen to be lower than that found for the unirradiated decomposition.

The rate constants k_1 and k_2 (equation 5.2 and 6.1), the lengths of the induction periods and the percentage decomposition of the runs done above,((i) and (ii)), appear in the table below. The p/t values for these results are tabulated in TABLE 8.8.

Specimen	Exposure (mins)	Point of Interruption	I.P. after interruption (mins)	Rate constant (mins^{-1})	Percentage decomposition
Unirradiated	Blank	-	48	8.71×10^{-3} (k_1)	93
Irradiated	Blank	-	16	9.08×10^{-3} (k_2)	84
"	0.5	t = 0	18	9.95×10^{-3}	74
"	"	0.5 I.P.	19	1.23×10^{-2}	55
"	"	End I.P.	41	7.70×10^{-3} (k_1)	32
"	"	$\alpha = 0.11$	45	5.38×10^{-3}	48
"	"	Inf. Pt.	33	8.12×10^{-3}	49
"	"	$\alpha = 0.60$	-	-	85
"	"	Successive	15 32 48 48 30 42	9.30×10^{-3}	66
Unirradiated	Blank	-	48	8.71×10^{-3} (k_1)	93
Irradiated	Blank	-	16	9.08×10^{-3} (k_2)	84
"	5	t = 0	55	7.66×10^{-3} (k_1)	68

8.3.8 The effect of thermal annealing

Powdered lithium azide, pre-irradiated for 15 secs with ultra-violet radiation, was thermally annealled in vacuo at 140°C for one hour with continuous pumping. The specimen was then further pumped for 10 hours and was then thermally decomposed after the pump section had been isolated. A blank run was done for comparative purposes, with no annealing. The reaction temperature was 185°C. Comparison of the normalised curves showed that thermal annealing had no effect on lithium azide, pre-irradiated with U.V.- radiation. The p/t results are given in TABLE 8.9 and the plots are illustrated in FIGURE 8.11.

8.3.9 Percentage decomposition

The percentage decomposition as described in 5.3.6 of the runs used for the varying temperature series of lithium azide pre-irradiated with ultra-violet light, was found to be as follows (decomposition temperature in brackets):

103 (170°); 100 (175°); 102 (180°); 98 (185°); 108 (190°); 91 (195°).

MEAN: 100%

The percentage decomposition of U.V.-irradiated azide used for the varying dose series was found to be as follows (irradiation time in brackets):

91 (0); 100 (2 secs); 93 (10 secs); 103 (80 secs); 81 (6 hrs); 77 (32 hrs);

MEAN: 94% (excluding 32 hours)

8.3.10 Photochemical decomposition of lithium azide

This study was made by Mr W G Sears. No evolution of gas was observed after 2 hours irradiation through an optically-flat quartz window, using the low intensity lamp 26 cm above the specimen. For longer irradiation times (6 hrs) a small amount of gas was measured indicating photochemical decomposition ($\ngtr$ 0.1%).

Irradiation of the lithium azide with the high intensity lamp resulted in instantaneous decomposition and approximately 5% decomposition was estimated after 30 mins, from gas pressure measurements.

8.3.11 Visual observations

It was observed that lithium azide turned a buff-cream colour after 20 mins irradiation with the high intensity lamp. On stirring the powder, fresh uncoloured particles were exposed. No colouration was observed after 30 hours irradiation at 26 cm below the low intensity lamp.

Colour changes during the thermal decomposition of the irradiated salt were similar to those reported for unirradiated and γ- and X-irradiated lithium azide.

8.4 RESULTS (PELLETED LITHIUM AZIDE)

8.4.1 The effect of varying pellet weight on the initial reaction

The effect of varying the pellet weight of ultra-violet pre-irradiated pelleted lithium azide was studied. Two pellets, weighing 8.5mg and 17.3mg were simultaneously irradiated for 35 mins 6.5cm beneath the low intensity lamp. The subsequent thermal decomposition of the irradiated pellets showed the initial reaction to be independent of the pellet weight. The reaction temperature was 190°C.

As a result of the low evolution of gas over the initial period of the thermal decomposition, no mathematical analysis could be attempted.

The p/t results obtained appear in TABLE 8.10 and the results are graphically illustrated in FIGURE 8.12. The results are not normalised for comparative purposes.

8.4.2 The effect of irradiating one and both faces of pelleted azide

Pelleted lithium azide was pre-irradiated with U.V.-radiation for 2 mins on one face and one minute on each face, so that the specimens both received the same total quanta of ultra-violet radiation. The irradiated pellets and a blank unirradiated pellet were decomposed in vacuo in the normal manner at 195°C.

It was observed that the induction period was the same for both irradiated specimens and the pellet irradiated on both faces decomposed with a higher rate than the sample irradiated on one face only. These results appear in TABLE 8.11 and are illustrated in FIGURE 8.13.

8.4.3 The effect of pelleting irradiated powdered lithium azide

The effect of pelleting powdered irradiated lithium azide irradiated for 4 hours with sunlight and then decomposing the pellet in the normal manner at 190°C was studied. A blank run of irradiated pelleted lithium azide was also done for comparative purposes.

It was observed that although the irradiated pelleted material yielded a sigmoid p/t plot, the p/t plot of the pelleted irradiated material had a double-sigmoid character (as found with γ-rays and X-rays). The results are presented in TABLE 8.12.

8.4.4 Visual observations

Only the high intensity U.V.-lamp coloured the pelleted azide. The low intensity lamp produced no noticeable colour change after 5 hours irradiation at 26cm. With the high intensity lamp only the irradiated face was coloured yellow-brown; the opposite face was white, as for unirradiated lithium azide.

Examination of the pellet faces under the optical microscope at the end of the induction period showed that the reaction always commenced on the irradiated face, while the opposite face was still unmarked at that point.

Examination of the pellet at the end of the initial reaction showed that the interior and the face opposite the reacting face were grey, indicating commencement of reaction at these points.

8.4.5 Photomicrography

As for previous photomicrographic studies, only pelleted lithium azide was used. The pellets were pre-irradiated with U.V. radiation for 30 mins at 26 cms, using the low intensity lamp. The thermal decomposition was done at $160^{\circ} \pm 2^{\circ}C$ and photomicrographs and differential pressure readings were taken during the course of the reaction.

Plate 4 shows the thermal decomposition of the irradiated surface of pelleted lithium azide. The magnification was 65X. FIGURE 8.14 shows the differential plot and the arrows indicate where the photomicrographs were taken. TABLE 8.13 contains the dp/dt results. (Figures in brackets below are the exposure times in printing the photographs as explained in 5.3.12).

(a) The photomicrograph shows the irradiated pellet surface at t = 0. The striations are due to the die face used in pelleting. The surface was white and uniform. (19)

(b) As the reaction proceeded into the acceleratory period of the first or initial reaction, characteristic of irradiated pelleted lithium azide, areas of decomposition begin to form, amidst general darkening of the entire pellet surface. (19)

(c) Just prior to the first inflexion point, distinct areas of decomposition are visible over the entire viewed surface. These have increased in number and have grown. (17)

(d) The photomicrograph was taken shortly after the previous one and shows the pellet surface at the inflexion point. The pellet surface had darkened considerably, while no further growth of the dark areas of product was seen. (16)

(e) In the first decay period more areas of decomposition were observed to appear, with the commencement of overlap of some of the areas of decomposition. (15)

(f) Further increase in the decomposition areas was observed at a point well into the first decay period. (14)

(g) and (h) These photomicrographs were taken prior to the commencement of the second reaction, at 50 and 100 mins respectively. It is seen that the entire surface of the pellet was covered with dark reaction product, prior to the second reaction. (12 and (11) respectively

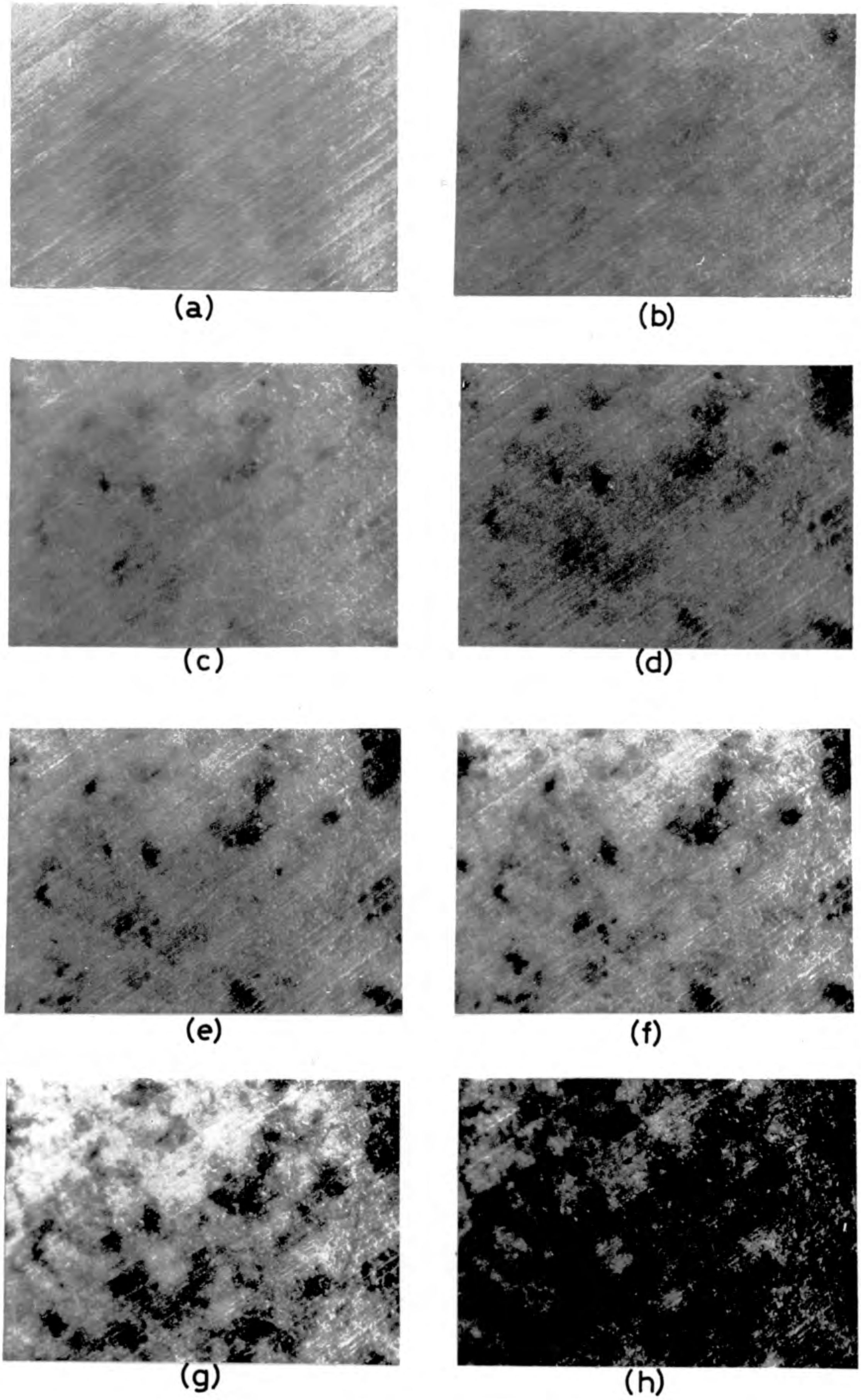

(a) (b) (c) (d) (e) (f) (g) (h)

PLATE 4. THE THERMAL DECOMPOSITION OF U.V.-IRRADIATED PELLETED LITHIUM AZIDE. 160° C.

8.5 DISCUSSION

The spectra of inorganic azides(37,89) have been studied, as these yield information on the formation of colour centres by ultra-violet radiation. Cunningham and Tompkins(89) have attributed the formation of F-centres in potassium and sodium azides to the production of excitons within the lattice in KN_3 and in the vicinity of dislocations and grain boundaries in NaN_3. The excitons formed primarily as a result of ultra-violet irradiation, lose electrons by the tunneling effect to vacant anion sites, resulting in F-centres and positive holes. The positive holes may in turn form V-centres or combine with an adjacent azide ion to liberate N_2.

Investigation of the effects of U.V. radiation on the thermal decomposition of strontium(68) and calcium(20) azides led the authors to propose that the formation of large numbers of anion vacancies on irradiation was responsible for the enhanced reaction rates on subsequent thermal decomposition. The effects of pre-irradiation on barium azide(68,109) and potassium azide(21) however, have been attributed to F-centre formation.

8.5.1 Powdered lithium azide

The effects of pre-irradiation with ultra-violet light on the subsequent thermal decomposition of lithium azide were found to be :

(i) a shortening of the length of the induction period,

(ii) an increase in the acceleratory period rate constant,

(iii) virtually no effect on the decay reaction rate constant.

The effects of varying doses of ultra-violet light on the thermal decomposition were observed to be a progressive shortening of the induction period and increase in the acceleratory period rate constant k_2, with increasing exposure to ultra-violet light. The decay period rate constant was found to change from 1.8×10^{-3} to 4.1×10^{-3} $\min^{-1}$ (unirradiated to 32 hours irradiation at 26 cms), while for γ-ray doses (6.3.1) the corresponding change was from 2.19×10^{-3} to 44.4×10^{-3} mins^{-1}, (unirradiated to 15000 roentgens).

The inflexion point of the p/t plot was also observed to decrease with increasing dose and for very heavy doses was found to be at $\alpha = 0.14$.

Although no colouration of the material was observed with light doses of U.V.-radiation, the material turned buff-cream with heavier doses suggesting the formation of F-centres. Nitrogen was also evolved and photochemical decomposition occurred. This effect was more pronounced when a high intensity ultra-violet source was employed.

Irradiation after interruption of the normal decomposition of the unirradiated salt is only effective at low values of α, ($\alpha \ngtr 0.15$), (FIGURE 8.9). This is due to the fact that the product layer on the surface of the particles will screen the unreacted azide from ultra-violet light.

Analysis of the acceleratory region of the p/t plot for the decomposition of U.V.-irradiated lithium azide was found to be described by the Avrami-Erofeyev equation with n = 2, as found for X-irradiated lithium azide. The decay period was well fitted by the contracting sphere formula.

The activation energies were found to have the following values:

(i) Induction period: 21 k.cals/mole

(ii) Acceleratory period: 25 k.cals/mole

(iii) Decay period: 27 k.cals/mole

The above observations are closely similar to those found on pre-irradiating lithium azide with X-rays (c.f. 7.5.1) and accordingly it is proposed that similar mechanisms are operative during the thermal decomposition of U.V.-irradiated lithium azide.

Erofeyev and Sviridov(131) have similarly reported that there exists a considerable degree of analogy between the effects produced by X-rays and ultra-violet light, when barium azide is pre-irradiated with these types of radiation.

The results of the "water interruption" series of runs, (FIGURE 8.10) were similar to those found for X-irradiated lithium azide, but as the series was done at a decomposition temperature of 20°C higher (185°C) than that used for the X-irradiated salt, the resulting p/t plots illustrate more clearly the extent to which the material was returned to an unirradiated state, after exposure to water vapour.

"Water interruption" experiments prior to decomposition and at various points during the course of the decomposition yielded information concerning the reaction mechanism. Similar effects were observed as found for γ- and X-irradiated lithium azide, when the U.V.-irradiated salt was exposed to water vapour prior to thermal decomposition. The 30 secs exposure had no effect, while 5 mins. exposure returned the salt to the unirradiated state indicating that the radiation damage was destroyed. The water destroyed the F-centre trapping sites and at the same time the F-centres, thus effectively removing the radiation damage and returning the salt to the unirradiated state. As previously found, the greater exposure time (5 mins) had a larger effect on the percentage decomposition, indicating a greater degree of hydrolytic reaction. "Water interruption" up to the point where the decay reaction commences, returned the salt to the unirradiated state, as is evident by the change from 2 to 3 in the value of n, the exponent in the Avrami-Erofeyev equation and the agreement of the values of rate constant k_1 (equation 5.1), after water interruption and for an unirradiated blank run.

The slightly higher value of the rate constant recorded as well as the small variation in the length of the new induction periods indicates that a small number of nuclei are still formed as a result of the irradiation effect. It is likely that these will be in the interior of the particle.

The rate determining steps for the induction, acceleratory and decay periods are considered to be the same as those proposed for the associated reactions in lithium azide pre-irradiated with γ- and X-rays (cf . 6.5.1, 7.5.1).

As previously found, (γ-, X-rays) the mean percentage decomposition was increased on pre-irradiating the azide.

8.5.2 Pelleted lithium azide

The initial reaction during the decomposition of irradiated pelleted lithium azide was found to be dependant on the irradiated surface area only, as doubling the weight of the pellet, with the same diameter pellet, produced the same initial gas evolution on decomposing the pellet. No activation energy determinations were attempted as the gas evolution during the initial reaction was not significant enough to obtain sufficient pressure readings for analysis purposes.

It was found that colouration of the irradiated surface <u>only</u>, was observed with suitable doses. Microscopic observations showed that only the irradiated face decomposed during the initial reaction. These facts confirm the initial reaction to be a surface one and to be the direct result of pre-irradiation with ultra-violet light.

By analogy from the results of U.V. radiation on the powdered material it is proposed that the same mechanisms apply to the initial reaction. The main reaction is the decomposition of unirradiated material at the reaction temperature employed (FIGURE 8.13). This decomposition is due to the unirradiated material within the pellet.

It was also found that irradiating the pelleted azide on one face with a certain quanta of energy, and then irradiating both faces of a similar pellet with the same total quanta produced an increase in the initial gas evolution, lending further support to the reaction being confined solely to the surface. It is seen for the material irradiated on both faces that the p/t plot is linear from $\alpha = 0.02$ to $\alpha = 0.20$, which can be expected if a rapid surface reaction covers the faces of the pellet with product and then the two interfaces move into the pellet. The decomposition of the unirradiated salt predominates after this.

A similar surface reaction can thus be expected with the powdered material. More efficient surface exposure was obtained by continuous stirring during irradiation in this case. The particles were very small and reaction was that of the irradiated material only, the first decay reaction being absent.

It was observed that pelleting irradiated lithium azide powder resulted in an "initial" reaction, (as found when pelleting γ- and X-irradiated powder) which is dependant upon the pellet weight. This "initial" reaction occurs at the "internal" surfaces (described previously, 6.5.2) and is considered analagous to the effect observed with the X-irradiated material. The proposed mechanism for the reaction is the same as that for the X-irradiated material.

The photomicrographs taken during the thermal decomposition of U.V.-irradiated pelleted lithium azide (Plate 4) are similar to those for the initial reaction in X-irradiated pelleted lithium azide (Plate 3). Whereas after the first decay period for X-irradiated material, the pellet was observed on cross-section to contain product throughout the mass and over the surfaces, for the U.V.-irradiated material at the end of the "initial" reaction, only the viewed (irradiated) surface consisted of dark product, penetrating a short distance into the interior of the pellet. The bulk of the pellet was grey in colour, indicating the early stages of the decomposition (acceleratory region) of the unirradiated material.

As for the X-irradiated pellets, the initial surface reaction was observed to commence at favoured sites. These sites did not increase to any extent in number, but grew in size until the surface was covered with reaction product, (photomicrograph (h), Plate 4).

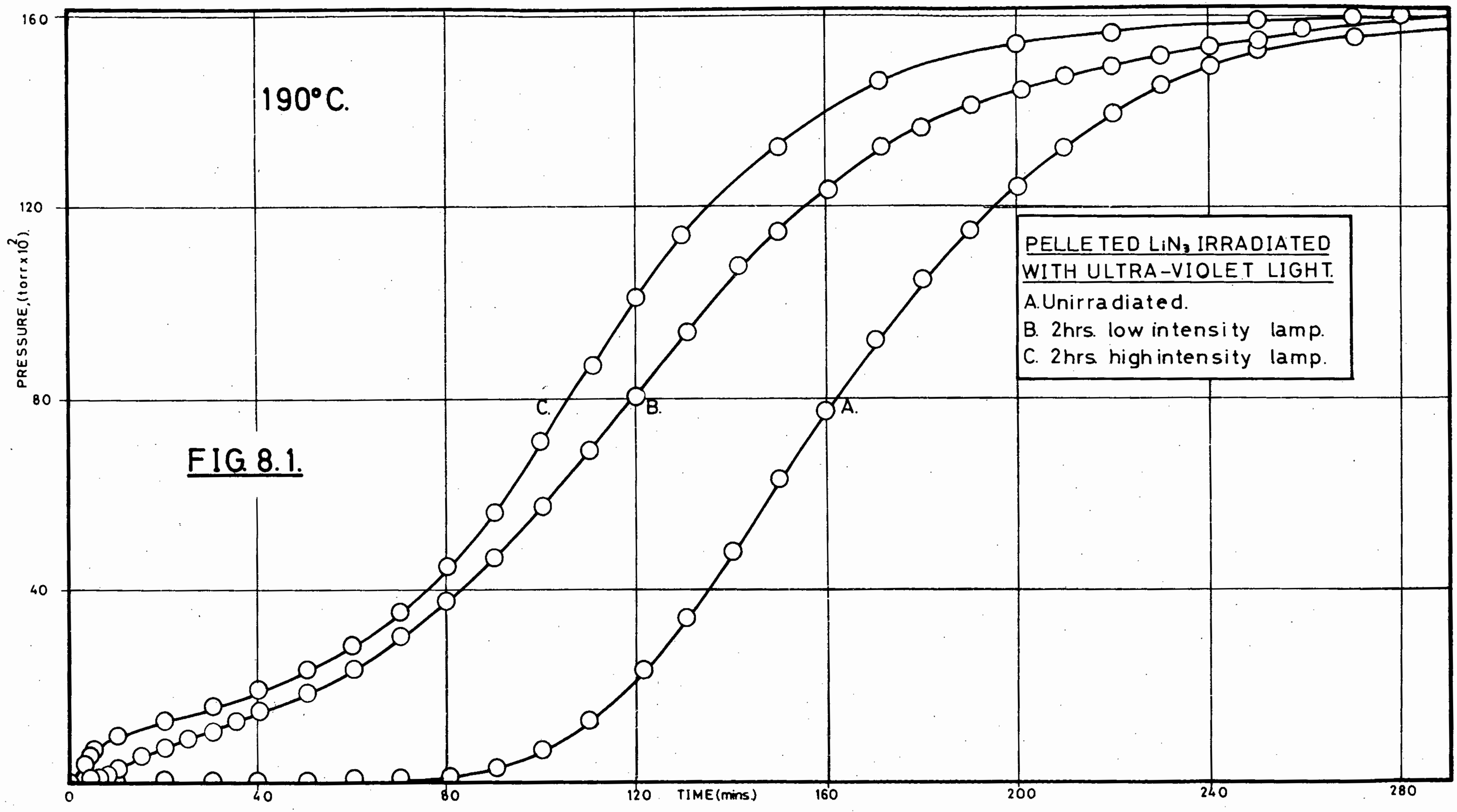
190°C.
PRESSURE, (torr x 10^2)
160
120
80
40
0
40
80
120
160
200
240
280
TIME (mins.)
C.
B.
A.
PELLETED LiN₃ IRRADIATED WITH ULTRA-VIOLET LIGHT.
A. Unirradiated.
B. 2hrs. low intensity lamp.
C. 2hrs. high intensity lamp.

FIG 8.1.

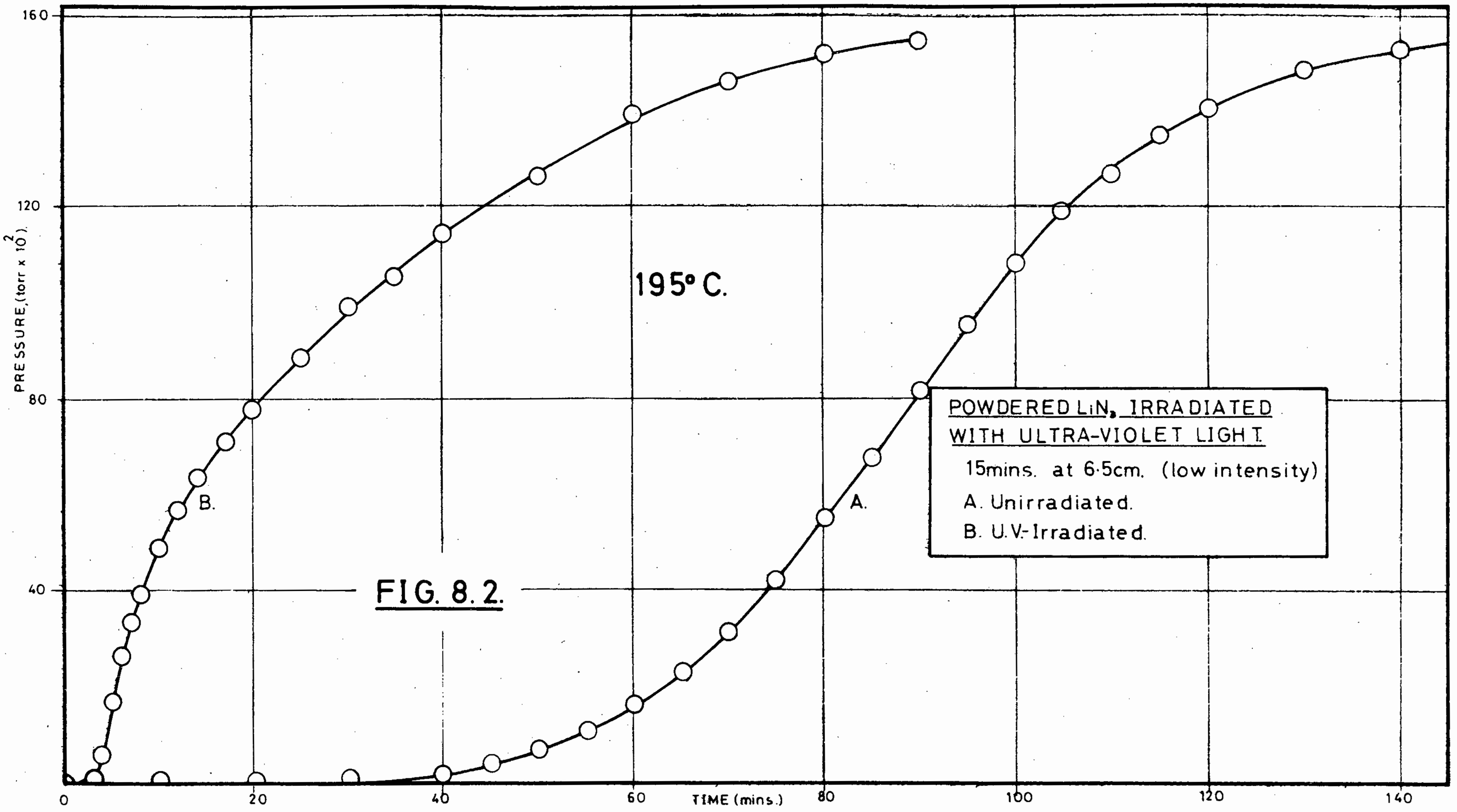

FIG. 8.2.

POWDERED LiN₃ IRRADIATED WITH ULTRA-VIOLET LIGHT.
15mins. at 6·5cm. (low intensity)
A. Unirradiated.
B. U.V.-Irradiated.
195° C.
A.
B.
PRESSURE, (torr x 10^2).
160
120
80
40
0
20
40
60
80
100
120
140
TIME (mins.)

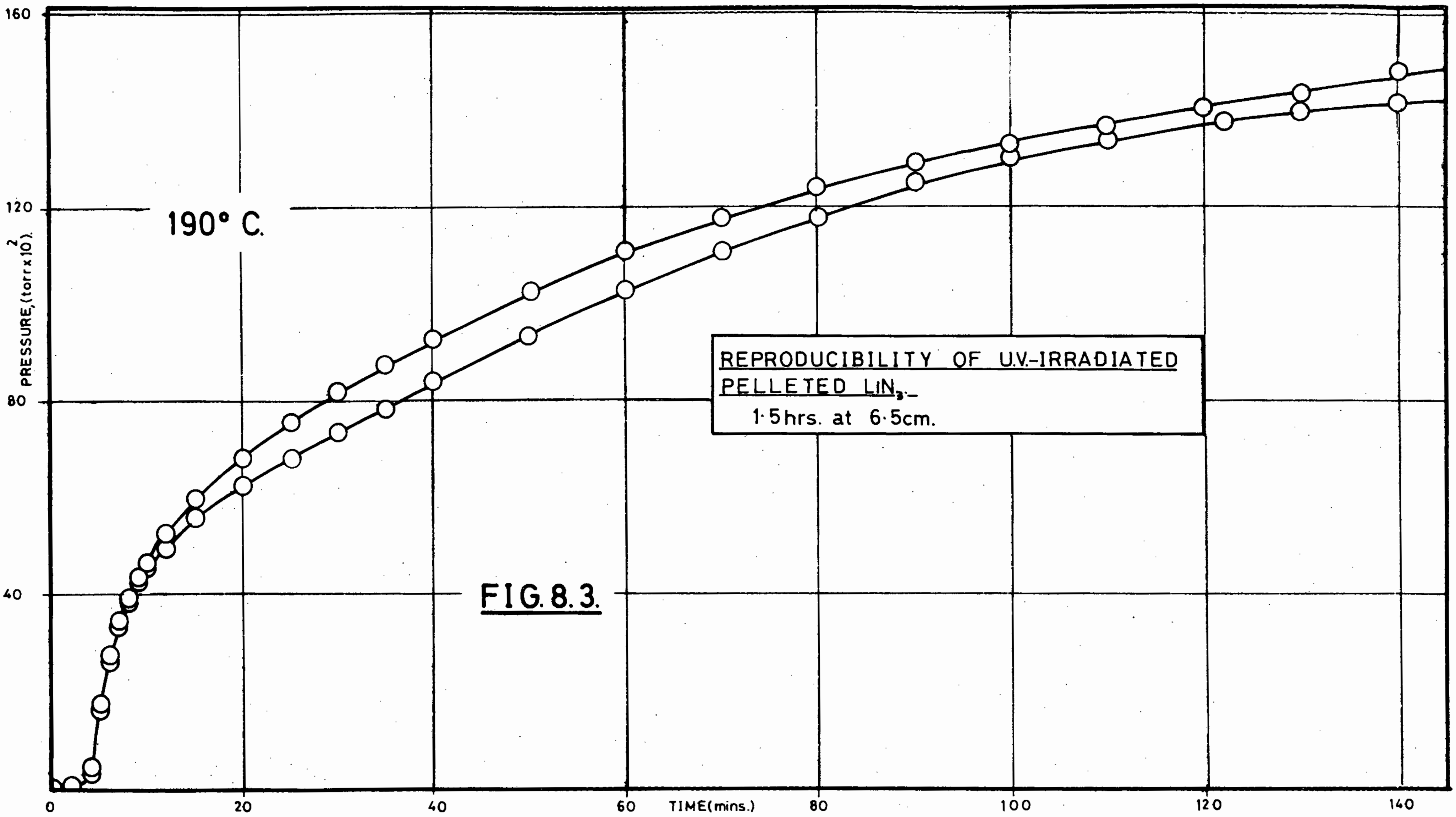
190° C.
REPRODUCIBILITY OF U.V.-IRRADIATED PELLETED LiN_3.
1·5 hrs. at 6·5 cm.
PRESSURE, (torr x 10^2).
160
120
80
40
0
20
40
60
TIME (mins.)
80
100
120
140

FIG. 8.3.

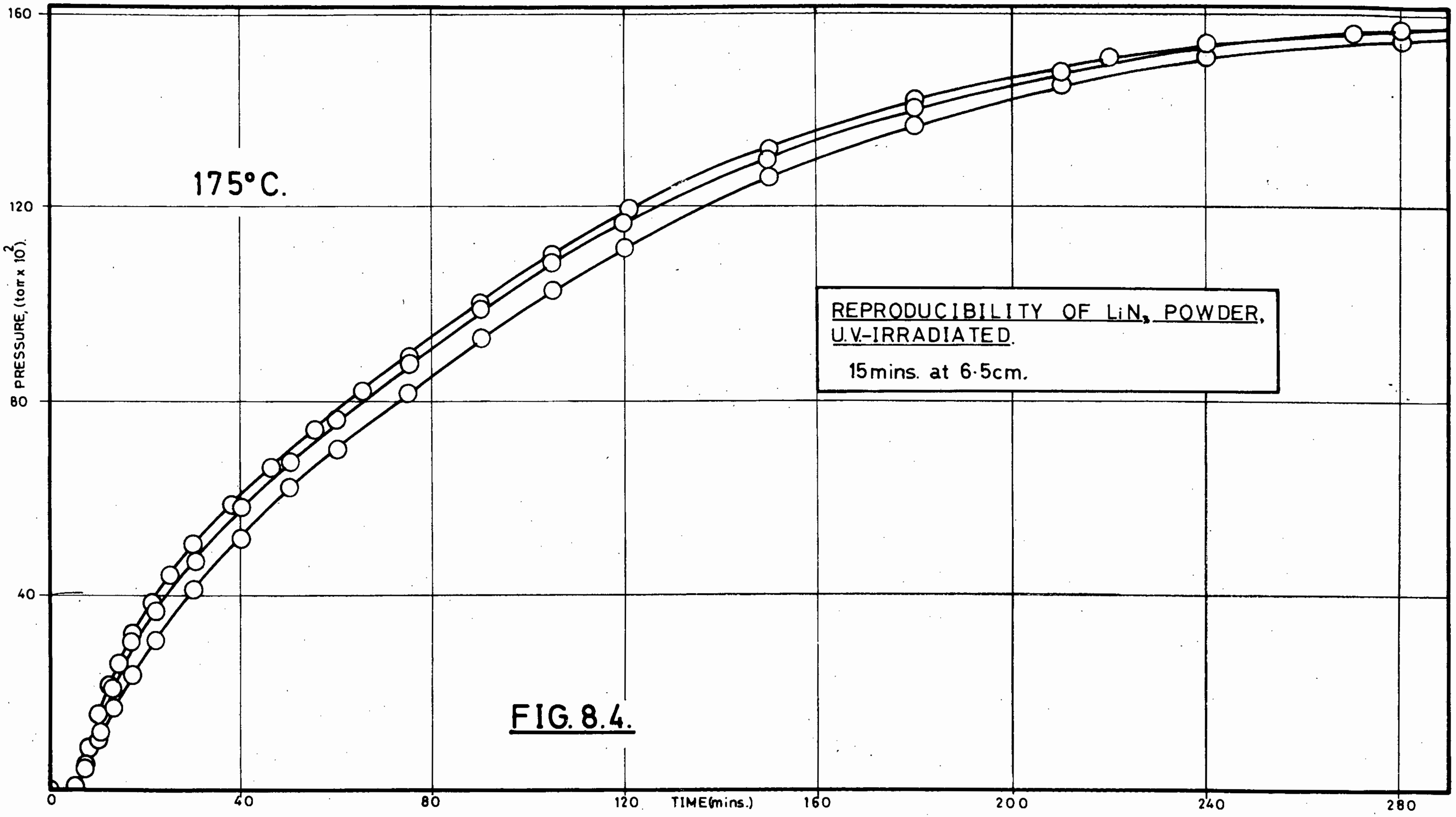

REPRODUCIBILITY OF LiN_3 POWDER, U.V.-IRRADIATED.

15mins. at 6·5cm.

FIG. 8.4.

FIG. 8.5.

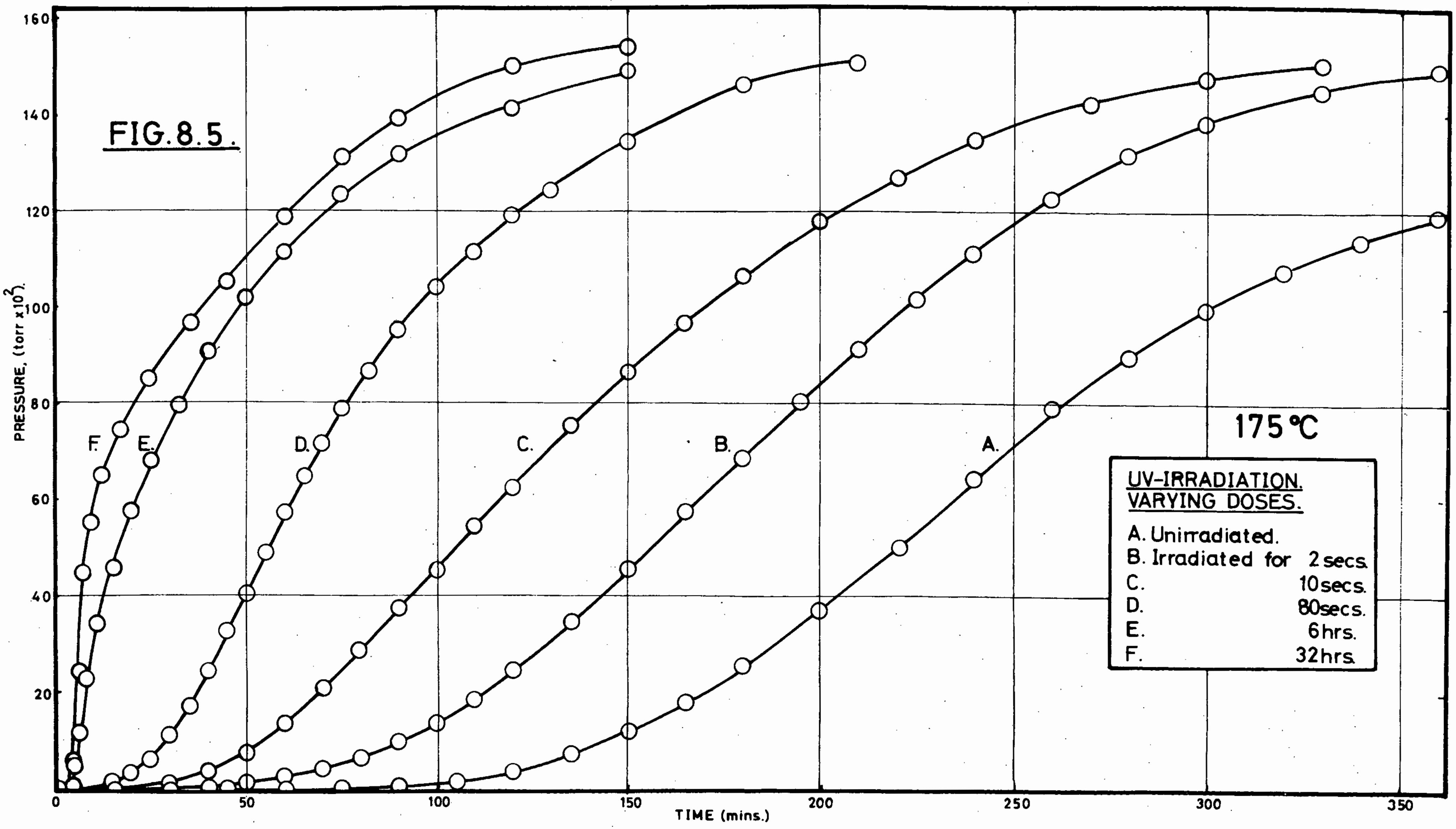
175 °C
UV-IRRADIATION.
VARYING DOSES.
A. Unirradiated.
B. Irradiated for 2 secs.
C. 10 secs.
D. 80 secs.
E. 6 hrs.
F. 32 hrs.
F.
E.
D.
C.
B.
A.
PRESSURE, (torr x10^2).
160
140
120
100
80
60
40
20
0
50
100
150
200
250
300
350
TIME (mins.)

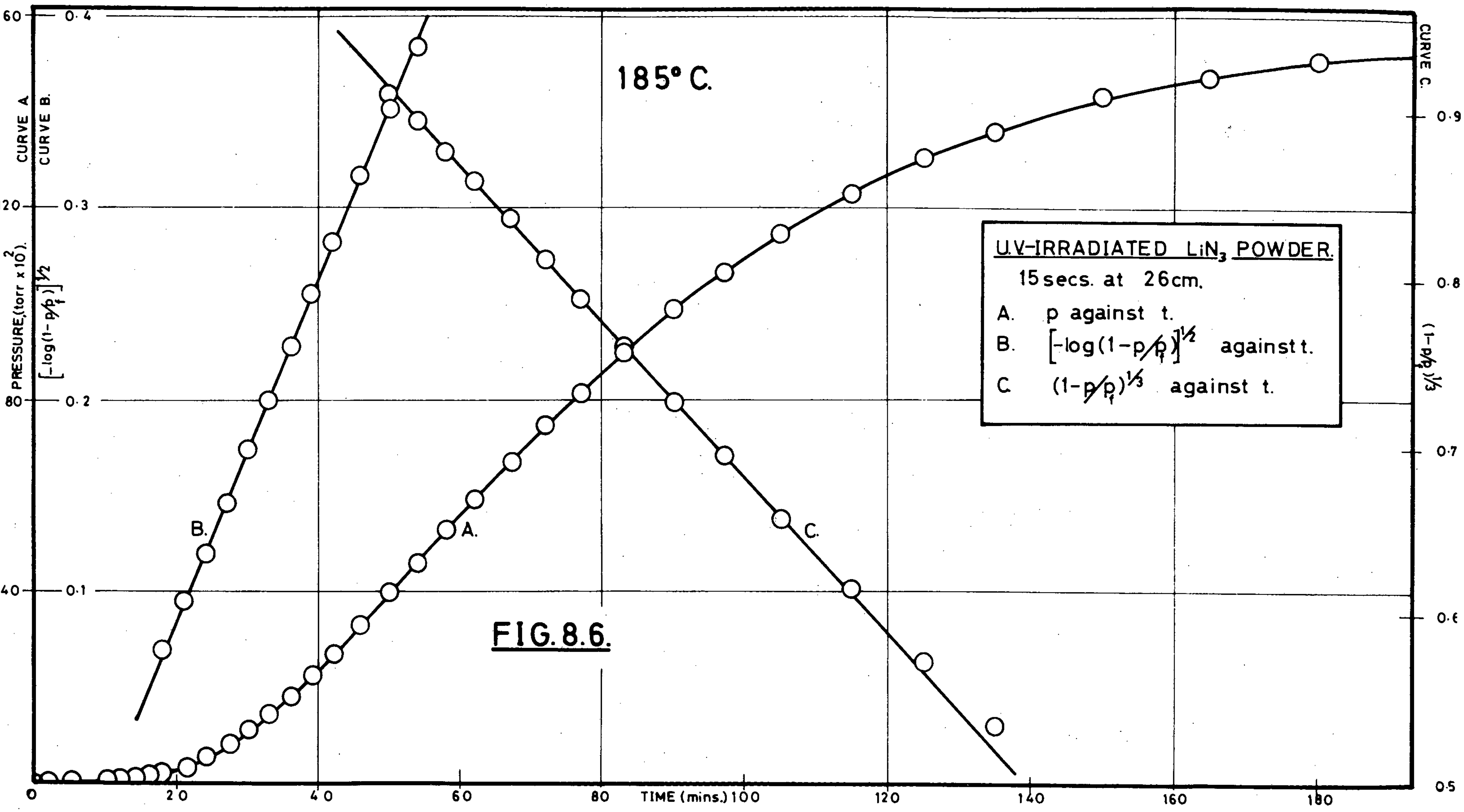
185° C.
U.V-IRRADIATED LiN_3 POWDER.
15 secs. at 26cm.
A. p against t.
B. $[-\log(1-p/p_f)]^{1/2}$ against t.
C. $(1-p/p_f)^{1/3}$ against t.
CURVE A
CURVE B.
PRESSURE (torr x 10^2).
$[-\log(1-p/p_f)]^{1/2}$
CURVE C.
$(1-p/p_f)^{1/3}$
TIME (mins.)
160
120
80
40
0·4
0·3
0·2
0·1
0·9
0·8
0·7
0·6
0·5
0
20
40
60
80
100
120
140
160
180
A.
B.
C.

FIG. 8.6.

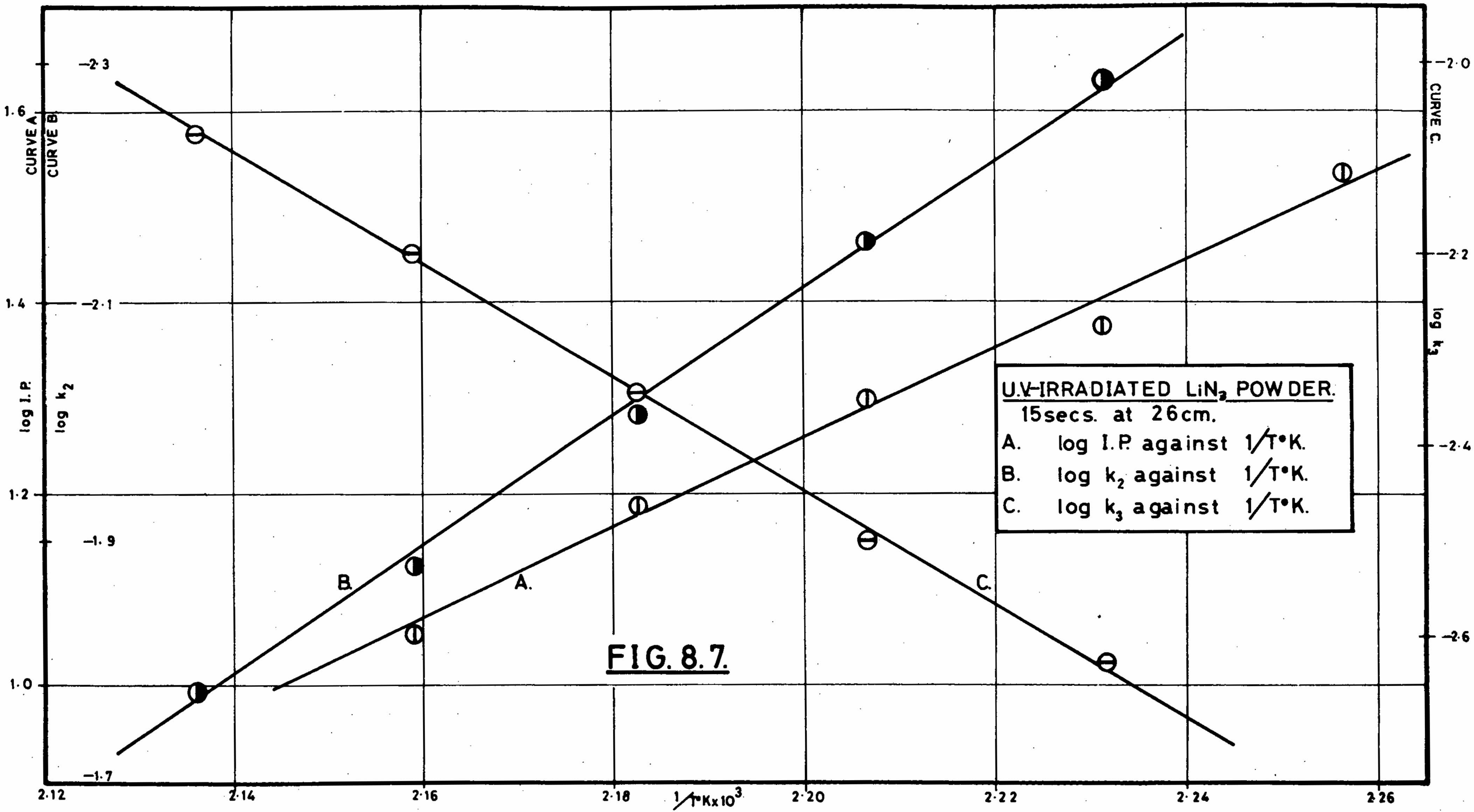
U.V-IRRADIATED LiN_3 POWDER.
15secs. at 26cm.
A. log I.P. against 1/T°K.
B. log k_2 against 1/T°K.
C. log k_3 against 1/T°K.
CURVE A
CURVE B
log I.P.
log k_2
CURVE C.
log k_3
1·6
1·4
1·2
1·0
−2·3
−2·1
−1·9
−1·7
−2·0
−2·2
−2·4
−2·6
2·12
2·14
2·16
2·18
2·20
2·22
2·24
2·26
1/T°K x 10^3
A.
B.
C.

FIG. 8.7.

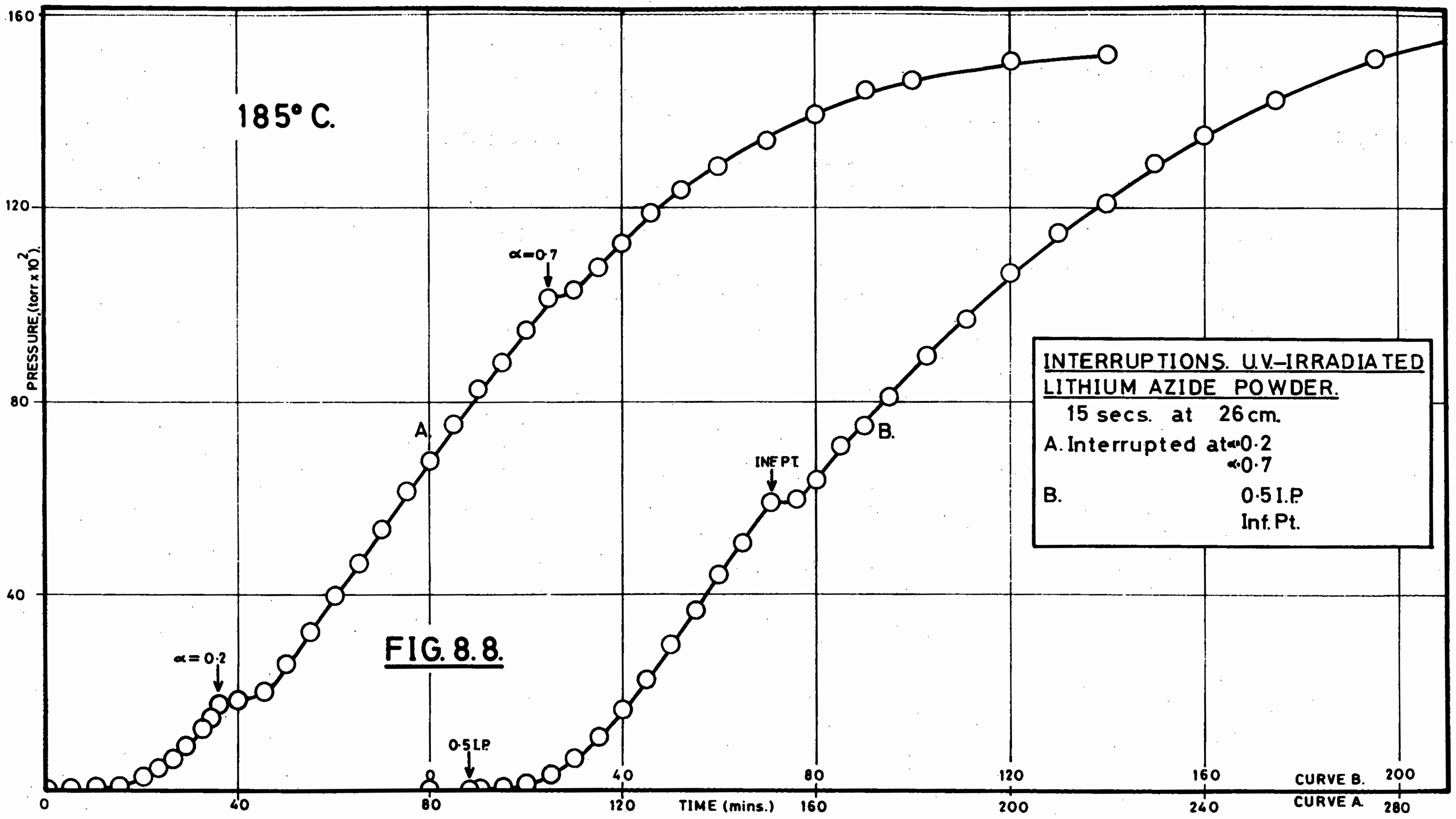
185° C.
PRESSURE, (torr x 10^2).
160
120
80
40
0
40
80
120
160
200
240
280
CURVE A.
0
40
80
120
160
200
CURVE B.
TIME (mins.)
α = 0·2
α = 0·7
0·5 I.P.
INF. PT.
A.
B.
INTERRUPTIONS. U.V.–IRRADIATED LITHIUM AZIDE POWDER.
15 secs. at 26 cm.
A. Interrupted at α 0·2
α 0·7
B. 0·5 I.P.
Inf. Pt.

FIG. 8.8.

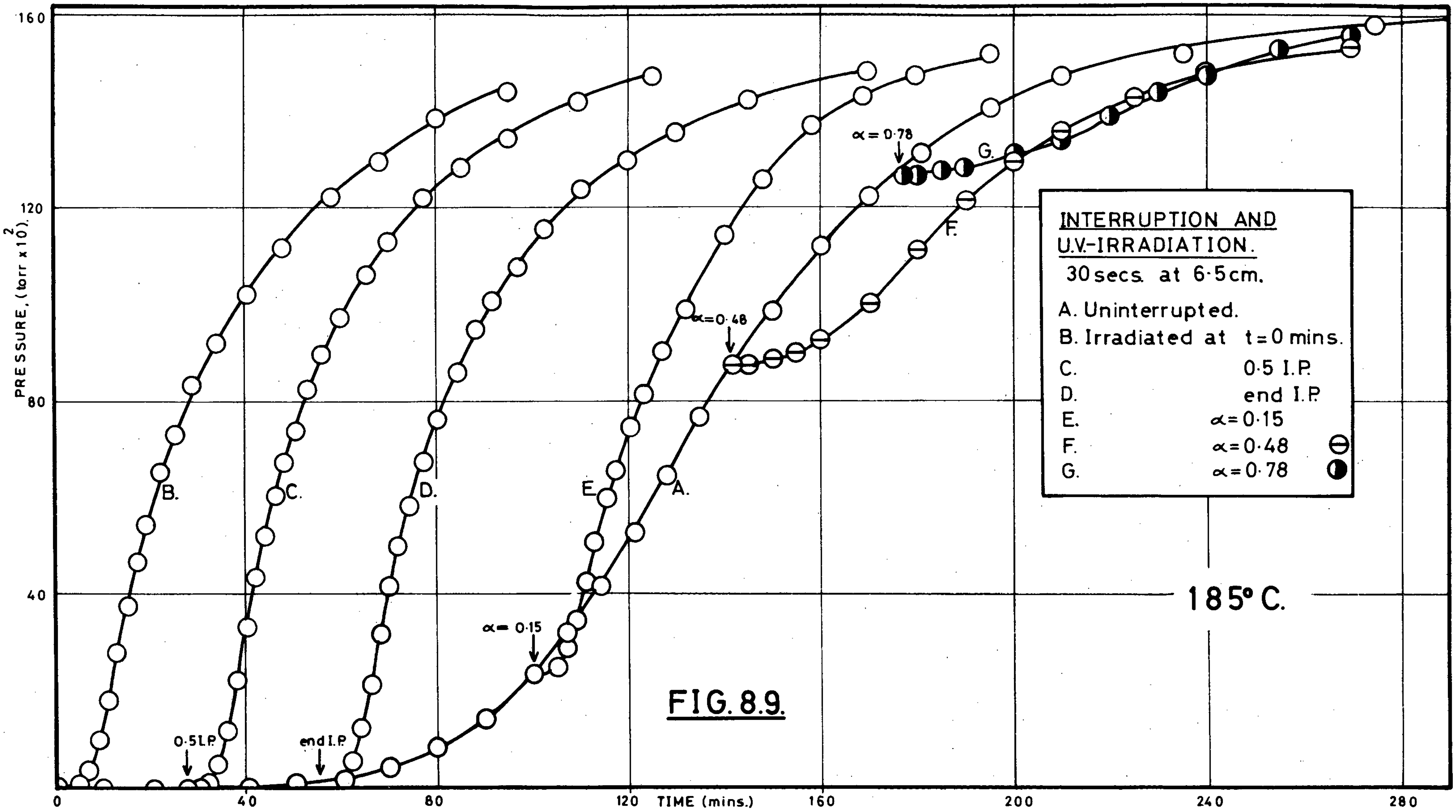
INTERRUPTION AND
U.V.-IRRADIATION.
30 secs. at 6·5 cm.
A. Uninterrupted.
B. Irradiated at t = 0 mins.
C. 0·5 I.P.
D. end I.P.
E. α = 0·15
F. α = 0·48 ⊖
G. α = 0·78 ◐
185° C.
PRESSURE, (torr x 10^2).
TIME (mins.)
0
40
80
120
160
200
240
280
160
120
80
40
A.
B.
C.
D.
E.
F.
G.
0·5 I.P.
end I.P.
α = 0·15
α = 0·48
α = 0·78

FIG. 8.9.

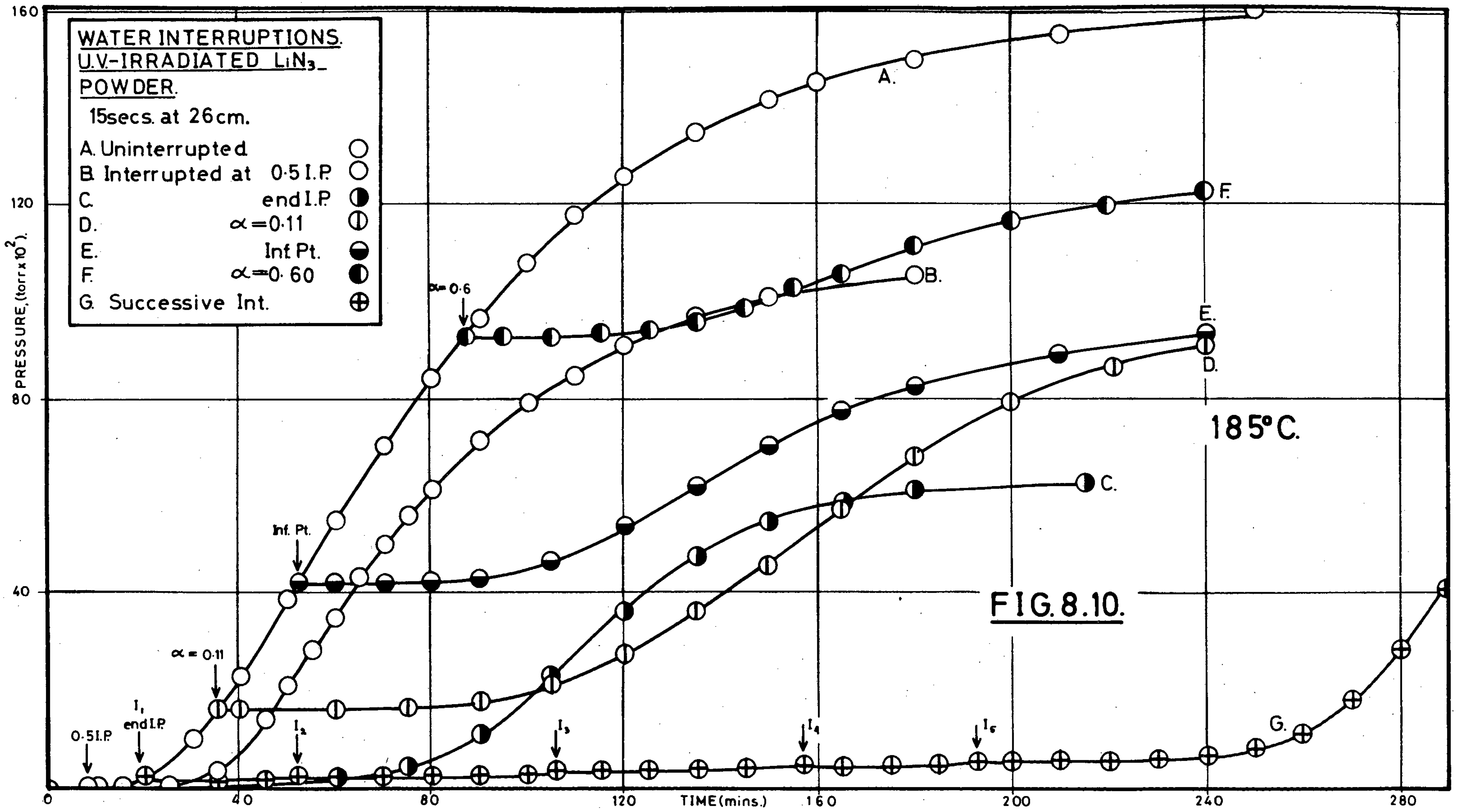
WATER INTERRUPTIONS.
U.V.-IRRADIATED LiN_3
POWDER.
15secs. at 26cm.
A. Uninterrupted ○
B. Interrupted at 0·5 I.P. ○
C. end I.P. ◐
D. $\alpha = 0{\cdot}11$ ⦶
E. Inf. Pt. ⊖
F. $\alpha = 0{\cdot}60$ ◐
G. Successive Int. ⊕
PRESSURE, (torr x 10^2).
TIME (mins.)
0
40
80
120
160
200
240
280
40
80
120
160
A.
B.
C.
D.
E.
F.
G.
185°C.
$\alpha = 0{\cdot}6$
Inf. Pt.
$\alpha = 0{\cdot}11$
0·5 I.P.
I_1
end I.P.
I_2
I_3
I_4
I_5

FIG. 8.10.

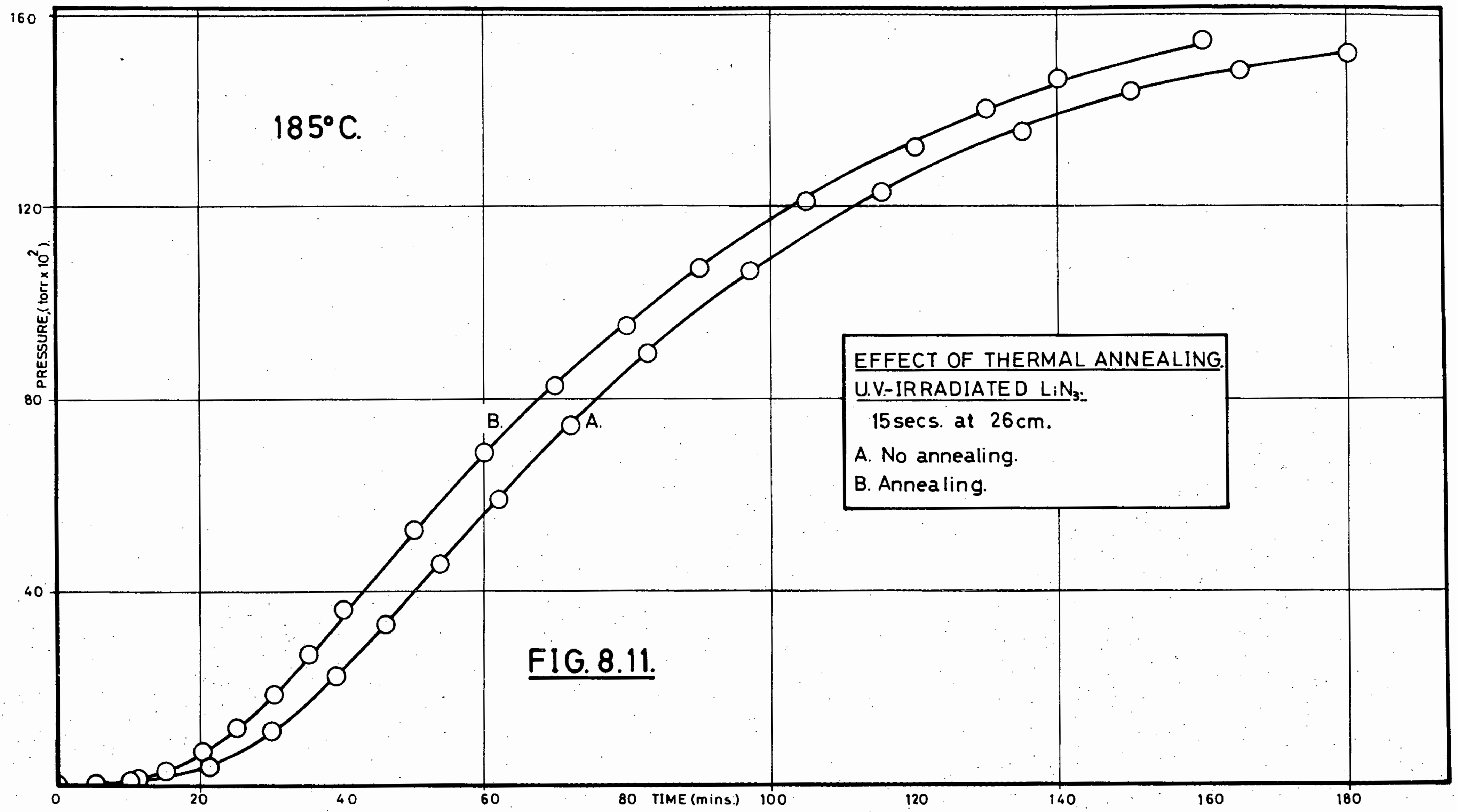
185°C.
EFFECT OF THERMAL ANNEALING.
U.V.-IRRADIATED LiN_3.
15 secs. at 26 cm.
A. No annealing.
B. Annealing.
B.
A.
PRESSURE, (torr x 10^{-2}).
160
120
80
40
0
20
40
60
80
TIME (mins.)
100
120
140
160
180

FIG. 8.11.

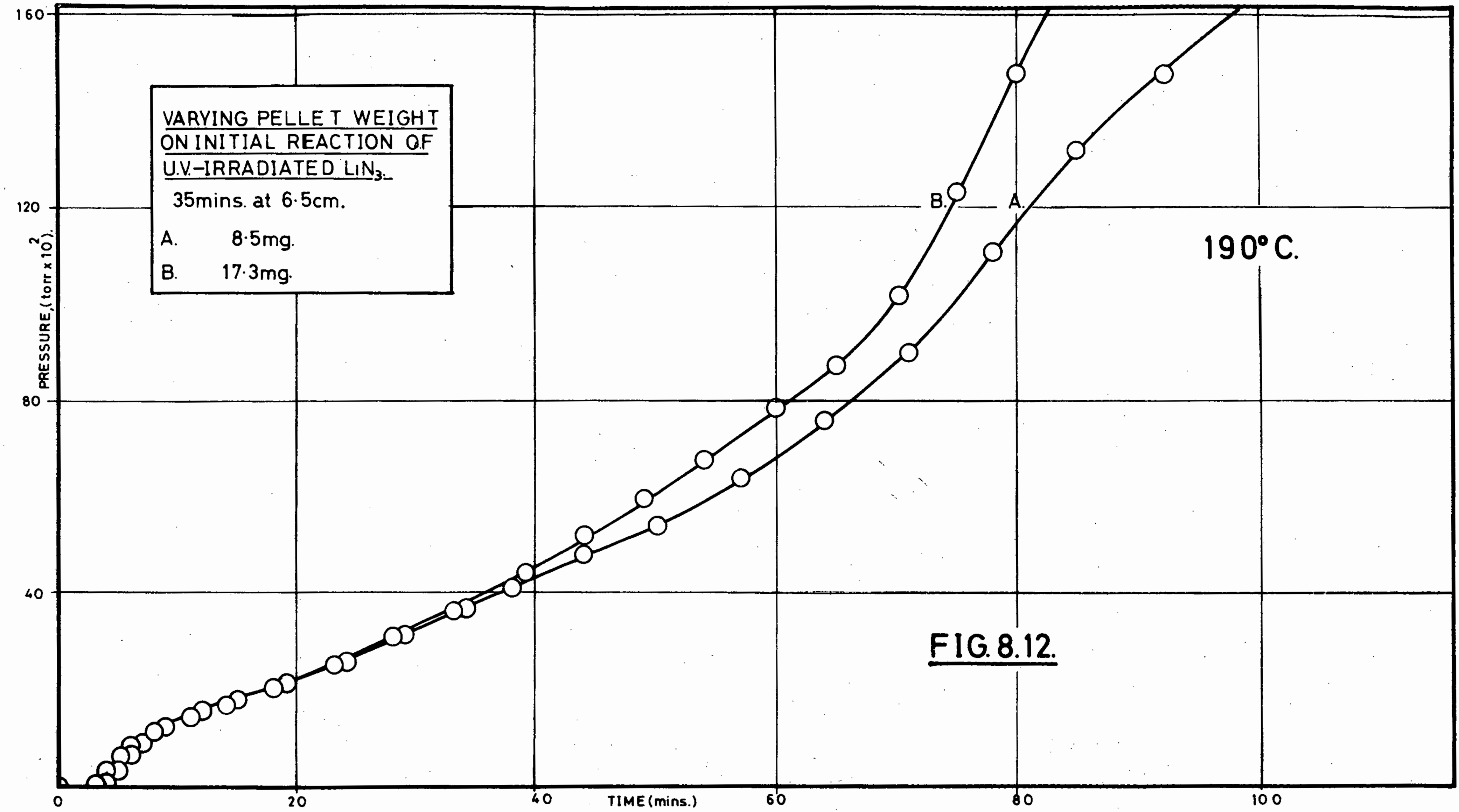
VARYING PELLET WEIGHT ON INITIAL REACTION OF U.V.-IRRADIATED LiN$_3$.
35mins. at 6·5cm.
A. 8·5mg.
B. 17·3mg.
190° C.
B.
A.
PRESSURE, (torr x 10^2).
160
120
80
40
0
20
40
60
80
100
TIME (mins.)

FIG. 8.12.

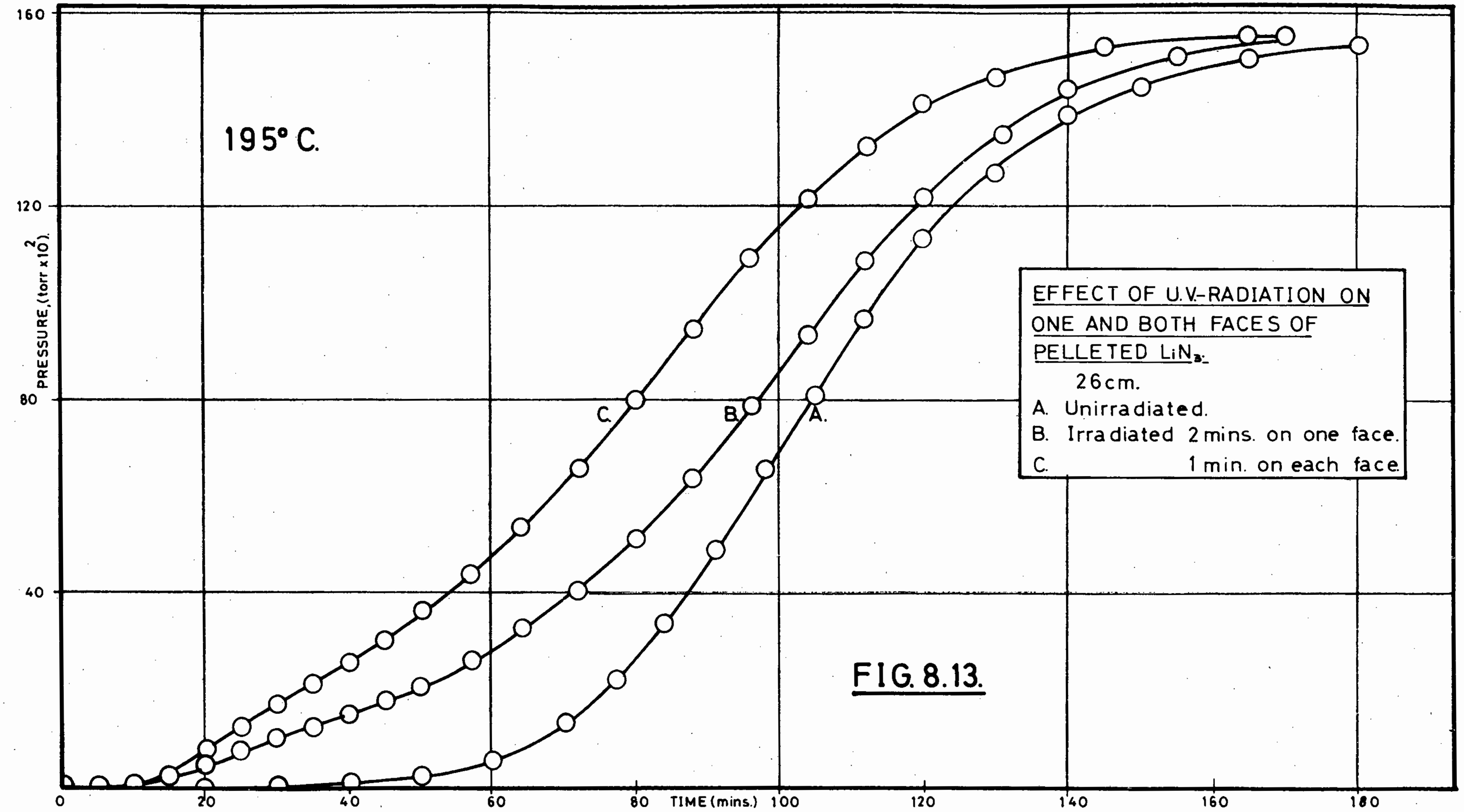
195° C.
EFFECT OF U.V-RADIATION ON ONE AND BOTH FACES OF PELLETED LiN_3.
26cm.
A. Unirradiated.
B. Irradiated 2 mins. on one face.
C. 1 min. on each face.
A.
B.
C.
PRESSURE, (torr x 10^2).
160
120
80
40
0
20
40
60
80
TIME (mins.)
100
120
140
160
180

FIG. 8.13.

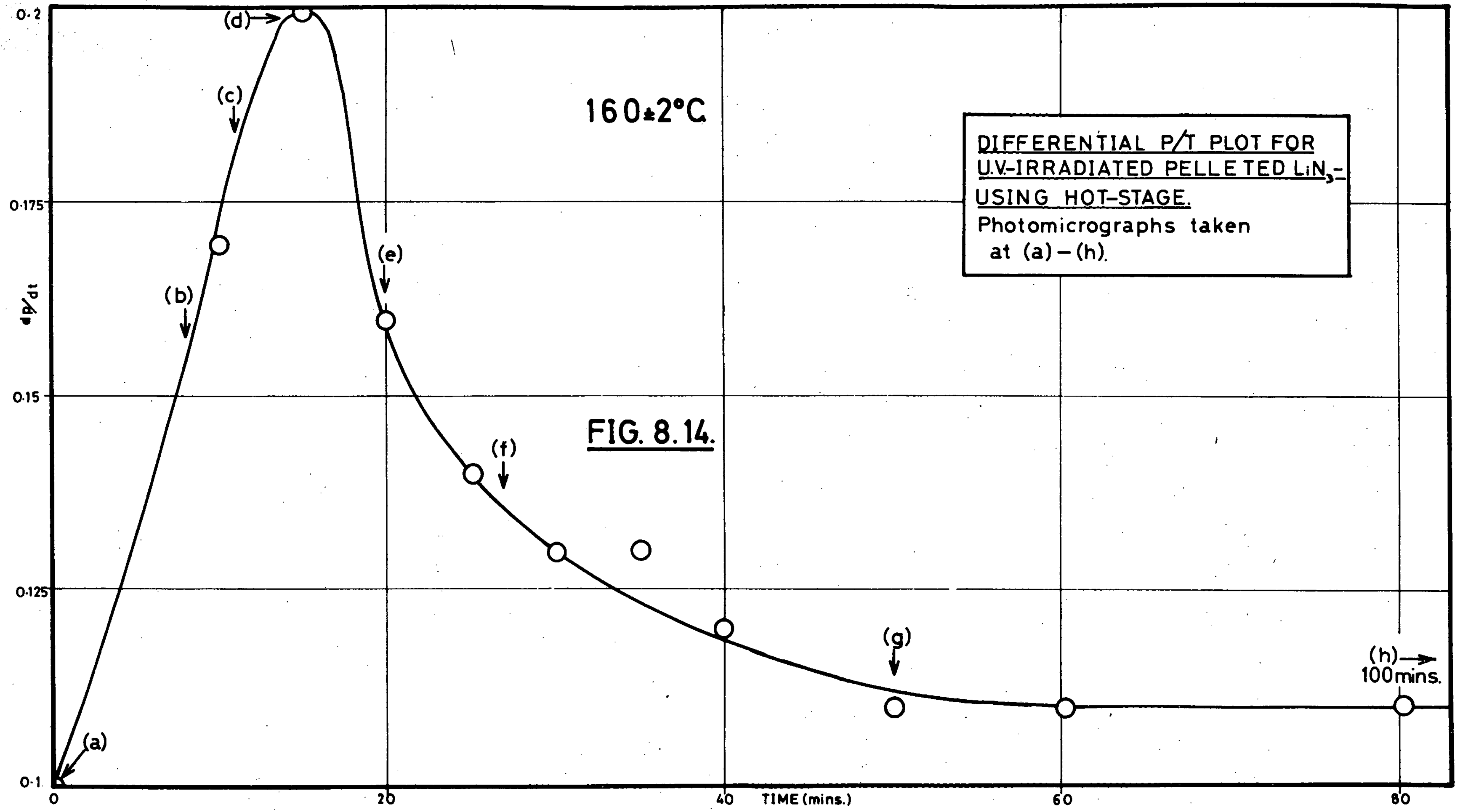

FIG. 8.14.

DIFFERENTIAL P/T PLOT FOR U.V.-IRRADIATED PELLETED LiN_3-USING HOT-STAGE.

Photomicrographs taken at (a) – (h).

9. SUPERIMPOSED IRRADIATIONS ON POWDERED LITHIUM AZIDE

Decompositions were performed on specimens irradiated prior to decomposition first with one type of irradiation and then superimposed with another type and vice versa. γ-, X- and U.V. radiations were used and three series were done, using combinations of these radiations.

In any particular series involving two irradiations, runs were done so that (a) the superimposed irradiation dose produced a maximum reaction rate greater than that found with the other radiation dose, when the irradiated azide samples were deocmposed and (b) vice versa, with the same particular two irradiations. Powdered lithium azide was used throughout the superimposed irradiations.

The methods used and the precautions taken when irradiating the lithium azide have been described previously in 4.2.3. Approximately 5.0 - 6.0mg samples were used. The p/t results for the decomposition runs appear in TABLE 9.1.

9.1 The effect of superimposing γ-radiation onto the salt, pre-irradiated with ultra-violet light

Blank runs were done at 175°C using lithium azide pre-irradiated with (a) a γ-ray dose of 15000 roentgens and (b) with U.V. radiation for 30 secs at a distance of 6.5cm beneath the tube. The γ-irradiated specimen had a greater reaction rate at the temperature used, than the U.V. irradiated specimen. Irradiating the U.V. irradiated specimen with 15000 roentgens γ-rays and decomposing this specimen at 175°C, showed that the rate of the reaction was the same as for the γ-irradiated specimen. The p/t plots for these runs are illustrated in FIGURE 9.1.

9.2 The effect of superimposing U.V.-radiation onto the salt, pre-irradiated with γ-rays

Blank runs were done at 155°C using lithium azide pre-irradiated with (a) 15000 roentgens γ-rays and (b) with U.V. radiation for 30 mins, at a distance of 6.5cm beneath the tube. The U.V. irradiated material had a greater rate than the γ-irradiated specimen, when decomposition at 155°C was studied. Irradiating the γ-irradiated specimen with U.V. radiation of the same dose as for the blank run and decomposign the salt at the above temperature it was observed that the superimposed p/t plot for this run resembled the plot for the U.V. - irradiated material, but reached the final pressure, p_f, before the U.V. p/t plot. These results are illustrated in FIGURE 9.2.

9.3 The effect of superimposing γ-radiation onto the salt, pre-irradiated with X-rays

Blank runs were done at 175°C using lithium azide pre-irradiated with (a) 15000 roentgens γ-rays and (b) 30 mins X-rays at 10 kV, 5 mA. The γ-irradiated specimen had a greater rate than the X-irradiated specimen. Superimposing 15000 roentgens γ-radiation onto the X-irradiated specimen resulted in a reaction having similar characteristics as the γ-irradiated run. The induction period of the superimposed run was slightly less than that for the γ-irradiated run. The reaction rates were about the same in these latter two decompositions. These results appear in FIGURE 9.3.

9.4 The effect of superimposing X-rays onto the salt, pre-irradiated with γ-radiation.

Blank runs were done at 155°C using lithium azide pre-irradiated with (a) X-rays for 60 mins at 10 kV, 5 mA and (b) 15000 roentgens γ-rays. The X-irradiated specimen had a greater reaction rate than the γ-irradiated specimen. Superimposing the above dose of X-rays onto the γ-irradiated specimen and decomposing the salt at 155°C, resulted in a pressure time plot showing the acceleratory period rate to be similar to that for the X-irradiated material, but the decay rate was enhanced. These results are graphically illustrated in FIGURE 9.4.

9.5 The effect of superimposing X-rays onto the salt, pre-irradiated with U.V. radiations

Blank runs were done at 165°C using material that was (a) irradiated with U.V. radiation for 30 secs at 6.5cm and material that was (b) irradiated for 30 mins at 20 kV and 10 mA. The X-irradiated specimen had a greater reaction rate than the U.V. irradiated specimen. Superimposing 30 mins X-rays and decomposing the salt at 165°C resulted in a p/t plot showing the acceleratory and decay periods rates to be greater that those for either the blank runs. The induction period of the superimposed irradiations thermal decomposition was shorter than that for the blank runs. These results are illustrated in FIGURE 9.5.

9.6 The effect of superimposing U.V. radiation onto the salt, pre-irradiated with X-rays

Blank runs were done at 160°C using material that was (a) irradiated with X-rays for 30 mins at 20 kV and 10 mA and material that was (b) irradiated with U.V. radiation for 30 mins at a distance of 6.5cm. The effect of superimposing 30 mins U.V. onto the X-irradiated salt resulted in a p/t plot with the same induction period as the U.V. irradiated specimen, and with an increased decay reaction, over the two blank runs. These results are illustrated in FIGURE 9.6.

9.7 DISCUSSION

Superimposing a particular radiation on material irradiated with another type of radiation and then comparing the p/t plots of the thermal decomposition of the three irradiated azide specimens, was observed to lend further support to the theories proposed concerning the nucleation and growth mechanisms occurring during the thermal decomposition of pre-irradiated lithium azide.

The effect of superimposing γ-radiation on ultra-violet pre-irradiated lithium azide (FIGURE 9.1) was seen to be the enhancement of all stages of the U.V. decomposition, the p/t plot for the reaction being indistinguishable from the p/t plot of the γ-irradiated blank run. This result indicates that the U.V. contribution is completely overridden by the γ-dose used which initiates reaction along internal grain boundaries and dislocation edges as well as on the surfaces of the crystal. The U.V. effect on the other hand is confined to the external surfaces of the particles only. It is seen (FIGURE 9.2) that irradiating γ-irradiated material with U.V. light exhibited the effect that could be expected if the U.V. effect was added to the γ-ray effect. In this case the surfaces of the particles would be further nucleated, enhancing the reaction rate as observed. However, although the U.V. dose employed was large and the decay reaction was observed to commence at a low value of α, no significant change in the decay period rate as compared to that of the γ-irradiated azide, is seen. This is to be expected, as reaction over this region proceeds via the contracting sphere mechanism on isolated "blocks" or "islands" of unirradiated material. The Ultra-violet light could not in any way decrease the size of these "blocks" and so enhance the decay rate.

Superimposing γ-irradiation onto X-irradiated lithium azide (FIGURE 9.3) and vice versa (FIGURE 9.4) can be expected to yield analagous results to the above, as it has been proposed that similar effects resulted on pre-irradiating lithium azide with X-rays and ultra-violet radiation. Similar effects as found above for γ-rays and ultra-violet radiation were recorded, supporting the porposal that X-rays and U.V. have similar effects on lithium azide.

Provided that a "saturation" effect on pre-irradiating lithium azide with X-rays or ultra-violet light was not achieved then superimposing either of these types of irradiation on material pre-irradiated with the other type, should result in the addition of these effects and a p/t plot representing addition of the p/t plots of the runs using the singly irradiated material. FIGURES 9.5 and 9.6 show that this was found to occur. No significant change in the decay reaction rate indicated that both types of irradiation resulted in nuclear formation and growth over the same topochemical regions of the particles i.e. the surfaces of the particles.

A significant feature of the six series of superimposed irradiation effects is that the length of the induction period of the p/t plot for the superimposed radiations was always approximately the same as that of the p/t plot having the shortest induction period. This indicated that the irradiation damage is not bleached or annealed out be exposure to radiation of another type. Generally (except in the case of γ-rays on X- or U.V.-irradiated azide), an increase in the number of nuclei results and the additive result gives rise to an enhanced acceleratory region rate.

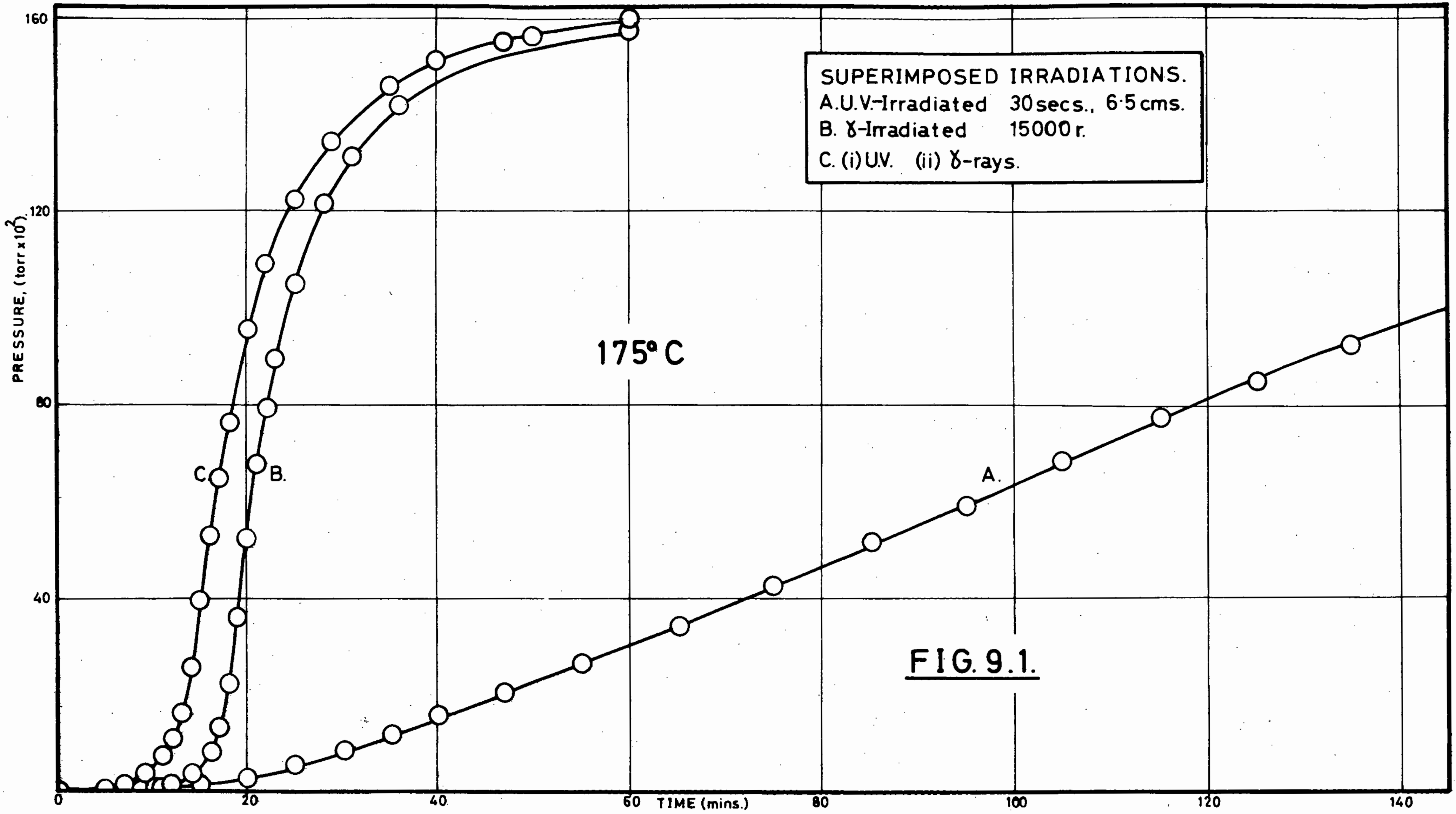
SUPERIMPOSED IRRADIATIONS.
A. U.V.-Irradiated 30 secs., 6·5 cms.
B. γ-Irradiated 15000 r.
C. (i) U.V. (ii) γ-rays.
175° C
C
B.
A.
PRESSURE, (torr x 10^2).
160
120
80
40
0
20
40
60
80
100
120
140
TIME (mins.)

FIG. 9.1.

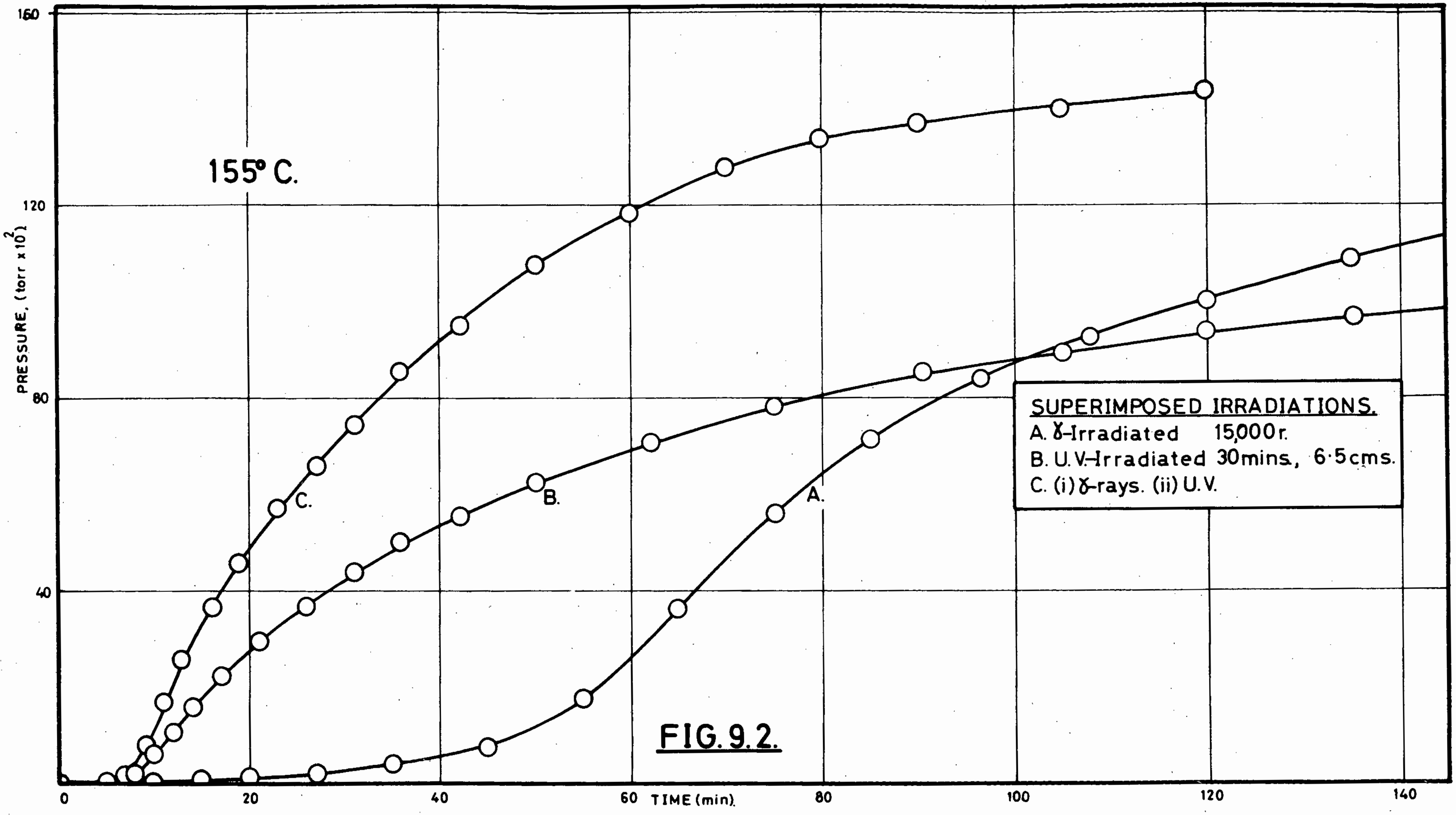
155° C.
160
120
80
40
PRESSURE, (torr x 10^2)
0
20
40
60
TIME (min).
80
100
120
140
C.
B.
A.
SUPERIMPOSED IRRADIATIONS.
A. γ-Irradiated 15,000 r.
B. U.V.-Irradiated 30 mins, 6·5 cms.
C. (i) γ-rays. (ii) U.V.

FIG. 9.2.

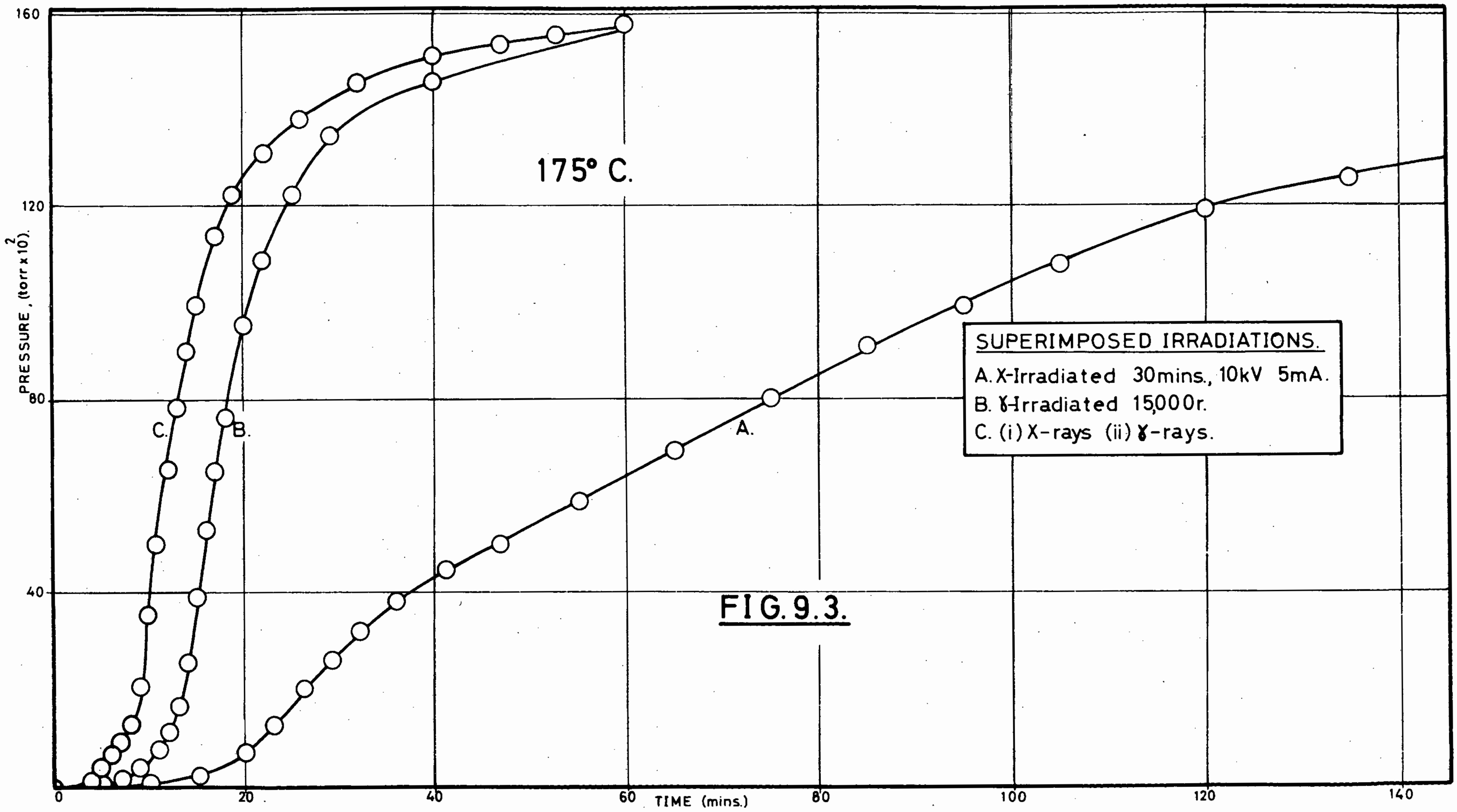
160
120
80
40
PRESSURE, (torr x 10^2).
0
20
40
60
TIME (mins.)
80
100
120
140
175° C.
C.
B.
A.
SUPERIMPOSED IRRADIATIONS.
A. X-Irradiated 30mins., 10kV 5mA.
B. γ-Irradiated 15,000r.
C. (i) X-rays (ii) γ-rays.

FIG. 9.3.

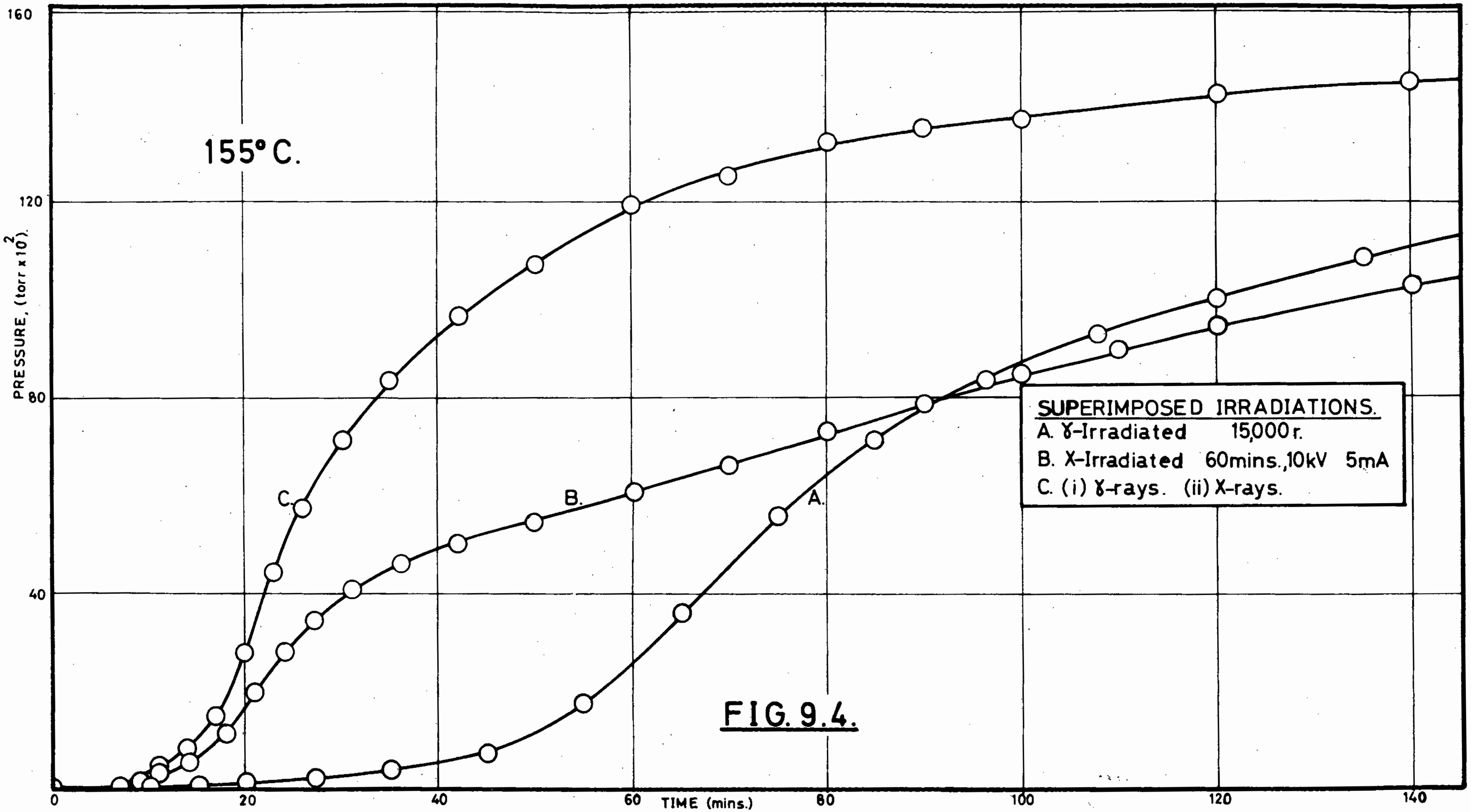
155° C.
PRESSURE, (torr x 10^2).
TIME (mins.)
160
120
80
40
0
20
40
60
80
100
120
140
C.
B.
A.
SUPERIMPOSED IRRADIATIONS.
A. γ-Irradiated 15,000 r.
B. X-Irradiated 60mins.,10kV 5mA
C. (i) γ-rays. (ii) X-rays.

FIG. 9.4.

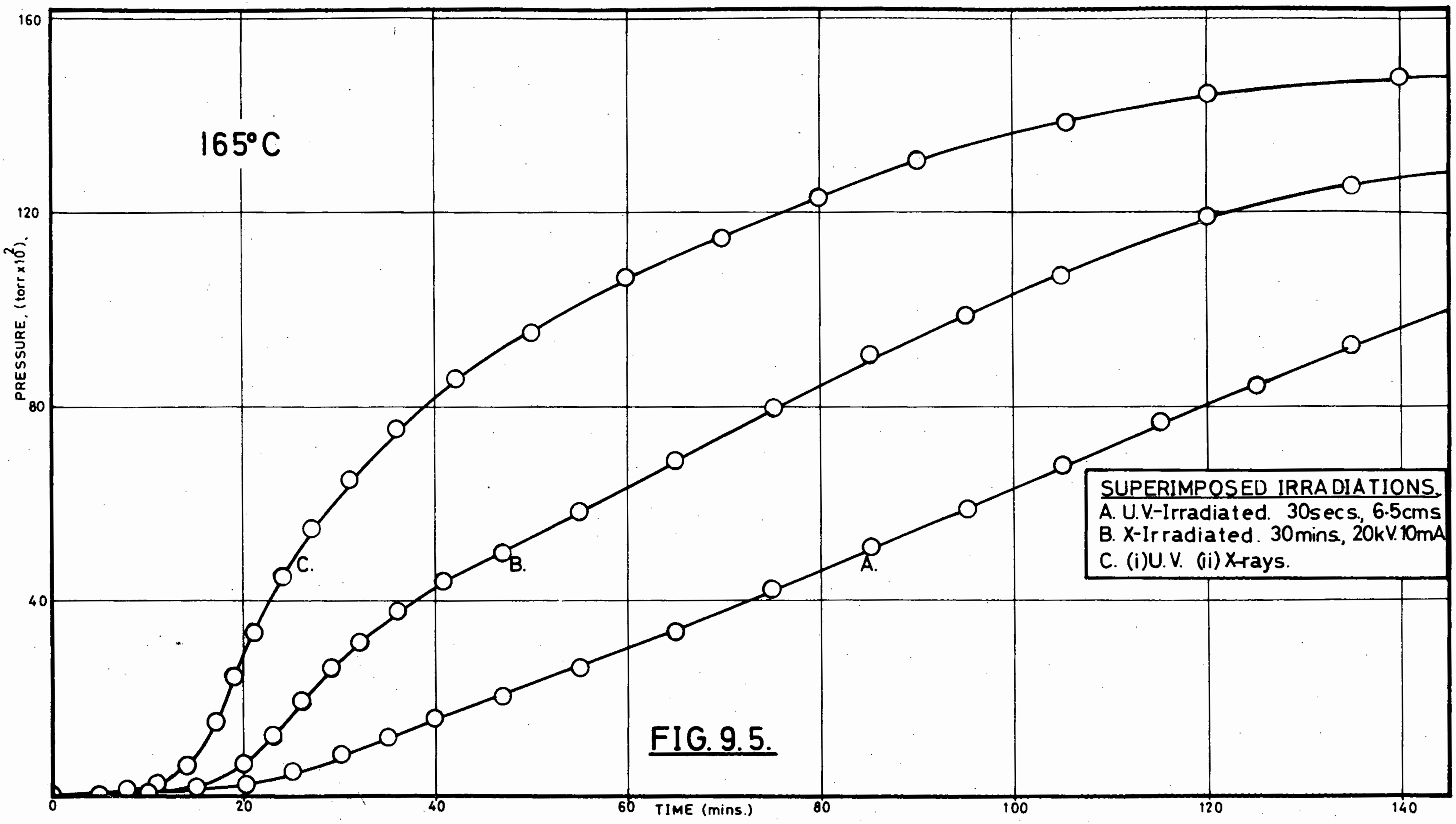
165°C
PRESSURE, (torr x10^2).
TIME (mins.)
0
20
40
60
80
100
120
140
160
A.
B.
C.
SUPERIMPOSED IRRADIATIONS.
A. U.V.-Irradiated. 30secs., 6·5cms
B. X-Irradiated. 30mins., 20kV.10mA
C. (i)U.V. (ii) X-rays.

FIG. 9.5.

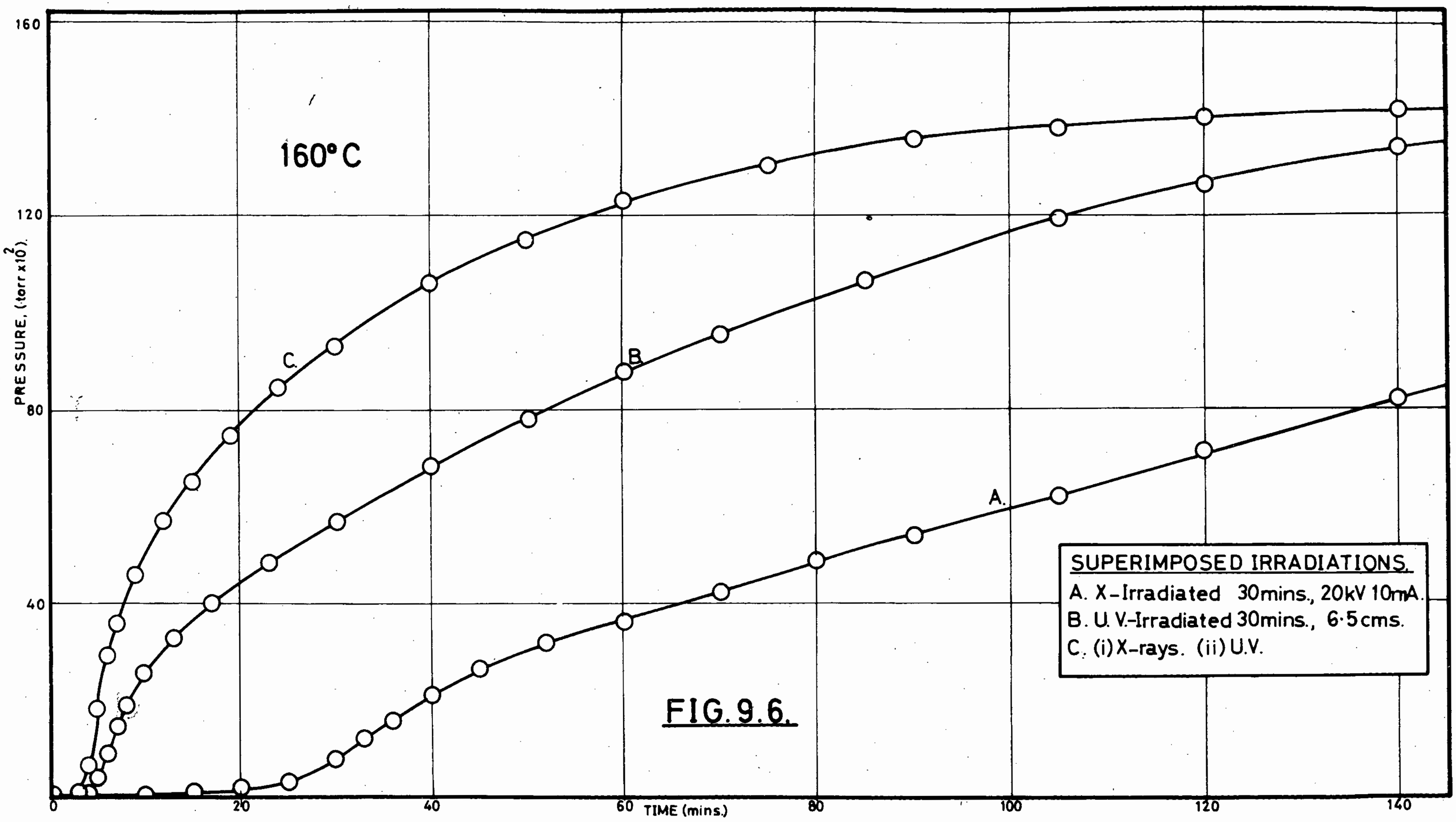
160° C
PRESSURE, (torr x 10^2).
160
120
80
40
0
20
40
60
80
100
120
140
TIME (mins.)
A.
B.
C.
SUPERIMPOSED IRRADIATIONS.
A. X-Irradiated 30mins., 20kV 10mA.
B. U.V.-Irradiated 30mins., 6·5cms.
C. (i) X-rays. (ii) U.V.

FIG. 9.6.

10. GENERAL DISCUSSION OF THE DECOMPOSITION OF THE ALKALI AND ALKALINE EARTH AZIDES

The thermal decomposition of powdered (polycrystalline) lithium azide yielded a sigmoid p/t plot over the temperature range studied (165°-205°C). This result is markedly different from the p/t plots obtained for the thermal decomposition of potassium(21,206) and sodium azides(206-208), but is similar to the p/t plots obtained for the thermal decomposition of the alkaline earth (Ca, Sr and Ba) metal azides(3,20,68,108,109,121,137,138). For sodium and potassium azides an initial reaction was observed which was identified as a unimolecular decomposition in the case of potassium azide(21). Although this reaction is not pronounced for sodium azide (for some preparations used it was not observed(84)), it was found(208) that it is enhanced if small single crystals are decomposed. This initial reaction has been shown to be related to the volatility of the metal nuclei at the reaction temperature.

Difficulties were experienced with reproducibility with lithium azide and as explained earlier, (5.4), it was necessary to pellet the material and then grind the pellets to obtain powdered lithium azide. Difficulties have also been experienced with reproducibility of the thermal decomposition of the other alkali and alkaline earth metal azides(17,84,206). It was found(84) that pelleting had the effect of decreasing the irreproducibility, which was attributed to the volatility of the metal.

Analysis of the p/t plots obtained for the thermal decomposition of lithium azide was carried out using the Avrami-Erofeyev ($n = 3$) and contracting sphere equations over the acceleratory and decay periods respectively. Previous workers(3,131) have made use of the Avrami-Erofeyev equation for the kinetic analysis of the acceleratory period for the decomposition of barium azide(3) reporting three-dimensional nuclear growth, with the number of nuclei increasing linearly with time. Jacobs and Kureishy(84) have reported growth of two-dimensional nuclei in the thermal decomposition of sodium azide. The Avrami-Erofeyev equation with n = 2 was used. Three-dimensional nuclei have also been postulated for barium azide(14) and calcium azide(20,47) using the less sophisticated power law. It has also been reported that the analysis of the acceleratory region for the thermal decomposition of calcium(137) and strontium azides(139) indicates two-dimensional growth, with the nuclei increasing in number linearly with time. The power law was also employed for these latter analyses. From these results it is seen that lithium azide is similar to the alkali and alkaline earth azides in that discrete nuclei are formed and these increase in number with time. Use of the more refined Avrami-Erofeyev equation indicates that overlap and ingestion of the nuclei play a significant role, whereas this was not observed for calcium or strontium azides.

The nuclei are considered to form on the external surface of the decomposing unirradiated lithium azide particle, as has been reported to be the case for the decomposition of calcium(137), strontium(138,139) and barium azide(3). Secco(17), however, reports decomposition in plate-like crystals of sodium azide as commencing along intermosaic grain boundaries. Early work(206) on the decomposition of potassium azide indicated that similar intermosaic reaction occurs in the azide, while later work(21) does not present a clear picture of the topochemical reaction, other than stressing the role played by the evaporation of surface nuclei. In this respect then (the topochemistry of nuclear formation) lithium azide resembles the alkaline earth azides, when nuclei are formed on the surface during decomposition and new nuclei are formed increasing in number linearly with time. These nuclei then grow two-dimensionally and overlap, after which point in the reaction the interface contracts radially inwards on blocks of unreacted material. The reaction, like those for the inorganic azides mentioned above, is autocatalytic and occurs at the product/reactant interface. This picture of the decomposition mechanism is consistent with the results obtained.

The activation energies reported in the literature for the thermal decomposition of the alkali and alkaline earth azides vary over the wide range 25 - 73 k.cals/mole. Values of 36 - 49 k.cals/mole have been reported for potassium azide(21,206), and 34 - 73 k.cals/mole for the decomposition of sodium azide(17,84,206,207). The larger values in the case of sodium azide were derived from dielectric constant investigations, while using the Avrami-Erofeyev equation a value of 38 has been reported. The activation energy found for the acceleratory process during the decomposition of lithium azide (28-29 k.cals/mole), however, appears to be of similar magnitude to those for barium (29(108), 27(3) k.cals/mole), strontium (25(139) k.cals/mole) and calcium azides (18-34(20,137,209) k.cals/mole).

Although the effects of pre-irradiation on the subsequent thermal decomposition of sodium azide have not been examined, it was reported(21) that pre-irradiation of potassium azide with U.V.-radiation had no effect on the subsequent decomposition. Considerable attention has been given, however, to the photochemical decomposition of these azides. F-centres are thought to be formed on irradiating potassium azide(21) and exciton peaks have been observed for both sodium and potassium azides(37), which have been supported by photoemission current experiments(88). The excitons are considered to react with anion vacancies, forming F-centres. F-centres(68,109) and vacancies(108) have been reported to result on pre-irradiating barium azide while vacancies are thought to result in strontium(68) and calcium azides(20,68).

The general characteristics observed as a consequence of pre-irradiating the above azides were a shortening of the length of the induction period in most cases and an increase in the rate of the reaction, when the material was decomposed isothermally. Similar changes have been observed for the thermal decomposition of U.V.-irradiated lithium azide and nuclear formation and growth is considered to be on the surface of the decomposing particles. It is thought that large numbers of F-centres are formed on irradiation, which then aggregate by thermal diffusion at room temperature. During the early stages of heating, these complex centres collapse with the eventual formation of lithium metal nuclei on the particle surface. This picture is consistent with the experimental results obtained.

Similar effects were found when lithium azide was pre-irradiated with X-rays and similar mechanisms have been proposed for the decomposition. The topochemical nature of the decomposition is also thought to be the same as that for the U.V-irradiated salt. It is not unexpected that these strong similarities in the effects exist. It has been reported that similar effects have been noticed when barium azide was pre-irradiated with X-rays and U.V-radiation(131). X-irradiation of barium azide at the threshold decomposition temperature(132) was found to have a greater effect on the thermal decomposition, than irradiation at room temperature. It was suggested that nuclei were aggregates of atoms or F-centres. When sodium azide was irradiated with X-rays at room temperature trapped electrons were identified(142) but no investigation of the thermal decomposition of the irradiated salt was done. Thus it appears that lithium azide resembles barium and sodium azides with regards the proposed radiation damage, (i.e. trapped electrons or F-centres). The reaction on heating lithium azide is indicated to be confined to the surface however, while damage is though to occur at both internal and external surfaces of the barium azide particles.

Such damage at the external surface and within the particles, was found to occur when lithium azide was pre-irradiated with γ-rays. F-centre aggregates are considered to result over the surface of the particle and along internal grain boundaries and dislocation lines. Similar damage and F-centre aggregation has been proposed for γ-irradiated barium azide(3), while for strontium(139) and calcium azides(48) it is considered that large numbers of vacancies are generated which in turn aggregate at the external and internal surfaces (i.e. along grain boundaries).

A characteristic of the p/t plots for the decomposition of γ-irradiated lithium azide is that the decay rate constant was considerably increased when compared to that of the unirradiated lithium azide. This feature of the decay rate constant was only observed on pre-irradiation with γ-rays and the topochemical picture presented is the only one consistent with the experimental results.

It was also seen that on X- and γ-irradiation, the subsequent decomposition rate constant was increased and the induction period shortened, as found when pre-irradiating the azide with U.V.

Although no work has been published on the effects of X- and γ-irradiation on the decomposition of sodium and potassium azides and comparing the results of the decomposition of unirradiated and U.V-irradiated sodium and potassium azides, it appears that lithium azide resembles the alkaline earth azides with regards the thermal decomposition of the unirradiated and irradiated (U.V., X- and γ-rays) azide.

11. BIBLIOGRAPHY

(1) Thomas and Renshaw: J. Chem. Soc., 2058 (1967).

(2) Bartlett, Tompkins and Young: Proc. Roy. Soc., A246, 206 (1958).

(3) Prout and Moore: A.S.T.M., Spec. Tech. Pub. No. 400, p.45 (1966).

(4) Tompkins and Young: Proc. Roy. Soc., A236, 10 (1956).

(5) Bowden and MacAuslan: Nature, 178, 408 (1956).

(6) Singh: Trans. Fara. Soc., 52, 1623 (1956).

(7) Bartlett, Tompkins and Young: J. Chem. Soc., 3323 (1956).

(8) Boldyrev: Kinet. i Katal., 1, 203 (1960).

(9) Boldyrev: ibid , 6, 934 (1965)

(10) Boldyrev: ibid , 8, 1179 (1967).

(11) Hill: Proc. Roy. Soc., A291, 208 (1966).

(12) Boldyrev, Kabanov, Trubitsyn, Oblivantsev, Uskov and Chelyshev: Zh. Fiz. Khim., 41, 1783 (1967).

(13) Yoffe: Developments in Inorganic Nitrogen Chemistry, Ed. Colburn, p.125 (Elsevier Pub. Co. 1966).

(14) Wischin: Proc. Roy. Soc., A172, 314 (1939).

(15) Torkar and Spath: Mh. Chem., 98, 1712 (1967).

(16) Secco: Canad. J. Chem., 40, 2191 (1961).

(17) Secco: J. Phys. Chem. Solids, 24, 469 (1963).

(18) Bowden and Yoffe: Fast Reactions in Solids, p.6 (Butterworths 1958).

(19) Hume and Colvin: Proc. Roy. Soc., A125, 635 (1929).

(20) Tompkins and Young: Trans. Fara. Soc., 61, 1470 (1965).

(21) Jacobs and Tompkins: Proc. Roy. Soc., A215, 265 (1952).

(22) Garner and Tanner: J. Chem. Soc., 47 (1930).

(23) Hill, Richardson and Rodger: Proc. Roy. Soc., A201, 208 (1966).

(24) Freeman, Anderson and Campisi: J. Phys. Chem., 64, 1727 (1960).

(25) Komarov, Boldyrev, Zhuravlev and Ivanov: Kinet. i Katal., 7, 788 (1966).

(26) Herley and Prout: Nature, 184, 445 (1959).

(27) Erofeyev and Protashchik: Dokl. Akad. Nauk SSSR, 172, 1129 (1967).

(28) Sviridov: Uchenye Zapiski Beloruss. Gosudarst Univ. im V.I. Lenina, Ser. Khim (1958) No. 42, p.233.

(29) Garner and Maggs: Proc. Roy. Soc., A172, 299 (1939).

(30) Groocock and Tompkins: ibid, A223, 267 (1954).

(31) Jach and Griffel: J. Phys. Chem., 68, 737 (1964).

(32) Flanagan: ibid, 66, 416 (1962).

(33) Torkar and Spath: Mh. Chem., 98, 1696 (1967).

(34) Wise: J. Phys. Chem., 71, 2843 (1967).

(35) Torkar and Herzog: Mh. Chem., 97, 765 (1966).

(36) Pringle and Noakes: Acta Cryst., B24, 262 (1968).

(37) Deb: J. Chem. Phys., 35, 2122 (1961).

(38) Torkar and Spath: Mh. Chem., 98, 2020 (1967).

(39) Bright and Garner: J. Chem. Soc., 1872 (1934)

(40) Bagdassarian: Acta Phys. Chim. U.R.S.S., 20, 441 (1945).

(41) Allnatt and Jacobs: Canad. J. Chem., 46, 111 (1968).

(42) Anous, Bradley and Colvin: J. Chem. Soc., 3348 (1951).

(43) Anous: Rec. Trav. Chim., 77, 822 (1958).

(44) Cooper and Garner: Proc. Roy. Soc., A174, 487 (1940).

(45) Young: Decomposition of Solids, (Pergamon Press 1966) p.14.

(46) Jacobs and Tompkins: Chemistry of the Solid State, Ed. Garner (Butterworths 1955) p.191.

(47) Tompkins and Young: Disc. Fara. Soc., 23, 202 (1957).

(48) Prout and Brown: Unpublished work. (Brown, Ph.D. thesis, Rhodes University 1965).

(49) Leiga: J. Phys. Chem., 70, 3254, 3260 (1966).

(50) Garner and Hailes: Proc. Roy. Soc., A139, 576 (1933).

(51) Hailes: Trans. Fara. Soc., 29, 544 (1933).

(52) Finch, Jacobs and Tompkins: J. Chem. Soc., 2053 (1954).

(53) Prout and Tompkins: Trans. Fara. Soc., 40, 488 (1944).

(54) Herley and Prout: J. Phys. Chem., 66, 961 (1962).

(55) Prout and Tompkins: Trans. Fara. Soc., 42, 482 (1946).

(56) Hill: ibid, 54, 685 (1958).

(57) Avrami: J. Chem. Phys., 7, 1103 (1939); 8, 212 (1940); 9, 177 (1941).

(58) Mampel: Z. Phys. Chem., A187, 43, 235 (1940).

(59) Erofeyev: Acad. Sci. U.R.S.S., 52, 511 (1946).

(60) Boldyrev, Eroshkin and Zakharov: Nauk Dokl. Vysshikh. Shkolei, 3 (1959).

(61) Boldyrev, Zakharov, Eroshkin and Sokolova: Dokl. Akad. Nauk, 129, 365 (1959).

(62) Protashchik and Erofeyev: Dokl. Akad. Nauk Beloruss. S.S.R., 10, 658 (1966).

(63) Ishkin and Dubil: Zh. Prikl. Khim., 41, 52 (1968).

(64) Galwey and Jacobs: Proc. Roy. Soc., A254, 455 (1960).

(65) Acheson and Galwey: J. Chem. Soc., 1174 (1967).

(66) Davies, Jacobs and Russell-Jones: Trans. Fara. Soc., 63, 1737 (1967).

(67) Herley and Levy: Nature, 211, 1287 (1966).

(68) Prout and Moore: Unpublished results (Moore, Ph.D. thesis, Rhodes University 1966).

(69) Razumov, Brounshtein and Kane: Tr. Gos. Inst. Prikl. Khim., No. 49, 170 (1962).

(70) Sakovich: Tr. Tomskogo Gos. Univ., Ser. Khim., 157, 37, 45 (1963).

(71) Mott and Gurney: Electronic Processes in Ionic Crystals, (Clarendon Press 1950).

(72) Eggert: Proc. Roy. Soc., A246, 216 (1958).

(73) Boldyrev and Medvinskii: Kinet. i Katal., 6, 550 (1965).

(74) Mott: Proc. Roy. Soc., A172, 325 (1939).

(75) Mott and Gurney: ibid, A164, 151 (1938).

(76) Thomas and Tompkins: ibid, A209, 550 (1951).

(77) Baidins: Disc. Fara. Soc., 28, 248 (1959).

(78) Jacobs, Tompkins and Young: ibid, 28, 234 (1959).

(79) Jacobs, Tompkins and Verneker: J. Phys. Chem., 66, 1113 (1962).

(80) Deb: Trans. Fara. Soc., 59, 1423 (1963).

(81) Verneker: J. Phys. Chem., 72, 1733 (1968).

(82) Jacobs and Tompkins: Proc. Roy. Soc., A215, 254 (1952).

(83) Jacobs, Sheppard and Tompkins: 5th Intern. Sym. Reac. Solids, Munich (1964), p.RS-45.

(84) Jacobs and Kureishy: J. Chem. Soc., 911, 4718, 4723 (1964).

(85) Verneker and Forsyth: J. Phys. Chem., 71, 3736 (1967).

(86) Jacobs and Kureishy: Canad. J. Chem., 44, 703 (1966).

(87) Dodd: J. Chem. Phys., 35, 1815 (1961).

(88) Deb: Trans. Fara. Soc., 59, 1414 (1963).

(89) Cunningham and Tompkins: Proc. Roy. Soc., A251, 27 (1959).

(90) Heal and Pringle: J. Phys. Chem. Solids, 15, 261 (1960).

(91) Papazian: ibid, 21, 81 (1961).

(92) Miller: J. Chem. Phys., 33, 889 (1960).

(93) Carlson, King and Miller: ibid, 33, 1266 (1960).

(94) King, Carlson, Miller and McMillan: ibid, 34, 1499 (1961).

(95) King, Miller, Carlson and McMillan: ibid, 35, 1442 (1961).

(96) Shuskus, Young, Giliam and Levy: ibid, 33, 622 (1960).

(97) Horst, Anderson and Milligan: J. Phys. Chem. Solids, 23, 157 (1962).

(98) Mees and James: The Theory of the Photographic Process, (The Macmillan Co., 1966).

(99) Mitchell: J. Phot. Sci., 5, 49 (1957).

(100) Dawood, Forty and Tubbs: Proc. Roy. Soc., 284, 272 (1965).

(101) Kaldor and Somorjai: J. Phys. Chem., 70, 3538 (1966).

(102) Tubbs: Proc. Roy. Soc., A280, 566 (1964).

(103) Maycock, Verneker and Witten: J. Phys. Chem., 71, 2107 (1967).

(104) Verneker and Maycock: ibid, 72, 2798 (1968).

(105) Herley and Levy: J. Chem. Phys., 46, 627 (1967).

(106) Levy and Herley: Intern. Symp. on Kinetics of Reactions in Ionic Systems, Ed. Alfred (Plenum Press).

(107) Levy and Herley: Presented at 6th Intern. Symp. on Reactivity of Solids.

(108) Thomas and Tompkins: Proc. Roy. Soc., A210, 111 (1951).

(109) Garner and Reeves: Trans. Fara. Soc., 51, 694 (1955).

(110) Herley and Prout: J. Am. Chem. Soc., 82, 1540 (1960).

(111) Boldyrev, Pinaevskaya, Boldyreva, Zakharov and Konyshev: Kinet. i Katal., 2, 184 (1961).

(112) Prout and Tompkins: Trans. Fara. Soc., 43, 148 (1947).

(113) Prout and Moore: A.S.T.M., Spec. Tech. Publ. No. 400, p.1, (1966).

(114) Benton and Cunningham: J. Am. Chem. Soc., 57, 2227 (1935).

(115) Tompkins: Trans. Fara. Soc., 44, 206 (1948).

(116) Macdonald: J. Chem. Soc., 832, 839 (1936).

(117) Bartlett: Thesis, (London 1956).

(118) Haynes and Young: Disc. Fara. Soc., 31, 229 (1961).

(119) Garner and Moon: J. Chem. Soc., 1398 (1933).

(120) Muraour: Chim. et Ind., 30, 39 (1933).

(121) Maggs: Trans. Fara. Soc., 35, 433 (1939).

(122) Bowden and Singh: Proc. Roy. Soc., A227, 22 (1954).

(123) Groocock: ibid, A246, 225 (1958).

(124) Jach: Trans. Fara. Soc., 59, 947 (1963).

(125) Jach: Nature, 196, 827 (1962).

(126) Todd and Parry: ibid, 186, 544 (1960).

(127) Hall and Walton: J. Inorg. and Nuc. Chem., 6, 288 (1958).

(128) Cunningham: J. Phys. Chem., 65, 628 (1961).

(129) Johnson: J. Am. Chem. Soc., 80, 4460 (1958).

(130) Cunningham and Heal: Trans. Fara. Soc., 54, 1355 (1958).

(131) Erofeyev and Sviridov: Inst. Khim., Sbornik Nauch. Rabot, Akad. Nauk Beloruss. S.S.R., 5, 113 (1956).

(132) Boldyrev and Skorik: Fiz. Shchel. Kristallov, Latv. Gos. Univ., Tr. 2 - go Vses., Riga p.527 (1961).

(133) Prout and Moore: Nature, 203, 860 (1964).

(134) Osinovik: Kand. dissertatsia, Minsk (1955).

(135) Boldyrev and Skorik: Dokl. Akad. Nauk S.S.S.R., 156, 1143 (1964).

(136) Skorik, Boldyrev and Komarov: Kinet. i Katal., 8, 1258 (1967).

(137) Prout and Brown: Nature, 205, 1314 (1965).

(138) Prout and Moore: ibid, 205, 1209 (1965).

(139) Prout and Moore: Unpublished results, in the Press.

(140) Sviridov: Dokl. Akad. Nauk Beloruss. S.S.R., 2, 291 (1958).

(141) Rosenwasser, Dreyfus and Levy: J. Chem. Phys., 24, 184 (1956).

(142) Heal: Trans. Fara. Soc., 53, 210 (1957).

(143) Gelerinter and Silsbee: J. Chem. Phys., 45, 1703 (1966).

(144) Keating and Krasner: J. Phys. Chem. Solids, 20, 150 (1961).

(145) Prout: J. Inorg. and Nucl. Chem., 7, 368 (1958).

(146) Prout and Sole: ibid, 9, 232 (1959).

(147) Herley and Prout: J. Phys. Chem., 65, 208 (1961).

(148) Herley and Prout: J. Inorg. and Nucl. Chem., 16, 16 (1960).

(149) Varley: Nature, 174, 886 (1954).

(150) Varley: J. Nucl. Energy, 1, 130 (1954).

(151) Varley: Progress in Nuclear Energy, (Pergamon Press, 1958).

(152) Boldyrev: Proc. of the 2nd All-Union Conf. on Radiation Chem., Moscow, 1962. p.p. 42-47.

(153) Boldyrev and Oblivantsev: Kinet. i Katal., 3, 887 (1962).

(154) Boldyrev and Bystrykh: Russ. Chem. Rev., 32, 426 (1963).

(155) Boldyrev: Zhur. Fiz. Khim., 35, 950 (1961).

(156) Huang: Proc. Roy. Soc., A190, 102 (1947).

(157) Senio and Tucker: Phys. Rev., 99, 1777 (1955).

(158) Prout and Woods: A.S.T.M., Spec. Tech. Publ. No. 359, p.50 (1963).

(159) Prout and Brown: Nature, 203, 398 (1965).

(160) Konazaki: J. Phys. Chem. Solids, 2, 107 (1957).

(161) Azaroff: Crystallography and Crystal Perfection, (Acad. Press, London 1963).

(162) Prout: (Unpublished), Lecture at Picatinny Arsenal, 1965.

(163) Young: J. Chem. Soc., 4533 (1960).

(164) Bircumshaw and Harris: ibid, 1898 (1948).

(165) Prout and Brown: A.S.T.M., Spec. Tech. Publ. No. 359, p.38 (1964).

(166) Daneš and Ponec: Coll. Czech. Chem. Comm., 23, 858 (1958).

(167) Zirkind and Freeman: Nature, 199, 1280 (1963).

(168) Freeman and Anderson: A.S.T.M., Spec. Tech. Publ. No. 359, p.58 (1963).

(169) Cole: J. Chem. Phys., 35, 1169 (1961).

(170) Boyarchuk, Buben, Dubovitskii and Manelis: Kinet. i Katal., 5, 823 (1964).

(171) Schneller and Flanagan: Nature, 215, 729 (1967).

(172) Boldyrev and Eroshkin: Zhur. Vses. Khim. Ob-va im. Mendeleeva, 9, 704 (1964).

(173) Herley and Prout: J. Chem. Ed., 37, 643 (1960).

(174) Marais, Potgieter, Hawkins and Hanekom: S. Afr. J. Agric. Sci., 7, 837 (1964).

(175) Gray and Waddington: Proc. Roy. Soc., A235, 106 (1956).

(176) Torkar and Spath: Mh. Chem., 99, 118 (1967).

(177) Dreyfus and Levy: Proc. Roy. Soc., A246, 233 (1958).

(178) Nuegebauer: The Structure and Properties of Thin Films, p.p. 39, 53, 244 (Wiley 1959).

(179) Reitzner: J. Phys. Chem., 65, 948 (1961).

(180) Young: J. Chem. Soc., 3141 (1964).

(181) Simpson, Taylor and Anderson: ibid, 2378 (1958).

(182) Verneker and Maycock: J. Inorg. and Nucl. Chem., 29, 2723 (1967).

(183) Mott: Proc. Phys. Soc., B64, 729 (1951).

(184) Seitz: Advanc. Phys., 1, 43 (1952).

(185) Koehler: Phys. Rev., 60, 397 (1941).

(186) Dexter: ibid, 86, 770 (1952).

(187) Mampel: Z. Phys. Chem., A187, 43, 255 (1940).

(188) Lambert and Guinier: Compt. Rend., 246, 1678 (1958).

(189) Gregg and Razouk: J. Chem. Soc., S36 (1949).

(190) Bircumshaw and Newman: Proc. Roy. Soc., A227, 228 (1955).

(191) Galavanov: Soviet Physics, Solid State, 1, 390 (1959).

(192) Dienes and Vineyard: Radiation Effects in Solids, p.48 (Interscience 1957).

(193) Cleland, Crawford and Holmes: Phys. Rev., 102, 722 (1956).

(194) Seitz: Rev. Mod. Phys., 18, 384 (1946); 26, 7 (1954); 23, 328 (1951).

(195) Mitchell, Wiegand and Smoluchowski: Phys. Rev., 117, 442 (1960).

(196) Crawford: Bull. Amer. Ceram. Soc., 44, 963 (1965).

(197) Prout and Herley: J. Phys. Chem., 66, 961 (1962).

(198) Sawkill: Proc. Roy. Soc., A229, 135 (1955).

(199) Hedges and Mitchell: Phil. Mag., 44, 223, 357 (1953).

(200) Evans and Mitchell: Rep. on Bristol Conf. on Defects in Crystal Solids, Phys. Soc., London (1955).

(201) Mitchell: Chemistry of the Solid State, Ed. Garner, Chap. 13 (Butterworths 1955).

(202) Amelinckx, Van der Worst, Gevers and Dekeyser: Phil. Mag., 46, 450 (1955).

(203) Seitz: Disc. Fara. Soc., 5, 271 (1949).

(204) Seitz: Solid State Physics, 2, 307 (1956).

(205) Heal: Canad. J. Chem., 31, 1153 (1953).

(206) Garner and Marke: J. Chem. Soc., 657 (1936).

(207) Ellis and Hall: Trans. Fara. Soc., 64, 1034 (1968).

(208) Walker, Gane and Bowden: Proc. Roy. Soc., 294, 417 (1966).

(209) Marke: Trans. Fara. Soc., 33, 770 (1937).

APPENDIX

TABLE 5.1

210°C		Run 1			3.5mg
t	p	t	p	t	p
5	0.04	45	77.61	85	175.51
10	0.67	50	96.57	95	181.79
20	1.44	55	116.42	105	184.11
25	7.81	60	133.47	120	186.23
30	20.22	65	146.63	140	188.06
35	38.24	70	157.03	p_a	190.01
40	58.46	75	165.17		

210°C		Run 2			5.5mg
t	p	t	p	t	p
3	0.07	20	4.42	29	135.66
6	0.11	22	6.71	30	160.67
9	0.20	24	10.19	31	177.63
12	0.41	25	13.69	32	188.56
14	0.74	26	20.32	33	195.16
16	1.47	27	48.62	40	208.66
18	2.63	28	102.11	p_a	211.21

210°C		Run 3			3.9mg
t	p	t	p	t	p
5	0.07	40	6.25	75	21.74
10	0.09	45	9.47	80	22.82
15	0.14	50	12.33	90	24.94
20	0.20	55	15.14	100	26.41
25	0.52	60	17.14	110	27.56
30	1.30	65	18.99	130	29.12
35	3.47	70	20.52	p_a	34.17

TABLE 5.2

200°C		Run 1			5.1mg
t	p	t	p	t	p
5	0.02	45	9.27	85	141.33
10	0.07	50	18.81	90	147.14
15	0.13	55	33.69	100	151.94
20	0.28	60	53.85	110	154.97
25	0.51	65	82.55	120	156.33
30	1.02	70	106.30	140	158.21
35	2.29	75	121.02	p_a	161.01
40	4.44	80	134.47		

200°C		Run 2			5.0mg
t	p	t	p	t	p
5	0.02	45	8.01	90	30.60
10	0.05	50	11.16	100	32.49
15	0.14	55.5	15.16	110	33.80
20	0.37	60	18.12	120	35.08
25	0.94	65	20.83	140	36.22
30	2.00	70	23.54	p_a	38.91
35	3.55	75	25.77		
40	5.58	80	27.58		

TABLE 5.3

195°C		Run 1			6.2mg pellet
t	p	t	p	t	p
20	0.13	62	55.51	95	138.78
30	0.66	65	67.95	105	144.91
40	3.28	68	79.95	120	152.06
45	6.64	71	90.88	140	156.07
50	13.58	74	100.96	p_f	160.00
53	21.42	78	112.87	p_a	210.03
56	31.65	82	120.48		
59	43.52	88	130.50		

195°C		Run 2		6.2mg pellet	
t	p	t	p	t	p
20	0.20	62	69.69	105	147.65
30	1.24	65	81.13	120	155.08
40	5.80	68	91.75	140	158.97
45	12.39	72	104.51	p_f	160.00
50	24.39	76	115.38	p_a	178.28
53	34.42	81	124.36		
56	46.03	88	134.73		
59	58.27	95	142.86		

210°C		Run 3		4.3mg pellet	
t	p	t	p	t	p
10	0.06	45	47.06	95	154.88
15	0.11	50	74.64	105	156.69
20	0.26	55	99.60	115	158.07
25	1.01	60	117.94	p_f	160.00
30	3.89	65	130.76	p_a	169.32
35	11.14	75	145.20		
40	25.27	85	151.54		

210°C		Run 4		4.2mg pellet	
t	p	t	p	t	p
10	0.39	45	54.88	95	158.09
15	0.93	50	81.31	105	158.98
20	1.81	55	104.35	115	160.00
25	3.73	60	123.44	p_f	160.00
30	5.83	65	136.55	p_a	160.00
35	14.89	75	150.62		
40	31.46	85	155.39		

TABLE 5.4

210°C		Run 1		4.6mg pellet	
t	p	t	p	t	p
5	0.06	39	54.49	65	155.86
10	0.11	41	71.43	75	159.53
15	0.16	43	88.31	85	160.00
20	0.39	45	104.15	p_f	160.00
25	1.15	47	117.32	p_a	193.21
30	7.49	50	132.63		
35	27.06	55	147.57		
37	39.34	60	153.05		

210°C		Run 2		4.7mg pellet	
t	p	t	p	t	p
10	0.16	41	65.49	75	159.12
15	0.26	43	80.62	85	160.00
20	0.64	45	94.85	p_f	160.00
25	1.66	47	106.99	p_a	189.01
30	7.89	50	123.81		
35	25.82	55	142.77		
37	37.26	60	153.16		
39	51.44	65	157.06		

210°C		Run 3		4.7mg pellet	
t	p	t	p	t	p
10	0.05	41	60.85	75	159.40
15	0.10	43	75.53	85	160.00
20	0.33	45	90.21	p_f	160 00
25	1.08	47	103.36	p_a	181.17
30	6.21	50	121.07		
35	22.30	55	142.55		
37	32.98	60	152.23		
39	45.86	65	156.83		

210°C		Run 4		4.7mg pellet	
t	p	t	p	t	p
10	0.06	41	56.20	75	159.05
15	0.11	43	70.54	85	160.00
20	0.34	45	84.49	p_f	160.00
25	1.00	47	97.62	p_a	211.29
30	5.71	50	116.04		
35	20.39	55	138.31		
37	30.49	60	150.37		
39	42.59	65	155.15		

TABLE 5.5

195°C		Run 1		1000 lbs/sq.in.	6.7mg pellet
t	p	t	p	t	p
10	0.02	66	46.34	97	153.06
20	0.05	69	62.77	120	157.22
30	0.21	72	80.51	p_f	160.00
40	0.87	75	97.98	p_a	211.08
50	4.02	78	113.73		
55	10.28	81	124.45		
60	22.23	85	136.85		
63	32.56	90	146.67		

195°C		Run 2		1000 lbs/sq.in.	6.7mg pellet
t	p	t	p	t	p
10	0.01	63	29.44	85	135.64
20	0.03	66	43.20	90	146.85
30	0.17	69	59.51	97	154.22
40	0.90	72	76.73	120	158.37
50	3.30	75	94.05	p_f	160.00
55	8.34	78	109.82	p_a	183.27
60	19.30	81	121.57		

195°C	Run 3		750 lbs/sq.in.		5.9mg pellet
t	p	t	p	t	p
30	0.19	69	43.74	107	139.49
40	0.66	72	58.00	120	143.54
50	2.72	75	73.29	140	145.22
55	7.00	80	97.14	p_f	160.00
60	15.24	85	112.75	p_a	178.12
63	22.24	90	125.49		
66	31.65	97	135.74		

195°C	Run 4		750 lbs/sq.in.		5.7mg pellet
t	p	t	p	t	p
30	0.20	69	72.42	107	154.14
40	1.27	72	85.63	120	158.20
50	5.67	75	97.91	140	158.99
55	13.71	80	116.67	p_f	160.00
60	30.36	85	129.65	p_a	187.11
63	44.25	90	140.90		
66	58.86	97	151.66		

195°C	Run 5		500 lbs/sq.in.		4.1mg pellet
t	p	t	p	t	p
20	0.06	65	19.11	97	135.67
30	0.21	70	34.04	106	142.28
40	0.71	75	55.84	120	148.70
50	2.50	80	82.96	140	153.51
55	5.21	85	105.98	p_f	160.00
60	10.34	90	122.42	p_a	148.02

195°C	Run 6		500 lbs/sq.in.		5.6mg pellet
t	p	t	p	t	p
20	0.02	65	31.68	97	122.99
30	0.14	70	51.48	106	131.34

40	1.09	75	69.99	120	140.15
50	4.25	80	85.86	140	148.01
55	8.16	85	99.32	p_f	160.00
60	16.39	90	110.90	p_a	172.51

195°C	Run 7	250 lbs/sq.in.		6.0 mg pellet	
t	p	t	p	t	p
20	0.06	70	38.51	110	111.71
30	0.24	75	52.61	120	118.89
40	0.82	80	63.64	140	127.56
50	2.54	85	73.61	p_f	160.00
60	11.40	92	87.50	p_a	157.81
65	23.08	100	101.71		

195°C	Run 8	250 lbs/sq.in.		4.9 mg pellet	
t	p	t	p	t	p
20	0.04	63	48.29	95	117.15
30	0.28	66	61.15	105	128.90
40	1.73	69	72.09	120	144.09
50	8.00	73	83.54	135	154.46
55	17.47	78	92.34	p_f	160.00
60	35.08	85	101.36	p_a	195.21

TABLE 5.6

195°C		Run 1			5.6mg
t	p	t	p	t	p
5	0.20	65	23.18	115	130.96
10	0.28	70	30.61	120	137.79
20	0.33	75	40.07	130	145.23
30	0.68	80	51.11	140	150.97
35	1.41	85	63.76	150	152.36
40	2.69	90	77.65	160	153.99
45	4.91	95	90.75	p_f	160.00

50	8.05	100	103.33	p_a	241.77
55	12.23	105	114.50		
60	17.29	110	123.29		

195°C		Run 2			5.6mg
t	p	t	p	t	p
5	0.02	70	37.90	120	138.56
10	0.06	75	48.18	130	145.84
20	0.14	80	59.91	140	150.04
30	0.55	85	71.83	150	153.13
40	3.19	90	84.43	160	153.97
45	6.37	95	96.08	180	155.71
50	10.83	100	107.29	p_f	160.00
55	16.18	105	117.38	p_a	218.36
60	22.42	110	125.03		
65	29.35	115	132.42		

195°C		Run 3			5.6mg
t	p	t	p	t	p
10	0.02	70	31.84	115	134.33
20	0.04	75	42.43	120	140.53
30	0.30	80	55.00	130	148.25
40	1.86	85	67.78	140	152.63
45	3.80	90	81.47	150	155.71
50	6.75	95	95.20	160	156.30
55	10.99	100	107.96	p_f	160.00
60	16.44	105	119.32	p_a	199.22
65	23.15	110	126.83		

TABLE 5.7

190°C	Run 1		1 cycle		5.0mg
t	p	t	p	t	p
30	0.16	101	43.61	180	149.86
40	0.45	108	58.70	200	155.24

50	1.13	115	73.09	220	157.16
60	2.40	122	86.26	240	157.36
70	4.32	130	101.21	p_f	160.00
80	9.93	140	118.00	p_a	184.01
87	17.93	150	129.58		
94	29.48	165	143.61		

190°C Run 2 3 cycles 5.1mg

t	p	t	p	t	p
40	0.37	114	65.45	200	155.99
50	1.04	121	79.81	220	159.54
60	2.37	128	95.40	p_f	160.00
70	4.72	137	111.62	p_a	179.86
80	9.00	146	127.07		
90	18.56	156	137.48		
100	34.75	167	145.25		
107	49.41	180	151.32		

TABLE 5.8

190°C Run 1 3 mins grinding 5.0mg

t	p	t	p	t	p
40	0.15	113	35.38	170	128.40
60	0.55	120	50.86	181	137.68
70	1.00	127	65.07	195	143.67
80	1.87	134.5	80.87	215	150.42
90	3.82	141	93.02	240	154.75
100	12.08	150	106.73	p_f	160.00
107	23.29	160	120.07	p_a	161.14

190°C Run 2 3 mins grinding 5.0mg

t	p	t	p	t	p
40	0.09	113	28.35	170	131.79
60	0.42	120	42.42	180	138.85
70	0.79	127	58.11	195	145.14
80	1.44	134	74.34	215	153.54

90	2.97	141	88.41	240	157.01
100	8.32	150	105.14	p_f	160.00
107	17.43	160	119.20	p_a	159.80

TABLE 5.9

185°C	Run 1		10 secs grinding		5.0mg
t	p	t	p	t	p
10	0.02	120	40.98	180	133.14
20	0.03	125	48.44	185.5	136.86
30	0.08	130	57.21	190	140.50
40	0.15	135	65.68	200	146.07
50	0.55	140	75.94	210	149.31
60	1.81	145	83.95	220	151.25
70	4.09	150	93.13	240	153.21
80	7.36	155	99.62	280	155.98
90	11.49	160	108.67	p_f	160.00
100	17.99	165	115.32	p_a	209.50
110	27.85	170	121.16		
115	33.82	175	126.50		

185°C	Run 2		30 secs grinding		4.7mg
t	p	t	p	t	p
10	0.03	105	29.56	160	134.65
20	0.06	110	39.47	165	137.92
30	0.10	115	50.02	175	146.07
40	0.20	120	61.50	185	149.19
50	0.56	125	71.94	195	152.14
60	1.44	130	83.19	205	153.95
70	2.88	135	92.93	215	155.43
80	5.33	140	103.66	225	156.49
90	10.62	145	113.52	p_f	160.00
95	15.27	150	123.07	p_a	217.50
100	21.47	155	128.80		

185°C	Run 3		3 mins grinding		4.8mg
t	p	t	p	t	p
10	0.03	120	8.61	175	117.91
20	0.07	125	14.68	180	123.38
30	0.11	130	24.09	190	131.81
40	0.16	135	35.31	200	138.38
50	0.25	140	47.25	210	143.43
60	0.43	145	59.46	220	147.47
70	0.70	150	71.06	230	150.81
80	1.20	155	82.37	240	153.29
90	1.83	160	93.12	p_f	160.00
100	2.83	165	102.68	p_a	187.00
110	4.55	170	111.25		

185°C	Run 4		10 mins grinding		4.8mg
t	p	t	p	t	p
10	0.04	110	1.85	210	44.24
20	0.12	120	2.69	220	51.27
30	0.15	130	5.18	230	58.30
40	0.19	140	6.24	240	64.12
51	0.24	150	9.25	260	75.92
60	0.30	160	13.83	280	86.81
70	0.39	170	19.41	p_f	160.00
80	0.56	180	25.11	p_a	218.54
90	0.83	190	31.41		
100	1.24	200	37.79		

TABLE 5.10

185°C	Run 1		Insufficient grinding		5.0mg
t	p	t	p	t	p
10	0.04	110	14.04	210	142.56
20	0.08	120	17.92	220	148.08
30	0.12	130	23.04	230	151.89
40	0.19	140	31.77	240	153.82

50	0.35	150	47.57	260	157.15
60	0.98	160	71.43	280	158.72
70	2.63	170	93.47	300	159.81
80	5.37	180	110.96	320	160.00
90	8.23	190	123.93	p_f	160.00
100	11.01	200	134.38	p_a	181.73

185°C	Run 2		Grindex		4.8mg
t	p	t	p	t	p
10	0.03	120	8.61	175	117.91
20	0.07	125	14.68	180	123.38
30	0.11	130	24.09	190	131.81
40	0.16	135	35.31	200	138.38
50	0.25	140	47.25	210	143.43
60	0.43	145	59.46	220	147.47
70	0.70	150	71.06	230	150.81
80	1.20	155	82.37	240	160.00
90	1.83	160	93.12	p_f	160.00
100	2.83	165	102.68	p_a	187.07
110	4.55	170	111.25		

TABLE 5.11

190°C	Run 1		Sunlight		4.5mg pellet
t	p	t	p	t	p
5	0.08	60	36.76	180	92.06
10	1.10	70	41.01	200	103.70
15	4.33	81	45.00	220	114.15
20	8.51	90	48.39	240	123.48
25	13.10	100	52.05	260	132.19
30	17.94	110	55.94	280	139.25
35	21.75	120	60.10	p_f	160.00
40	25.32	140	68.95	p_a	170.94
50	31.80	160	80.31		

190°C	Run 2		No Sunlight		4.5mg pellet
t	p	t	p	t	p
10	0.04	110	38.34	210	148.34
20	0.05	120	55.42	220	151.47
30	0.08	130	73.03	230	153.66
40	0.13	140	89.72	240	156.07
50	0.28	150	103.58	250	157.96
60	0.75	160	115.82	260	158.40
70	2.08	170	123.76	270	158.80
80	5.69	180	132.75	p_f	160.00
90	12.77	190	139.51	p_a	168.92
100	23.67	200	144.61		

TABLE 5.12

210°C	Run 1		Rough handling		4.5mg pellet
t	p	t	p	t	p
10	0.03	40	53.68	75	157.55
15	0.08	45	82.98	85	159.07
20	0.46	50	117.78	95	159.74
25	2.41	55	136.87	105	160.00
30	10.35	60	140.98	p_f	160.00
35	27.16	65	148.69	p_a	154.44

210°C	Run 2		Blank		4.7mg pellet
t	p	t	p	t	p
10	0.05	39	45.86	60	152.23
15	0.10	41	60.85	65	156.83
20	0.33	43	75.53	75	159.40
25	1.08	45	90.21	85	160.00
30	6.21	47	103.36	p_f	160.00
35	22.30	50	121.07	p_a	182.11
37	32.98	55	142.55		

195°C	Run 3		Rough handling		5.0mg
t	p	t	p	t	p
20	0.06	63	71.02	95	154.25
30	0.26	66	93.60	105	155.47
40	1.54	69	113.25	120	157.29
45	3.27	72	127.85	p_f	160.00
50	7.21	75	137.98	p_a	177.35
55	18.35	79	143.29		
60	48.58	85	150.74		

195°C	Run 4		Blank		5.0mg
t	p	t	p	t	p
20	0.09	63	38.54	95	146.34
30	0.25	66	59.89	105	149.86
40	1.16	69	80.56	120	153.77
45	2.51	72	99.07	140	155.42
50	5.30	75	114.28	p_f	160.00
55	10.99	79	126.18	p_a	190.91
60	24.25	85	138.66		

TABLE 5.13

200°C	Run 1		Dry air admitted		5.0mg
t	p	t	p	t	p
5	0.11	55	34.66	110	153.03
10	0.14	60	48.92	120	155.25
15	0.23	65	64.88	131	156.86
20	0.41	70	82.22	145	158.29
25	0.92	75	98.90	161.5	159.00
30	2.19	80	114.02	176	160.00
35	4.48	85	126.00	p_f	160.00
40	7.88	90	136.02	p_a	204.10
45	13.51	95	142.35		
50	22.38	100	147.69		

200°C	Run 2		Blank		5.0mg
t	p	t	p	t	p
5	0.11	50	15.32	95	145.30
10	0.12	55	27.45	100	149.60
15	0.14	60	44.77	110	154.25
20	0.20	65	65.09	120	156.88
25	0.40	70	86.05	130	158.17
30	1.01	75	104.89	p_f	160.00
35	2.16	80	119.96	p_a	212.89
40	4.37	85	131.23		
45	8.12	90	139.79		

TABLE 5.14

200°C	Run 1		Annealing		5.0mg
t	p	t	p	t	p
5	0.01	60	24.28	120	150.49
10	0.02	65	35.32	130	154.80
15	0.03	70	48.98	140	157.21
20	0.10	75	63.74	150	158.34
25	0.27	80	79.89	160	159.29
30	0.75	85	94.34	170	159.53
35	1.58	90	108.63	180	160.00
40	3.13	95	119.65	190	160.00
45	5.64	100	129.81	p_f	160.00
50	9.66	105	136.54	p_a	192.90
55	15.69	110	143.01		

200°C	Run 2		Blank		5.0mg
t	p	t	p	t	p
5	0.02	50	10.47	95	121.51
10	0.03	55	18.10	100	131.24
15	0.05	60	28.72	105	138.38
20	0.12	65	41.33	110	144.43
25	0.26	70	55.48	120	151.97
30	0.63	75	69.89	130	155.72
35	1.43	80	84.73	140	157.66

40	2.90	85	97.99	p_f	160.00
45	5.74	90	111.28	p_a	219.01

TABLE 5.15

195°C			Run 1		4.6mg pellet
t	p	t	p	t	p
10	0.02	105	28.37	190	118.17
20	0.03	110	32.97	200	126.26
30	0.05	115	38.07	210	133.17
40	0.20	120	43.63	220	137.58
45	0.42	125	49.12	230	142.06
50	0.87	130	54.57	240	145.80
55	1.55	135	60.27	250	149.32
60	2.54	140	65.95	262	153.29
65	3.98	145	72.56	270	154.39
70	5.52	150	77.70	280	156.13
75	7.54	155	82.77	290	157.16
80.5	10.22	160	88.19	300	158.34
85	13.31	165	94.64	310	159.00
90	16.12	170	99.34	320	160.00
95	19.77	175	104.80	p_f	160.00
100	23.81	180	109.58	p_a	159.00

200°C			Run 2		4.6mg pellet
t	p	t	p	t	p
5	0.09	55	8.29	130	106.38
10	0.14	60	10.52	135	113.47
15	0.19	65	13.74	140	118.81
20	0.22	70	17.91	150	130.66
25	0.24	75	22.79	160	139.52
30	0.32	80	28.56	170	145.44
35	0.47	85	35.13	180	150.50
40	1.49	90	42.64	190	153.95
42	2.87	95	50.11	200	155.79
44	3.82	100	58.27	210	156.58
45	4.43	105	66.66	222	157.09

46	4.84	110	74.36	230	158.27
48	5.71	115	83.23	240	160.00
50	6.74	120	92.07	p_f	160.00
52	7.14	125	99.89	p_a	111.00

205°C		Run 3		4.5mg pellet	
t	p	t	p	t	p
5	0.01	70	58.84	135	150.98
10	0.01	75	69.56	140	151.41
15	0.03	80	80.10	146	153.25
20	0.17	85	89.18	150	154.23
25	0.78	90	98.62	160	156.69
30	2.50	95	108.39	170	158.18
35	5.43	100	115.69	180	158.51
40	9.83	105	123.71	190	159.17
45	15.53	110	130.18	200	160.00
50.5	23.03	115	135.69	p_f	160.00
55	30.43	120	141.38	p_a	222.51
60	39.41	125	144.52		
65	48.65	130	147.87		

210°C		Run 4		4.6mg pellet	
t	p	t	p	t	p
2	0.16	30	3.21	62	63.55
4	0.19	32	4.36	65	71.05
6	0.24	34	5.83	70	83.74
8	0.30	36	7.44	75	96.74
10	0.32	38	9.87	80	107.55
12	0.37	40	12.31	85	118.06
14	0.43	42	15.40	90	126.72
16	0.50	44	18.80	95	131.71
18	0.62	46	22.83	105	142.30
20	0.73	48	27.11	115	148.76
22	0.94	50	31.73	125	152.28

24	1.30	53	39.06	135	154.35
26	1.71	56	47.21	p_f	160.00
28	2.37	59	55.04	p_a	168.07

215°C			Run 5		4.5mg pellet
t	p	t	p	t	p
5	0.02	33	19.33	62	129.88
7	0.02	35	25.30	65	137.14
9	0.02	37	32.56	68	142.93
10	0.02	39	40.44	71	147.74
15	0.15	41	49.17	75	152.42
17	0.36	43	57.77	80	156.27
19	0.75	45	66.76	85	156.89
20	1.09	47	75.62	91	157.96
21	1.41	49	84.33	95	158.46
23	2.46	51	93.16	100	158.75
25	4.12	53	101.17	105	158.86
27	6.49	55	108.95	110	158.97
29	9.66	57	116.09	p_f	160.00
31	13.95	59	122.36	p_a	212.60

220°C			Run 6		4.6mg pellet
t	p	t	p	t	p
2	0.01	25	32.77	50	142.22
4	0.02	26	38.27	53	144.55
6	0.03	27	44.33	56	148.22
8	0.04	28	50.53	60	150.54
10	0.11	29	56.44	65	150.71
12	0.39	30	61.50	70	153.32
14	1.18	31	67.65	75	151.99
15	2.00	32	73.63	80	153.48
16	3.09	33	79.54	85	154.08
17	4.41	34	85.07	90	154.77
18	6.27	35	90.18	95	155.47
19	8.57	37	100.65	100	155.91
20	11.42	39	110.50	110	157.47

21	14.80	41	119.27	120	158.08
22	18.82	43	126.41	p_f	160.00
23	22.64	45	131.48	p_a	228.50
24	27.50	47	136.60		

TABLE 5.16

185°C		Run 1			5.5 mg
t	p	t	p	t	p
10	0.02	70	35.63	118	123.55
20	0.04	73	40.60	127	132.68
30	0.25	76	46.22	136	139.02
35	0.68	79	52.23	147	144.09
39	1.41	83	60.43	158	147.32
44	3.20	87	68.98	170	149.76
49	6.64	91	78.00	185	151.41
54	11.70	95	85.57	p_f	160.00
59	18.26	100	95.35	p_a	195.15
63	24.04	105	103.96		
67	30.35	111	114.54		

190°C		Run 2			5.3mg
t	p	t	p	t	p
10	0.03	56	37.08	90	123.94
20	0.13	59	43.77	94	129.26
25	0.42	62	51.31	99	135.03
30	1.44	65	59.35	104	138.82
35	4.12	68	67.83	110	143.88
38	6.92	71	76.54	117	147.06
41	10.54	74	85.32	125	149.57
44	14.97	77	93.74	p_f	160.00
47	19.75	80	102.14	p_a	195.01
50	24.92	83	109.32		
53	30.83	86	116.34		

195°C		Run 3			5.8mg
t	p	t	p	t	p
5	0.02	41	30.09	65	107.51
10	0.04	43	36.12	68	114.64
15	0.12	45	41.93	71	118.42
20	0.47	47	49.23	74	123.12
23	1.05	49	56.66	78	128.67
26	2.30	51	64.11	82	131.78
29	4.87	53	71.32	89	136.30
32	9.30	55	78.23	95	140.85
35	15.19	57	84.87	101	144.10
37	19.61	59	91.10	p_f	160.00
39	24.58	62	99.38	p_a	207.63

200°C		Run 4			5.4mg
t	p	t	p	t	p
10	0.01	34	50.76	63	150.38
15	0.20	36	62.09	69	154.51
18	0.73	38	73.45	75	156.10
20	1.68	40	85.27	85	158.36
22	3.59	42	95.99	95	158.90
24	6.92	44	106.36	105	159.37
26	12.13	46	115.76	115	159.70
28	19.35	48	123.19	125	159.84
29	23.85	51	132.69	p_f	160.00
30	28.80	54	139.44	p_a	182.06
32	39.30	58	145.59		

205°C		Run 5			5.4mg
t	p	t	p	t	p
5	0.02	25	57.80	46	141.62
10	0.11	26	65.07	49	143.86
12	0.36	27	72.62	53	147.06
14	0.94	28	79.93	58	149.73

16	2.86	29	87.06	65	152.54
18	6.89	30	93.68	75	156.86
19	10.80	31	98.19	85	158.47
20	16.89	33	108.99	95	159.28
21	27.28	35	118.29	105	160.00
22	35.27	37	123.58	p_f	160.00
23	42.89	40	131.16	p_a	205.01
24	50.54	43	136.61		

Runs 6 - 10 Repeat I.P. series

180°C	5.7mg	185°C	4.8mg	190°C	5.8mg
t	p	t	p	t	p
10	0.03	10	0.03	5	0.01
20	0.03	20	0.04	10	0.01
30	0.04	30	0.06	20	0.02
40	0.06	40	0.14	30	0.09
50	0.16	45	0.30	40	1.12
60	0.52	55	1.20	45	2.84
70	1.55	60	2.21	p_f	160.00
p_f	160.00	p_f	160.00	p_a	208.05
p_a	226.63	p_a	173.27		

195°C	6.0mg	200°C	4.8mg
t	p	t	p
5	0.04	5	0.03
10	0.23	10	0.04
15	0.25	15	0.06
20	0.28	20	0.20
25	0.41	25	1.25
30	1.26	28	3.19
32	1.94	30	5.19
p_f	160.00	p_f	160.00
p_a	248.06	p_a	210.40

TABLE 5.17

Acceleratory period		Split Run		4.6mg pellet	
195°C		170°C		185°C	
t	p	t	p	t	p
20	0.04	6	16.48	5	46.73
40	0.52	8	16.99	6	48.41
60	4.81	10	17.77	7	50.15
70	10.42	12	18.54	8	51.74
160°C		13	18.96	9	53.58
4	10.46	14	19.30	10	55.53
5	10.68	15	19.58	11	57.12
6	10.59	16	19.90	190°C	
7	10.44	175°C		5	69.42
8	10.75	6	23.11	6	71.50
10	10.85	7	23.44	7	74.24
12	11.00	8	23.97	8	76.35
14	11.24	9	24.52	9	78.58
16	11.45	10	24.93	10	80.94
18	11.66	11	25.64	11	83.09
20	11.88	12	26.11	12	85.33
22	12.02	13	26.86	20	105.04
24.5	12.51	14	27.51	30	119.28
165°C		15	28.00	40	134.19
6	13.23	180°C		50	141.29
8	13.39	6	32.43	60	150.09
10	13.67	7	33.47	70	154.51
12	14.11	8	34.53	80	157.40
13	14.21	9	35.48	90	159.43
14	14.27	10	36.72	100	161.26
15	14.55	11	37.48	110	162.91
16	14.86	12	38.63	p_f	165.90
17	14.96	13	39.34	p_a	165.90
18	14.98				

Decay period		Split Run		4.6mg pellet	
200°C		175°C		190°C	
t	p	t	p	t	p
40	4.72	6	105.30	6	151.95
45	9.53	8	105.52	7	152.78
50	21.07	10	105.78	8	154.44
55	41.31	12	107.17	9	155.60
60	68.33	14	108.03	10	156.38
63	86.30	16	109.06	11	157.09
166°C		18	109.87	210°C	
7	90.72	20	110.84	20	179.64
8	89.93	180°C		30	198.79
9	89.98	6	116.25	40	206.59
10	89.59	8	116.30	50	206.67
12	90.08	10	118.27	60	206.59
14	90.47	12	119.68	p_f	206.62
16	91.31	14	121.61	p_a	206.62
18	91.90	16	123.04		
20	92.55	18	125.41		
22	92.70	185°C			
24	93.65	6	132.57		
26	94.10	7	134.79		
28	94.70	8	134.99		
30	95.46	9	135.63		
32	96.42	10	136.84		
34	96.88	11	137.39		
170°C		12	139.03		
6	97.39	13	140.07		
8	98.36	14	141.11		
10	98.88				
12	99.70				
14	100.53				
16	101.41				

195°C		Blank			5.5mg pellet
t	p	t	p	t	p
10	0.01	75	17.25	114	116.04
20	0.03	79	24.56	118	124.92
30	0.09	83	33.40	122	131.38
40	0.47	87	42.75	127	140.28
45	1.02	91	53.38	133	147.00
50	1.75	94	61.46	140	152.86
55	2.94	98	72.44	150	157.04
60	4.53	102	83.53	160	158.60
65	6.81	106	94.86	p_f	160.00
70	10.92	110	106.15	p_a	202.66

TABLE 5.18.

Acceleratory period		Split run			5.0mg
180.5°C		170.6°C		180.8°C	
t	p	t	p	t	p
20	0.05	12	27.40	12	66.68
35	0.09	15	28.91	13	68.68
45	0.17	18	30.89	14	70.71
55	0.47	21	33.32	15	72.78
60	0.84	23	35.14	16	74.78
80	6.72	175.4°C		17	76.67
100	14.29	12	41.91	185.7°C	
166.0°C		14	44.70	12	103.09
15	18.31	15	46.17	13	105.63
20	19.94	16	47.30	14	108.94
25	21.55	17	48.63	15	111.71
30	23.33	18	50.01	16	114.52
35	25.27	19	51.41	210°C	
				p_f	226.31
				p_a	226.31

190°C			Blank		5.6mg
t	p	t	p	t	p
10	0.02	65	19.55	110	130.31
20	0.05	70	28.69	115	136.75
30	0.21	75	40.75	120	142.31
35	0.52	80	54.87	125	145.98
40	1.22	85	69.95	130	148.90
45	2.68	90	87.68	140	153.00
50	4.78	95	98.81	p_f	160.00
55	8.05	100	111.29	p_a	240.01
60	12.91	105	121.99		

TABLE 5.19

190°C		Run 1	Interruptions		5.6mg pellet
t	p	t	p	t	p
10	0.02	77	10.14	119	106.09
20	0.04	81	12.43	121	107.09
30	0.08	84	17.55	123	110.67
40	0.19	87	23.25	125	114.51
50.5	1.03	90	30.17	128	120.00
55	1.75	94	41.12	132	126.63
Interruption		98	52.74	137	134.40
59	2.02	102	65.75	142	140.01
62	2.45	106	77.95	152	149.76
66	4.36	110	90.30	162	156.80
70	7.22	114	100.34	172	158.24
73	9.69	117	106.03	p_f	160.00
Interruption		Interruption		p_a	238.64

195°C		Run 2	Interruptions		5.1mg
t	p	t	p	t	p
10	0.03	44	11.34	68	82.22
15	0.05	Interruption		70	89.09
20	0.12	48	11.34	72	95.79

25	0.34	50	15.90	75	103.77
29	0.74	52	23.06	79	113.14
Interruption		54	31.75	83	121.02
30	0.75	56	40.86	88	127.44
32	1.27	58	49.68	94	134.42
34	1.54	60	58.10	101	139.36
36	2.33	62	65.44	110	143.87
38	3.55	Interruption		120	148.39
40	5.43	64	66.45	p_f	160.00
42	8.23	66	74.24	p_a	231.40

TABLE 5.20

190°C Run 1 Water interruption (30 secs) 5.2mg pellet

t	p	t	p	t	p
10	0.03	89	13.39	186	71.48
20	0.07	94	13.68	Interruption	
30	0.13	98	15.99	193	71.55
40	0.26	102	19.38	206	71.57
50	0.61	106	23.47	226	71.62
62	3.35	108	23.87	266	73.33
Interruption		Interruption		296	78.66
65	3.37	113	23.75	336	86.97
70	3.77	118	25.09	p_a	94.88
75	5.38	126	28.39		
78	7.26	134	31.94		
81	10.82	146	38.41		
84	13.38	161	49.24		
Interruption		176	63.57		

190°C Run 2 Interruption blank 5.6mg pellet

t	p	t	p	t	p
10	0.03	77	15.13	119	158.22
20	0.06	81	18.54	121	159.73
30	0.12	84	26.17	123	165.05
40	0.29	87	34.67	125	170.89
50.5	1.54	90	44.99	128	179.04

50	2.61	94	61.32	132	188.86
Interruption		98	78.66	137	200.45
59	3.02	102	98.06	142	208.99
62	3.65	106	116.26	152	223.35
66	6.50	110	134.69	162	233.86
70	10.77	114	149.65	172	238.43
73	14.45	117	158.14	p_a	238.64
Interruption		Interruption			

190°C Run 3 t = 0 Water interruption (5 mins) 5.6mg pellet					
t	p	t	p	t	p
10	0.00	60	2.62	110	105.15
15	0.00	65	5.17	115	113.97
20	0.00	70	10.70	120	122.30
25	0.01	75	18.14	130	136.41
30	0.01	80	28.00	140	144.64
35	0.03	85.5	41.61	150	152.14
40	0.05	90	54.07	160	156.17
45	0.17	95	68.34	170	157.86
50	0.46	101	84.09	180	159.63
55	1.23	105	93.40	p_a	160.33

190°C Run 4 Blank 5.6mg pellet					
t	p	t	p	t	p
10	0.02	65	3.11	120	135.14
15	0.04	70	5.64	125	145.01
20	0.06	75	10.56	130	154.62
25	0.08	80	17.22	140	168.72
30	0.10	85	27.05	150	178.11
35	0.15	90	40.25	160	183.83
40	0.20	95	56.15	170	187.56
45	0.32	100	73.62	180.5	190.20
50	0.59	105	91.65	190	191.56
55	1.52	110	107.23	200	192.49
60	1.69	115	122.12	p_a	229.32

190°C Run 5 Successive Interruptions (5 mins) 5.6mg pellet

t	p	t	p	t	p
5	0.03	65	1.32	120	7.51
10	0.04	70	1.68	125	9.13
15	0.06	74	2.33	130	10.69
20	0.06	75	2.50	140	15.31
25	0.08	Interruption		150	22.09
30	0.11	80	2.50	160	30.67
35	0.15	85	2.52	170	40.78
40	0.23	90	3.40	180	50.11
45	0.41	91	3.49	190	56.26
50	0.83	Interruption		200	62.62
52	1.04	95	3.51	210	65.81
53	1.22	100	3.87	220	68.16
Interruption		105	4.50	230	69.75
55	1.22	111	5.50	245	71.61
60	1.22	115	6.21	p_a	112.33

195°C Run 1 Water interruptions (30 secs) Blank 5.0 mg

t	p	t	p	t	p
10	0.02	70	39.64	115	167.24
20	0.05	75	52.83	120	174.96
30	0.37	80	68.48	130	184.57
40	2.32	85	84.39	140	190.03
45	4.73	90	101.43	150	193.86
50	8.40	95	118.52	160	194.60
55	13.68	100	134.41	p_a	199.22
60	20.47	105	148.56		
65	28.82	110	157.90		

195°C		Run 2	t = 0		5.0mg
t	p	t	p	t	p
20	0.01	60	37.11	100	101.61
30	0.15	65	47.24	110	109.71
40	2.59	70	57.46	120	116.93
45	7.27	75	66.78	135	123.10
50	15.43	80	75.21	150	126.63
55	26.22	90	89.54	p_a	135.44

195°C		Run 3	0.5 I.P.		5.0mg
t	p	t	p	t	p
17	0.11	55	3.10	115	92.04
Interruption		65	11.30	125	100.39
25	0.11	75	25.74	135	106.82
35	0.12	85	43.98	150	111.93
45	0.50	95	62.60	180	115.29
50	1.35	105	79.71	p_a	115.78

195°C		Run 4	End I.P.		5.0mg
t	p	t	p	t	p
10	0.09	75	2.57	160	111.49
20	0.16	80	4.19	170	119.96
30	0.77	90	10.51	180	126.54
33	1.19	100	21.39	195	133.53
Interruption		110	36.73	210	138.69
40	1.21	120	54.58	240	146.45
50	1.22	130	72.17	p_a	153.20
60	1.30	140	88.39		
70	1.80	150	101.05		

195°C Run 5 $\alpha = 0.06$ 5.0mg

t	p	t	p	t	p
10	0.03	70	11.87	150	76.37
20	0.14	80	12.77	160	88.05
30	0.93	90	15.91	170	96.98
40	2.56	100	22.61	180	106.70
50	9.09	110	31.46	190	113.06
53	11.70	120	42.24	200	119.46
Interruption		130	53.41	220	125.45
60	11.71	140	65.36	p_a	138.50

195°C Run 6 Inf. pt. 5.0mg

t	p	t	p	t	p
10	0.01	75	55.04	140	103.32
20	0.05	80	68.37	150	104.40
30	0.48	90	101.43	160	105.33
40	3.25	Interruption		190	107.96
50	10.60	100	101.44	220	110.73
60	22.33	110	101.46	250	113.14
65	31.10	120	101.65	p_a	120.01
70	41.76	130	102.28		

195°C Run 7 $\alpha = 0.75$ 5.0mg

t	p	t	p	t	p
30	0.95	100	141.48	160	150.76
55	26.86	105	146.32	170	152.20
65	49.02	Interruption		180	153.42
75	76.21	110	146.42	202	155.75
80	91.21	120	146.46	240	158.14
85	104.99	130	146.76	p_a	162.34
90	119.23	140	147.78		
95	132.28	150	149.32		

195°C		Run 8	Successive		5.0mg
t	p	t	p	t	p
15	0.10	111	4.67	215	6.93
25	0.39	Interruption		225	7.43
30	0.98	120	4.68	235	9.69
35	1.67	130	4.76	245	17.06
Interruption		140	5.19	255	30.99
40	1.67	145	5.77	265	48.76
50	1.69	Interruption		275	63.78
60	1.73	155	5.78	285	75.68
70	2.12	165	6.04	300	85.49
77	3.22	175	6.43	315	91.10
Interruption		185	6.82	330	92.63
85	3.23	Interruption		p_a	95.57
95	3.29	195	6.83		
105	3.79	205	6.84		

190°C		Run 9	Water interruptions (5 mins)	t = 0	5.0mg
t	p	t	p	t	p
10	0.01	70	3.48	140	38.66
20	0.01	80	6.69	160	42.28
30	0.02	90	12.11	180	45.01
40	0.14	100	18.60	200	47.12
50	0.61	110	24.89	220	47.62
60	1.63	120	30.32	p_a	55.80

190°C		Run 10	Blank		4.8mg
t	p	t	p	t	p
20	0.02	70	28.66	110	112.49
30	0.09	75	37.83	115	122.52
40	0.68	80	46.83	120	131.74
45	1.73	85	57.59	128	142.59
50	3.99	90	69.07	136	152.14
55	7.84	95	80.52	145	158.00
60	13.29	100	92.05	160	164.38
65	20.39	105	102.25	p_a	180.68

TABLE 5.21

195°C		Run 1	Aged LiN_3		5.0mg
t	p	t	p	t	p
5	0.01	67	29.25	119	137.74
10	0.01	73	40.14	130	146.19
20	0.04	79	53.13	145	151.88
30	0.39	85	67.55	161	155.04
40	2.32	91	82.99	180	156.03
48	6.44	97	96.48	p_f	160.00
55	12.70	104	112.59	p_a	180.48
61	20.25	111	125.63		

195°C			Run 2		5.6mg
t	p	t	p	t	p
5	0.02	65	19.60	116	122.29
10	0.03	70	26.24	124	133.26
20	0.09	75	33.90	135	144.71
30	0.40	80	42.40	150	151.36
40	1.89	85	52.81	170	155.65
45	3.56	90	64.56	p_f	160.00
50	6.05	95	75.91	p_a	145.08
55	9.64	102	93.39		
60	14.31	109	108.28		

195°C			Run 3		5.5mg
t	p	t	p	t	p
10	0.01	67	30.58	116	130.54
20	0.05	72	39.70	125	139.84
30	0.49	80	56.93	140	148.10
40	2.74	87	73.05	160	152.87
48	7.31	94	89.72	p_f	160.00
55	13.88	101	104.80	p_a	158.96
62	22.64	108	117.55		

195°C		Run 4	Blank		5.6mg
t	p	t	p	t	p
5	0.02	60	17.29	105	114.50
10	0.09	65	23.18	110	123.29
20	0.23	70	30.61	115	130.96
30	0.68	75	40.07	120	137.79
35	1.41	80	51.11	130	145.23
40	2.69	85	63.76	140	150.97
45	4.91	90	77.65	150	152.36
50	8.05	95	90.75	p_f	160.00
55	12.23	100	103.33	p_a	219.80

195°C			Run 5		5.6mg
t	p	t	p	t	p
5	0.02	65	29.35	110	125.03
10	0.06	70	37.90	115	132.42
20	0.14	75	48.18	120	138.56
30	0.55	80	59.91	130	145.84
40	3.19	85	71.83	140	150.04
45	6.37	90	84.43	150	153.16
50	10.83	95	96.08	160	153.97
55	16.18	100	107.29	p_f	160.00
60	22.42	105	117.38	p_a	218.36

195°C			Run 6		5.6mg
t	p	t	p	t	p
10	0.02	70	31.84	115	134.33
20	0.06	75	42.43	120	140.53
30	0.30	80	55.00	130	148.25
40	1.86	85	67.78	140	152.63
45	3.80	90	81.47	150	155.71
50	6.75	95	95.20	p_f	160.00
55	10.99	100	107.96	p_a	199.22
60	16.44	105	119.32		
65	23.15	110	126.83		

TABLE 5.22

195°C	Run 1		Pyrex		4.8mg
t	p	t	p	t	p
10	0.01	47	22.49	73	126.34
15	0.02	50	29.45	76	134.50
20	0.04	53	37.62	80	142.41
25	0.21	56	48.93	85	147.46
30	1.17	58	58.30	90	151.57
35	4.38	60	68.49	100	158.17
37	6.56	62	78.15	110	158.70
39	9.23	64	89.64	122	159.99
41	12.08	66	99.18	p_f	160.00
43	15.35	68	108.76	p_a	186.80
45	18.74	70	116.90		

195°C	Run 2		Platinum		6.0mg
t	p	t	p	t	p
10	0.03	54	38.93	88	146.37
20	0.28	58	53.63	95	151.05
30	1.20	62	71.24	110	156.29
34	3.11	66	89.12	130	158.12
38	6.75	70	106.02	150	159.04
42	12.13	74	119.56	170	159.87
46	19.23	78	130.41	p_f	160.00
50	28.00	82	138.43	p_a	242.79

TABLE 5.23.

195°C	Run 1		With end product	5.3mg + 1.9mg pellet	
t	p	t	p	t	p
5	0.10	42	37.12	74	135.15
10	0.15	45	47.26	79	143.58
15	0.35	48	58.72	85	147.82
20	1.36	51	70.82	92	154.48
24	3.32	54	81.56	100	155.98
27	5.92	57	93.09	110	158.43
30	9.66	60	103.89	120	159.22

33	14.46	64	113.28	p_f	160.00
36	20.59	66	119.95	p_a	217.13
39	28.36	70	129.78		

195°C	Run 2		Blank		7.2mg pellet
t	p	t	p	t	p
5	0.02	43	16.27	71	120.18
10	0.02	46	25.14	76	130.66
15	0.04	49	36.98	82	139.79
20	0.13	52	48.97	90	146.46
25	0.42	55	62.74	100	150.77
30	1.22	58	76.79	110	152.96
34	2.79	61	88.56	120	154.28
37	5.42	64	99.71	p_f	160.00
40	10.04	67	109.65	p_a	261.42

195°C	Run 3		With end product		6.1mg + 1.7mg
t	p	t	p	t	p
5	0.11	40	27.20	68	129.11
10	0.14	43	38.96	72	134.66
15	0.22	46	51.41	77	142.00
20	0.55	49	63.91	83	147.56
25	1.74	52	75.56	90	151.35
28	3.32	55	88.74	110	156.00
31	5.90	58	100.80	120	157.35
34	10.06	61	111.56	p_f	160.00
37	17.21	64	118.74	p_a	216.13

195°C	Run 4		Blank		5.6mg
t	p	t	p	t	p
10	0.02	49	53.21	81	134.68
20	0.20	52	64.39	86	139.64
25	0.92	55	74.15	92	144.57
30	3.53	58	84.70	100	150.08
34	8.01	61	93.22	110	153.16
37	13.50	64	101.73	120	155.26
40	21.38	68	111.27	p_f	160.00
43	31.04	72	119.60	p_a	197.61
46	42.15	76	126.52		

TABLE 5.24

195°C	Run 1	Illuminated with "Ultropak"			5.0mg pellet
t	p	t	p	t	p
5	0.08	40	56.46	90	141.05
10	0.85	45	69.70	100	145.63
15	3.05	50	82.44	110	148.87
20	8.23	56	96.53	120	152.16
25	17.70	63	108.69	p_f	160.00
30	30.27	70	121.00	p_a	192.17
35	43.69	80	132.03		

195°C	Run 2		Blank		5.0mg pellet
t	p	t	p	t	p
10	0.01	60	7.85	95	112.74
20	0.03	65	14.04	102	131.31
30	0.09	70	24.20	110	144.33
40	0.52	75	38.88	120	153.72
45	1.16	80	57.06	137	159.20
50	2.40	85	76.55	p_f	160.00
55	4.40	90	96.38	p_a	188.07

TABLE 5.25

188 ± 2°C				6.0mg pellet	
t	dp/dt	t	dp/dt	t	dp/dt
5	0.01	100	0.15	150	2.73
10	0.01	105	0.20	155	2.58
20	0.01	110	0.26	160	1.77
30	0.01	115	0.34	165	1.18
60	0.01	120	0.47	170	0.90
75	0.01	125	0.70	175	0.72
80	0.02	130	1.09	180	0.58
85	0.03	135	1.46	190	0.37
90	0.06	140	1.95		
95	0.10	145	2.61		

TABLE 6.1

190°C	Run 1		500 r.		4.6mg pellet
t	p	t	p	t	p
5	0.04	50	58.44	190	130.54
10	0.48	60	64.25	200	137.08
13	1.66	70	68.68	210	140.98
15	3.82	80	72.38	220	145.27
17	7.15	90	76.45	230	148.98
19	11.35	100	80.86	240	151.71
21	16.05	110	85.59	250	154.03
23	20.56	120	90.35	260	155.63
25	25.38	130	96.00	270	156.28
27	29.64	140	101.99	280	157.84
30	35.83	150	108.04	290	158.55
33	40.14	160	113.55	p_f	160.00
38	47.63	170	119.88	p_a	164.72
43	52.05	180	125.51		

190°C	Run 2		Blank, unirradiated		4.6mg pellet
t	p	t	p	t	p
10	0.02	110	22.41	210	121.44
20	0.04	120	31.12	220	128.74
30	0 05	130	40.85	230	135.87
40	0.09	140	50.79	240	141.26
50	0.31	150	61.87	251	146.99
60	1.04	160	72.19	270	155.87
70	2.55	170	83.03	280	157.78
80	5.23	180	93.60	290	158.63
90	9.31	190	103.61	p_f	160.00
100	15.15	200	112.79	p_a	155.01

190°C	Run 3		15,000 r.		4.9mg
t	p	t	p	t	p
3	0.01	11	104.11	40	157.24
4	0.46	12	113.63	60	160.16
5	3.50	13	121.05	70	159.50
6	10.41	14	126.99	80	159.81
7	29.53	16	135.49	p_f	160.00
8	54.41	18	141.60	p_a	192.07
9	76.16	23	149.47		
10	92.78	30	155.05		

190°C	Run 4		Blank, unirradiated		5.6mg
t	p	t	p	t	p
10	0.03	75	7.92	130	120.86
20	0.05	80	12.65	135	128.72
30	0.11	85	19.52	140	133.68
35	0.13	90	28.18	145	138.08
40	0.21	95	37.90	150	143.12
45	0.35	100	51.20	160	148.56
50	0.65	105	64.92	170	152.28
55	1.10	110	79.01	180	155.29
60	1.75	115	90.67	190	156.86

65	2.95	120	102.34	p_f	160.00
70	4.84	125	111.34	p_a	228.71

TABLE 6.2

175°C Run 1 15,000 r. 4.6mg pellet					
t	p	t	p	t	p
5	0.01	50	47.39	135	116.53
7	0.64	55	48.90	140	120.06
8	1.69	60	52.45	145	121.97
9	3.14	65	54.50	150	126.06
10	5.51	70	58.76	160	131.64
11	8.72	75	62.33	170	136.10
12	12.95	80	67.51	180	139.67
13	16.99	85	72.87	190	142.42
14	20.77	90	78.67	200	145.70
15	23.77	95	83.31	210	149.33
17	28.67	100	89.38	220	151.70
20	33.26	105	93.24	230	152.84
25	37.30	110	97.01	240	155.55
30	40.43	115	102.35	250	157.18
35	42.07	120	106.80	260	159.99
40	43.99	125	109.65	p_f	160.00
45	45.32	130	113.80	p_a	171.03

175°C Run 2 15,000 r. 4.6mg pellet					
t	p	t	p	t	p
5	0.04	26	42.71	105	106.98
6	0.27	30	46.49	110	110.73
7	0.72	35	49.87	115	114.38
8	1.38	40	52.59	120	117.03
9	2.24	45	55.50	130	123.62
10	3.60	50	58.26	140	127.83
11	5.21	55	61.67	150	133.35
12	7.46	60	65.24	170	141.06
13	10.39	65	69.15	180	144.98
14	13.70	70	74.15	200	150.60

15	17.41	75	79.43	210	152.19
16	21.03	80	85.15	230	154.99
17	24.61	85	90.01	250	158.00
19	30.88	90	94.44	270	159.18
21	35.31	95	99.25	p_f	160.00
23	38.88	100	103.76	p_a	162.20

190°C	Run 3		5,000 r.	4.7mg pellet	
t	p	t	p	t	p
5	0.21	24	49.37	80	124.77
7	0.59	27	54.04	85	131.49
9	1.20	30	56.85	90	138.40
11	3.62	35	60.58	95	143.71
13	9.67	40	65.29	100	148.81
15	18.93	45	70.58	105	151.29
16	24.18	50	76.90	110	154.44
17	28.81	55	83.47	120	157.55
18	33.05	60	91.18	130	159.46
19	36.89	65	99.11	140	159.72
20	40.23	70	108.10	p_f	160.00
22	45.45	75	116.24	p_a	166.20

190°C	Run 4		5,000 r.	4.6mg pellet	
t	p	t	p	t	p
5	0.16	24	25.37	80	137.23
7	0.41	27	31.06	90	146.87
9	0.71	30	36.66	100	153.36
12	1.68	35	46.47	110	157.25
13	3.13	40	57.73	120	158.52
15	6.21	45	69.82	130	158.94
16	8.34	50	82.68	140	159.99
17	10.67	55	93.99	p_f	160.00
18	12.78	60	104.78	p_a	137.08
20	17.52	65	114.06		
22	21.59	70	122.67		

33	46.85	65	130.66	p_a	186.00
36	61.75	70	135.26		

170°C	Run 8		15,000 r.		5.0mg
t	p	t	p	t	p
5	0.02	36	63.46	70	133.07
8	0.39	39	77.53	80	138.75
11	1.87	42	88.40	90	141.50
15	4.20	45	98.10	100	144.34
20	9.34	50	110.22	110	146.16
25	18.16	55	117.98	120	147.51
30	33.50	60	124.82	p_f	160.00
33	46.92	65	129.44	p_a	173.60

TABLE 6.3

170°C	Run 1		Unirradiated		4.8mg
t	p	t	p	t	p
10	0.01	100	0.37	190	16.35
20	0.01	110	0.80	200	20.13
30	0.01	120	1.40	210	24.34
40	0.02	130	2.44	220	28.68
50	0.02	140	3.75	240	39.67
60	0.02	150	5.56	260	52.91
70	0.03	160	7.66	280	67.12
80	0.06	171	10.47	p_f	160.00
90	0.17	180	12.96	p_a	182.40

170°C	Run 2		10 r.		4.8mg
t	p	t	p	t	p
5	0.01	70	0.28	180	20.06
10	0.02	80	0.63	195	24.73
15	0.02	90	1.36	210	29.69
20	0.04	105	3.35	225	35.99

30	0.05	120	6.34	240	43.86
40	0.06	135	9.40	280	72.24
50	0.09	150	12.87	p_f	160.00
60	0.14	165	16.29	p_a	180.26

170°C	Run 3		50 r.		4.8mg
t	p	t	p	t	p
10	0.01	110	20.36	210	98.43
20	0.03	120	25.76	220	105.15
30	0.07	130	31.91	230	112.77
40	0.17	140	39.53	240	118.27
50	0.36	150	47.93	265	127.02
60	0.97	160	56.69	275	135.61
70	2.77	170	65.69	p_f	160.00
80	6.28	180	74.32	p_a	202.20
90	10.78	190	82.23		
100	15.58	200	90.08		

170°C	Run 4		250 r.		4.8mg
t	p	t	p	t	p
5	0.02	65	13.87	135	99.53
10	0.04	70	17.86	145	107.11
15	0.12	75	22.02	155	114.19
20	0.36	80	27.19	165	119.90
25	0.60	85	35.05	175	125.15
30	0.84	90	43.12	190	132.96
35	1.10	95	52.07	205	137.41
40	1.59	100	60.75	220	138.60
45	2.58	105	67.94	240	139.43
50	4.45	110	74.64	p_f	160.00
55	7.07	115	80.57	p_a	182.70
60	10.22	125	91.57		

170°C	Run 5		500 r.		4.8mg
t	p	t	p	t	p
5	0.01	55	18.54	110	118.32
10	0.01	60	25.34	120	128.69
15	0.31	65	35.98	130	137.02
20	0.74	70	47.67	140	142.97
25	1.06	75	59.41	150	147.01
30	1.48	80	70.87	160	149.62
35	2.32	85	80.95	180	153.43
40	4.44	90	90.25	200	155.38
45	8.25	95	97.87	p_f	160.00
50	13.14	100	105.53	p_a	187.64

170°C	Run 6		1500 r.		4.8mg
t	p	t	p	t	p
5	0.01	46	37.94	75	127.98
10	0.51	49	56.14	80	134.24
15	1.76	51	64.91	85	138.64
20	2.70	53	73.45	90	142.52
25	4.12	55	81.22	100	147.70
30	6.95	58	91.99	110	151.10
35	12.28	61	100.07	120	153.02
39	18.56	65	110.14	p_f	160.00
43	26.86	70	120.42	p_a	215.80

170°C	Run 7		5000 r.		5.0mg
t	p	t	p	t	p
6	0.02	26	27.92	52	136.86
8	0.46	28	33.21	56	142.98
9	1.03	30	39.64	60	146.58
10	1.59	33	54.67	65	149.73
12	2.52	36	78.11	70	152.47
15	4.20	38	91.60	80	155.37
18	7.32	40	102.38	90	156.76

20	11.35	42	110.82	100	157.98
22	16.49	45	121.30	p_f	160.00
24	22.16	48	129.14	p_a	200.07

170°C	Run 8		15000 r.		5.0mg
t	p	t	p	t	p
4	0.01	19	28.92	29	121.15
6	0.04	20	33.96	30	127.25
8	1.03	21	39.03	31	132.23
9	2.31	22	45.53	32	134.84
10	3.07	23	53.23	34	140.59
11	4.99	24	63.99	36	145.33
12	5.88	25	77.39	40	151.49
14	10.71	26	91.49	45	154.41
16	16.10	27	103.90	p_f	160.00
18	24.68	28	113.50	p_a	181.50

170°C	Run 9		700000 r.		5.0mg
t	p	t	p	t	p
2	0.01	5	152.81	11	159.87
3	25.12	6	157.21	p_f	160.00
4	115.04	8	158.98	p_a	195.03

TABLE 6.4

Induction Period series		Runs 1 - 6		15000 r.	± 4.8mg per run
121.3°C		126.0°C		135.3°C	
t	p	t	p	t	p
5	0.01	10	0.01	27	0.74
10	0.01	20	0.01	28	1.01
20	0.01	30	0.04	29	1.33
40	0.04	37	0.13	30	1.52
50	0.10	40	0.20	31	1.75
53	0.15	43	0.41	32	1.98

<table>
<tr><td>56</td><td>0.26</td><td>46</td><td>0.71</td><td>34</td><td>2.45</td></tr>
<tr><td>59</td><td>0.41</td><td>49</td><td>1.02</td><td>p_a</td><td>203.10</td></tr>
<tr><td>62</td><td>0.56</td><td>52</td><td>1.32</td><td colspan="2">140.1°C</td></tr>
<tr><td>65</td><td>0.74</td><td>55</td><td>1.61</td><td>5</td><td>0.03</td></tr>
<tr><td>68</td><td>0.99</td><td>58</td><td>1.85</td><td>10</td><td>0.04</td></tr>
<tr><td>70</td><td>1.08</td><td>p_a</td><td>165.20</td><td>15</td><td>0.08</td></tr>
<tr><td>72</td><td>1.23</td><td colspan="2">130.1°C</td><td>18</td><td>0.28</td></tr>
<tr><td>74</td><td>1.34</td><td>10</td><td>0.01</td><td>20</td><td>0.82</td></tr>
<tr><td>76</td><td>1.42</td><td>20</td><td>0.03</td><td>21</td><td>1.16</td></tr>
<tr><td>78</td><td>1.54</td><td>33</td><td>0.23</td><td>22</td><td>1.46</td></tr>
<tr><td>80</td><td>1.66</td><td>35</td><td>0.57</td><td>23</td><td>1.78</td></tr>
<tr><td>p_a</td><td>121.20</td><td>37</td><td>0.93</td><td>24</td><td>2.05</td></tr>
<tr><td></td><td></td><td>39</td><td>1.32</td><td>p_a</td><td>164.10</td></tr>
<tr><td></td><td></td><td>41</td><td>1.73</td><td></td><td></td></tr>
<tr><td></td><td></td><td>p_a</td><td>219.80</td><td></td><td></td></tr>
<tr><td colspan="6">144.4°C</td></tr>
<tr><td>t</td><td>p</td><td>t</td><td>p</td><td>t</td><td>p</td></tr>
<tr><td>5</td><td>0.01</td><td>15</td><td>0.36</td><td>19</td><td>2.47</td></tr>
<tr><td>10</td><td>0.03</td><td>16</td><td>0.85</td><td>p_a</td><td>177.84</td></tr>
<tr><td>13</td><td>0.10</td><td>17</td><td>1.42</td><td></td><td></td></tr>
<tr><td>14</td><td>0.14</td><td>18</td><td>1.98</td><td></td><td></td></tr>
</table>

<table>
<tr><td>140.8°C</td><td>Run 7</td><td colspan="2">15000 r.</td><td colspan="2">4.9mg</td></tr>
<tr><td>t</td><td>p</td><td>t</td><td>p</td><td>t</td><td>p</td></tr>
<tr><td>5</td><td>0.01</td><td>50</td><td>7.63</td><td>130</td><td>73.91</td></tr>
<tr><td>10</td><td>0.02</td><td>55</td><td>9.26</td><td>140</td><td>89.65</td></tr>
<tr><td>15</td><td>0.05</td><td>60</td><td>11.20</td><td>150</td><td>101.67</td></tr>
<tr><td>20</td><td>1.03</td><td>70</td><td>16.57</td><td>160</td><td>110.26</td></tr>
<tr><td>25</td><td>2.27</td><td>80</td><td>23.23</td><td>170</td><td>116.09</td></tr>
<tr><td>30</td><td>3.35</td><td>90</td><td>30.07</td><td>180</td><td>120.77</td></tr>
<tr><td>35</td><td>4.27</td><td>100</td><td>37.10</td><td>200</td><td>128.74</td></tr>
<tr><td>40</td><td>5.24</td><td>110</td><td>45.59</td><td>p_f</td><td>160.00</td></tr>
<tr><td>45</td><td>6.32</td><td>120</td><td>58.22</td><td>p_a</td><td>176.20</td></tr>
</table>

145.0°C		Run 8		15000 r.	5.0mg
t	p	t	p	t	p
5	0.01	60	20.24	120	101.11
10	0.01	65	24.23	130	110.05
15	0.39	70	28.38	140	116.22
17	0.98	75	32.24	150	120.46
20	1.85	80	36.55	160	123.64
25	3.14	85	41.72	170	125.94
30	4.41	90	48.67	180	127.89
35	5.92	95	57.74	200	130.49
40	7.66	100	68.27	p_f	160.00
45	9.92	105	79.06	p_a	215.80
50	12.89	110	87.87		
55	16.47	115	94.96		

150.3°C		Run 9		15000 r.	5.0mg
t	p	t	p	t	p
15	1.30	60	30.94	105	115.82
18	2.53	65	36.77	110	120.08
22	3.95	70	45.12	120	125.10
26	5.08	75	57.03	130	128.58
30	6.43	78	65.65	140	131.31
35	8.41	81	74.34	150	133.30
40	11.43	84	83.27	160	134.73
44	14.39	87	90.73	p_f	160.00
48	18.15	91	98.47	p_a	240.35
52	22.33	95	104.78		
56	26.37	100	111.60		

155.0°C		Run 10		15000 r.	5.0mg
t	p	t	p	t	p
6	0.01	36	19.51	67	109.73
8	0.01	39	23.41	70	117.99
10	0.11	42	28.19	75	129.04
12	1.30	45	33.91	80	134.30

14	2.26	48	40.32	85	138.52
16	3.06	51	47.18	90	142.52
18	3.97	54	56.05	95	144.53
20	4.92	56	63.56	100	147.08
23	6.84	58	72.62	105	148.09
26	9.10	60	82.45	110	149.80
30	12.61	62	91.24	p_f	160.00
33	16.11	64	99.61	p_a	206.20

160.0°C	Run 11		15000 r.		4.8mg
t	p	t	p	t	p
4	0.01	34	47.01	55	138.61
6	0.02	38	65.61	60	144.44
8	0.30	40	79.32	65	148.37
10	2.15	41	86.63	70	152.04
12	3.98	42	93.12	79	156.76
14	5.62	43	99.85	90	157.86
17	8.30	44	106.14	100	158.01
20	11.93	45	111.01	110	158.84
22	15.33	46	115.78	120	159.13
24	19.85	47	119.89	p_f	160.00
26	24.96	48	123.48	p_a	136.90
28	29.91	50	129.52		
30	35.43	52	133.78		

170.0°C	Run 12		15000 r.		5.0mg
t	p	t	p	t	p
4	0.01	19	28.92	29	121.15
6	0.07	20	33.96	30	127.25
8	1.03	21	39.03	31	132.23
9	2.31	22	45.53	32	134.84
10	3.07	23	53.23	34	140.59
11	4.99	24	63.99	36	145.33
12	5.88	25	77.39	40	151.49
14	10.71	26	91.49	45	154.41
16	16.10	27	103.90	p_f	160.00
18	24.68	28	113.50	p_a	181.50

Acceleratory period		Split-run	Run 13	15000 r	5.0mg
150.5°C		t	p	t	p
t	p				
5	0.01	27	9.88	18	40.09
10	0.07	30	10.75	19	42.04
15	0.46	35	12.20	165.0°C	
20	1.25	154.8°C		10	52.23
25	2.01	16	14.86	11	54.30
30	2.89	19	16.08	12	56.07
35	3.65	22	17.72	13	58.66
40	4.89	25	20.46	14	61.51
43	5.68	28	23.84	15	64.71
46	6.65	159.5°C		16	67.53
49	7.70	12	30.74	17	70.84
144.9°C		14	33.29	210°C	
21	8.41	16	36.47	p_a	212.10
24	9.14	17	38.40		

TABLE 6.5

170°C	Run 1		15000 r.		4.8mg
t	p	t	p	t	p
2	0.01	40	45.33	100	140.65
5	0.04	45	59.45	110	145.73
7	0.33	50	73.26	121.5	150.18
9	0.88	55	85.04	130	153.85
11	1.42	60	96.12	140	155.53
14	2.25	65	105.00	150	157.02
17	3.70	70	113.20	160	158.54
20	6.10	75	119.10	170	159.01
25	11.94	80	125.23	p_f	160.00
30	20.42	85	129.36	p_a	210.00
35	31.60	90	133.93		

130°C	Run 2		0.7 Mr.		7.5mg
t	p	t	p	t	p
5	0.01	31	41.27	58	118.23
10	0.03	33	47.39	61	121.82
15	1.23	35	54.37	65	127.36
16	2.56	37	61.29	70	131.83
17	4.25	39	68.01	75	134.32
18	6.25	41	74.64	80	136.83
19	8.50	43	79.94	90	139.72
20	10.87	45	86.39	100	140.89
21	13.11	47	92.43	110	142.33
23	18.10	49	97.90	120	142.95
25	23.05	51	103.27	p_f	160.00
27	28.72	53	108.05	p_a	242.80
29	34.89	55	112.54		

TABLE 6.6

170°C	Run 1	15000 r.		Platinum bucket	4.8mg
t	p	t	p	t	p
5	0.06	39	76.08	75	137.43
8	1.04	42	87.77	80	140.33
11	2.69	45	97.38	90	143.74
15	5.18	48	105.17	100	146.38
20	10.54	51	112.84	110	147.88
25	19.39	55	118.70	120	149.56
30	33.75	60	125.97	p_f	160.00
33	46.85	65	130.66	p_a	186.00
36	61.75	70	135.26		

170°C	Run 2	15000 r		Pyrex bucket	5.0mg
t	p	t	p	t	p
5	0.02	36	63.46	70	133.07
8	0.39	39	77.53	80	138.75
11	1.87	42	88.40	90	141.50
15	4.20	45	98.10	100	144.34

20	9.34	50	110.22	110	146.16
25	18.16	55	117.98	120	147.51
30	33.50	60	124.82	p_f	160.00
33	46.93	65	129.44	p_a	197.90

TABLE 6.7

175°C	Run 1		Unirradiated		5.0mg
t	p	t	p	t	p
20	0.03	140	17.98	240	120.55
30	0.05	150	24.00	250	126.25
50	0.08	160	31.87	260	130.55
70	0.18	170	42.03	280	135.93
80	0.32	180	55.18	300	140.84
90	0.73	190	69.46	321	145.76
100	1.76	200	82.55	360	150.27
110	4.23	210	94.65	p_f	160.00
120	7.85	220	104.61	p_a	200.40
130	12.71	230	113.50		

175°C	Run 2		200 r. at t = 0		5.0mg
5	0.03	55	12.81	100	123.75
10	0.04	60	30.94	110	130.55
15	0.05	65	58.51	120	135.27
20	0.08	70	76.81	140	142.91
30	0.52	75	88.31	170	148.20
40	1.55	80	98.02	p_f	160.00
50	3.96	90	112.92	p_a	203.11

175°C	Run 3		200 r. at $\alpha = 0.23$		5.0mg
t	p	t	p	t	p
100	1.16	169	36.01	214	92.82
120	4.05	174	36.35	224	102.57
130	9.27	179	36.82	234	109.91
140	15.81	184	37.39	244	115.14

150	23.40	194	45.69	264	122.54
160	35.99	199	63.79	284	127.66
164	36.09	204	77.18	p_f	160.00
Interruption		209	85.72	p_a	172.11

175°C	Run 4		1000 r. at t = 0		5.0mg
t	p	t	p	t	p
5	0.02	28	102.29	65	151.24
10	1.41	30	112.14	75	153.14
15	3.46	34	124.28	p_f	160.00
20	11.29	39	133.68	p_a	182.98
23	35.57	45	140.48		
26	81.97	55	147.15		

175°C	Run 5		1000 r. at 0.5 I.P.		5.0mg
t	p	t	p	t	p
20	0.03	60	3.28	95	125.08
30	0.03	65	13.77	100	130.05
40	0.06	70	59.29	110	136.70
45	0.07	75	86.33	130	143.42
Interruption		80	100.10	145	147.33
50	0.08	85	109.95	p_f	160.00
55	0.21	90	118.71	p_a	186.17

175°C	Run 6		1000 r. at end I.P.		5.0mg
t	p	t	p	t	p
20	0.03	100	2.51	145	115.51
30	0.05	105	4.35	155	125.84
40	0.07	110	7.54	165	131.03
50	0.10	112	14.65	175	135.27
60	0.16	114	38.59	190	141.73
70	0.29	116	52.53	220	149.71
80	0.67	118	63.56	p_f	160.00

90	1.67	122	76.59	p_a	163.23
Interruption		128	89.57		
95	1.69	136	103.49		

175°C	Run 7		1000 r at α = 0.18		5.0mg
t	p	t	p	t	p
155	28.20	177	75.13	215	138.08
Interruption		179	85.96	230	145.88
160	28.27	182	97.17	250	152.14
165	30.13	186	106.98	p_f	160.00
170	32.48	192	117.07	p_a	172.21
175	61.18	202	129.74		

175°C	Run 8		1000 r at α=0.37		5.0mg
t	p	t	p	t	p
180	58.42	203	89.63	252	144.50
Interruption		206	95.95	262	147.37
182	58.45	210	102.56	272	149.54
187	59.36	215	111.05	p_f	160.00
192	60.48	222	122.08	p_a	158.97
197	67.95	232	132.69		
200	80.99	242	139.96		

175°C	Run 9		1000 r at α=0.47		5.0mg
t	p	t	p	t	p
195	75.30	224	101.45	269	143.22
Interruption		229	107.73	279	146.49
199	75.40	234	114.15	299	152.08
204	76.34	239	120.62	319	154.74
209	77.97	244	125.92	p_f	160.00
214	86.90	249	130.61	p_a	182.42
219	94.62	259	138.24		

175°C Run 10 1000 r at α= 0.78 5.0mg

t	p	t	p	t	p
245	125.36	278	128.08	338	148.34
Interruption		288	130.68	358	150.93
253	125.49	298	135.26	378	152.05
258	125.69	308	140.19	p_f	160.00
263	126.40	318	144.13	p_a	157.38
268	126.40	328	146.58		

175°C Run 11 Unirradiated blank 5.0 g

t	p	t	p	t	p
20	0.03	140	17.98	240	120.55
30	0.05	150	24.00	250	126.25
50	0.08	160	31.87	260	130.55
70	0.18	170	42.03	280	135.93
80	0.32	180	55.18	300	140.84
90	0.73	191	69.46	321	145.76
100	1.76	200	82.55	360	150.27
110	4.23	210	94.65	p_f	160.00
120	7.85	220	104.61	p_a	200.40
130	12.71	230	113.50		

TABLE 6.8

165°C Run 1 Water Interruption 15000 r Blank run 5.0mg

t	p	t	p	t	p
5	0.01	33	52.26	85	122.94
10	0.06	36	64.72	100	127.17
15	2.91	40	78.90	120	133.47
20	7.13	45	91.36	140	138.91
24	14.43	51	100.31	p_a	169.01
27	25.32	60	110.89		
30	38.52	70	116.81		

165°C Run 2 15000 r t = 0 (30 secs) 5.0mg

t	p	t	p	t	p
10	0.92	34	66.07	80	126.33
15	3.18	39	80.55	95	133.99
20	9.44	45	91.81	110	137.10
25	26.48	52	102.01	135	142.40
28	41.13	60	111.68	p_a	154.08
31	54.61	70	120.50		

165°C Run 3 15000 r 0.5 I.P. 5.0mg

t	p	t	p	t	p
6	0.04	50	17.93	100	74.28
Interruption		55	26.20	110	77.98
15	0.09	60	34.69	120	81.49
25	0.43	65	42.52	135	84.65
35	1.79	72	51.89	150	87.72
40	4.26	80	60.33	p_a	102.00
45	9.99	90	67.69		

165°C Run 4 15000 r End I.P. 5.0mg

t	p	t	p	t	p
12	1.71	60	11.11	115	66.81
Interruption		65	16.41	130	75.90
20	1.74	70	22.66	145	80.65
30	1.92	75	29.79	160	84.76
40	2.46	80	36.66	180	89.20
45	3.19	85	41.61	p_a	108.74
50	4.71	90	48.97		
55	7.07	100	56.65		

165°C Run 5 15000 r = 0.24 5.0mg

t	p	t	p	t	p
30	37.50	75	45.67	135	85.10

Interruption		80	49.98	150	89.59
40	37.98	90	58.94	180	96.38
50	38.07	100	67.18	p_a	105.18
60	38.56	110	73.48		
70	41.98	120	78.94		

165°C	Run 6	15000 r	$\alpha = 0.47$		5.0mg
t	p	t	p	t	p
40	78.88	80	80.33	135	103.17
Interruption		90	82.39	145	105.61
50	78.98	100	86.75	180	112.50
60	79.18	110	92.40	p_a	121.11
70	79.47	120	97.62		

165°C	Run 7	15000 r	$\alpha = 0.66$		5.0mg
t	p	t	p	t	p
10	0.07	70	110.87	150	117.34
20	8.21	80	111.05	180	119.54
30	40.01	95	111.90	200	121.76
60	110.77	110	114.03	p_a	124.97
Interruption		135	115.93		

180°C	Run 8		Unirradiated Blank		5.0mg
t	p	t	p	t	p
17	0.09	139	68.58	261	176.62
35	0.16	157	98.59	278	180.50
52	0.39	174	119.40	296	183.71
70	1.09	191	138.08	313	185.30
87	4.67	209	152.53	331	186.29
104	16.45	226	163.19	p_a	187.21
122	39.03	244	170.72		

180°C	Run 9		15000 r	t = 0 (5 mins)	4.9mg
t	p	t	p	t	p
5	0.00	70	0.59	185	66.01
10	0.00	80	1.16	200	77.21
15	0.00	90	2.30	215	85.85
20	0.00	100	4.39	240	98.17
25	0.00	110	7.47	260	99.70
30	0.02	120	11.93	280	102.98
35	0.03	130	17.33	300	105.31
40	0.06	140	23.59	320	107.54
50	0.14	155	36.85	p_a	117.37
60	0.28	170	51.78		

195°C	Run 10		Unirradiated Blank		6.0mg
t	p	t	p	t	p
5	0.06	50	38.08	82	188.27
10	0.31	54	52.95	88	199.06
20	0.38	58	72.94	95	205.42
30	1.63	62	96.88	110	212.55
34	4.23	66	121.20	130	215.04
38	9.18	70	144.19	150	216.29
42	16.50	74	162.60	170	216.92
46	26.15	78	177.36	p_a	248.06

195°C	Run 11		Irradiated blank	15000 r	5.0mg
t	p	t	p	t	p
2	0.03	8	80.07	20	159.61
4	0.08	9	134.21	30	161.01
5	7.91	10	147.81	p_a	161.44
6	16.81	12	154.41		
7	32.01	15	157.21		

195°C Run 12 1st t = 0 interruption 5.0mg

t	p	t	p	t	p
5	0.10	65	9.02	160	130.68
8	0.92	70	10.76	170	141.48
10	1.28	80	14.55	180	150.92
15	1.37	90	21.28	190	158.72
20	1.37	100	31.93	200	164.71
25	1.41	110	46.59	210	170.05
30	1.49	120	65.41	220	173.93
35	1.84	130	84.89	240	181.17
40	2.62	135	93.80	260	184.32
45	3.74	140	102.98	280	186.22
50	4.86	145	110.19	p_a	186.50
55	6.12	150	118.10		
60	7.51	155	124.42		

195°C Run 13 Irradiated (2nd 15000 r) 5.0mg

t	p	t	p	t	p
2	0.01	8	121.54	15	178.82
4	0.02	9	152.53	20	180.77
5	3.22	10	165.87	25	180.84
6	23.17	11	171.69	p_a	181.00
7	73.04	13	176.65		

195°C Run 14 Irradiated (2nd 15000r 2nd t = 0 interruption) 5.0mg

t	p	t	p	t	p
10	0.24	65	8.26	165	128.12
20	0.55	70	10.66	180	138.00
30	0.81	80	17.44	200	146.11
35	1.09	90	28.32	220	151.07
40	1.91	100	41.01	240	153.22
45	2.95	110	55.83	260	156.11
50	3.72	120	71.69	p_a	165.10

55	5.03	135	94.55		
60	6.71	150	113.94		

195°C	Run 15		Irradiated (3rd 15000 r)		5.0mg
t	p	t	p	t	p
4	6.25	8	119.51	20	156.57
5	26.73	9	129.96	30	160.87
6	69.33	11	142.10	50	162.58
7	102.09	14	149.21	p_a	163.01

195°C	Run 16	Irradiated (3rd 15000r, 3rd t = 0 interruption)			5.0mg
t	p	t	p	t	p
5	0.10	70	33.14	140	130.07
10	0.19	80	48.98	150	135.09
20	1.02	90	65.13	160	139.15
30	2.24	100	80.61	180	146.88
40	4.26	110	95.36	200	150.87
50	10.15	120	106.69	p_a	155.22
60	20.62	130	120.36		

195°C	Run 17		Irradiated (4th 15000 r)		5.0mg
t	p	t	p	t	p
2	0.03	6	56.16	11	113.99
3	0.06	7	87.94	15	114.90
4	4.43	8	103.08	25	116.22
5	20.13	9	103.78	p_a	117.01

195°C	Run 18	Irradiated (4th 15000 r, 4th t = 0 interruption)			4.3mg
t	p	t	p	t	p
10	0.01	70	3.24	140	22.04

20	0.02	80	5.49	160	24.36
30	0.06	90	8.61	180	25.96
40	0.29	100	12.35	p_a	29.95
50	0.84	110	15.65		
60	1.77	120	18.15		

TABLE 6.9

190°C	Run 1		Unirradiated blank		5.0mg pellet
t	p	t	p	t	p
10	0.02	110	22.41	210	121.44
20	0.04	120	31.12	220	128.74
30	0.05	130	40.85	230	135.87
40	0.09	140	50.79	240	141.26
50	0.31	150	61.87	251	146.99
60	1.04	160	72.19	270	155.81
70	2.55	170	83.03	280	157.78
80	5.23	180	93.60	290	158.63
90	9.31	190	103.61	p_f	160.00
100	15.15	200	112.79	p_a	155.00

190°C	Run 2		50r		4.9mg pellet
t	p	t	p	t	p
5	0.05	75	8.50	125	111.94
10	0.07	79	13.57	132	121.13
15	0.09	82	18.77	139	127.34
20	0.13	85	25.14	147	133.12
25	0.17	88	32.31	158	140.91
30	0.23	91	40.17	169	148.52
35	0.28	94	47.63	180	154.08
40	0.37	97	55.81	190	158.54
45	0.50	100	63.37	200	159.90
50	0.78	103	70.37	210	160.00
55	1.27	106	77.24	p_f	160.00
60	1.83	110	85.20	p_a	159.10
65	2.83	115	95.99		
70	4.80	120	104.96		

190°C	Run 3		250r		4.9mg pellet
t	p	t	p	t	p
5	0.02	66	25.65	135	136.00
10	0.06	70	29.04	140	140.68
15	0.09	75	33.91	150	147.89
20	0.16	80	40.02	160	152.25
25	0.39	85	47.17	170	155.01
30	1.22	90	55.84	180	156.21
34	2.45	95	65.73	190	157.53
38	4.32	100	76.93	200	157.80
42	6.63	105	88.21	210	159.00
46	9.52	110	99.47	220	159.51
50	12.75	115	107.90	p_f	160.00
54	15.94	120	117.30	p_a	152.20
58	19.16	125	124.49		
62	22.36	130	131.21		

190°C	Run 4		500r		5.0mg pellet
t	p	t	p	t	p
5	0.04	38	47.63	150	108.04
10	0.48	43	52.05	160	113.55
13	1.66	50	58.44	170	119.88
15	3.82	60	64.25	180	125.51
17	7.15	70	68.68	190	130.54
19	11.35	80	72.38	210	140.98
21	16.05	90	76.45	230	148.98
23	20.56	100	80.86	250	154.03
25	25.38	110	85.59	270	156.28
27	29.64	120	90.35	290	158.55
30	35.83	130	96.00	p_f	160.00
33	40.14	140	101.99	p_a	159.50

190°C	Run 5		5000r		5.0mg pellet
t	p	t	p	t	p
5	0.21	24	49.37	80	124.77

7	0.59	27	54.04	85	131.49
9	1.20	30	56.85	90	138.40
11	3.62	35	60.58	95	143.71
13	9.67	40	65.29	100	148.81
15	18.93	45	70.58	105	151.29
16	24.18	50	76.90	110	154.44
17	28.81	55	83.47	120	157.55
18	33.05	60	91.18	130	159.46
19	36.89	65	99.11	140	159.72
20	40.23	70	108.10	p_f	160.00
22	45.45	75	116.24	p_a	166.20

190°C Run 6 15000r 4.4mg pellet

t	p	t	p	t	p
4	0.94	18	71.42	75	141.32
5	4.67	24	77.22	90	148.51
6	17.72	30	81.76	105	153.63
7	38.37	37	91.23	120	156.23
8	49.21	43	99.43	p_f	160.00
9	55.20	49	108.95	p_a	134.65
11	61.88	55	118.45		
14	66.80	64	129.08		

190°C Run 7 1.0 M r. 4.6mg pellet

t	p	t	p	t	p
1	0.02	10	107.84	60	156.15
2	0.02	15	120.99	78	160.00
3	44.75	20	129.14	80	160.00
3.75	66.97	25	135.19	90	160.00
4.5	77.94	30	139.79	p_f	160.00
6	91.62	40	147.31	p_a	169.99
8	101.33	50	152.41		

TABLE 6.10

Induction period series. Runs 1 - 5 50r					
165°C	5.7mg	175°C	6.1mg		
t	p	t	p	t	p
25	0.24	10	0.06	p_a	182.85
30	0.48	15	0.24	185°C	4.8mg
35	0.80	18	0.48	5	0.04
40	1.26	21	0.83	8	0.05
44	1.76	24	1.39	10	0.16
p_a	188.10	27	2.17	12	0.39
170°C	6.4mg	p_a	178.06	14	0.74
20	0.35	180°C	5.9mg	16	1.27
25	0.79	15	0.69	18	2.20
28	1.18	17	1.17	p_a	130.73
31	1.70	19	1.92		
33	2.15	21	2.94		
p_a	192.00	23	4.38		

Acceleratory period		Split run	Run 6	50r	11.0mg pellet
t	p	t	p	t	p
160.4°C		20	52.79	11	93.70
10	37.67	25	55.61	12	95.05
15	38.01	30	58.70	13	96.17
20	38.50	35	61.95	14	97.49
25	39.01	175.3°C		15	99.13
30	39.83	8	68.90	185.0°C	
35	40.61	10	70.71	8	119.00
40	41.34	12	71.68	9	121.61
45	42.48	14	73.93	10	124.08
50	43.50	16	76.31	11	126.62
55	44.43	18	77.98	12	128.79
170.0°C		20	80.29	13	131.80
10	48.09	180.2°C		14	133.95
15	50.45	10	93.42	p_a	370.63

Decay period		Split-run		Run 7	50r 4.4mg pellet
t	p	t	p	t	p
190°C		14	52.60	172°C	
40	1.10	16	52.81	6	60.37
70	10.92	18	52.90	8	60.84
86	25.25	20	53.13	10	61.22
94	36.41	23	53.74	12	61.75
102	47.51	26	54.27	14	62.57
157°C		29	54.88	16	63.26
24	48.66	32	55.30	18	63.92
28	49.02	167°C		182°C	
32	49.68	6	55.22	9	72.22
36	50.04	8	55.57	10	72.53
40	50.26	10	55.80	11	73.17
44	51.18	12	56.23	14	74.87
47	51.48	14	56.89	16	75.49
162°C		16	57.55	18	76.44
6	51.48	18	57.86	20	76.89
8	51.67	20	58.26	22	77.48
10	51.97	22	58.82	24	77.80
12	52.34	24	59.05	p_a	98.01

Induction period series		Runs 8 - 12		15000r	
t	p	t	p	t	p
140.4°C	4.7mg	55	0.80	20	0.08
18	0.17	60	1.13	25	0.39
20	0.40	65	1.49	29	0.90
22	0.70	p_a	129.22	32	1.38
24	1.09	131.7°C	6.9mg	35	1.94
26	1.52	30	0.16	p_a	169.45
28	2.02	35	0.55	145.5°C	4.5mg
p_a	149.01	38	0.91	15	0.18
126.0°C	4.4mg	41	1.32	19	0.82
35	0.07	44	1.76	20	1.21
40	0.15	47	2.33	22	1.87
45	0.30	p_a	215.00	p_a	137.00
50	0.53	135.7°C	5.8mg		

175°C		Run 13		15000r	4.9mg pellet
t	p	t	p	t	p
5	0.04	26	42.71	105	106.98
6	0.27	30	46.49	110	110.73
7	0.72	35	49.87	115	114.38
8	1.38	40	52.59	120	117.03
9	2.24	45	55.50	130	123.62
10	3.60	50	58.26	140	127.83
11	5.21	55	61.67	150	133.35
12	7.46	60	65.24	170	141.06
13	10.39	65	69.15	180	144.98
14	13.70	70	74.15	200	150.60
15	17.41	75	79.43	210	152.19
16	21.03	80	85.15	230	154.99
17	24.61	85	90.01	250	158.00
19	30.88	90	94.44	270	159.18
21	35.31	95	99.25	p_f	160.00
23	38.88	100	103.76	p_a	162.20

Acceleratory period		Split- run	Run 14	15000r	11.0mg pellet
t	p	t	p	t	p
130°C		15	13.96	10	25.35
200	8.88	19	14.21	12	25.64
114.6°C		23	14.60	14	26.04
7	11.14	27	14.90	16	26.22
11	11.26	31	15.29	18	26.70
15	11.30	125.0°C		20	27.10
21	11.47	7	20.29	22	27.43
27	11.73	11	20.69	150°C	
33	11.86	15	21.12	30	58.11
39	12.18	19	21.76	60	67.84
45	12.38	23	22.18	80	73.91
51	12.69	27	22.69	100	79.54
120.7°C		30	23.31	110	81.04
7	13.35	130.0°C		140	82.03
11	13.73	7	24.91	p'_a	86.00

Decay period Split-run Run 15 15000r 5.0mg pellet

t	p	t	p	t	p
160°C		11	77.84	14	97.49
140	56.15	12	78.58	190°C	
144	58.90	13	79.46	1	96.83
148	60.49	14	80.71	3	98.05
152	62.56	15	81.31	5	101.41
154	64.01	180°C		7	106.58
157	65.67	1	80.01	8	108.52
159	65.88	3	81.68	9	110.79
161	66.77	5	85.04	10	111.88
170°C		7	88.12	11	112.87
1	68.73	8	89.29	12	114.14
3	69.93	9	91.21	13	115.19
5	72.16	10	92.65	14	116.64
7	74.20	11	93.84	210°C	
8	75.00	12	95.00	p_a	127.00
10	76.80	13	96.11		

110°C 5.0 M r. Run 16 4.6mg pellet

t	p	t	p	t	p
10	0.02	65	61.72	140	134.98
20	0.02	70	71.98	150	138.53
25	0.56	75	80.68	160	141.02
30	3.61	80	87.52	170	143.66
35	8.19	85	96.11	180	146.07
40	14.27	90	101.39	195	148.68
45	21.54	100	111.59	210	150.83
50	31.16	110	119.68	p_f	160.00
55	41.36	120	126.31	p_a	140.00
60	51.73	130	131.08		

185°C		Run 17	15000 r.	4.4mg pellet	
t	p	t	p	t	p
3	0.02	19	46.80	70	120.59
5	0.13	23	49.90	75	130.05
6	0.87	27	53.81	80	139.67
7	2.49	31	57.26	85	146.48
8	6.53	35	61.06	90	153.22
9	15.36	40	66.13	95	156.79
10	24.42	45	71.37	101	161.44
11	30.10	50	79.06	110	164.89
12	34.23	55	86.99	p_a	166.04
14	39.88	60	97.84		
16	43.32	65	108.36		

185°C		Run 18	15000 r	11.0mg pellet	
t	p	t	p	t	p
1	0.01	11	51.48	32	123.67
2	0.06	12	63.92	37	127.50
3	0.12	13	74.24	43	134.13
4	1.16	14	82.01	50	142.28
5	3.00	15	87.98	60	162.71
6	4.72	16	93.40	65	173.93
7	7.03	18	101.41	70	187.92
8	12.15	20	107.48	75	204.14
9	22.39	23	113.75	80	251.21
10	36.88	27	118.94	p_a	489.52

TABLE 6.11

165°C		Run 1	Powder	15000r.	4.8mg
t	p	t	p	t	p
5	0.13	30	53.77	80	130.68
10	1.73	33	67.28	100	137.71
15	4.01	37	82.06	130	146.62

18	6.64	42	95.71	p_f	160.00
21	12.18	49	107.55	p_a	161.53
24	23.08	60	120.07		
27	38.30	70	126.28		

165°C Run 2 Pellet 15000r 4.3mg pellet					
t	p	t	p	t	p
5	0.03	36	40.61	135	91.21
8	1.26	41	45.11	145	98.89
10	1.60	46	48.22	155	106.48
12	2.80	52	50.36	165	111.21
14	4.45	60	52.70	175	117.40
16	6.84	68	55.50	185	121.26
18	9.95	76	58.12	205	126.84
20	13.62	85	60.20	240	132.94
22	17.81	95	64.50	p_f	160.00
25	23.58	105	69.22	p_a	153.67
28	29.02	115	76.11		
32	35.50	125	83.32		

165°C Run 3 Pelleted irradiated powder 15000r 5.5mg pellet					
t	p	t	p	t	p
5	0.01	45	28.65	135	107.18
10	0.20	50	35.13	150	117.31
15	0.68	57	42.71	165	125.44
20	1.41	65	49.26	180	132.81
25	3.10	75	56.75	200	140.03
30	7.47	90	66.64	240	149.00
35	14.59	105	78.87	p_f	160.00
40	22.23	120	92.59	p_a	174.21

TABLE 6.12

160° ± 2°C		15000r		6.0mg pellet	
t	dp/dt	t	dp/dt	t	dp/dt
5	0.03	35	1.13	70	0.48
10	0.05	40	1.36	80	0.42
15	0.10	45	1.34	95	0.39
20	0.20	50	1.10	115	0.36
25	0.34	55	0.74	140	0.34
30	0.67	60	0.60		

TABLE 7.1

195°C	2 hrs	X-irradiated		Run 1	6.3mg pellet
t	p	t	p	t	p
5	0.27	19	45.32	77	139.12
7	0.92	25	51.66	85	150.63
9	3.78	35	56.88	95	157.22
10	8.39	45	65.91	105	159.83
11	15.98	52	76.02	p_f	160.00
12	23.27	59	92.58	p_a	210.10
13	28.99	65	108.40		
15	36.90	71	125.62		

195°C	Unirradiated blank		Run 2		6.1mg pellet
t	p	t	p	t	p
10	0.01	60	7.85	95	112.74
20	0.03	65	14.04	102	131.31
30	0.09	70	24.20	110	144.53
40	0.52	75	38.88	120	153.72
45	1.16	80	57.06	137	159.20
50	2.40	85	76.55	p_f	160.00
55	4.40	90	96.38	p_a	193.40

175°C	30 mins	X-irradiated		Run 3	5.0mg
t	p	t	p	t	p
10	0.07	55	41.67	120	119.56
15	0.33	60	52.24	135	128.55
20	0.60	65	61.28	150	134.91
25	1.06	70	70.25	180	145.96
30	2.21	75	77.23	200	151.01
35	5.52	80	84.62	p_f	160.00
40	11.92	90	96.37	p_a	201.12
45	20.77	100	105.60		
50	31.14	110	113.23		

175°C		Unirradiated blank		Run 4	5.0mg
t	p	t	p	t	p
10	0.02	100	7.68	190	118.49
20	0.03	110	14.57	200	125.62
30	0.04	120	24.81	210	131.94
40	0.06	130	38.23	225	140.20
50	0.10	140	53.36	240	144.88
60	0.26	150	69.30	260	148.64
70	0.67	160	83.96	280	150.02
80	1.66	170	97.14	p_f	160.00
90	3.74	180	108.25	p_a	198.20

TABLE 7.2

175°C	Reproducibility series		30mins	X-irradiated	Run 1 5.0mg
t	p	t	p	t	p
10	0.05	60	30.01	120	103.23
20	0.31	65	37.89	135	114.03
30	0.73	70	45.90	150	122.21
40	3.11	80	60.64	170	134.37
45	7.14	90	73.33	190	144.10
50	14.06	100	84.33	p_f	160.00
55	21.75	110	96.57	p_a	198.11

175°C	Run 2				5.0mg
t	p	t	p	t	p
10	0.06	60	32.53	110	98.85
20	0.30	65	45.37	120	107.60
30	0.83	70	49.11	130	114.79
35	1.78	75	56.27	145	124.92
40	4.47	80	64.43	160	132.50
45	9.19	85	70.25	185	142.18
50	16.14	90	77.78	p_f	160.00
55	23.82	100	89.02	p_a	189.10

175°C	Run 3				5.0mg
t	p	t	p	t	p
10	0.04	60	33.97	110	99.45
20	0.29	65	42.41	120	108.58
30	0.82	70	51.50	130	114.64
35	1.89	75	58.58	145	123.24
40	4.52	80	66.58	160	130.67
45	9.41	85	72.49	185	142.39
50	16.33	90	79.50	p_f	160.00
55	24.71	100	90.39	p_a	202.10

TABLE 7.3

175°C	Run 1	30 mins	X-irradiated		5.0mg
t	p	t	p	t	p
10	0.09	45	31.61	100	93.91
15	0.62	48	36.42	110	102.70
20	1.35	52	42.47	120	110.47
25	3.05	56	48.16	140	124.92
30	7.50	61	53.83	165	141.91
33	11.51	67	60.69	p_f	160.00
36	16.49	74	68.23	p_a	193.80
39	21.91	82	76.51		
42	27.04	90	84.80		

TABLE 7.4

175°C	Run 1	Unirradiated blank			5.0mg
t	p	t	p	t	p
10	0.02	100	7.68	190	118.49
20	0.03	110	14.56	200	125.62
30	0.04	120	24.81	210	131.94
40	0.06	130	38.23	225	140.20
50	0.10	140	53.36	240	144.88
60	0.26	150	69.30	260	148.64
70	0.67	160	83.96	280	150.20
80	1.66	170	97.14	p_f	160.00
90	3.74	180	108.25	p_a	198.21

175°C	Run 2	2 mins X-irradiated			5.0mg
t	p	t	p	t	p
10	0.04	90	23.87	175	114.53
20	0.08	100	36.20	190	123.58
30	0.13	110	48.48	210	132.61
40	0.26	120	61.15	220	144.88
50	0.78	130	73.07	260	148.64
61	2.94	140	83.95	280	150.02
70	7.04	150	93.99	p_f	160.00
80	13.97	160	102.70	p_a	163.71

175°C	Run 3	5 mins X-irradiated			5.0mg
t	p	t	p	t	p
10	0.02	80	40.50	155	123.07
20	0.06	90	56.98	170	129.79
30	0.20	100	71.68	190	137.31
40	0.70	110	84.78	210	143.00
50	3.34	120	96.33	240	149.32
60	11.23	130	104.85	p_f	160.00
70	24.35	140	113.66	p_a	169.10

175°C	Run 4	10 mins X-irradiated			5.4mg
t	p	t	p	t	p
10	0.03	80	51.42	160	130.74
20	0.13	90	65.82	180	140.59
30	0.39	100	78.86	210	150.52
40	1.90	110	90.21	p_f	160.00
50	7.77	120	99.73	p_a	223.00
60	19.36	130	109.16		
70	34.20	145	121.13		

175°C	Run 5	15 mins X-irradiated			5.0mg
t	p	t	p	t	p
10	0.05	60	30.01	120	103.23
20	0.31	65	37.89	135	114.03
30	0.73	70	45.90	150	122.21
40	3.11	80	60.64	170	134.37
45	7.14	90	73.33	190	144.10
50	14.06	100	84.33	p_f	160.00
55	21.75	110	96.57	p_a	188.80

175°C	Run 6	30 mins X-irradiated			5.0mg
t	p	t	p	t	p
10	0.07	55	41.67	120	119.56
15	0.33	60	52.24	135	128.55
20	0.60	65	61.28	150	134.91
25	1.01	70	70.25	180	145.96
30	2.21	75	77.23	200	151.01
35	5.52	80	84.62	p_f	160.00
40	11.92	90	96.37	p_a	201.12
45	20.77	100	105.60		
50	31.14	110	113.23		

175°C	Run 7	1 hour X-irradiated			5.0mg
t	p	t	p	t	p
5	0.02	37	31.70	80	112.01
10	0.30	40	41.64	90	118.41
15	0.93	43	50.51	105	125.49
20	1.54	47	62.69	130	136.14
25	3.92	51	72.69	160	145.32
28	7.67	56	82.42	p_f	160.00
31	13.88	62	91.83	p_a	198.60
34	22.24	70	103.08		

175°C	Run 8	3 hours X-irradiated			5.5mg
t	p	t	p	t	p
5	0.02	29	41.86	65	115.30
9	0.83	31	49.47	75	123.11
13	1.68	34	60.11	86	129.87
17	3.19	37	69.24	100	137.38
20	7.74	41	79.61	120	144.41
23	17.14	45	88.60	p_f	160.00
25	25.20	50	98.40	p_a	231.70
27	33.46	56	106.30		

175°C	Run 9	16 hours X-irradiated			5.0mg
t	p	t	p	t	p
5	0.09	16	16.20	42	97.27
6	0.58	18	25.14	50	107.27
7	1.16	20	34.17	60	114.40
8	1.67	22	42.82	70	118.45
9	2.15	25	54.84	80	121.07
10	2.62	28	65.63	p_f	160.00
12	4.03	32	77.29		
14	8.13	36	86.78		

TABLE 7.5

Varying temperature series.		30 mins.	X-irradiated		Runs 1 - 7
t	p	t	p	t	p
150°C	4.3mg	36	1.11	p_a	187.20
40	0.42	39	1.26	175°C	5.1mg
45	0.66	p_a	157.11	5	0.03
50	0.74	165°C	5.0mg	10	0.18
55	0.88	22	0.73	15	1.14
60	1.04	24	0.88	20	2.25
65	1.17	25	0.97	25	4.79
70	1.38	26	1.08	30	12.52
p_a	134.11	27	1.13	33	19.35
155°C	4.9mg	28	1.19	p_a	207.10
30	0.45	29	1.28	180°C	5.0mg
35	0.67	30	1.41	5	0.01
40	0.92	p_a	174.11	10	0.42
43	1.09	170°C	5.1mg	15	1.75
46	1.22	10	0.09	18	3.34
49	1.38	15	0.59	21	7.03
52	1.55	16	0.75	24	14.05
p_a	175.94	17	0.90	p_a	171.51
161°C	4.8mg	18	1.07		
10	0.02	19	1.25		
20	0.27	20	1.40		
25	0.54	21	1.55		
30	0.84	22	1.73		
33	1.00	24	2.11		

165°C		Run 8			5.5mg
t	p	t	p	t	p
10	0.03	75	30.65	163	82.28
20	0.49	79	33.99	171	87.87
25	0.86	84	38.25	179	90.93
30	1.31	89	41.82	190	95.94
35	1.90	93	44.51	200	100.30
40	2.91	99	48.04	210	104.51

45	4.45	107	53.09	220	108.44
50	7.48	115	57.07	230	112.14
55	11.74	123	61.48	240	116.01
59	15.44	131	66.39	280	130.07
63	19.47	139	70.12	p_f	160.00
67	23.12	147	74.61	p_a	215.30
71	27.01	155	79.72		

170°C		Run 9			5.0mg
t	p	t	p	t	p
5	0.01	47	18.26	97	75.33
10	0.04	49	21.28	105	81.64
15	0.32	51	24.15	115	89.64
20	0.86	54	28.72	125	96.77
25	1.40	57	33.49	135	103.05
28	1.92	60	37.59	145	109.21
31	2.74	63	41.47	155	114.45
34	4.12	67	46.39	170	122.03
37	6.10	71	51.46	195	133.66
39	7.90	75	55.23	p_f	160.00
41	10.06	80	60.12	p_a	174.96
43	12.67	85	64.78		
45	15.42	90	69.19		

175°C		Run 10			5.0mg
t	p	t	p	t	p
10	0.10	39	20.27	72	69.48
15	0.60	40	21.90	76	74.16
20	1.17	41	23.79	80	79.48
25	2.39	42	25.59	85	85.44
28	4.21	43	27.33	90	91.57
30	6.30	44	29.27	95	96.32
31	7.67	46	32.80	100	101.72
32	9.05	48	36.14	105	105.97

33	10.40	51	40.63	110	110.73
34	11.76	54	44.96	115	114.23
35	13.43	57	49.22	120	118.24
36	15.00	60	53.66	p_f	160.00
37	16.73	64	58.86	p_a	208.91
38	18.45	68	65.50		

180°C		Run 11			5.5mg
t	p	t	p	t	p
5	0.02	29	22.57	66	80.57
10	0.50	30	25.07	71	86.30
12	0.84	32	29.74	76	92.24
14	1.24	34	34.19	81	97.66
16	1.74	36	38.31	87	104.06
19	3.20	38	41.98	93	109.43
21	5.15	40	45.38	100	115.43
22	6.54	42	48.62	107	120.24
23	8.23	45	52.99	115	125.32
24	10.46	48	57.27	125	130.44
25	12.68	51	61.04	135	135.30
26	15.18	54	65.05	p_f	160.00
27	17.66	57	68.91	p_a	258.10
28	20.18	61	73.90		

185°C		Run 12			4.9mg
t	p	t	p	t	p
5	0.02	27	40.25	66	110.75
8	0.25	28	42.81	70	115.60
10	0.84	30	47.84	74	119.82
12	1.50	32	52.21	79	125.31
14	2.58	34	56.65	84	129.64
16	4.92	36	60.71	89	133.71
18	9.93	38	64.66	96	137.79
19	12.97	40	68.67	104	142.04

20	15.92	43	74.17	115	146.36
21	19.02	46	79.76	130	151.13
22	22.87	49	85.13	140	154.12
23	26.86	52	90.55	p_f	160.00
24	30.80	55	94.90	p_a	181.60
25	34.23	58	99.79		
26	37.37	62	105.30		

190°C		Run 13			5.5mg
t	p	t	p	t	p
5	0.03	24	47.89	46	108.67
8	0.73	25	51.41	48	110.43
10	1.66	26	54.73	50	113.89
12	6.07	27	58.20	54	118.96
13	8.18	28	61.73	56	122.56
14	10.37	29	64.88	60	127.86
15	13.18	30	68.37	64	131.44
16	16.62	31	71.33	69	136.13
17	20.86	32	73.48	75	138.60
18	25.39	34	79.28	82	143.46
19	29.74	36	84.42	90	147.51
20	33.69	38	89.68	100	150.46
21	37.49	40	94.44	p_f	160.00
22	41.03	42	98.42	p_a	230.85
23	44.38	44	102.74		

TABLE 7.6

180°C	Run 1	30 mins X-irradiated			5.8mg
t	p	t	p	t	p
3	0.04	21	45.67	44	122.70
5	0.08	22	52.63	46	128.20
7	1.62	23	58.37	Interruption	
8	4.10	24	64.30	49	130.32
9	7.96	Interruption		52	135.21
10	13.74	26	64.25	56	142.72
11	21.09	28	64.75	60	149.66

Interruption		30	66.81	67	158.52
13	22.02	32	73.66	75	166.37
14	22.27	34	83.61	90	178.74
16	23.06	36	93.75	p_a	232.10
18	26.00	38	101.15		
20	34.07	40	108.73		

TABLE 7.7

175°C	Run 1		Unirradiated blank		5.0mg
t	p	t	p	t	p
20	0.08	140	32.13	242	117.22
40	0.16	150	40.09	255	124.86
60	0.64	160	48.63	270	131.86
70	1.47	170	57.84	290	139.38
80	3.06	180	67.37	320	144.15
90	5.59	190	77.08	360	149.17
100	8.99	200	86.19	420	153.81
110	13.22	210	94.81	p_f	160.00
120	18.50	220	102.52	p_a	222.10
130	24.99	230	109.47		

175°C	Run 2	t = 0	2hrs X-irradiated		5.0mg
t	p	t	p	t	p
10	0.79	50	59.59	95	114.99
15	2.56	55	67.73	100	119.67
20	7.49	60	75.96	110	127.48
25	16.08	65	82.54	120	133.96
28	21.84	70	89.50	160	149.90
31	26.98	75	94.79	p_f	160.00
35	34.20	80	100.75	p_a	187.90
40	43.09	85	105.48		
45	51.86	90	111.26		

175°C Run 3 End I.P. 2 hrs. X-irradiated 5.0mg

t	p	t	p	t	p
10	0.01	75	4.25	105	102.81
20	0.02	78	7.48	110	106.18
30	0.08	81	12.91	120	113.55
40	0.21	84	24.09	135	121.56
50	0.64	87	39.91	150	128.68
60	0.89	90	56.63	170	133.21
65	1.00	93	69.59	200	137.38
Interruption		96	81.98	p_f	160.00
70	1.04	100	93.54	p_a	192.70

175°C Run 4 $\alpha = 0.25$ 2 hrs X-irradiated 5.0mg

t	p	t	p	t	p
20	0.06	173	51.81	210	112.02
90	4.67	176	57.43	217	117.41
130	23.12	179	62.99	230	125.21
150	39.10	182	69.04	250	133.03
Interruption		185	74.94	280	140.35
155	40.05	188	80.79	310	143.28
158	40.19	191	85.85	p_f	160.00
161	41.58	195	92.82	p_a	174.90
165	43.05	200	100.77		
169	46.01	205	106.36		

175°C Run 5 $\alpha = 0.48$ 2 hrs X-irradiated 4.2mg

t	p	t	p	t	p
40	0.19	198	78.89	239	128.26
90	6.11	202	79.88	247	133.55
120	19.07	207	85.05	262	140.52
150	42.01	212	95.33	282	146.51
185	75.23	217	104.08	312	152.65

Interruption		222	110.72	352	156.09
190	77.34	227	116.95	p_f	160.00
194	78.15	232	122.37	p_a	110.21

175°C Run 6 α = 0.80 2 hrs X-irradiated 5.0mg

t	p	t	p	t	p
40	0.18	260	126.70	330	145.20
100	9.21	265	127.75	360	152.03
150	41.91	275	128.53	390	154.04
210	96.71	285	130.41	p_f	160.00
250	124.76	300	136.92	p_a	192.00
Interruption		315	141.59		

TABLE 7.8

165°C Water interruptions. 30 mins X-irradiated Uninterrupted blank 5.0mg

t	p	t	p	t	p
20	0.88	90	49.31	180	92.89
30	1.27	100	56.57	200	101.00
40	3.40	110	61.91	220	108.52
50	8.96	120	66.47	240	115.18
60	19.48	137	75.90	260	120.17
70	31.38	150	80.89	280	124.19
80	41.60	165	86.96	p_a	202.20

165°C Run 2 t = 0 (30 secs) 4.8mg

t	p	t	p	t	p
10	0.02	70	17.02	125	47.82
20	0.13	75	21.27	135	51.03
30	0.34	80	25.23	145	53.41
40	0.77	85	29.02	160	56.80
50	2.60	95	35.19	180	61.37

60	8.57	105	40.21	p_a	133.42
65	12.84	115	44.39		

165°C	Run 3	0.5 I.P.	(30 secs)		4.8mg
t	p	t	p	t	p
15	0.04	75	5.68	180	31.33
Interruption		85	9.64	210	34.85
25	0.06	95	13.54	240	37.52
35	0.10	105	16.94	280	39.29
45	0.21	120	21.00	p_a	111.26
55	0.80	140	25.42		
65	2.45	160	28.51		

165°C	Run 4	End I.P.	(30 secs)		5.0mg
t	p	t	p	t	p
30	1.34	90	5.52	200	35.80
Interruption		100	8.18	220	40.29
40	1.35	110	11.52	240	44.40
50	1.37	120	14.71	280	50.40
60	1.47	140	20.19	p_a	159.99
70	2.22	160	25.74		
80	3.59	180	30.84		

165°C	Run 5	$\alpha = 0.15$		(30 secs)	5.0mg
t	p	t	p	t	p
10	0.01	Interruption		135	23.28
20	0.34	70	19.01	150	24.87
30	0.93	80	19.04	180	28.27
40	2.92	90	19.24	210	32.45
50	8.21	100	19.95	240	37.24
60	15.27	110	20.84	280	40.80
65	19.00	120	21.74	p_a	135.21

165°C Run 6 $\alpha = 0.25$ (30 secs) 4.8mg

t	p	t	p	t	p
20	0.07	110	41.94	180	51.08
50	7.91	120	42.52	200	55.00
80	40.99	130	43.46	220	59.25
Interruption		140	44.56	240	63.66
90	41.57	150	45.88	280	71.37
100	41.66	160	47.43	p_a	102.31

165°C Run 7 $\alpha = 0.50$ (30 secs) 5.0mg

t	p	t	p	t	p
20	0.71	140	67.05	225	74.08
50	7.01	150	67.17	240	77.08
80	39.47	160	67.38	270	85.11
100	55.88	170	67.68	300	95.95
120	66.90	180	68.24	p_a	162.17
Interruption		195	69.43		
130	66.99	210	71.52		

165°C Run 8 Unirradiated blank 5.0mg

t	p	t	p	t	p
30	0.02	210	0.76	395	20.88
60	0.04	240	1.71	420	28.57
90	0.05	270	3.34	450	35.63
120	0.06	300	5.96	480	44.82
150	0.13	330	9.61	p_a	204.29
180	0.31	360	14.17		

165°C Run 9 $t = 0$ (5 mins) 5.1mg

t	p	t	p	t	p
10	0.01	100	0.45	285	11.45

20	0.01	120	0.53	300	15.57
30	0.01	140	0.59	315	19.42
40	0.03	160	0.64	330	22.52
50	0.12	180	0.84	345	25.17
60	0.21	210	0.99	360	27.26
70	0.27	240	2.17	390	30.03
80	0.32	270	7.31	p_a	114.63

TABLE 7.9

175°C	Run 1		Irradiated powder		5.0mg pellet
t	p	t	p	t	p
10	0.13	57	50.39	161	131.85
15	0.74	65	58.63	180	138.16
20	1.62	75	68.65	210	145.00
25	3.48	85	78.56	240	148.79
30	8.26	95	87.28	280	152.11
35	15.24	105	95.30	p_f	160.00
40	24.22	115	104.07	p_a	200.31
45	32.88	125	111.19		
50	40.99	140	120.90		

175°C	Run 2		Irradiated pellet		7.0mg pellet
t	p	t	p	t	p
10	0.13	55	35.12	160	107.84
15	0.51	60	39.71	180	122.10
20	1.06	70	46.74	200	133.17
30	5.82	80	53.18	220	140.96
35	11.41	90	58.45	240	146.56
40	17.95	105	66.69	280	150.54
45	24.04	120	76.81	p_f	160.00
50	29.87	140	91.91	p_a	243.58

175°C Run 3 Pelleted irradiated powder 7.0mg pellet

t	p	t	p	t	p
10	0.02	60	28.18	150	105.71
15	0.15	65	34.07	160	111.21
20	0.41	70	39.71	170	116.66
25	0.71	80	49.25	180	122.70
30	1.20	90	58.01	200	131.43
35	2.40	100	66.05	220	137.65
40	4.58	110	75.19	240	143.41
45	8.45	120	82.68	280	151.07
50	14.29	130	91.14	p_f	160.00
55	21.25	140	98.02	p_a	244.36

TABLE 7.10

195°C Run 1 Unirradiated blank 5.1mg pellet

t	p	t	p	t	p
10	0.01	60	7.85	95	112.74
20	0.03	65	14.04	102	131.31
30	0.09	70	24.20	110	144.33
40	0.52	75	38.88	120	153.72
45	1.16	80	57.06	137	159.20
50	2.40	85	76.55	p_f	160.00
55	4.40	90	96.38	p_a	193.40

195°C Run 2 X-irradiated on brass 5.0mg pellet

t	p	t	p	t	p
4	0.07	18	45.01	69	120.39
5	0.32	22	49.16	73	130.85
6	0.65	27	51.70	77	139.74
7	1.00	33	55.53	81	146.46
8	1.72	38	59.15	85	150.53
9	3.81	43	64.01	92	153.75

10	10.91	48	69.11	100	156.82
11	22.03	53	78.11	110	156.33
12	28.95	57	87.26	120	157.61
13	33.57	61	97.63	p_f	160.00
15	39.84	65	109.04	p_a	192.90

$195^\circ C$	Run 3		X-irradiated on glass		5.2mg pellet
t	p	t	p	t	p
5	0.10	30	21.15	75	106.38
7	0.32	35	25.74	80	119.60
9	0.95	40	31.74	86	132.64
11	2.44	45	37.98	94	142.46
13	5.22	50	45.95	105	152.11
15	8.31	55	55.25	120	155.11
18	12.12	60	66.42	p_f	160.00
22	15.61	65	78.39	p_a	200.17
26	18.83	70	92.16		

TABLE 7.11

$164^\circ \pm 2^\circ C$		2 hours	X-irradiated		5.0mg pellet
t	dp/dt	t	dp/dt	t	dp/dt
15	0.01	75	0.22	125	0.36
20	0.01	80	0.24	130	0.34
25	0.02	85	0.31	140	0.31
30	0.02	90	0.34	150	0.28
35	0.03	95	0.37	170	0.24
45	0.05	100	0.40	190	0.19
50	0.07	105	0.42	210	0.16
60	0.10	110	0.42	250	0.13
65	0.15	115	0.41		
70	0.18	120	0.39		

TABLE 8.1

190°C	Run 1		Unirradiated blank		4.5mg pellet
t	p	t	p	t	p
10	0.02	110	12.78	210	132.42
20	0.03	121	23.16	220	139.29
30	0.05	130	34.18	230	145.39
40	0.06	140	48.01	240	149.50
50	0.09	150	63.08	250	153.12
60	0.16	160	77.82	260	157.84
70	0.42	170	92.20	270	159.26
80	1.04	180	104.63	280	160.00
90	2.94	190	115.22	p_f	160.00
100	6.59	200	124.19	p_a	177.69

190°C	Run 2		Low intensity lamp		4.1mg pellet
t	p	t	p	t	p
2	0.05	60	23.79	180	136.51
4	0.15	70	30.23	190	141.08
6	0.76	80	37.89	201	144.65
8	1.73	90	46.97	210	147.16
10	2.76	100	57.25	220	148.84
15	5.12	110	68.60	230	151.69
20	7.04	120	80.37	240	153.02
25	8.92	131	94.12	250	153.31
30	10.71	142	106.72	p_f	160.00
35	12.59	150	114.75	p_a	120.51
40	14.35	160	123.46		
50	18.69	172	132.31		

190°C	Run 3	High intensity lamp			4.5mg pellet
t	p	t	p	t	p
1	0.20	50	23.26	150	132.57
2	0.60	60	28.63	171	146.19
3	3.79	70	35.50	200	154.30
4	5.42	80	44.80	220	156.36
5	6.40	90	56.28	270	160.00
10	9.09	100	70.96	p_f	160.00
20	12.41	111	87.39	p_a	192.00
30	15.70	120	101.25		
40	19.19	130	114.30		

TABLE 8.2.

195°C	Run 1	Unirradiated blank			5.4mg
t	p	t	p	t	p
10	0.02	70	31.84	115	134.33
20	0.04	75	42.43	120	140.53
30	0.30	80	55.00	130	148.25
40	1.86	85	67.78	140	152.63
45	3.80	90	81.47	150	155.71
50	6.75	95	95.20	160	156.30
55	10.99	100	107.96	p_f	160.00
60	16.44	105	119.32	p_a	199.22
65	23.15	110	126.83		

195°C	Run 2	15 mins U.V. - irradiated			5.0mg
t	p	t	p	t	p
3	0.35	14	63.31	60	139.02
4	5.87	17	70.75	70	146.23
5	17.07	20	77.85	80	151.80
6	26.12	25	88.87	90	154.68
7	33.21	30	98.64	p_f	160.00
8	39.13	35	105.13	p_a	189.19

10	48.77	40	114.04		
12	56.50	50	126.25		

TABLE 8.3

190°C	Run 1	1.5 hrs U.V. - irradiated			4.6mg pellet
t	p	t	p	t	p
2	0.80	25	75.83	120	140.21
4	4.71	30	82.26	130	143.24
5	17.75	35	87.74	150	148.25
6	27.81	40	93.13	170	152.36
7	34.38	50	102.67	190	154.67
8	39.25	60	110.93	220	157.59
9	43.56	70	117.37	240	158.93
10	46.86	80	123.69	260	159.78
12	52.56	90	128.66	280	160.00
15	59.55	100	132.95	p_f	160.00
20	68.25	110	136.95	p_a	214.86

190°C			Run 2		4.6mg pellet
t	p	t	p	t	p
2	0.02	25	67.87	130	139.15
3	0.03	30	73.27	140	141.09
4	3.33	35	77.98	160	145.45
5	16.05	40	83.99	180	148.06
6	26.93	50	93.11	200	151.71
7	33.81	60	102.93	220	151.82
8	38.85	70	110.52	240	152.95
9	42.56	80	117.90	260	154.32
10	45.57	90	124.73	280	155.63
12	49.89	100	129.97	p_f	160.00
15	55.67	110	133.38	p_a	186.12
20	62.49	122	137.06		

175°C	Run 3	15 mins U.V. - irradiated			5.0mg
t	p	t	p	t	p
5	0.44	40	57.96	150	130.01
7	4.08	50	67.61	180	140.27
10	11.86	60	76.22	210	148.01
13	20.94	75	88.10	240	153.72
17	30.61	90	99.01	280	156.98
22	36.82	105	108.71	p_f	160.00
30	47.11	120	117.04	p_a	203.10

175°C		Run 4			5.0mg
t	p	t	p	t	p
5	0.46	25	44.03	121	119.86
7	4.44	30	50.26	150	132.08
8	8.33	38	58.62	180	142.21
9	12.24	46	66.35	210	150.00
10	15.56	55	74.21	220	151.12
12	21.37	65	82.04	240	155.22
14	26.19	75	89.35	270	156.21
17	31.92	90	100.27	p_f	160.00
21	38.41	105	110.12	p_a	197.70

175°C		Run 5			5.0mg
t	p	t	p	t	p
5	0.60	40	51.65	150	126.43
7	3.87	50	62.20	180	136.84
10	10.80	60	70.08	210	145.01
13	16.93	75	82.07	240	151.24
17	23.59	90	92.97	280	154.51
22	30.90	105	103.18	p_f	160.00
30	41.10	120	111.90	p_a	205.10

TABLE 8.4

175°C	Run 1		Unirradiated blank		5.0mg
t	p	t	p	t	p
15	0.03	150	11.97	320	107.12
30	0.03	165	18.03	340	113.56
45	0.07	180	25.40	360	118.67
60	0.13	200	36.84	390	123.33
75	0.30	220	49.95	420	126.94
90	0.78	240	64.13	450	129.04
105	1.85	260	78.77	p_f	160.00
120	4.02	280	89.48	p_a	189.91
135	7.30	300	99.17		

175°C	Run 2		2 secs U.V. - irradiated		5.0mg
t	p	t	p	t	p
10	0.01	110	18.94	260	122.28
20	0.05	120	24.85	280	131.27
30	0.21	135	34.86	300	138.16
40	0.62	150	45.66	330	144.90
50	1.56	165	57.25	360	149.33
60	2.85	180	68.84	390	152.95
70	4.53	195	80.31	420	154.65
80	6.75	210	91.24	p_f	160.00
90	9.88	225	101.40	p_a	217.10
100	13.94	240	110.90		

175°C	Run 3		10 secs U.V. -irradiated		5.0mg
t	p	t	p	t	p
10	0.05	90	37.28	200	117.94
20	0.40	100	45.66	220	126.83
30	1.50	110	54.86	240	134.39
40	3.82	120	62.78	270	142.05

50	7.76	135	75.38	300	146.95
60	13.60	150	86.84	330	150.32
70	20.71	165	96.78	p_f	160.00
80	29.06	180	106.45	p_a	194.30

175°C	Run 4	80 secs U.V. - irradiated			5.7mg
t	p	t	p	t	p
6	0.14	50	40.69	110	111.76
10	0.64	55	49.26	120	119.37
15	1.58	60	57.48	130	124.59
20	3.36	65	64.91	150	134.65
25	6.58	70	72.01	180	146.25
30	11.39	75	79.02	210	150.33
35	17.64	82	86.96	p_f	160.00
40	24.91	90	95.63	p_a	245.50
45	32.90	100	104.20		

175°C	Run 5	6 hrs U.V. - irradiated			5.0mg
t	p	t	p	t	p
3	0.01	20	57.59	90	131.62
4	0.96	25	68.05	120	141.84
5	4.98	32	79.74	150	148.93
6	11.79	40	91.23	p_f	160.00
8	22.98	50	102.19	p_a	169.21
11	34.48	60	111.51		
15	45.66	75	123.65		

175°C	Run 6	32 hrs U.V. - irradiated			5.0mg
t	p	t	p	t	p
3	0.05	12	65.21	75	131.09
4	5.97	17	74.51	90	139.08
5	24.53	25	85.33	120	150.23

6	36.94	35	96.88	150	153.16
7	44.98	45	105.20	p_f	160.00
9	55.26	60	118.89	p_a	161.00

TABLE 8.5

170°C	Run 1	Varying temperature series		15 secs U.V.-irradiated	5.0mg
t	p	t	p	t	p
10	0.03	30	0.68	p_f	160.00
15	0.12	35	1.08	p_a	214.70
20	0.25	40	1.70		
25	0.42	45	2.55		

175°C			Run 2		5.1mg
t	p	t	p	t	p
3	0.03	63	19.78	158	98.18
8	0.13	68	24.25	173	106.32
13	0.29	73	28.86	188	114.09
18	0.52	78	33.75	203	120.55
23	0.87	83	38.58	218	126.34
28	1.53	90	44.71	233	130.86
33	2.77	97	52.35	263	139.64
38	4.62	104	57.50	293	145.09
43	6.92	113	65.93	323	149.31
48	9.71	123	73.52	353	152.05
53	12.90	133	80.45	p_f	160.00
58	16.06	143	88.39	p_a	213.20

180°C			Run 3		6.0mg
t	p	t	p	t	p
10	0.10	65	37.50	150	103.10
15	0.36	70	44.30	165	109.22
20	0.98	75	49.30	180	114.48

25	2.25	80	54.20	200	120.83
30	4.37	86	59.75	220	125.70
35	7.35	93	65.75	240	130.25
40	11.34	100	71.85	270	135.04
45	16.24	108	77.94	300	139.10
50	21.62	118	85.12	330	142.90
55	27.49	128	91.35	p_f	160.00
60	33.18	139	97.20	p_a	256.00

185°C			Run 4		5.0mg
t	p	t	p	t	p
5	0.01	39	22.08	97	106.24
10	0.26	42	26.59	105	114.46
12	0.43	46	32.83	115	122.66
14	0.71	50	39.52	125	129.96
16	1.15	54	45.83	135	135.56
18	1.78	58	52.68	150	143.13
21	3.23	62	58.80	165	147.16
24	5.11	67	66.83	180	150.63
27	7.57	72	74.64	195	152.66
30	10.69	77	81.61	p_f	160.00
33	14.14	83	89.83	p_a	204.40
36	17.84	90	98.82		

190°C			Run 5		5.3mg
t	p	t	p	t	p
5	0.05	38	46.23	83	123.66
8	0.31	41	53.38	89	130.31
11	0.93	44	60.19	95	134.41
14	2.45	47	66.05	105	142.60
17	4.96	50	72.33	116	147.81
20	8.62	53	78.37	126	151.60
23	13.39	57	84.07	140	155.76
26	19.29	62	95.06	155	158.16

29	25.70	67	102.52	180	159.78
32	32.33	72	110.89	p_f	160.00
35	39.38	77	116.32	p_a	239.51

195°C		Run 6			5.0mg
t	p	t	p	t	p
5	0.05	28	39.47	65	125.01
8	0.42	30	45.48	70	132.37
10	1.09	32	51.60	75	138.75
12	2.41	34	56.76	82	144.29
14	4.63	37	65.82	90	150.53
16	7.63	40	74.51	100	154.45
18	11.41	43	82.68	110	156.73
20	16.14	46	90.42	p_f	160.00
22	21.46	50	98.06	p_a	190.50
24	27.13	55	108.67		
26	33.24	60	118.29		

TABLE 8.6

185°C	Run 1	15 secs U.V. - irradiated			5.0mg
t	p	t	p	t	p
5	0.03	55	32.27	120	112.36
10	0.22	60	39.69	126	118.58
15	0.74	65	46.36	132	121.35
20	2.45	70	53.68	140	128.39
23	4.07	75	61.27	150	133.69
26	6.24	80	67.62	160	138.57
29	9.01	85	75.03	170	143.84
32	12.57	90	82.37	180	146.13
34	14.62	95	87.87	200	149.99
36	17.30	100	94.72	220	151.50
Interruption		105	101.14	p_f	160.00
40	17.98	Interruption		p_a	249.94
45	19.83	110	102.74		
50	25.67	115	107.28		

185°C Run 2 5.0mg

t	p	t	p	t	p
8	0.09	60	43.95	120	106.11
Interruption		65	50.93	130	114.43
10	0.10	70	57.37	140	120.70
15	0.30	71	58.61	150	129.27
20	0.91	Interruption		160	134.68
25	2.98	76	59.23	175	142.14
30	6.03	80	63.37	195	150.31
35	10.62	85	70.35	215	153.40
40	16.27	90	74.93	p_f	160.00
45	22.88	95	79.65	p_a	204.58
50	29.63	103	89.14		
55	36.75	111	96.63		

TABLE 8.7

185°C Run 1 Interruption and Irradiation series. Unirradiated blank 5.0mg

t	p	t	p	t	p
10	0.01	100	23.61	170	122.23
20	0.02	107	31.97	181	131.06
30	0.06	114	41.80	195	140.77
40	0.15	121	52.94	210	147.16
50	0.55	128	64.56	235	151.82
60	1.57	135	76.92	275	157.88
70	4.00	142	87.62	p_f	160.00
80	8.21	150	98.82	p_a	218.05
90	14.43	160	111.88		

185°C Run 2 U.V. -irradiated at t = 0 5.0mg

t	p	t	p	t	p
5	0.50	19	54.69	58	122.48
7	3.84	22	65.12	68	129.66
9	9.88	25	73.50	80	138.37

11	18.14	29	83.33	95	143.34
13	28.15	34	92.11	p_f	160.00
15	37.57	40	102.16	p_a	229.35
17	46.32	48	111.58		

185°C	Run 3		0.5 I.P.		5.0mg
t	p	t	p	t	p
27	0.05	44	51.99	70	113.28
Interruption		46	59.99	77	122.28
32	0.70	48	67.22	85	128.17
34	4.69	50	73.77	95	134.51
36	12.11	53	82.53	110	141.99
38	22.16	56	89.98	125	147.20
40	33.09	60	97.25	p_f	160.00
42	43.45	65	105.79	p_a	212.40

185°C	Run 4		End I.P.		5.2mg
t	p	t	p	t	p
10	0.02	66	21.63	97	107.69
20	0.03	68	31.65	103	115.59
30	0.05	70	41.27	110	123.59
40	0.11	72	50.01	120	129.93
50	0.34	74	57.91	130	135.36
55	0.99	77	67.32	145	142.15
Interruption		80	75.86	160	146.95
60	1.29	84	85.97	p_f	160.00
62	5.32	88	94.63	p_a	241.20
64	12.41	92	100.44		

185°C	Run 5		α = 0.15		4.6mg
t	p	t	p	t	p
20	0.03	113	51.13	158	136.66
50	0.73	115	59.48	169	142.98
80	8.94	117	65.40	180	147.54
100	24.11	120	74.54	195	152.04
Interruption		123	81.83	210	153.94
105	24.88	127	90.61	p_f	160.00
107	28.89	132	99.00	p_a	188.20
109	34.58	140	114.20		
111	42.50	148	125.82		

185°C	Run 6		α = 0.48		5.0mg
t	p	t	p	t	p
50	0.66	150	88.50	210	135.79
80	9.10	155	90.23	225	142.91
100	25.03	160	92.75	240	147.40
120	53.07	170	100.08	270	152.94
140	84.10	180	111.21	p_f	160.00
Interruption		190	121.35	p_a	198.71
145	87.70	200	129.31		

185°C	Run 7		α = 0.78		5.4mg
t	p	t	p	t	p
90	12.13	180	126.66	240	148.11
110	32.74	185	127.36	255	152.55
130	80.01	190	128.43	270	153.30
150	97.99	200	130.98	p_f	160.00
170	122.77	210	134.19	p_a	215.11
Interruption		220	138.95		
177	126.45	230	143.86		

TABLE 8.8

185°C Run 1 Water interruptions. Uninterrupted blank 15 secs U.V. 5.0mg

t	p	t	p	t	p
10	0.16	80	84.15	160	144.76
20	2.29	90	96.31	180	149.58
30	9.83	100	107.96	210	155.63
40	22.58	110	117.89	240	161.89
50	38.44	120	125.43	p_a	175.76
60	54.85	135	134.53		
70	70.32	150	141.17		

185°C Run 2 Unirradiated blank 5.0mg

t	p	t	p	t	p
5	0.02	95	32.17	165	166.57
15	0.03	102	43.57	175	178.60
25	0.08	109	56.97	190	191.84
35	0.21	116	72.15	205	200.54
45	0.75	123	87.98	230	206.89
55	2.14	130	104.83	270	215.16
65	5.45	137	119.40	p_a	218.05
75	11.19	145	134.67		
85	19.67	155	152.46		

185°C Run 3 t = 0 (30 secs) 4.3mg

t	p	t	p	t	p
10	0.04	45	27.69	105	91.16
15	0.28	50	34.34	120	101.53
20	1.37	55	40.99	135	108.50
25	4.05	60	46.72	150	115.25
30	8.51	70	59.19	p_a	131.77
35	14.17	80	70.25		
40	20.71	90	79.30		

185°C Run 4 0.5 I.P. (30 secs) 4.9mg

t	p	t	p	t	p
8	0.12	55	28.12	100	78.75
Interruption		60	34.58	110	84.80
15	0.10	65	42.96	120	90.70
25	0.33	70	49.54	135	96.46
35	3.12	75	55.87	150	100.96
45	13.57	80	61.02	180	105.28
50	20.62	90	71.20	p_a	112.85

185°C Run 5 End I.P. (30 secs) 5.0mg

t	p	t	p	t	p
19	1.40	75	4.07	150	54.36
Interruption		90	10.94	165	58.36
25	1.47	105	22.93	180	61.16
45	1.49	120	36.24	215	62.76
60	1.88	135	47.36	p_a	63.35

185°C Run 6 $\alpha = 0.11$ (30 secs) 5.0mg

t	p	t	p	t	p
25	3.11	75	16.13	165	57.57
30	9.10	90	17.68	180	68.19
35	13.11	105	21.06	200	79.18
Interruption		120	27.21	221	86.76
40	15.91	135	36.01	240	91.02
60	15.95	150	46.46	p_a	107.67

185°C Run 7 Inflexion point (30 secs) 5.0mg

t	p	t	p	t	p
10	0.29	80	42.26	165	77.57

30	11.47	90	42.94	180	82.87
55	40.19	105	46.57	210	89.54
Interruption		120	53.58	240	93.24
60	42.04	135	62.22	p_a	107.19
70	42.08	150	70.38		

185°C	Run 8	α = 0.60	(30 secs)		5.0mg
t	p	t	p	t	p
30	9.04	105	93.13	165	105.98
50	33.29	115	93.37	180	111.35
70	67.21	125	94.17	200	116.58
90	92.19	135	95.96	220	119.71
Interruption		145	98.74	240	122.17
95	93.04	155	102.27	p_a	129.62

185°C	Run 9	Successive	(30 secs)		5.0mg
t	p	t	p	t	p
5	0.01	115	3.32	240	6.36
10	0.30	125	3.33	250	7.79
19	1.15	135	3.36	260	11.23
Interruption		145	3.57	270	18.03
25	1.16	155	4.18	280	28.65
35	1.19	157	4.36	290	41.18
45	1.50	Interruption		300	53.02
52	2.25	165	4.37	310	64.80
Interruption		175	4.44	321	73,58
60	2.25	185	4.81	330	78.85
70	2.26	193	5.45	346	87.13
80	2.27	Interruption		361	89.89
90	2.34	200	5.45	390	93.74
100	2.78	210	5.46	420	95.30
106	3.32	220	5.53	p_a	101.60
Interruption		230	5.78		

185°C Run 10 t = 0 (5 mins) 4.4mg

t	p	t	p	t	p
10	0.01	90	6.36	170	89.29
20	0.02	105	14.51	180	97.97
30	0.10	120	28.79	200	109.05
40	0.26	130	41.23	220	115.47
50	0.59	140	55.88	241	120.96
60	1.13	150	68.57	p_a	121.96
75	2.66	160	80.77		

TABLE 8.9

185°C Run 1 Blank 15 secs U.V. - irradiated 5.0mg

t	p	t	p	t	p
5	0.01	39	22.08	97	106.24
10	0.26	42	26.59	105	114.46
12	0.43	46	32.83	115	122.66
14	0.71	50	39.52	125	129.96
16	1.15	54	45.83	135	135.56
18	1.78	58	52.68	150	143.13
21	3.23	62	58.80	165	147.16
24	5.11	67	66.82	180	150.63
27	7.57	72	74.64	195	152.66
30	10.69	77	81.61	p_f	160.00
33	14.14	83	89.83	p_a	204.07
36	17.84	90	98.82		

185°C Run 2 Thermally annealed. 15 secs U.V. irradiated 5.0mg

t	p	t	p	t	p
5	0.20	40	36.41	120	131.78
10	0.79	50	53.16	135	140.08
15	2.93	60	68.97	150	146.42
20	6.63	70	82.85	180	154.28
25	11.78	80	95.31	p_f	160.00

30	19.08	90	107.14	p_a	199.70
35	27.40	105	120.96		

TABLE 8.10

190°C Run 1 35 mins U.V. irradiated 8.5mg pellet					
t	p	t	p	t	p
3	0.09	33	36.08	99	178.84
4	2.92	38	40.78	107	202.68
5	6.05	44	47.81	115	212.98
6	8.21	50	53.68	125	227.87
8	11.08	57	63.30	135	237.53
11	14.18	64	75.56	155	248.19
14	16.82	71	90.10	175	252.51
18	20.08	78	110.56	197	254.01
23	25.15	85	131.40	225	254.34
28	30.62	92	157.29	p_a	254.30

190°C Run 2 35 mins U.V. irradiated 17.3mg pellet					
t	p	t	p	t	p
4	0.21	44	51.95	105	384.40
5	3.01	49	59.02	110	421.47
6	6.36	54	67.52	115	449.65
7	8.77	60	78.12	120	469.88
9	12.00	65	87.05	130	492.11
12	15.31	70	101.80	140	502.84
15	17.77	75	122.96	160	511.85
19	21.10	80	147.78	180	512.14
24	25.53	85	185.51	200	514.37
29	31.12	90	230.67	p_a	601.00
34	36.88	95	286.22		
39	44.14	100	337.62		

TABLE 8.11

195°C	Run 1		Unirradiated blank		5.0mg pellet
t	p	t	p	t	p
10	0.02	77	22.00	130	126.51
20	0.04	84	33.81	140	138.75
30	0.16	91	48.65	150	144.14
40	0.61	98	65.22	165	150.12
50	2.02	105	80.94	180	153.01
60	5.41	112	96.40	p_f	160.00
70	13.07	120	113.16	p_a	191.21

195°C	Run 2	60 secs	U.V.-irradiated on each face		4.4mg pellet
t	p	t	p	t	p
5	0.14	45	30.45	104	121.22
10	0.77	50	35.96	112	132.05
15	3.06	57	43.79	120	141.15
20	7.58	64	53.67	130	146.50
25	12.12	72	65.62	145	152.80
30	17.02	80	80.09	165	155.27
35	21.18	88	94.22	p_f	160.00
40	25.53	96	109.34	p_a	168.39

195°C	Run 3	120 secs	U.V.-irradiated on one face		5.0mg pellet
t	p	t	p	t	p
5	0.04	50	20.47	120	121.90
10	0.38	57	25.90	131	134.59
15	2.02	64	32.64	140	144.44
20	4.39	72	40.57	155	150.60
25	7.53	80	51.04	170	154.43
30	9.74	88	63.68	p_f	160.00
35	12.02	96	78.34	p_a	158.30
40	14.48	104	93.42		
45	17.37	112	108.27		

TABLE 8.12

190°C	Run 1	Sunlight irradiation pellet			4.5mg pellet
t	p	t	p	t	p
5	0.04	50	19.56	160	142.23
10	0.34	60	33.36	180	149.23
15	0.70	70	48.45	200	153.50
20	1.36	80	64.87	220	155.97
26	2.40	90	81.29	240	158.50
30	3.68	100	95.87	p_f	160.00
35	6.00	110	107.98	p_a	179.21
40	9.49	120	117.88		
45	14.16	140	132.46		

190°C	Run 2	Pelleted sunlight irradiated powder			4.5mg pellet
t	p	t	p	t	p
5	0.09	60	39.27	180	98.36
10	1.17	70	43.81	200	110.79
15	4.63	81	48.08	220	121.95
20	9.09	90	51.70	240	131.92
25	14.00	100	55.61	260	141.25
30	19.17	110	59.77	280	148.77
35	23.24	120	64.21	p_f	160.00
40	27.05	140	73.66	p_a	170.94
50	33.95	160	85.80		

TABLE 8.13

160° ± 2°C			Run 1		6.0mg pellet
t	dp/dt	t	dp/dt	t	dp/dt
10	0.17	30	0.13	60	0.11
15	0.20	35	0.13	80	0.11
20	0.16	40	0.12	100	0.10
25	0.14	50	0.11	120	0.09

TABLE 9.1

175°C Run 1 30 secs U.V.-irradiated at 6.5 cm. 5.0mg

t	p	t	p	t	p
5	0.05	55	26.52	150	105.53
10	0.35	65	34.11	165	119.35
15	1.02	75	42.51	180	131.42
20	2.74	85	51.52	195	136.46
25	5.44	95	58.92	210	144.79
30	8.43	105	68.07	p_f	160.00
35	11.82	115	77.36	p_a	174.21
40	15.50	125	84.59		
47	20.44	135	92.73		

175°C Run 2 30 secs U.V. 15000 r. γ. 5.0mg

t	p	t	p	t	p
4	0.02	14	35.96	31	141.48
5	0.26	15	52.24	40	151.18
6	0.87	16	67.73	50	156.32
7	1.53	17	78.94	60	159.06
9	3.55	18	89.35	p_f	160.00
11	8.10	20	104.76	p_a	180.21
12	13.35	23	120.70		
13	22.06	26	131.08		

175°C Run 3 15000 r. γ. 4.9mg

t	p	t	p	t	p
5	0.26	15	39.13	29	134.19
7	1.61	16	52.84	35	145.46
9	3.64	17	65.10	47	154.64
11	7.50	18	76.07	60	157.63
12	10.77	20	95.45	p_f	160.00
13	16.43	22	108.81	p_a	172.00
14	25.64	25	122.00		

155°C Run 4 15000 r. γ. 5.0mg

t	p	t	p	t	p
10	0.12	55	17.51	120	100.16
15	0.70	65	36.02	135	108.66
20	1.26	75	55.94	150	113.25
27	2.24	85	71.11	170	117.92
35	3.69	97	83.94	p_f	160.00
45	7.28	108	93.02	p_a	194.07

155°C Run 5 30 mins U.V. at 6.5 cm 5.0mg

t	p	t	p	t	p
5	0.03	26	37.10	91	84.96
8	2.07	31	43.94	105	89.12
10	6.04	36	50.04	120	93.74
12	10.91	42	55.38	140	97.01
14	16.09	50	62.13	p_f	160.00
17	22.57	62	70.25	p_a	172.81
21	29.52	75	78.07		

155°C Run 6 15000 r. γ., 30 mins U.V. 5.5mg

t	p	t	p	t	p
5	0.03	23	56.70	70	127.20
7	2.02	27	65.34	80	133.48
9	8.06	31	74.53	90	136.87
11	17.22	36	84.99	105	139.98
13	25.66	42	94.81	120	143.85
16	36.52	50	107.59	p_f	160.00
19	45.75	60	117.93	p_a	192.11

175°C Run 7 30 mins X-rays (20, 10) 5.0mg

t	p	t	p	t	p
5	0.04	41	44.34	135	125.27
10	0.54	47	50.14	150	131.07
15	1.92	55	58.68	165	138.69
20	6.77	65	69.21	180	144.60
23	12.70	75	79.98	200	146.23
26	19.66	85	91.10	p_f	160.00
29	26.06	95	98.90	p_a	173.38
32	31.58	105	107.53		
36	38.19	120	118.96		

175°C Run 8 30 mins X-rays 15000 r. γ. 5.0mg

t	p	t	p	t	p
3	0.04	11	49.95	26	137.70
4	0.83	12	65.29	32	145.28
5	3.73	13	78.53	40	151.06
6	6.08	14	89.99	53	155.60
7	8.67	15	99.53	p_f	160.00
8	12.58	17	113.83	p_a	180.20
9	20.38	19	121.82		
10	35.25	22	130.59		

155°C Run 9 60 mins X-rays (40, 20) 5.2mg

t	p	t	p	t	p
5	0.02	27	34.35	90	78.92
7	0.67	31	40.63	100	85.18
9	1.88	36	45.97	110	89.56
11	3.25	42	50.22	120	94.92
14	5.60	50	54.47	140	102.78
18	11.56	60	60.37	p_f	160.00
21	19.59	70	66.09	p_a	187.98
24	27.96	80	73.18		

155°C Run 10 15000 r. γ. 60 mins X-rays (40, 20) 4.7mg

t	p	t	p	t	p
5	0.01	26	57.40	90	134.67
7	0.14	30	71.33	100	136.90
9	1.75	35	83.63	120	142.27
11	4.09	42	96.70	140	144.75
14	8.19	50	106.87	p_f	160.00
17	15.29	60	119.35	p_a	150.70
20	27.91	70	125.29		
23	44.21	80	132.13		

175°C Run 11 30 secs U.V., 30 mins X-rays 4.9mg

t	p	t	p	t	p
5	0.23	27	55.01	90	130.57
8	1.32	31	65.01	106	138.31
11	2.64	36	75.59	120	144.14
14	6.06	42	85.67	140	147.89
17	15.40	50	95.35	p_f	160.00
19	24.38	60	106.63	p_a	172.09
21	33.56	70	114.66		
24	45.47	80	123.37		

165°C Run 12 30 mins U.V. 5.0mg

t	p	t	p	t	p
4	0.75	17	39.71	85	106.29
5	3.81	23	48.23	105	119.30
6	9.18	30	56.24	120	126.08
7	14.62	40	67.85	140	134.11
8	19.04	50	77.95	p_f	160.00
10	25.57	60	87.81	p_a	211.46
13	32.75	70	95.23		

165°C Run 13 30 mins X-rays (20, 10) 5.2mg

t	p	t	p	t	p
10	0.34	40	20.94	105	62.06
15	0.90	45	26.15	120	71.69
20	1.58	52	31.70	140	82.24
25	3.26	60	35.91	p_f	160.00
30	7.60	70	41.92	p_a	229.04
33	11.79	80	48.05		
36	15.85	90	52.84		

165°C Run 14 30 mins, X-rays, 30 mins U.V. 5.0mg

t	p	t	p	t	p
2	0.02	15	64.69	90	135.33
3	1.04	19	74.30	105	137.87
4	6.72	24	84.23	120	139.12
5	18.77	30	92.90	140	142.19
6	29.43	40	106.09	p_f	160.00
7	35.88	50	114.92	p_a	209.95
9	45.61	60	122.86		
12	56.37	75	130.01		